UNIVERSITY OF SOUTHAMPTON

FACULTY OF ENGINEERING AND THE ENVIRONMENT

Institute of Sound and Vibration Research

Variability in the dynamic response of connected structures possessing spatially slowly varying properties

by

Marcos Ricardo Souza

Thesis for the degree of Doctor of Philosophy

September 2018

UNIVERSITY OF SOUTHAMPTON

ABSTRACT

FACULTY OF ENGINEERING AND THE ENVIRONMENT

Institute of Sound and Vibration Research

Thesis for the degree of Doctor of Philosophy

Variability in the dynamic response of connected structures possessing spatially slowly varying properties

by Marcos Ricardo Souza

This thesis covers the modelling and analysis of the dynamic behaviour of coupled structures possessing slowly varying properties. A mobility method is used to dynamically couple beams to a plate through a series of point connections comprising rigid links or flexible ones, the latter in the form of elastic springs. This is a relevant problem for cable bundles providing electrical power or for communications in cars, satellites and airplanes. In the case of rigid links, the response of the coupled system will generally be governed by the response of the least mobile structure, but with additional modes. For flexible links, there is a frequency at which the response of the combined system uncouples. The flexible links can also be used to reduce the uncertainties due to one of the sub-structures. Uncertainties in the positioning of the connection points were also considered and they can be as important as uncertainties in the mechanical properties of the structures in terms of the coupled system response variability.

The slowly varying properties are then introduced using a description given by a random field using the Karhunen–Loève expansion. For the slowly varying beams, the Wentzel–Kramers–Brillouin approximation is used to find analytical solutions of the flexural wave equation and subsequently expressions for the input and transfer mobilities. The slowly varying plate is solved combining Finite Element Analysis and a Perturbation Method in order to find the required mode shapes, natural frequencies and mobilities. Infinite and finite coupled structures were considered. The work presented here thus proposes an alternative to the standard technique used in the industry of considering the cable bundles as lumped mass at the connection points. This approximation is valid at lower frequencies, where they indeed behave as an additional mass. However, at higher frequencies they can contribute to adding some stiffness and apparent damping, as the response of the coupled system is now shared into more modal resonances, from the modes of the host structure and the attached cables.

Experimental validation is presented showing the effects of randomly spaced connections and are in good agreement with numerical simulations. In order to capture the varying properties, a novel technique is proposed that combines a wavenumber correlation technique within a Bayesian framework in order to estimate the values of the bending stiffness of the particular cable bundles. The Bayes' technique was also used to reconstruct random fields from synthetic data. It could subsequently be applied experimentally and provide the required input for models possessing slowly varying properties.

Table of Contents

Table of Tables

Table of Figures

Table of Figures

Table of Figures

Table of Figures

Academic Thesis: Declaration of Authorship

I, Marcos Ricardo Souza, declare that this thesis entitled Variability in the dynamic response of connected structures possessing spatially slowly varying properties and the work presented in it are my own and has been generated by me as the result of my own original research.

I confirm that:

1. This work was done wholly or mainly while in candidature for a research degree at this University;
2. Where any part of this thesis has previously been submitted for a degree or any other qualification at this University or any other institution, this has been clearly stated;
3. Where I have consulted the published work of others, this is always clearly attributed;
4. Where I have quoted from the work of others, the source is always given. With the exception of such quotations, this thesis is entirely my own work;
5. I have acknowledged all main sources of help;
6. Where the thesis is based on work done by myself jointly with others, I have made clear exactly what was done by others and what I have contributed myself;
7. Parts of this work have been published as:

    - Souza, M.R.; Ferguson, N.S.; Identification of bending stiffness via wavenumber estimation and Bayes inference. ICVRAM-ISUMA Uncertainties 2018, 2018, Florianópolis. Proceedings of the joint ICVRAM ISUMA UNCERTAINTIES conference, 2018.
    - Souza, M.R.; Ferguson, N.S.; The dynamics of coupled structures possessing inhomogeneous attachments. Procedia Engineering, v. 199, p. 1264-1269, 2017.
    - Souza, M.R.; Ferguson, N.S.; Experimental investigation of the variability in the dynamics of connected structures. Journal of physics. Conference Series (print), v. 744, p. 012200, 2016.
    - Souza, M.R.; Ferguson, N.S.; Variability in the dynamic response of connected structures. Uncertainties 2016 - 3rd International Symposium on Uncertainty Quantification and Stochastic Modeling, 2016, Maresias. Proceedings of the 3rd International Symposium on Uncertainty Quantification and Stochastic Modeling, 2016.

Signed: .....

Date: 03/09/2018

Acknowledgements

Firstly, I would like to thank my supervisor, Doctor Neil Ferguson for his guidance and patience throughout this work, as well as his friendship and support.

I would also like to thank Doctor Adriano T. Fabro and Professor Brian Mace for their helpful suggestions and comments on this work on every occasion we were able to meet.

I'm grateful for all the friends and colleagues from the ISVR that made these almost 4 years a brilliant experience filled with coffees and laughs.

This work was financially supported by the Brazilian National Council for Scientific and Technological Development, CNPq, through the Science without Borders program under the code 231744-2013/7. I would also like to acknowledge Jaguar Land Rover for providing the cable bundle samples.

And finally, I would like to thank my parents Geraldo and Ivonete. Even from afar they were able to be supportive and I could always feel their unconditional love.

Nomenclature

Symbols

a, b, c Amplitude of the propagating waves

$\boldsymbol{a}, \boldsymbol{b}, \boldsymbol{c}$ Vector of amplitude of the propagating waves

a_Γ Shape parameter for the Gamma distribution

b_L Correlation length

b_Γ Scale parameter for the Gamma distribution

c_{eq}^b Equivalent lumped damper for the beam

c_{eq}^p Equivalent lumped damper for the plate

c_l Local phase velocity

$\boldsymbol{e}$ Prediction error

ϵ Random factor sampled from a distribution

ϵ_i Average modal spacing

f Distributed force per unit length

$\boldsymbol{f}$ Vector of external forces

$\boldsymbol{f'}$ Vector of transmitted forces

f_j Eigenfunctions of the Fredholm integral equation of the second kind

f_X Probability density function

$\widehat{f_X}$ Kernel density estimator

h Thickness

h_K Estimator bandwidth

i Imaginary unit

k Wavenumber

k_{tx} Trial wavenumber

$[\boldsymbol{k}]_e$ Element stiffness matrix

m Mass per unit area

m_{eq}^b Equivalent lumped mass for the beam

$[\boldsymbol{m}]_e$ Element inertia matrix

p Distributed transverse force per unit area

$p(\boldsymbol{y})$ Normalising constant

$p(\boldsymbol{y}|\boldsymbol{\theta})$ Likelihood function

$p(\boldsymbol{\theta})$ Prior distribution

$\boldsymbol{q}(\boldsymbol{\theta})$ Outputs of the modelled system under the excitation $\boldsymbol{\theta}$

r Distance between the points

t Time

u Longitudinal displacement as function of x and t

w Transverse displacement as function of x and t

$\dot{\boldsymbol{w}}$ Vector of velocities

x Coordinate x

A Cross-sectional area

B Bending stiffness of the plate

C Arbitrary constant

Cov Covariance

D Geometrical domain

E Young's modulus

E_0 Nominal Young's modulus

$\mathbb{E}[x]$ Expected value of a random variable x

F Force

F_X Cumulative distribution function

H Random field

H_0 Mean value of the random field

$H_i^{(2)}$ i[th] order Hankel function of the second kind

I Second moment of area

$\boldsymbol{I}$ Identity matrix

K Kernel estimator

K_i i[th] order modified Bessel function of the second kind

$[\boldsymbol{K}]$ Global stiffness matrix

$[\widetilde{\boldsymbol{K}}]$ Global stiffness matrix from random field

$\Delta[\boldsymbol{K}]$ Difference in the global stiffness matrix

L Length of the Domain

L_i i[th] length of interest for rod or beam

M_i Modal mass

$[\boldsymbol{M}]$ Global inertia matrix

$\Delta[\boldsymbol{M}]$ Difference in the global inertia matrix

N_{KL} Number of terms in the KL expansion

N_p Number of points

P Internal forces on the rod

R^2 Coefficient of determination

S *Eikonal* function

T Applied tension

U Longitudinal displacement as function of x

$\widetilde{U}$ Amplitude of the longitudinal travelling wave on the *eikonal* solution

V Velocity

W Transverse displacement as function of x

$\widetilde{W}$ Amplitude of the flexural travelling wave on the *eikonal* solution

$\boldsymbol{W}$ Vector of the propagating and evanescent waves of transverse displacement

Y Mobility

Y^{b_r} Envelope for one dimensional waveguides

Y^{p_r} Envelope for plates

Y^c Characteristic mobility line

$\hat{Y}$ Correlation function

$\boldsymbol{Y}$ Mobility matrix

Greek symbols

α , β Coordinates points α and β

γ Amplitude change of the travelling wave

Δ Spacing between the point connections

η Loss factor

θ Phase change of the travelling wave

$\boldsymbol{\theta}$ Set of model parameters

κ Spring stiffness

$\boldsymbol{\kappa}$ Diagonal matrix with the stiffness of the springs

λ Wavelength

λ_j Eigenvalues of the Fredholm integral equation of the second kind

$\widetilde{\Delta}\lambda_m$ Change in the m^{th} eigenvalue

λ_m Unperturbed m^{th} eigenvalue

μ Mean value

ν Poisson's ration

ξ_j Gaussian uncorrelated random variables

ρ Density

σ Spreading factor in the random field

σ^2 Variance

$\hat{\sigma}^2$ Most probable value of the Variance

$\boldsymbol{\phi}_m$ Unperturbed m^{th} eigenvector

$\widetilde{\Delta}\boldsymbol{\phi}_m$ Change in the m^{th} eigenvector

ψ_n Modal shape for a beam

ψ_{mn} Modal shape for a plate

ω Angular frequency

ω_n Natural frequency for a beam

ω_{mn} Natural frequency for a plate

ω_B Modal bandwidth

Γ Factor for the envelope of complex vibrators

$\boldsymbol{\Gamma}$ Reflection matrices

Λ Propagation element

$\boldsymbol{\Lambda}$ Propagation matrix

$\Delta\boldsymbol{\Phi}_m$ Mass normalised perturbed modal shapes

Subscripts

b Relative to the beam

dof Degrees of freedom

l Longitudinal

p Relative to the plate

x, y, z Relative to the directions x, y or z

B Bending

K Relative to the springs

KL Relative to the KL expansion

L, R Left or Right

N Near-field wave

Superscripts

b Relative to the beam

p Relative to the plate

$-$ Negative-going wave

$+$ Positive-going wave

Abbreviations

cdf Cumulative distribution function

pdf Probability density function

CLF Coupling loss factor

FE Finite Element

FEA Finite Element Analysis

FEM Finite Element Method

KL Karhunen-Loève expansion

MAC Modal Assurance Criterion

MC Monte Carlo

SEA Statistical Energy Analysis

WBM Wave based method

WFE Wave Finite Element method

WKB Wentzel–Kramers–Brillouin approximation

Chapter 1 Introduction

In the design process of structures, control of vibrations is a relevant factor as excessive vibration might lead to problems ranging from noise and vibration nuisance to complete failure of a structure. Therefore, it is imperative to carry out an analysis of the vibration profile for structures to predict and assure that vibration responses, forces, stresses and radiated sound can be estimated and judged if they are within an acceptable level under typical operating conditions. Vibration analysis requires the dynamic characteristics of a structure to be known, so geometry and mechanical properties such as density, Young's modulus of elasticity, Poisson's ratio, boundary conditions, connections between the sub-elements of the structure are all necessary as input parameters for the subsequent analysis [**1**].

Problems can arise, because it is known that manufacturing processes produce variability in the nominal properties of the materials and that these deviations lead to different dynamic responses of nominally identical components [**2**]. It is also common to have discrepancies between measured performance and a structural model [**1**]. Models are not an exact representation of the actual structure and are assembled assuming physical properties that might not match the real properties or are incomplete models. Even when the model is assumed to be adequate albeit approximate, the predictions can differ from the measured data of the actual structures simply because the model parameters are not known with sufficient accuracy, i.e. they are uncertain [**1**].

Analysis of structures comprising a one-dimensional vibration waveguide attached to a host-structure, which are commonly found in engineering was developed in this study. The one-dimensional waveguide can represent structures such as cable bundles, hydraulic pipes, reinforcement ribs etc., whilst the host structure can be an aircraft fuselage, a satellite body or a car body-in-white. To some extent, it is possible to relate those structures to beams attached to plates and model them as such to better understand how they behave when attached together through a set of point connections. In addition, it might then be possible to consider how to deal with and analyse the effect of uncertainties in their parameters.

It is of interest to know how to take into account these effects of uncertainties, especially in the so called mid to higher frequencies where they are more significant. This study introduces these variations in the form of varying the properties of the one-dimensional waveguides and host structure and varying the position of the attachment points. Scenarios with perfectly rigid links and flexible connections are also presented. The flexible connections are treated as elastic springs and variations around the nominal value of the stiffness of the springs are considered. Slowly varying properties of the beams and plate are considered.

A wave propagation approach is used to describe and model the one-dimensional waveguides in order to find their mobility expressions. The analysis of the plate is made using the Finite Element method combined with the perturbation method. Once the input and the transfer mobilities are known, it is possible to use matrix and vector algebra to attach the beam to the plate. Design engineers frequently consider these attachments, the one-dimensional waveguide, as simply lumped masses at the attachment points, which is not enough to fully predict all of the structural dynamic interaction of structures such as cables or determining when this interaction is relevant [**3**]. An overview of the relevant background structural dynamic modelling and previous studies is now presented.

1.1 Modelling techniques in structural dynamics

This section explores some of the most common modelling techniques that are used to predict the dynamic behaviour of structures. Yoo [**4**] brings together a fine summary of the different methods that are used for different frequency bands, each one has its own particularities and limitations.

These different behaviours for each different frequency band can be illustrated by the industrial problem of a simplified car model, as shown in Figure 1.1, where one is interested in calculating the mechanical energy in the areas identified from A1 to A12. The force excitation is randomly distributed over the panel A7 and it has frequency components within the range 0 to 300 Hz. The spatial distribution for the variability of the Young's modulus is known and Figure 1.2 shows three simulated typical samples of this spatial distribution with the same statistical features [**2**], in other words, the values for the Young's modulus at each position.

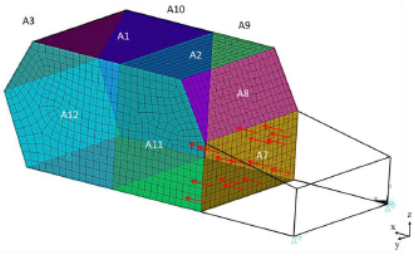

Figure 1.1 – Simplified structural model (FE) for a car.
Model comprising a number of plates with spatial variability. The cavity is not modelled.
(From: [**2**])

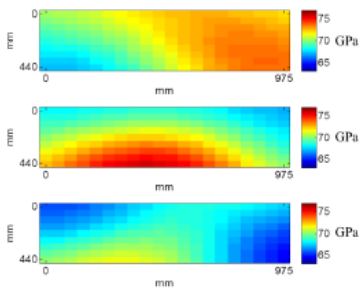

Figure 1.2 – Three simulated typical samples of Young's modulus spatial distribution for the panel A7.
(From: [**2**])

If one evaluates the effects of the material on the dynamic response of all the possible cars produced, the typical 95% percentile of frequency response of the mechanical energy on the windshield, panel A8, can be seen on Figure 1.3. This result can be typically calculated by running the finite element model hundreds (or even thousands) of times, each time using different samples with the same statistical features of the material distribution of the panel A7. This approach is called Monte Carlo sampling, but it can be computationally prohibitive [**2**].

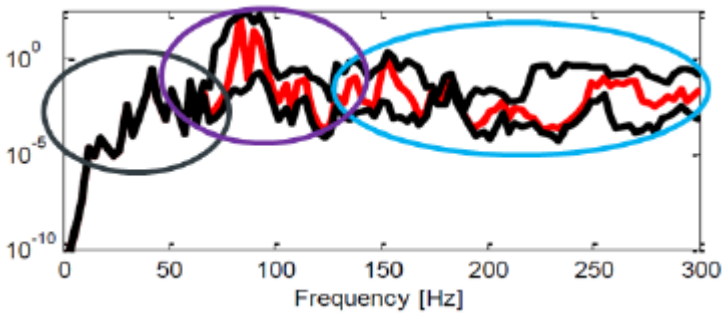

Figure 1.3 – 95% percentile of the potential energy in the windshield.
Three distinct frequency bands are highlighted: low frequency (black), mid frequency (magenta) and high frequency (cyan).
(From: [**2**])

However, there are three clearly distinguishable frequency bands shown in Figure 1.3. In the first region, at low frequencies a deterministic model can be useful. The second identifiable region, highlighted in cyan, is the so called high frequencies. It has a high modal density and it is highly sensitive to the variability of the panel. For this region, energy-like methods are well suited. The mid frequency region, which is between the low and high frequency regions, still has distinguishable modal behaviour and it is affected by variability. Wave-based methods are one of the tools to analyse this region of the response spectrum [**2**].

At higher frequencies, structures can be very sensitive to variability in the manufacturing processes, presenting significant differences in the dynamic behaviour. An example is shown in Figure 1.4, where the measured noise levels in the cabin of 57 nominally identical trucks due a force input at a wheel show large variations [**4**] [**5**]. In that case, a model considering only one of the vehicles would be incapable of fully representing the response of the others accurately. A number of numerical (FE) solutions containing slight differences in the geometry or material properties, although feasible, would not be efficient and one would need to have a description of the variability to include within said models. It is possible though to extend the frequency range of a FE model, but it is usually inappropriate due the variation of the responses at high frequencies, which occurs due to the numerical results of FE models at high frequencies being sensitive and different for slight refinement to the mesh, etc. [**4**] [**6**].

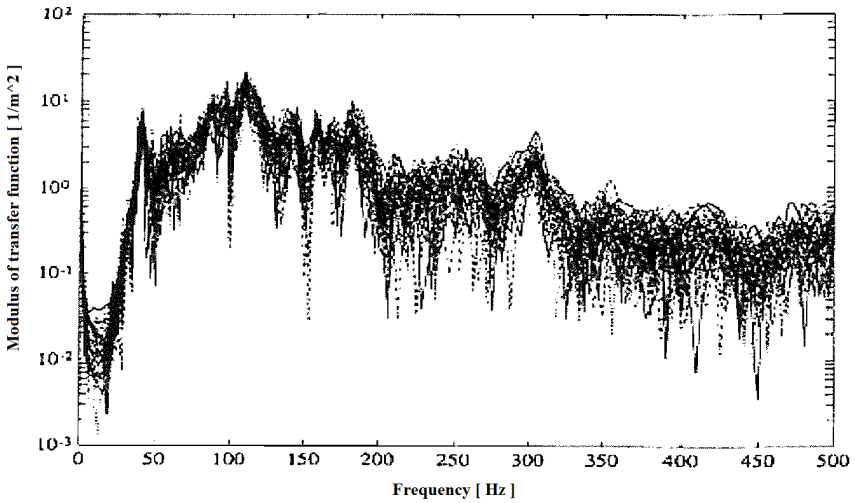

Figure 1.4 – Modulus of transfer functions between the input force at the front left wheel and sound pressure level at the location of driver's head measured on 57 nominally identical vehicles.
(From: [**4**] and [**5**])

1.1.1 *Low frequency methods*

The first band of interest is the so called low frequencies. At these frequencies one can find the fundamental lowest order modal characteristics of a given structure. The most common method used to describe or even predict the dynamic behaviour of structures is the finite element method, FEM. Instead of using physical experiments, it is the de facto engineering designing tool in engineering companies for virtual prototyping. FEM is actually capable of predicting both static and dynamic characteristics of a product before manufacturing it [**4**]. It is also widely used in the automotive industry to predict body vibrations and interior noise [**4**] [**7**] [**8**].

FEM is a deterministic method. It is, in principle, possible to determine the exact behaviour of the system once geometric and material properties are known [**4**]. To predict this behaviour, the method is based on a discrete system of equations written as the stiffness and mass matrices of a continuous structure. The structure is divided into small areas, or volumes, called elements. There is no restriction on the geometric complexity of the structure, since the stiffness and mass matrices are assembled from the individual contribution of each finite element, which are simpler structures. Each element has a mathematical representation and formulation associated with its simple geometry, regardless of the complexity of the whole structure. The nodes of an element are shared with its surrounding elements; therefore, the displacement field is continuous [**9**].

Shannon's sampling theorem is fundamental to frequency detection in acoustic and vibrations, stating that at least two points per wavelength are necessary to detect the corresponding waveform [**10**] and it is one reason behind using greater than a minimum fixed number of elements per wavelength [**11**]. Two linear elements per wavelength are sufficient, but might not lead to accurate modal shapes and a factor of 3 to 5 should be used on top of that [**12**]. Therefore, to correctly represent

the continuous dynamic deformation, it is typically necessary to have between 6 and 10 linear elements per wavelength [**4**] [**12**] [**13**] [**14**]. There is one very clear implication of that; the higher the frequency, the higher the number of elements necessary for an accurate result, which can be prohibitive in a computational sense [**4**]. One way of dealing with the problem is to use higher order elements, the so called Hierarchical Finite Elements. These elements use higher order polynomial or slope functions that allow the model to have fewer elements and retain the accuracy [**4**] [**15**] [**16**]. However, regardless of those requirements, uncertainties can play a major role in modelling, causing the predictions to be inaccurate.

1.1.2 *High frequency methods*

In the high frequency region, the most widely accepted modelling method is Statistical Energy Analysis, SEA. This method consists in dividing the system into a number of smaller subsystems and the response is described in terms of energy and power flow. The modal characteristics of a structure vary according to detailed properties. Therefore, even subsystems that might have the same gross physical and geometrical properties can have some scattering in their dynamic response [**4**]. SEA predicts the ensemble response and some work has been conducted to investigate the variance in the SEA predictions.

One does not use SEA to predict a detailed response of the structure at every single frequency, for this method one only predicts the average response. There are three averages involved in SEA: the spatial average, the ensemble average and the frequency average. The first one arises from the fact that SEA calculates the total vibrational energy in a region of the system, rather than the response at a specific point. The ensemble average takes into account the variability of nominally identical structures, which might have random dynamic properties due to manufacturing tolerances. Finally, the frequency average is the result of SEA being an analysis over a frequency band. These bands can have a constant bandwidth or may consist of octave (or 1/3 octave) bands. The total vibrational energy is predicted for each of those bands. To summarise, SEA predicts the average vibrational energy stored in various subsystems of the structure in different frequency bands [**17**].

Figure 1.5 shows the time-averaged energy and the power balance relationship of a simple SEA model that comprises two subsystems. The coupling loss factor, CLF, and the difference between mean modal stored energy in the source and receiver are the factors that regulate the power transferred between the subsystems [**4**]. The values for the CLFs involved in a SEA might require numerical calculations, or they can also be estimated through wave methods. They are highly dependent on physical and geometrical properties of the structures [**4**] [**18**] [**19**] [**20**].

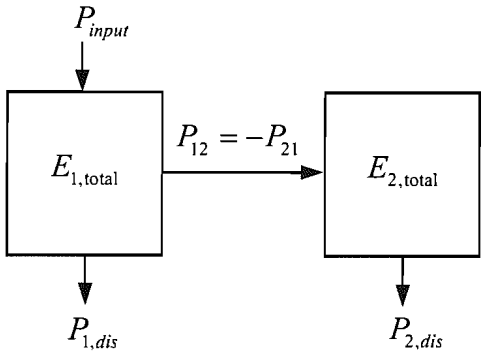

Figure 1.5 – Power balance relationship of a coupled structure consisting of subsystems 1-2.
E is the storage energy in each subsystem, *P* is the dissipated or transferred net power and subscripts indicate the corresponding subsystem in the coupled system.
(From: [**4**])

In order to obtain good accuracy, SEA is very dependent of the modal overlap, that is, the ratio of the half-power bandwidth to the average spacing between resonances [**4**] [**21**]. To obtain no clear resonance peaks, as they merge, this ratio needs to be in the region of the unity or greater. High modal overlap typically results in low variance of the response, despite the structural uncertainties [**4**] [**17**]. Especially because of such assumption, there is a lower limit in frequency for the applicability of SEA [**4**].

1.1.3 *Mid frequency methods*

In this region of the spectrum, the uncertainties in the dynamic characteristics are increasing and therefore the accuracy of low frequency methods are decreasing. However, the behaviour in these frequencies are still not adequate for SEA calculations. For a given structure, the mid frequency region can be especially broad when the said structure is a mixture of stiff and flexible substructures. These different elements may exhibit very distinct behaviours. For instance, the stiff substructures can be treated as in a "low frequency region" for a quite higher frequency than the flexible elements, which will present "high frequency behaviour" at a much lower frequency. Thus, such structures have a very broad mid-frequency region where neither of the previously presented methods can satisfactorily predict the structural response [**4**]. In a finite element analysis, the shortest wavelength of all types of occurring waves in the structure is what usually defines the element size for the mesh. An element size that is be adequate for the flexible substructure will result in a mesh that may be too large to analyse in an acceptable time. In addition, the stiff substructure may not have enough modal density for SEA [**22**].

One of the methods used for the mid frequency region is a wave approach, which is based on how waves are propagated, reflected and transmitted along or across a structure and its joints [**4**]. The forced response of a beam in flexure for example can be expressed as the sum of the propagating

wave and an infinite number of its reflections [**23**]. The response of a beam with length l and excited at $x = 0$ with an harmonic point force F_0 can be considered as shown in Figure 1.6.

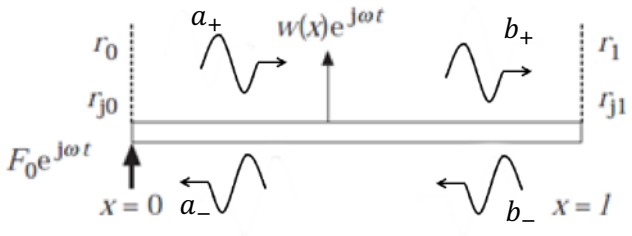

Figure 1.6 – Beam of length l excited by a harmonic point force.

(Adapted from: [**23**])

In [**22**], the authors used a wave analysis to study a structure comprising a stiff beam and a flexible plate. They considered the beam as the source and the plate as the receiver. When the wavenumber in the plate is at least twice as large as the wavenumber in the beam, the plate can be idealized as set of independent plate strips and then the dynamic behaviour of the beam can be described in terms of a locally reacting impedance of the plate and the dispersion relationship of the coupled structure [**4**].

Castel et al. [**24**] used a hybrid FE-SEA model to extend the applicability of both approaches to the mid frequency region in the space industry. This hybrid method is widely used in the automotive industry to couple components with high modal density (ideal for the SEA method) to low modal density components (FE subsystems). The method uses the concept of direct and reverberant fields, where the direct fields can be seen as the contribution from the generated waves, whilst the reverberant field takes into account the contribution from the waves reflected by the boundaries [**25**].

1.2 The Monte Carlo approach for variability calculations

The analysis of uncertainties has been increasing in the last decades and the inclusion of uncertainties in the model parameters means that the structure modelled has a range of performance when operating. Its response might vary within this given range. It is then necessary to use tools that can determine this range of operation or response [**1**].

One way to consider variability when modelling a structure is to use the Monte Carlo (MC) approach [**26**]. The numerical solution of a stochastic process can be divided in three parts. Firstly, one designs a deterministic model of the system. Secondly, a probabilistic model to the uncertain variables involved is created, assigning a probability density function, PDF, to each of the uncertain variables. Lastly, samples of the uncertain variables are created and to each one of these samples a deterministic response is calculated. Figure 1.7 illustrates this process. It is important to note that this is a tool to solve the stochastic process, it is not a technique for stochastic modelling. A stochastic

modelling approach is defined by the strategy of adopting PDF's of the input variables. Thus, the determination of these probability density functions is fundamental to a probabilistic model [**27**].

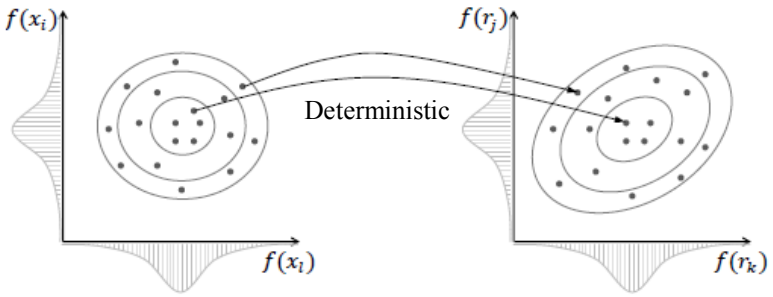

Figure 1.7 – Monte Carlo sampling.
On the left side, the input uncertain variables and their PDF. On the right, the deterministic responses for each one of the inputs.
(Adapted from: [**27**])

The Monte Carlo method makes use of the law of large numbers to ensure that the average of the response from the independent sampled input converges to the actual expected value of the response, whilst the central limit theorem says that the distribution of the error converges to a normal distribution [**28**]. The Monte Carlo method has a somewhat slow convergence rate, as it converges with the square root of the number of samples. Therefore, to increase accuracy by a factor of 10, it is necessary to increase the number of samples by a factor of 100 [**28**].

The Monte Carlo method is actually the most commonly used technique found in the literature [**29**]. It consists of sampling the random parameters from their distributions and each one of these samples defines a deterministic problem that then leads to one solution. After many realisations and responses, the statistics of the response can be processed [**29**] [**30**] [**31**] [**32**]. One advantage of the MC approach is that if there is one code to compute the response of a deterministic model, the MC does not require a new code to compute the responses. It is only necessary to run the available code multiple times, different from other common techniques used for uncertainty quantification, like generalised Polynomial Chaos [**29**] [**33**].

The MC method started to be used during the 1980s [**34**] in order to take into account uncertainties in FEA, introducing uncertain parameters to compute the statistical features of the response of the structure [**1**].

In the case of epistemic uncertainty, in other words, lack of precise knowledge about the statistical features of the processes or quantities, a possibilistic approach can be used in an interval arithmetic approach [**35**] [**36**].

1.3 Statistical tools

This section brings together some concepts from statistics that will be useful within this work.

Firstly, the cumulative distribution function, cdf, is the probability that X is less than or equal to x and it is defined as $F_X(x) = \mathbb{P}(X \leq x)$ and $F_X : \mathbb{R} \to [0,1]$ [**37**]. Secondly, the concept of percentile: The n^{th} percentile of a random variable x is the smallest number X_n such that $n = \mathbb{P}(X \leq X_n)$ [**38**]. In the next chapters, the regions within which 95% of the response lies are calculated using the 2.5% percentile and the 97.5% percentile. Also, the derivative of the cdf is called the probability density function, pdf, $f_X(x) = \frac{dF_X(x)}{dx}$ [**38**], so they are related by $\mathbb{P}(a < X < b) = \int_a^b f_X(x)dx$ [**37**].

The expected value of a random variable x, $\mathbb{E}[x]$, also known as the mean of x, is defined by $\mathbb{E}[x] = \int_{-\infty}^{\infty} x\, f_X(x)dx$ and its variance is given by $\sigma^2 = \int_{-\infty}^{\infty} (x - \mathbb{E}[x])^2 f_X(x)dx$ [**38**]. The variance can be seen as a measure of the spread of the population around its mean.

Statistical inference is defined as the process of using data to infer the distribution that generated said data [**37**]. Chapters 2 and 3 use a frequentist approach to identify distributions from the simulated data, using the kernel density estimator. It is defined as [**37**]:

$$\widehat{f_X}(x) = \frac{1}{n}\sum_{j=1}^{n} \frac{1}{h_K} K\left(\frac{x - X_j}{h_K}\right) \tag{1.1}$$

where $h_K > 0$ is the estimator bandwidth and the kernel K is a smooth function such that $K(x) \geq 0$, which means that there is no negative probability; $\int_D K(x)dx = 1$, the total probability is 1; $\int_D xK(x)dx = 0$, the mean of the kernel is 0 and $\int_D x^2K(x)dx > 0$, the variance of the kernel has to be positive [**37**] [**39**].

Details on a Bayesian approach, for a different case, are given in Chapter 5.

1.4 Slowly varying properties

Wave-based methods have been developed as a prediction tool in the mid frequency region in order to extend the applicability of deterministic approaches to higher frequencies. However, they are usually limited to the assumption that the waveguide properties are homogeneous in the direction of the travelling wave. Some examples are the Wave Based Method (WBM), based on the indirect Trefftz approach, the spectral element method, that uses analytical solutions for the wave propagation to assemble dynamic stiffness matrices for waveguides, the Semi-Analytical FE method, that uses FE formulation for the cross section of waveguides and assumes a wave-like solution in the

propagation direction and the Wave and Finite Element method (WFE), that applies the theory of periodic structures for homogeneous waveguides using FE model of the cross section [**2**] [**40**].

Pierce [**41**] seems to be the first to suggest using the Wentzel-Kramers-Brillouin (WKB) approximation for beams and plates. Fabro [**2**] used the WKB approximation and the Karhunen-Loève expansion to treat random fields with slowly varying properties in finite rods and finite beams in order to find their input mobilities and natural frequencies via a wave propagation approach. The work done here extends Fabro's approach to infinite beams and it also generalises the expressions for the case of transfer mobilities. Details on this are shown in Chapter 2 and Chapter 3. Also, for coupled one and two dimensional structures possessing spatial variability a hybrid method with the WKB approach for the one-dimensional structures and an FE model for the two-dimensional structure has been developed in this thesis.

1.5 Envelope of complex vibrators

Infinite homogeneous beams and infinite plates have exact and concise analytical solutions for the point and transfer mobilities, which capture the general characteristic behaviour of the structures. However, when dealing with infinite structures, there are no reflections by the boundaries and therefore no modes. At lower frequencies, when the resonances are well separated, the peaks and valleys of the mobility response extend greatly above and below the characteristic line, whereas, at higher frequencies, the behaviour of the frequency averaged response of a finite structure converges to the characteristic line, or the infinite system response [**42**] [**43**].

1.6 Practical applications of variability in connected structures

This section will explore what the effects are of adding cable bundles to a host structure. There are a variety of areas that could take advantage of a good modelling technique for the interaction between these attached structures. Some studies have previously taken place in the aerospace and in the automotive industries.

Cable bundles can reach up to 50 mm in diameter in the automotive industry and most of them are used to transmit signals through the car. The type of wrapping for these cable bundles depends on the location of the cables within the vehicle. Internal cables are wrapped with a soft fabric to increase damping, cables in the engine bay are usually only wrapped in a black tape in order to hide them and cables that are out of sight in the engine bay can actually not be wrapped at all. For the same manufacturer, the bundles are usually made with a standard length, which means that the bundle is not always fixed in a straight configuration; it depends on the car model. When the body is shorter, the bundles are curved and fixed at additional locations. Moreover, the thick bundles usually branch

out into bundles of smaller diameter to connect to various parts in the vehicle [**44**]. Figure 1.8 shows some details of these bundles.

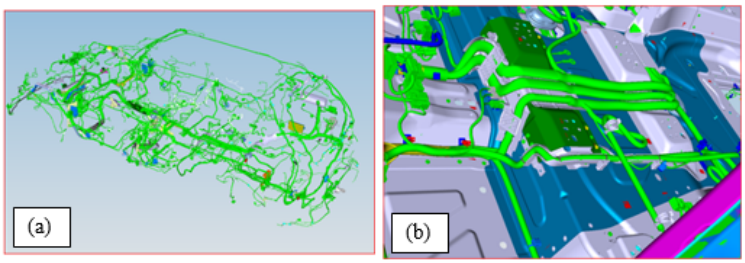

Figure 1.8 – Cable bundles in a vehicle's body.
All the harness in (a) and bundles and mixture of fixture in (b).
(Adapted from: [**44**])

Since the aerospace industry is always aiming to use lighter materials, power and signal cable harnesses are often 10% of the mass, but they could be as much as 30% of the total mass of a spacecraft. Despite being rarely considered in the design phases of a spacecraft, aerospace cables have a more appreciable effect on the dynamics of the structure, especially as the number of the electronic components onboard increases both in quantity and power demand. The current standard method of modelling cable bundles as lumped masses at attachment locations is not sufficiently accurate to predict all of the structural dynamic interaction of cables or determining when this interaction is relevant. A model able to predict the effects of cable harnesses, for example, has many benefits, especially in increasing the confidence in vibration control systems [**3**].

The effects of adding light (harness-to-beam mass ratio of roughly 8%) cable bundles to a beam can be divided in two: at low frequencies, due to mass loading, the natural frequencies of the beam are slightly lower. At high frequencies, the harness increases the system modal damping ratios. Moreover, cable dynamics that strongly couple with base structure modes can result in a dramatic reduction in the system quality factors [**45**]. These effects were also observed in [**46**] and [**47**]. Some results are shown in Figure 1.9 and Figure 1.10.

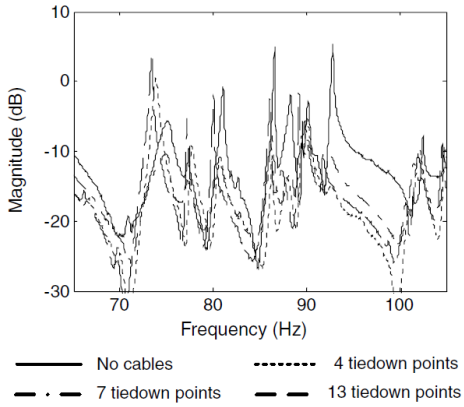

Figure 1.9 – FRF: The effects of adding cable bundles to a beam and varying the number of attachment points.

(From: [**46**] – no information on dB reference or what type of FRF were given)

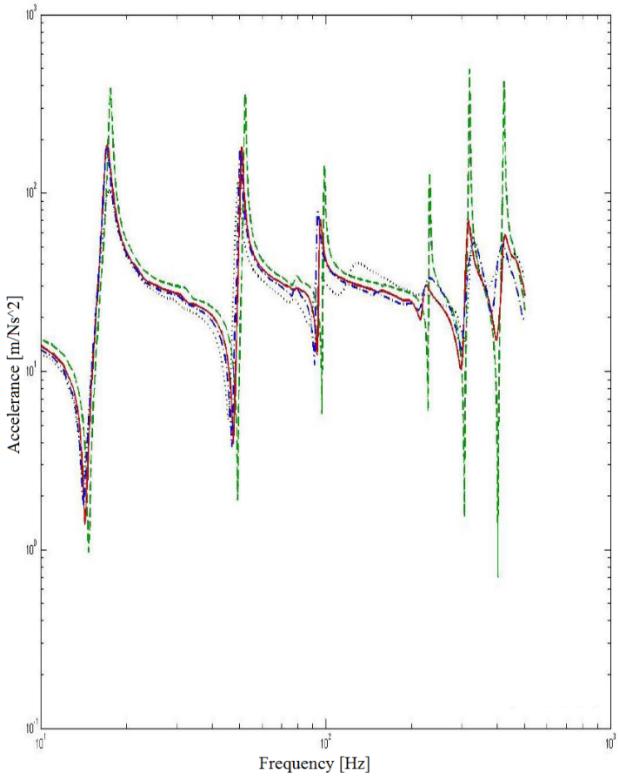

Figure 1.10 – The effects of adding cable bundles varying the number of cables.
(From: [**47**] — — is the bare beam, — 3 wires bundle, — · — · 5 wires bundle and ···· 8 wires bundle)

The previous two figures show that all cables affected the response of the host structure, beams in these cases. At low frequencies, the cable effect was dominated by mass and stiffness. At higher frequencies they had a dissipative effect, adding damping [**46**].

It was also highlighted in [**46**] that the effects on the structure due to the cables are sensitive to relatively small changes in the cable properties and therefore, it would be wiser to use the specific cable properties that will be coupled in the real structure when modelling. This research aims to get around this issue by introducing slowly varying properties and uncertainty for these attachments.

Moshrefi-Torbati et al. [**48**] analyses the effects of adding point masses to a plate and suggests a method to minimise the response of the mass-loaded plate over a frequency band optimising the positions of the masses, a passive structural vibration control. In the case where the control of excessive vibration is required, a common method would be to add heavy viscoelastic damping materials, which result in raising the costs and weight of the structure [**49**]. Another common method of control that could benefit from the use of attachments is the use of the properties of periodic structures, as they have frequency stop-bands [**48**] where travelling waves are attenuated and there is no occurrence of natural frequencies in these bands [**50**] [**51**].

1.7 Aims and objectives

The general aims of this study are to analyse the effect of variability on the dynamics of coupled structures and to develop a methodology to introduce the variability into coupled models.

One question that needs to be addressed is what the basic features of the interaction are, when connecting a beam to a plate. Whether they are dependent of the number of point connections or not; the effects of the spacing between the connection points; how uncertainties in the positioning of the attachments or in its properties affect the vibrational response of the coupled structure.

Moreover, one also needs to address the problem of variability and uncertainties in the actual structures that will be coupled together. Cable bundles can be highly uncertain and manufacturing processes in general lead to deviations from the original design. Therefore, one might be interested in analysing what governs the response of the coupled structure; if it is the uncertainties in the attached one-dimensional element, namely the cable bundles, or the uncertainties in the host structure. How do different beam to plate bending wavenumber relations change the behaviour of the coupled system? Also, if one is interested in statistical properties of the response of nominally identical systems, a fast, computationally cheap and robust numerical modelling technique needs to be used in order to keep a MC approach from being prohibitive.

Satellites are not mass produced, so one might be interested in getting the properties of the actual cable bundles that are going to be used in the manufacturing of the spacecraft. So it would be useful to have an experimental analysis that could identify the dynamical properties of cable bundles, even when they vary along the cable harnesses.

To summarise, the research questions are:

- What are the basic features of the coupled system comprising a beam and a plate?
- Does the number of attachment points and the spacing between them play a relevant role in the response of the coupled system?
- How does uncertainty in the positioning of the attachment points affect the response of the coupled system?
- How to model the uncertainties in the structures that from the coupled system, i.e. beams and plates?
- Is the response of the coupled system governed by uncertainties in one of the substructures?
- How to identify uncertain properties in cable bundles?

1.7.1 *Outline of thesis*

Chapter 1 gives an introduction to the work done, posing the problem and interests that will be investigated along with a short first literature review and contributions of this work.

In Chapter 2, a first analysis of the problem of coupling the structures is made using infinite beams and plates. A mobility method is used in order to couple the structures together and analytical solutions for the point and transfer mobilities are either taken from the literature or developed. For the case of the infinite beam with slowly varying properties, this is performed via the WKB approximation. Results for coupled system structural response comprising different beams, number of connection points, rigid or flexible links are presented.

Chapter 3 extends the analysis of the previous chapter to finite structures, using the same mobility approach. Analytical solutions for the mobilities of the one-dimensional waveguides are used, whilst a combination of FEA and perturbation method is used to introduce variability into the plate and determine its mobilities.

An experimental investigation of the effects of randomly spaced connections is made in Chapter 4, along with a validation of the mobility approach used to model the connections.

Chapter 5 deals with experimental and pseudo-experimental identification of the bending stiffness of cable bundles. It proposes a combination of the wavenumber estimation technique with Bayesian inference in order to identify the parameters. It starts by treating the cable bundle as a uniform beam and, then, it moves on to identify local bending stiffnesses along the length of the one-dimensional waveguide.

Finally, Chapter 6 brings the final remarks of the work done, summarising the conclusions and proposing future research topics.

1.7.2 *Contributions of the thesis*

This thesis proposes an improvement to the industrial state of the art approach and common practice of modelling attachments. Rather than simply using lumped masses at the connections points, a methodical approach considering the mobilities of the attachments is formulated and proposed. This allows the designer or researcher to capture the effects of the stiffness and dissipation due to the attachments. It also captures and includes the modal characteristics of the attachment, which is especially noticeable when the modal density of the attached structure is higher than that of the host plate or shell.

Rigid and flexible links in the form of elastic springs were considered for the coupling of a beam to a plate. For the rigid links, the response of the coupled system is governed by the response of the least mobile structure. However, additional modes are present in the response of the coupled system. In the presence of flexible links, the system uncouples at a frequency given by the mobilities of the attached beam, plate and elastic spring. An equivalent lumped parameter system is used in this thesis to estimate this frequency of uncoupling. The effects of uncertainties in the spacing or, in other words, the positioning of the connection points was also studied in this thesis.

In order to keep computational costs low, analytical solutions are used for the one-dimensional waveguides and a perturbation method applied to an FE model for the finite plates. This is used for the uncertain structures. The analytical solutions for the one-dimensional waveguides are found through the WKB approximation, which allows to calculate the changes in phase and amplitude of the waves propagating through a slowly varying field. For the uncertain plate, the perturbation method avoids the reanalysis of the eigenproblem, lowering the computational costs but maintaining the accuracy when the variations are small.

The approach formulated by Fabro [**2**] in finding input mobilities for spatially varying finite beams and rods is applied to the case of an infinite Euler-Bernoulli beam. Expressions for the input and transfer mobilities for the infinite beam were subsequently derived in this thesis. Moreover, a generalised expression for the input and transfer mobilities for a finite Euler-Bernoulli beam using the WKB approximation was derived, extending Fabro's approach.

Also, in order to support the basis for the spatial variability of material properties, a novel approach is introduced and implemented. It combines the estimation of the flexural wavenumbers in a one-dimensional wave bearing structure with Bayesian parameter identification. In particular, it was developed in order to find the bending stiffness of cable bundles, even if the bending stiffness is given by a random field. This could also be extended in principle to determine the properties of different structures, such as corroded pipes, for example.

Chapter 2 The coupling of infinite structures using mobilities

This chapter presents a formulation for the modelling of structures connected through a finite number of points. The structures of interest are thin infinite plates and infinite beams. Firstly, homogeneous Euler-Bernoulli beams are considered and then beams with slowly varying spatial properties are introduced. A mobility approach was chosen for the coupling of the structures and the method is described in the first section of the chapter. Expressions for the input and transfer mobilities are required to calculate the response of the coupled system. In order to describe the one-dimensional waveguides with slowly varying properties, the Wentzel–Kramers–Brillouin (WKB) approximation is used. This allows one to find the changes in phase and amplitude of the waves propagating in the structure and, therefore, to find the required expressions for the mobilities. The slowly varying properties are treated as strongly correlated random fields and are described using the Karhunen–Loève (KL) expansion.

In order to reduce computational costs, it was chosen to focus on analytical solutions for the expressions, which reflects in the choice of the covariance function used in the KL expansion. The connection points are firstly modelled as rigid links, i.e., the same displacement in the plate and the beam at the connected points, and then as flexible connections in the form of translational elastic springs only. The excitation loads are considered to be acting on the plate, but the method could also be applied if the loads were applied on the one-dimensional waveguides (beams, rods, etc.).

Results comprising different beam-to-plate flexural wavenumbers, different spacing between the connections, random spacing between the connections, different spring stiffnesses and different slowly varying beams are presented. For convenience, the Young's modulus was chosen to be the slowly varying property, but the approach can be expanded for any other of the mechanical and geometrical properties or even multiple properties.

2.1 A mobility method

A mechanical response quantity, named mobility, is a particular form of a scaled dynamic frequency response of a mechanical system. Mobility is defined as a function of frequency to be the ratio of velocity to force. In a three-dimensional system, one can measure (or estimate) the translational velocity in the three coordinate directions, X, Y, and Z, and one can also measure the rotational response. Mobility is in general a complex function in the frequency domain [**52**].

$$Y(\beta,\beta)(i\omega) = \left.\frac{V(i\omega)_x}{F(i\omega)_x}\right|_{point\beta} \tag{2.1}$$

where the subscripts in the above denote the direction of the excitation or response and ω is the circular frequency.

One can find the driving point (also known as input or point) mobility, when the velocity and force are in the same direction and at the same point, Equation (2.1).

$$Y(\beta,\beta)_{xy}(i\omega) = \left.\frac{V(i\omega)_y}{F(i\omega)_x}\right|_{point\beta} \tag{2.2}$$

Whereas the cross mobility is defined when one measures the force and velocity in different directions, Equation (2.2).

$$Y(\alpha,\beta)(i\omega) = \frac{V(i\omega)_x|_{point\beta}}{F(i\omega)_x|_{point\alpha}} \tag{2.3}$$

Finally, one has the transfer mobility, when one considers the velocity and force at different points, Equation (2.3).

Mobility (or impedance) methods are a useful and straightforward tool to analyse linear mechanical systems under periodic, transient or random loads. It can be used for describing the behaviour of simple lumped parameters or more elaborate systems, in the form of a mobility matrix [**53**]. This method was chosen due to the existence of analytical solutions for the mobilities of both infinite and finite structures. This kind of approach was developed in order to be able to consider the dynamic behaviour, in the frequency domain, of both the source and receiver of the vibration and then predict a coupled system performance in a manner analogous to what electrical engineers use for circuit analysis [**52**]. It is important to note that shear deformation and rotary inertia are neglected in the work presented here and that linear models are assumed throughout this thesis. Likewise, at the point beam to plate connection, there is only coupling through the transverse out-of-plane deflections. In the case of the later cable to plate models, it is assumed that the cable is represented by a low stiffness linear beam, with no contact other than the discrete attachment points.

2.2 The Wentzel-Kramers-Brillouin approximation to estimate point and transfer mobilities of infinite beams

Infinite structures were the first to be analysed, because they can represent the general behaviour of finite structures, but have simpler expressions. At higher frequencies, finite structures also tend to the behaviour of an infinite structure. Moreover, the frequency-averaged response of a finite structure also tends to that of an infinite structure [**52**] [**54**] [**55**]. The mobilities for the homogeneous infinite

beam and infinite plate are given in Appendix A, whilst the WKB approximation is used to derive the input and transfer mobility of an infinite Euler-Bernoulli beam possessing slowly varying properties.

This method (WKB) was initially developed in order to solve the Schrödinger equation in quantum mechanics. It is named after Wentzel, Kramers and Brillouin and it is used for finding suitable modifications of plane-wave solutions for propagation in slowly varying media when compared to the wavelength [**2**] [**41**]. The fundamental assumption of this formulation is that the properties of the waveguide along the propagation axis vary slowly enough and do not lead to reflections due to local changes or that they can be neglected, even if the net change is large [**2**] [**56**]. It also retains the interpretation of positive-going and negative-going travelling waves, which allows one to use a wave approach that is similar to the one of homogeneous waveguides and it also allows the inclusion of random fields to treat the random variability [**2**].

If the travelling wave reaches a local cut-off, or cut-on, region, the WKB approximation fails. Those are known as turning points and they lead to internal reflection, when the main assumption of the method breaks down [**2**].

2.2.1 *The WKB approximation applied to rods*

In order to become familiar with the WKB approximation, the method was applied to wave propagation in a finite rod by Fabro [**2**] and is applied again here to find the mobilities of an infinite rod. Consider a rod with slowly varying Young's modulus along its propagation length, such that there are no reflections of the propagating wave due to local changes in the impedance or that they can be neglected. The governing equation of a rod is then given by:

$$\frac{\partial^2 u(x,t)}{\partial t^2} - c_l^2(x)\frac{\partial^2 u(x,t)}{\partial x^2} = 0 \tag{2.4}$$

where $u(x,t)$ is the axial displacement and $c_l(x) = \sqrt{\frac{E(x)}{\rho}}$ is the local phase velocity at position x.

Assuming a harmonic response in the form of $u(x,t) = U(x)e^{i\omega t}$ and defining a local wavenumber $k_l(x) = \omega/c_l(x)$, it is possible to write:

$$\frac{d^2 U(x)}{dx^2} + k_L^2(x)U(x) = 0 \tag{2.5}$$

Introducing the *eikonal* function:

$$S(x) = \ln \widetilde{U}(x) - i\theta(x) \tag{2.6}$$

$$U(x) = e^{S(x)} = \widetilde{U}(x)e^{-i\theta(x)} \tag{2.7}$$

where $\widetilde{U}(x)$ is the local amplitude at point x and $\theta(x)$ is equivalent to the change in phase.

Then, rewriting Equation (2.5) with Equation (2.7):

$$\frac{d^2\widetilde{U}(x)e^{-i\theta(x)}}{dx^2} + k_l^2(x)\widetilde{U}(x)e^{-i\theta(x)} = 0 \tag{2.8}$$

$$-2\mathrm{i}e^{-i\theta(x)}\frac{d\widetilde{U}(x)}{dx}\frac{\partial\theta(x)}{\partial x} + e^{-i\theta(x)}\frac{d^2\widetilde{U}(x)}{dx^2} + \widetilde{U}(x)\left(-e^{-i\theta(x)}\left(\frac{d\theta(x)}{dx}\right)^2 - ie^{-i\theta(x)}\frac{d^2\theta(x)}{dx^2}\right) + k_l^2(x)\widetilde{U}(x)e^{-i\theta(x)} = 0 \tag{2.9}$$

Dividing Equation (2.9) by $e^{-i\theta(x)}$:

$$-2\mathrm{i}\frac{d\widetilde{U}(x)}{dx}\frac{d\theta(x)}{dx} + \frac{d^2\widetilde{U}(x)}{dx^2} + \widetilde{U}(x)\left[-\left(\frac{d\theta(x)}{dx}\right)^2 - i\frac{d^2\theta(x)}{dx^2}\right] + k_l^2(x)\widetilde{U}(x) = 0 \tag{2.10}$$

Therefore, both the real and imaginary parts of Equation (2.10) have to be equal to zero:

$$\frac{d^2\widetilde{U}(x)}{dx^2} - \widetilde{U}(x)\left[\frac{d\theta(x)}{dx}\right]^2 + k_l^2(x)\widetilde{U}(x) = 0 \tag{2.11}$$

$$-2\frac{d\widetilde{U}(x)}{dx}\frac{d\theta(x)}{dx} - \widetilde{U}(x)\frac{d^2\theta(x)}{dx^2} = 0 \tag{2.12}$$

Dividing Equation (2.11) by $k_l^2(x)\widetilde{U}(x)$:

$$\frac{1}{k_l^2(x)\widetilde{U}(x)}\frac{d^2\widetilde{U}(x)}{dx^2} - \frac{1}{k_l^2(x)}\left[\frac{d\theta(x)}{dx}\right]^2 + 1 = 0 \tag{2.13}$$

Then, ignoring the term of second order, $\frac{1}{k_l^2(x)\widetilde{U}(x)}\frac{d^2\widetilde{U}(x)}{dx^2}$:

$$\theta(x) = \int k_l(x)dx \tag{2.14}$$

Using Equation (2.14) to rewrite Equation (2.12):

$$-2k_l(x)\frac{d\widetilde{U}(x)}{dx} - \widetilde{U}(x)\frac{dk_l(x)}{dx} = 0 \tag{2.15}$$

which, by direct integration, has solutions in the form of:

$$\widetilde{U}(x) = \frac{C}{\sqrt{k_l(x)}} \tag{2.16}$$

where C is an arbitrary constant.

Hence:

$$U(x) = \frac{C_1}{\sqrt{k_l(x)}}e^{-i\int_{x_o}^{x} k_l(x)dx} + \frac{C_2}{\sqrt{k_l(x)}}e^{i\int_{x_o}^{x} k_l(x)dx} \tag{2.17}$$

$$U(x) = C_1 e^{-i\int_{x_o}^{x} k_l(x)dx - \frac{1}{2}\ln k_L(x)} + C_2 e^{i\int_{x_o}^{x} k_l(x)dx - \frac{1}{2}\ln k_L(x)} \tag{2.18}$$

The term $\frac{1}{k_l^2(x)\widetilde{U}(x)}\frac{d^2\widetilde{U}(x)}{dx^2}$ represents the contribution given by the reflections and neglecting them to derive Eq. (2.14) is equivalent to say:

$$\left|\frac{1}{k_l^2(x)\widetilde{U}(x)}\frac{d^2\widetilde{U}(x)}{dx^2}\right| \ll 1 \tag{2.19}$$

If $\widetilde{U}(x) = \frac{C}{\sqrt{k_l(x)}}$, it is possible to rewrite Eq. (2.19) as:

$$\left|\frac{3\frac{d}{dx}k_l^2(x) - 2k_l(x)\frac{d^2}{dx^2}k_l(x)}{4k_l^4(x)}\right| \ll 1 \tag{2.20}$$

Assuming that $k_l(x)$ is locally linear implies that $\frac{d^2}{dx^2}k_l(x) \approx 0$, the WKB approximation holds if:

$$\left|\frac{3\frac{d}{dx}k_l^2(x)}{4k_l^4(x)}\right| = \sqrt{\frac{3}{4}}\left|\frac{\frac{d}{dx}k_l(x)}{k_l^2(x)}\right| \ll 1 \rightarrow \boxed{\frac{1}{k_l^2(x)}\left|\frac{d}{dx}k_l(x)\right| \ll 1} \tag{2.21}$$

The boxed equations mark the contribution presented by this thesis in terms of using the WKB approximation.

Equation (2.21) is equivalent to the expression mostly found in the literature [**2**] [**57**]:

$$\frac{1}{k_l(x)}\left|\frac{d}{dx}\ln k_l(x)\right| \ll 1 \tag{2.22}$$

Once $U(x)$ is known, it is possible to find the mobility of the rod with slowly varying properties. When excited by an harmonic load F, Figure 2.1, this excitation creates a positive going wave a_2^+ and a negative going wave a_1^-. Using the force-deformation relationship for a rod excited by a harmonic load, one can find the internal forces related to those waves:

$$P^+ = EA(L_1)\frac{dU^+(x)}{\mathrm{d}x} \tag{2.23}$$

$$P^- = EA(L_1)\frac{dU^-(x)}{\mathrm{d}x} \tag{2.24}$$

where, $U^{\pm}(x) = C_1 e^{\pm i\int_{x_o}^{x} k_L(x)dx - \frac{1}{2}\ln k_L(x)}$.

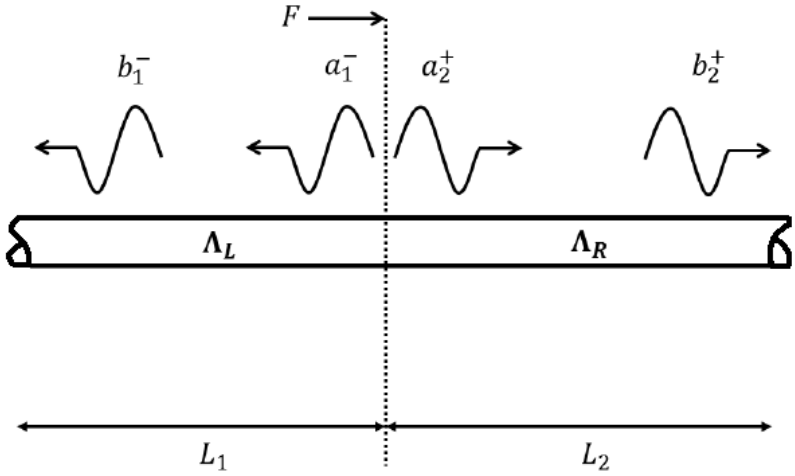

Figure 2.1 – Infinite rod under a point harmonic excitation and the propagating waves. (adapted from: [**2**])

$$\frac{dU^+(x)}{\mathrm{d}x} = \left[-k_l(x)\left(i + \frac{1}{2}\frac{1}{k_l^2(x)}\frac{dk_l(x)}{dx}\right)\right]U^+(x) \tag{2.25}$$

$$\frac{dU^-(x)}{\mathrm{d}x} = \left[k_l(x)\left(i + \frac{1}{2}\frac{1}{k_l^2(x)}\frac{dk_l(x)}{dx}\right)\right]U^-(x) \tag{2.26}$$

The WKB assumptions require that the spatial derivative $\frac{1}{k_l^2(x)}\frac{dk_l(x)}{dx}$ is small. Therefore, the terms that involve $\frac{1}{k_l^2(x)}\frac{dk_l(x)}{dx}$ are neglected and the internal forces can be expressed as [**2**] [**57**] [**58**]:

$$P^+ = -ik_l(x)EA(x)U^+(x) \tag{2.27}$$

$$P^- = ik_l(x)EA(x)U^-(x) \tag{2.28}$$

Equilibrium and continuity of displacement lead to:

$$F = -2P^+ = -2P^- \tag{2.29}$$

Then, the amplitudes a_2^+ and a_1^- can be found by:

$$a_2^+ = a_1^- = a = -\frac{iF}{2k_l(0)EA(0)} \tag{2.30}$$

and mobility can be written as:

$$Y = \frac{i\omega}{F} a_i \tag{2.31}$$

where a_i is the amplitude of the incident wave at a given point.

So, for the input mobility:

$$Y = \frac{\omega}{2k_l(0)EA(0)} \tag{2.32}$$

Equation (2.32) is analogous to the solution of the homogenous rod.

For a transfer mobility between points at $x = 0$ and $x = L_2$, where the amplitude of the incident wave is b_2^+, it is possible to relate the amplitudes of the waves by:

$$b_2^+ = \Lambda_R a_2^+ = e^{-i\theta_R + \gamma_R} a_2^+ \tag{2.33}$$

where Λ_R is the propagation element, $\theta_R = \int_0^{L_2} k_l(x)dx$ and $\gamma_R = \frac{1}{2}\ln\frac{k_l(0)}{k_l(L_2)}$ are the phase and amplitude changes of the propagating wave, respectively.

It is then possible to write the transfer mobility as:

$$Y = \frac{i\omega}{F} a_i = \frac{i\omega}{F} b_2^+ = \frac{i\omega}{F} \Lambda_R a_2^+ \tag{2.34}$$

$$Y = \sqrt{\frac{k_l(0)}{k_l(L_2)}} \frac{\omega e^{-i\int_0^{L_2} k_l(x)dx}}{2k_l(0)EA(0)} \tag{2.35}$$

Equation (2.35) can be reduced to Equation (2.32) if $L_2 = 0$, which would be the input mobility. Moreover, if the rod is homogenous, one can write $k_l(x) = k_l$ and $EA(x) = EA$, so Equation (2.35) simplifies to the exact solution of the homogenous rod, that can be found in [**53**]:

$$Y = \frac{\omega}{2k_l EA} e^{-ik_l x} \tag{2.36}$$

2.2.2 *The WKB approximation applied to beams*

After the simpler case of the rod, used for the introduction to the WKB approximation, it is easier to understand and apply the method to an inhomogeneous beam with slowly varying properties as presented in the work published by Pierce [**41**] and Fabro [**2**]. In the work found in the literature the change in phase and amplitude are found by considering an energy conservation relation, as no energy should be lost from a propagating wave. This thesis uses a direct derivation from the equation of motion to obtain the same expressions for the changes in phase and amplitude. It also uses free wave propagation, as in Fabro [**2**], but applied to an infinite one-dimensional waveguide. Starting from:

$$\frac{\partial^2}{\partial x}\left(EI(x)\frac{\partial^2 w(x,t)}{\partial x^2}\right) + \rho A(x)\frac{\partial^2 w(x,t)}{\partial t^2} = 0 \tag{2.37}$$

Assuming again a harmonic response and a similar *eikonal*:

$$w(x,t) = W(x)e^{i\omega t} \tag{2.38}$$

$$\frac{d^2}{dx}\left(EI(x)\frac{d^2 W(x)}{dx^2}\right) - \omega^2 \rho A(x) W(x) = 0 \tag{2.39}$$

$$S(x) = \ln \widetilde{W}(x) - i\theta(x) \tag{2.40}$$

$$W(x) = e^{S(x)} = \widetilde{W}(x)e^{-i\theta(x)} \tag{2.41}$$

Rewriting Equation (2.39) with Equation (2.41):

$$\frac{d^2}{dx}\left(EI(x)\frac{\partial^2 \widetilde{W}(x)e^{-i\theta(x)}}{\partial x^2}\right) - \omega^2 \rho A(x)\widetilde{W}(x)e^{-i\theta(x)} = 0 \tag{2.42}$$

It is possible then to calculate the derivatives. In a process similar to the case of the rod, one can divide the expressions by $e^{-i\theta(x)}$ and consider that both the real and imaginary parts have to be equal to zero.

The approximation for the real part, considering only the lowest order terms and dividing them by $\omega^2\rho A(x)\widetilde{W}(x)$, is given by:

$$-1+\frac{EI(x)}{\omega^2\rho A(x)}\left[\frac{d\theta(x)}{dx}\right]^4=0 \tag{2.43}$$

Therefore:

$$\theta(x)=\int\left[\frac{\rho A(x)}{EI(x)}\right]^{\frac{1}{4}}\sqrt{\omega}dx\ \equiv\int k_b(x)dx \tag{2.44}$$

Similarly, using a first order approximation, the imaginary part is given by:

$$2\widetilde{W}(x)\frac{dEI(x)}{dx}\left[\frac{d\theta(x)}{dx}\right]^3+4EI(x)\frac{d\widetilde{W}(x)}{dx}\left[\frac{d\theta(x)}{dx}\right]^3+6EI(x)\widetilde{W}(x)\left[\frac{d\theta(x)}{dx}\right]^2\frac{d^2\theta(x)}{dx^2}=0 \tag{2.45}$$

Equation (2.45) has a solution in the form of:

$$\widetilde{W}(x)=\frac{C}{EI(x)^{\frac{1}{8}}\rho A(x)^{\frac{3}{8}}} \tag{2.46}$$

which matches the solution found in [**41**] through an energetic method. Then the total beam response is given by:

$$W(x)=\ EI(x)^{-\frac{1}{8}}\rho A(x)^{-\frac{3}{8}}\left[C_1e^{-i\int_{x_0}^{x}k_b(x)dx}+C_{1N}e^{-\int_{x_0}^{x}k_b(x)dx}+C_2e^{i\int_{x_0}^{x}k_b(x)dx}+C_{2N}e^{\int_{x_0}^{x}k_b(x)dx}\right. \tag{2.47}$$

In terms of the validity of the WKB assumption, analogous to the case of the rod, the absolute value of the terms neglected to find Eq. (2.43) must be much smaller than 1:

$$\frac{1}{|\omega^2 \rho A(x)\widetilde{W}(x)|}\Big|-6EI'(x)\widetilde{W}'(x)k_b^2(x) - \widetilde{W}(x)k_b^2(x)EI''(x) - 6EI(x)k_b^2(x)\widetilde{W}''(x) + EI''(x)\widetilde{W}''(x) - 6\widetilde{W}(x)EI'(x)k_b(x)k_b'(x) - 12EI(x)\widetilde{W}'(x)k_b(x)k_b'(x) - 3EI(x)\widetilde{W}(x)k_b^{2\prime}(x) + 2EI'(x)\widetilde{W}'''(x) - 4EI(x)\widetilde{W}(x)k_b(x)k_b''(x) + EI(x)\widetilde{W}''''(x)\Big| \ll 1 \tag{2.48}$$

where the superscript $'$ denotes the derivative in x.

In a method analogous to that of the rod, it is possible to find the mobility of the inhomogeneous beam under a point harmonic load, which creates propagating waves, Figure 2.2. The load creates a positive going wave a^+ and a negative going wave a^- and also creates the near-field waves a_N^+ and a_N^-. Using the force-deformation relationship for a beam excited by a harmonic load, one can find the internal forces related to those waves:

$$F = 2EI(0)\frac{d^3\boldsymbol{W}^+(x)}{dx^3}\bigg|_{x=0} = 2EI(0)\frac{d^3\boldsymbol{W}^-(x)}{dx^3}\bigg|_{x=0} \tag{2.49}$$

where $\boldsymbol{W}^+$ and $\boldsymbol{W}^-$ are the two components, propagating and evanescent, of the right-going and left-going waves.

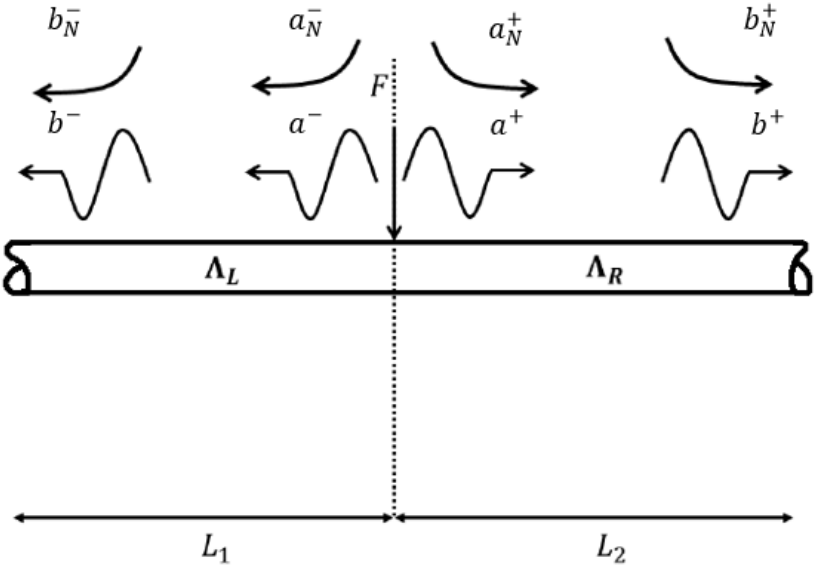

Figure 2.2 – Infinite beam under a point harmonic excitation and the propagating waves and near-field waves.
(adapted from: [**2**])

It is possible to generalise Equations (2.25) and (2.26) and under the same WKB assumptions to say that [**2**]:

$$\frac{d^n W^{\pm}(x)}{dx^n} = [\mp ik_b(x)]^n W^{\pm}(x) \tag{2.50}$$

$$\frac{d^n W_N^{\pm}(x)}{dx^n} = [\mp k_b(x)]^n W_N^{\pm}(x) \tag{2.51}$$

Therefore, Equation (2.49) can be rewrite as:

$$F = 2EI(0)[-ik_b(0)]^3 W^+ + 2EI(0)[-k_b(0)]^3 W_N^+ \tag{2.52}$$

$$F = 2EI(0)\left[ik_b^3(0)a^+ - k_b^3(0)a_N^+\right] \tag{2.53}$$

The slope boundary condition implies:

$$\frac{d\boldsymbol{W}^+(x)}{dx} = -ik_b(0)a^+ - k_b(0)a_N^+ = 0 \tag{2.54}$$

Thus:

$$a_N^+ = -ia^+ \tag{2.55}$$

$$F = 2EI(0)\left[ik_b^3(0)a^+ + ik_b^3(0)a^+\right] \tag{2.56}$$

$$F = 4iEI(0)k_b^3(0)a^+ \tag{2.57}$$

Then, the amplitude of the waves are given by:

$$a^+ = a^- = \frac{-iF}{4EI(0)k_b^3(0)} \tag{2.58}$$

$$a_N^+ = a_N^- = \frac{-F}{4EI(0)k_b^3(0)} \tag{2.59}$$

So, for the input mobility:

$$Y = \frac{i\omega}{F}(a^+ + a_N^+) = \frac{i\omega}{F}\frac{-F}{4EI(0)k_b^3(0)}(i+1) \tag{2.60}$$

$$\boxed{Y = \frac{\omega(1-i)}{4EI(0)k_b^3(0)}} \tag{2.61}$$

which is also analogous to the solution of the homogeneous beam and it only requires the local properties and free wavenumber.

In order to find the transfer mobility between the points at $x = 0$ and $x = L_2$, one can relate the amplitude of the incident waves $\boldsymbol{b}^+$ using the propagation matrix $\boldsymbol{\Lambda_R}$, as follows:

$$\boldsymbol{b}^+ = \boldsymbol{\Lambda_R}\boldsymbol{a}^+ \tag{2.62}$$

$$\begin{Bmatrix} b^+ \\ b_N^+ \end{Bmatrix} = \begin{bmatrix} e^{-i\theta_R+\gamma_R} & 0 \\ 0 & e^{-\theta_R+\gamma_R} \end{bmatrix} \begin{Bmatrix} a^+ \\ a_N^+ \end{Bmatrix} \tag{2.63}$$

Therefore:

$$Y = \frac{i\omega}{F}(b^+ + b_N^+) = \frac{\omega}{4EI(0)k_b^3(0)}(e^{-i\theta_R+\gamma_R} - ie^{-\theta_R+\gamma_R}) \tag{2.64}$$

where $\theta_R = \int_0^{L_2} k_b(x)dx$ and $\gamma_R = \ln\frac{\widetilde{W}(L_2)}{\widetilde{W}(0)}$ are now the changes in phase and amplitude of the bending waves, respectively.

The transfer mobility can be then written as:

$$Y = \frac{\omega}{4EI(0)k_B^3(0)}\left[e^{-i\int_0^{L_2} k_b(x)dx + \ln\frac{\widetilde{W}(L_2)}{\widetilde{W}(0)}} - ie^{-\int_0^{L_2} k_b(x)dx + \ln\frac{\widetilde{W}(L_2)}{\widetilde{W}(0)}}\right] \tag{2.65}$$

$$Y = \frac{\widetilde{W}(L_2)}{\widetilde{W}(0)}\frac{\omega}{4EI(0)k_b^3(0)}\left[e^{-i\int_0^{L_2} k_b(x)dx} - ie^{-\int_0^{L_2} k_b(x)dx}\right] \tag{2.66}$$

Again, Equation (2.66) reduces to that of the input mobility when $L_2 = 0$ and, if the beam is homogeneous, $k_b(x) = k_b$ and $EI(x) = EI$, it simplifies to Equation (A.8).

2.3 Using mobilities to couple an infinite beam to an infinite plate

The previous section focused on finding the input and transfer mobilities of inhomogeneous beams with slowly varying properties. The mobility of the homogeneous beams and plates are readily found in the literature and are summarised in Appendix A. For the homogeneous beam [**53**] $Y_b(\alpha,\beta)$ is the transfer mobility of an infinite beam between points α and β and is given by $Y_b(\alpha,\beta) = \frac{-\omega}{4EIk_b{}^3}\left(ie^{-k_b r} - e^{-ik_b r}\right)$, ω is the angular frequency, E is the Young's modulus, I is the second moment of area about the neutral axis, whilst $k_b = \left[\frac{\rho A}{EI}\right]^{\frac{1}{4}}\sqrt{\omega}$ is the bending wavenumber of the beam and r is the distance between the points. The input mobility is obtained when $r = 0$. Whereas the transfer mobility of the infinite homogenous plate is [**53**] $Y_p(\alpha,\beta) = \begin{cases} \frac{\omega}{8Bk_p^2}\left[H_0^{(2)}(k_p r) - \frac{2i}{\pi}K_0(k_p r)\right], & \alpha \neq \beta \\ \frac{1}{8\sqrt{Bm}}, & \alpha = \beta \end{cases}$,where $H_i^{(2)}$is an i[th] order Hankel function of the second kind, K_i is an i[th] order modified Bessel function of the second kind, $k_p = \sqrt[4]{\frac{m}{B}}\sqrt{\omega}$ is the flexural wavenumber in the plate, ω is the circular frequency and r is the distance between points α and β in the plate.

Once the input and transfer mobilities are known, it is possible to couple the structures using the continuity and equilibrium conditions expressed in terms of the mobility matrices. For simplicity, an external harmonic point force is applied to the plate at one of the attachments. In addition, the numbers of points of interest in the plate and in the beam are the same as are the attachment points. Firstly, rigid links are considered and then flexible connections in the form of elastic transverse springs are used as links. The analysis neglects the offset of the beam neutral axis from the plate,

with both beam and plate vibrating in flexure only. Figure 2.3 shows schematically the coupled system.

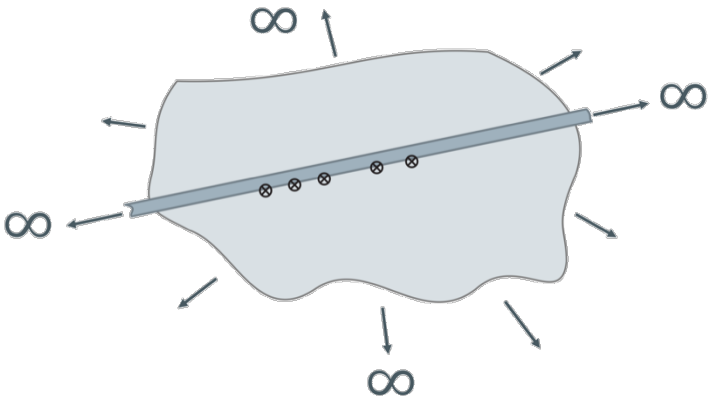

Figure 2.3 – Diagram of an infinite beam attached to an infinite plate through 5 discrete point connections.

2.3.1 *Rigid links*

As rigid links, the velocity continuity implies that at the attachment points:

$$\dot{\boldsymbol{w}}^p = \dot{\boldsymbol{w}}^b \tag{2.67}$$

The separate beam and plate velocities can be calculated using:

$$\dot{\boldsymbol{w}}^p = \boldsymbol{Y}^p(\boldsymbol{f} - \boldsymbol{f}') \tag{2.68}$$

$$\dot{\boldsymbol{w}}^b = \boldsymbol{Y}^b\boldsymbol{f}' \tag{2.69}$$

where $\boldsymbol{f}$ is the vector of external forces applied to the plate and $\boldsymbol{f}'$ is the vector of transmitted internal forces between the beam and plate. A certain proportion of this applied force $\boldsymbol{f}$ is transmitted from the plate to the beam through the rigid link connecting them and, as a reaction, the beam applies the same transmitted force, $\boldsymbol{f}'$, on the plate in the opposite direction (c.f. Newton's third law of motion).

From the previous set of equations, one can determine the vector for the transmitted forces:

$$\boldsymbol{f}' = \left(\boldsymbol{Y}^p + \boldsymbol{Y}^b\right)^{-1}\boldsymbol{Y}^p\boldsymbol{f} \tag{2.70}$$

The previous equations consider that the number of points of interest are the attachment points connecting the beam to the plate. If one is interested, for instance, in the response at points on the

plate that are not connected to the beam, some transformation matrices are required to match the matrix dimensions and ensure that the relationships agree with the required transfer mobilities. Appendix B shows how reciprocity holds in the case where the load is applied at a connection point on the beam.

In the particular case of one single point of connection, a simple system with equivalent lump parameters can be used to give some insight on the general trends of the coupled system. For one single attachment point, only the input point mobilities of the beam and plate are required and from Equations (A.8) and (A.11) one can notice that the input mobility of the beam is analogous to a mass, $m_{eq}^{b} = 4\rho A/k_b$, and a frequency-dependent damper, $c_{eq}^{b} = 4\omega\rho A/k_b$, with their respective mobilities in series, whilst the input mobility of the plate is analogous to a damper, $c_{eq}^{p} = 8\sqrt{\frac{EI\rho h}{1-\nu^2}}$ [**43**] [**59**]. The point mobility of the coupled system is the combination of the mobilities of the beam and plate in parallel:

$$Y = \left[\left(Y^{c_{eq}^{b}} + Y^{m_{eq}^{b}}\right)^{-1} + Y^{c_{eq}^{p}\,-1}\right]^{-1} = \left[\left(\frac{1}{c_{eq}^{b}} + \frac{1}{i\omega m_{eq}^{b}}\right)^{-1} + \frac{1}{c_{eq}^{p}}^{-1}\right]^{-1} \tag{2.71}$$

2.3.2 *Flexible connections*

In order to get a more realistic model of the attachments, it is reasonable to consider some flexibility in the connections. It is possible for example to achieve that using linear elastic translational springs to connect the beam and plate. At each attachment point one will find a force that is produced by the spring on the connected beam and plate. These forces, at end of the spring, are equal in magnitude, but opposite in direction. The force on the beam, for example, is by Hooke's Law equal to the spring stiffness, κ, multiplied by the extension of the spring, which is given by the difference in the displacement of its ends. This extension is the difference in the displacement of the beam and the displacement of the plate at the respective attachment points. Figure 2.4 shows the forces on a system comprising an infinite plate connected to an infinite beam through a finite number of spring connections. In this diagram, the external forced is applied at the second of the N connection points but in principle could be at any alternative location, which would require suitable reformulation.

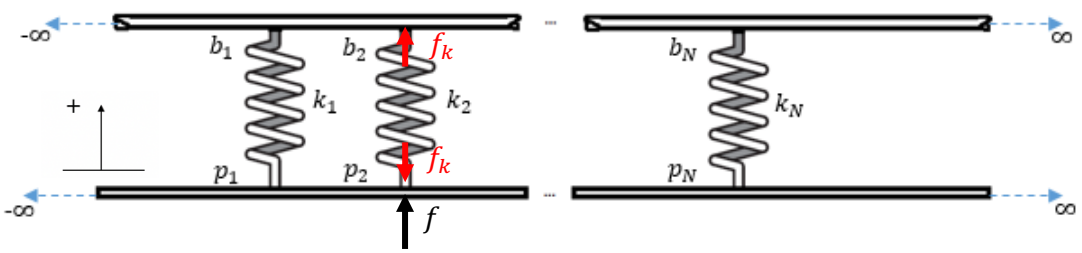

Figure 2.4 – Infinite beam attached to infinite plate through an arbitrary and finite number *N* of elastic spring attachments.

In a case analogous to the rigid link, it is possible to write:

$$\dot{\boldsymbol{w}}^p = \boldsymbol{Y}^p \boldsymbol{f} - \boldsymbol{Y}^p \boldsymbol{f}_{\boldsymbol{K}} \tag{2.72}$$

$$\dot{\boldsymbol{w}}^b = \boldsymbol{Y}^b \boldsymbol{f}_{\boldsymbol{K}} \tag{2.73}$$

where $\boldsymbol{f}$ is the vector of external forces applied to the plate and $\boldsymbol{f}_K$ is the vector of the internal forces due to the compression of the springs.

Rewriting for $\boldsymbol{f}_K$:

$$\boldsymbol{f}_{\boldsymbol{K}} = \boldsymbol{Y}^{b^{-1}} \dot{\boldsymbol{w}}^b \tag{2.74}$$

By Hooke's Law, one can evaluate the spring forces in terms of the displacement (or velocities) at the two ends, i.e.

$$\boldsymbol{f}_{\boldsymbol{K}} = \frac{1}{i\omega} \boldsymbol{\kappa} \left(\dot{\boldsymbol{w}}^p - \dot{\boldsymbol{w}}^b \right) \tag{2.75}$$

relating the spring forces to the vectors representing the velocities at the spring attachment points on the two components. $\boldsymbol{\kappa}$ is a diagonal matrix containing the stiffness of the connecting springs.

Then:

$$\boldsymbol{Y}^{b^{-1}} \dot{\boldsymbol{w}}^b = \frac{1}{i\omega} \boldsymbol{\kappa} \left(\dot{\boldsymbol{w}}^p - \dot{\boldsymbol{w}}^b \right) \tag{2.76}$$

$$\frac{1}{i\omega} \boldsymbol{\kappa} \dot{\boldsymbol{w}}^p = \boldsymbol{Y}^{b^{-1}} \dot{\boldsymbol{w}}^b + \frac{1}{i\omega} \boldsymbol{\kappa} \dot{\boldsymbol{w}}^b \tag{2.77}$$

$$\frac{1}{i\omega} \boldsymbol{\kappa} \dot{\boldsymbol{w}}^p - \left(\boldsymbol{Y}^{b^{-1}} + \frac{1}{i\omega} \boldsymbol{\kappa} \right) \dot{\boldsymbol{w}}^b = \boldsymbol{0} \tag{2.78}$$

Also:

$$\dot{\boldsymbol{w}}^p = \boldsymbol{Y}^p \boldsymbol{f} - \boldsymbol{Y}^p \boldsymbol{Y}^{b\,-1} \dot{\boldsymbol{w}}^b \tag{2.79}$$

$$\dot{\boldsymbol{w}}^p + \boldsymbol{Y}^p \boldsymbol{Y}^{b\,-1} \dot{\boldsymbol{w}}^b = \boldsymbol{Y}^p \boldsymbol{f} \tag{2.80}$$

$$\begin{cases} \dot{\boldsymbol{w}}^p + \boldsymbol{Y}^p \boldsymbol{Y}^{b\,-1} \dot{\boldsymbol{w}}^b = \boldsymbol{Y}^p \boldsymbol{f} \\ \frac{1}{i\omega} \boldsymbol{\kappa} \dot{\boldsymbol{w}}^p - \left(\boldsymbol{Y}^{b\,-1} + \frac{1}{i\omega} \boldsymbol{\kappa} \right) \dot{\boldsymbol{w}}^b = \boldsymbol{0} \end{cases} \tag{2.81}$$

In a matrix form:

$$\begin{bmatrix} \boldsymbol{I} & \boldsymbol{Y}^p \boldsymbol{Y}^{b\,-1} \\ \frac{1}{i\omega} \boldsymbol{\kappa} & -\left(\boldsymbol{Y}^{b\,-1} + \frac{1}{i\omega} \boldsymbol{\kappa} \right) \end{bmatrix} \begin{Bmatrix} \dot{\boldsymbol{w}}^p \\ \dot{\boldsymbol{w}}^b \end{Bmatrix} = \begin{Bmatrix} \boldsymbol{Y}^p \boldsymbol{f} \\ \boldsymbol{0} \end{Bmatrix} \tag{2.82}$$

Rearranging for the velocity vectors in terms of the subsystems and spring mobilities in conjuction with the applied force vector, one has:

$$\begin{Bmatrix} \dot{\boldsymbol{w}}^p \\ \dot{\boldsymbol{w}}^b \end{Bmatrix} = \begin{bmatrix} \boldsymbol{I} & \boldsymbol{Y}^p \boldsymbol{Y}^{b\,-1} \\ \frac{1}{i\omega} \boldsymbol{\kappa} & -\left(\boldsymbol{Y}^{b\,-1} + \frac{1}{i\omega} \boldsymbol{\kappa} \right) \end{bmatrix}^{-1} \begin{Bmatrix} \boldsymbol{Y}^p \boldsymbol{f} \\ \boldsymbol{0} \end{Bmatrix} \tag{2.83}$$

Once again, in the particular case of one single point of connection, a simple system with equivalent lump parameters can be used to give some insight on the general trends of the coupled system. The input mobility of the beam is analogous to a mass, $m_{eq}^b = 4\rho A / k_b$, and a frequency-dependent damper, $c_{eq}^b = 4\omega\rho A / k_b$, with their respective mobilities in series, whilst the input mobility of the plate is analogous to a damper, $c_{eq}^p = 8\sqrt{\frac{EI\rho h}{1-\nu^2}}$ [**43**] [**59**]. The system now has a spring connecting the elements and the mobility of the coupled system is the combination of the mobilities of the beam+spring and plate in parallel:

$$Y = \left[\left(Y_K + Y^{c_{eq}^b} + Y^{m_{eq}^b} \right)^{-1} + Y^{c_{eq}^p\,-1} \right]^{-1} = \left[\left(\frac{i\omega}{\kappa} \frac{1}{c_{eq}^b} + \frac{1}{i\omega m_{eq}^b} \right)^{-1} + \frac{1}{c_{eq}^p}^{-1} \right]^{-1} \tag{2.84}$$

Simulations showing the frequency response behaviour of the coupled systems will be shown later in sections 2.5 and 2.6. Inclusion of damping in either the beam, plate or springs is by introduction of a hysteretic loss factor. Also, the above analysis is general in that it is not required that the springs are equally spaced or have the same stiffness or damping values.

2.4 The description of random fields using the Karhunen-Loève expansion formulation

Since manufacturing processes usually lead to variability of the mechanical properties of the actual structure when compared to the original design [**2**], these properties, or even loads, are sometimes treated as random fields [**60**]. The latter is a useful representation, which can be modelled using spatially correlated variability [**2**] [**61**] [**62**] [**63**] [**64**]. One can describe a random field $H(x,q)$ as a set of random variables described by a continuous parameter $x \in D$, where D describes the system geometry or domain [**2**] [**63**]. For a given position x_0, $H(x_0,q)$ is a random variable, whilst for an outcome q, $H(x,q)$ is a realisation of the random field [**2**]. Also, when a random field $H(x,q)$ can be completely defined by its mean value and auto covariance function or autocorrelation for a zero-mean process, it is said to be of second order [**2**]. The covariance function is given by [**2**]:

$$Cov(x_1,x_2) = \langle [H(x_1,q)-\mu][H(x_2,q)-\mu] \rangle \tag{2.85}$$

Another parameter of interest in a random field is the correlation length, which gives a measure at the spatial variability of the random field. A larger correlation length leads to a smooth spatial variability [**2**]. Figure 2.5 illustrates the correlation length for a one-dimensional case. Material and geometrical uncertainty often exhibits spatial correlation, which qualifies it as being a candidate on which to use the theory of random fields to model this spatially distributed variability [**40**].

Figure 2.5 – General effect of the correlation length on the spatial distribution of a random field.
(From: [**2**])

It is possible to use a set of deterministic functions with random coefficients to represent a random field in the form of a series expansion [**2**] [**60**] [**63**] [**64**] [**65**]. A usual technique for representing a sample function of a random field is the Karhunen-Loève (KL) expansion [**66**],which is a Fourier-like series [**2**].

The KL expansion comprises a series of deterministic eigenfunctions weighted by uncorrelated random variables [**2**]. Moreover, the KL is said to be bi-orthogonal, which means that not only the deterministic basis functions are orthogonal, but also the corresponding random coefficients are orthogonal (uncorrelated) [**60**]. This property allows for the optimal encapsulation of the random field into uncorrelated random variables [**60**] [**62**]. In addition, the KL is the optimal expansion in the sense that the mean-square error associated by approximating the infinite series with a finite number of terms is minimized [**66**] [**67**] [**68**] and it is especially suited for strongly correlated random fields, i.e. slowly varying [**2**].

A Gaussian distribution has the maximum entropy when the process has a finite mean μ and a finite variance σ^2 [**69**] and therefore it is the one that best describe the knowledge about the process. Hence it will be used to describe the random field, but the KL expansion could be applied to other distributions, when others are more adequate. A Gaussian homogenous random field $H(x,q)$ with a finite, symmetric and positive definite covariance function $Cov(x_1,x_2)$ on a bounded domain D can be expressed as [**2**] [**60**] [**62**] [**70**]:

$$H(x,q) = H_0(x) + \sum_{j=1}^{\infty} \sqrt{\lambda_j}\xi_j(q)f_j(x) \tag{2.86}$$

where $\xi_j(q)$ are Gaussian uncorrelated random variables, λ_j and $f_j(x)$ are the eigenvalues and eigenfunctions of the Fredholm integral equation of the second kind given by:

$$\int_D Cov(x_1,x_2)f_j(x_1) = \lambda_j f_j(x_2) \tag{2.87}$$

Usually, Equation (2.87) can only be solved numerically, discretizing the covariance function, using some collocation method and finding the eigenvalues and eigenfunctions [**2**] [**63**]. It is possible to find analytical solutions for some families of correlation functions though, for instance the one-dimensional exponentially decaying autocorrelation function [**2**]:

$$Cov(x_1,x_2) = e^{-\frac{|x_1-x_2|}{b_L}} \tag{2.88}$$

where b_L is the correlation length in the interval $0 \leq x \leq L$ and L is the length of the domain.

Then, the KL expansion for the zero-mean random field, truncating the series at N_{kl} terms, can be written as [**2**] [**62**]:

$$H(x,q) = \sum_{j=1}^{N_{kl}} \left\{ \alpha_j \xi_{1j}(q) \sin\left[w_{1j}\left(x - \frac{L}{2}\right)\right] + \beta_j \xi_{2j}(q) \cos\left[w_{2j}\left(x - \frac{L}{2}\right)\right] \right\} \tag{2.89}$$

where ξ_{1j} and ξ_{2j} are Gaussian zero-mean, unit standard-deviation, independent random variables with the properties [**2**]:

$$\langle \xi_{1j} \rangle = \langle \xi_{1i} \rangle = 0;\ \langle \xi_{1i} \xi_{2j} \rangle = 0;\ \langle \xi_{1i} \xi_{1j} \rangle = \delta_{ij} \tag{2.90}$$

where $\delta_{ij} = 1$ for $i = j$ and $\delta_{ij} = 0$ for $i \neq j$.

$$\alpha_j = \sqrt{\frac{\lambda_{1j}}{\frac{L}{2} - \frac{\sin(w_{1j}L)}{2w_{1j}}}} \tag{2.91}$$

$$\beta_j = \sqrt{\frac{\lambda_{2j}}{\frac{L}{2} + \frac{\sin(w_{2j}L)}{2w_{2j}}}} \tag{2.92}$$

$$\lambda_{ij} = \frac{2c}{w_{ij}^2 + c^2} \tag{2.93}$$

$$c = \frac{1}{b_L} \tag{2.94}$$

where w_{1j} and w_{2j} are the j^{th} roots of the transcendental equations $c \tan w_1 + w_1 = 0$ and $w_2 \tan w_2 - c = 0$, respectively.

For instance, it is possible to describe the Young's modulus as a random field by the KL expansion. Assuming that the Young's modulus is given by [**2**]:

$$E(x,q) = E_0[1 + \sigma H(x,q)] \tag{2.95}$$

where E_0 is the nominal value for the Young's modulus and σ is a dispersion term to quantify the influence of $H(x,q)$ in the mean nominal value E_0.

Therefore, assuming that only the Young's modulus is varying, it is possible to rewrite Equation (2.14) for the phase change in a propagating wave in an infinite rod as:

$$\int k_l(x)dx = \omega\sqrt{\frac{\rho}{E_0}}\int\sqrt{\frac{1}{[1+\sigma H(x,q)]}}dx \tag{2.96}$$

For the case when the Young's modulus variation also has small dispersion around its nominal value, $|\sigma H(x,q)| \ll 1$, it is possible to use a first order approximation such that [**2**]:

$$\sqrt{\frac{1}{[1+\sigma H(x,q)]}} \approx 1-\frac{\sigma}{2}H(x,q) \tag{2.97}$$

Then, for propagation from $x = x_1$ to $x = x_2$, the phase change is:

$$\int_{x_1}^{x_2} k_l(x)dx \approx \ \omega\sqrt{\frac{\rho}{E_0}}\int_{x_1}^{x_2}\left[1-\frac{\sigma}{2}H(x,q)\right]dx \tag{2.98}$$

If $H(x,q)$ is given by the KL expansion in Equation (2.89), it is possible to write:

$$\int_{x_1}^{x_2} k_l(x)dx \approx \omega\sqrt{\frac{\rho}{E_0}}\left[x-\sigma\sum_{j=1}^{N_{kl}}\frac{\xi_{2j}(q)\beta_j}{w_{2j}}\sin\left(\frac{w_{2j}x}{2}\right)\right]\Bigg|_{x=x_1}^{x=x_2} \tag{2.99}$$

which can be substituted into Equation (2.35) to obtain the transfer mobility for a rod, for example, with slowly varying Young's modulus by the KL expansion.

The point mobility for a rod with slowly varying Young's modulus by the KL expansion is given by substituting Equation (2.95) in Equation (2.32):

$$Y = \frac{\omega}{2k_l(0)E(0)A} \tag{2.100}$$

$$Y = \frac{1}{2A\sqrt{\rho\left[E_0\left(1+\sigma H(x,q)\right)\right]}} \tag{2.101}$$

where $H(x,q)$ is given by Equation (2.89). A first order approximation could also be made if necessary.

A similar procedure can be applied for propagating flexural waves in a beam, also assuming small dispersion so that $|\sigma H(x,q)| \ll 1$ and that $[1+\sigma H(x,q)]^{-\frac{1}{4}} \approx 1-\frac{\sigma}{4}H(x,q)$, as in [**2**]. Therefore, one can rewrite Equation (2.44) as:

$$\int k_B(x)dx \approx \sqrt{\omega}\left(\frac{\rho A}{E_0 I}\right)^{1/4}\int\left[1-\frac{\sigma}{4}H(x,q)\right]dx \tag{2.102}$$

$$\int_{x_1}^{x_2} k_B(x)dx \approx \sqrt{\omega}\left(\frac{\rho A}{E_0 I}\right)^{\frac{1}{4}}\left[x-\frac{\sigma}{2}\sum_{j=1}^{N_{kl}}\frac{\xi_{2j}(q)\beta_j}{w_{2j}}\sin\left(\frac{w_{2j}x}{2}\right)\right]\Bigg|_{x=x_1}^{x=x_2} \tag{2.103}$$

One can also substitute Equation (2.103) in Equation (2.66) to obtain the transfer mobility of an infinite beam with slowly varying Young's modulus by the KL expansion.

The point mobility can be obtained by substituting Equation (2.95) in Equation (2.61):

$$Y = \frac{\omega(1-i)}{4IE_0[1+\sigma H(x,q)]\omega^{\frac{3}{2}}\left[\frac{\rho A}{IE_0[1+\sigma H(x,q)]}\right]^{\frac{3}{4}}} \tag{2.104}$$

$$Y = \frac{1-i}{4\sqrt{\omega}[\rho A]^{\frac{3}{4}}\left[IE_0[1+\sigma H(x,q)]\right]^{\frac{1}{4}}} \tag{2.105}$$

where $H(x,q)$ is given by Equation (2.89). A first order approximation could also be made if necessary.

Alternatively, the integrals involving $H(x,q)$ could also be solved numerically. Likewise, other geometric or material properties could have been considered instead of the Young's modulus which would produce similar formulations and expressions.

2.5 Numerical results and discussion for infinite beams connected to homogeneous plates through a single point

This section presents the results that can be obtained numerically using the models developed in the chapter. The results were obtained with codes written in Matlab. Firstly, results comprising homogeneous infinite beams and homogeneous infinite plates connected through one single point are investigated, considering rigid and flexible links. In all cases, the external harmonic force was applied on the plate at one of the attachment points.

Before the analysis of the beams with slowly varying Young's moduli, an analysis considering different homogeneous beams was made, with a beam to plate bending wavenumber ratio ranging between $\frac{k_b}{kp} = 0.35$ to $\frac{k_b}{kp} = 2.00$. For this, the plate properties were fixed and, therefore, the Young's modulus of the beam is in the range between 146 GPa and 0.137 GPa. For $\frac{k_b}{kp} = 1.00$, the Young's modulus of the beam is 2.20 GPa. The nominal properties of the beams and plates are given in Table 2.1. Damping is introduced in the form of a complex Young's modulus $E = (1 + i\eta)$, considering the loss factor η. The value used for the loss factor η was the same for both the beam and plate, but they could be different, if necessary.

Table 2.1 – Nominal properties of the modelled beams and plates.

Properties	Value
Density (kg/m^3)	7850
Plate thickness (m)	0.002
Plate Young's modulus (GPa)	200
Beam cross-sectional side – square section (m)	0.02
Poisson's ratio	0.30
Loss factor	0.001
Stiff beam to plate bending wavenumber ratio	0.35
Flexible beam to plate bending wavenumber ratio	2.00

Before moving to the actual results of the coupled systems, it is important to verify if the shear deformation can indeed be neglected. For that, it is important to know the flexural wavelengths in the beam compared to the cross-sectional dimensions. Figure 2.6 shows a diagram of the wavelengths for the stiffer beam and more flexible beam.

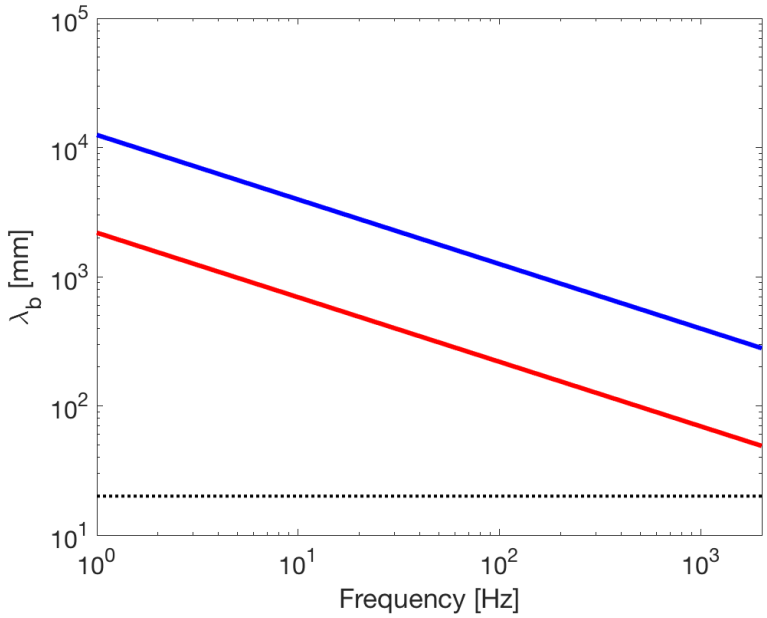

Figure 2.6 – Flexural wavelengths in the beams compared to height of the beam.

— is the stiffer beam $E = 146$ GPa, — is the more flexible beam $E = 0.137$ GPa. The cross-section of the beam is a square of side 20 mm, ·····.

The assumption that shear deformation can be neglected may not be valid over all the frequency range, as the usual criterion for that is that the wavelength should be at least six times larger than the height of the beam, but the Euler-Bernoulli beam is nevertheless used for simplicity.

2.5.1 *Results for a single connection point between an infinite plate and beam*

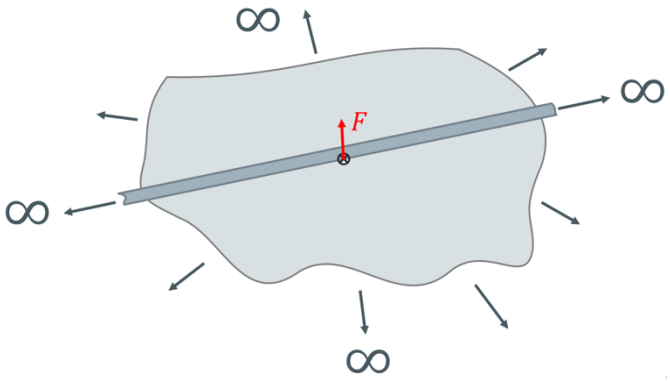

Figure 2.7 – Single point connection.

The first simulation comprises a beam coupled to a plate through a single rigid attachment. A single point harmonic force is applied to the plate at this attachment point, Figure 2.7. Three different beams were studied. Results for the point mobility are shown in Figure 2.8. It is possible from this figure to see how the coupled system tends to the behaviour of the attached beam at higher frequencies. At lower frequencies, the results are dominated by the low mobility component namely the plate.

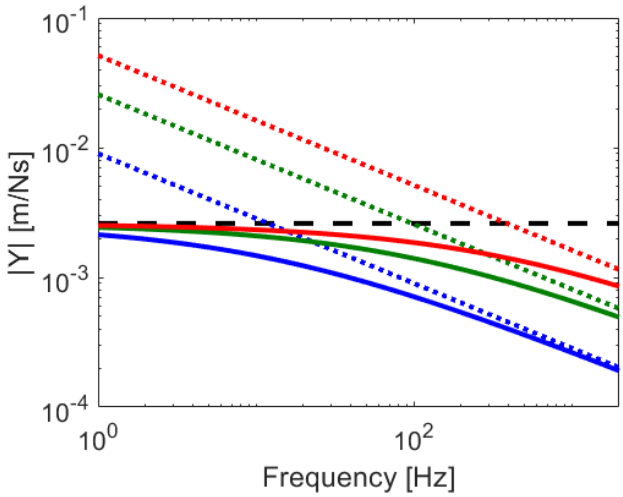

Figure 2.8 – Point mobility. Infinite beam attached to an infinite plate through one single rigid connection.

— is the coupled system $\frac{k_b}{kp} = 0.35$, — is the coupled system $\frac{k_b}{kp} = 1.00$, — is the coupled system $\frac{k_b}{kp} = 2.00$, ····, ····, ···· are respectively the beam mobilities and — — is the plate mobility.

The overall mobility response is being governed by the least mobile (lowest mobility) component.

The comparison between the input mobility using the beam and plate mobility expressions versus the representative lumped parameter system, $Y = \left[\left(Y^{c_{eq}^b} + Y^{m_{eq}^b}\right)^{-1} + Y^{c_{eq}^p}{}^{-1}\right]^{-1} = \left[\left(\frac{1}{c_{eq}^b} + \frac{1}{i\omega m_{eq}^b}\right)^{-1} + \frac{1}{c_{eq}^p}{}^{-1}\right]^{-1}$, is shown in Figure 2.9. The two approaches are in full agreement, as expected.

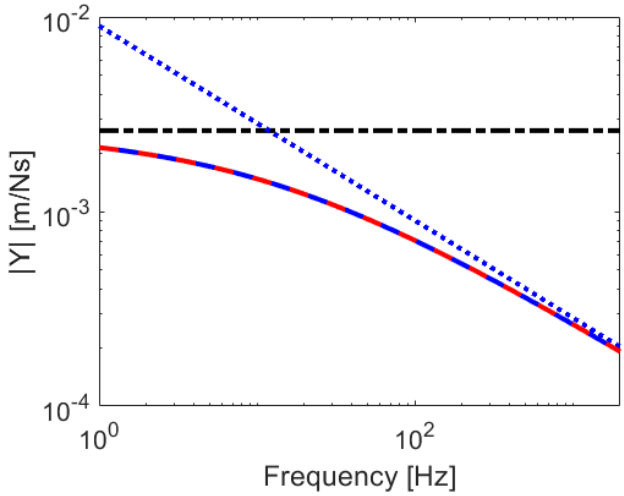

Figure 2.9 – Point mobility. Comparison between lumped parameter system and modelling.

— is the coupled system $\frac{k_b}{kp} = 0.35$, — is the equivalent lumped parameter coupled system, ···· is the mobility of the beam and — · — · is the mobility of the plate.

The response of the systems with one single connection point using the equivalent lumped parameters approach agrees well with the response calculated using the full formulation for the input

mobilities. This helps to visualise how the beam can be seen as a mass and damper in series, whilst the plate can be seen as a damper.

2.5.2 *Single elastic spring connection between beam and plate*

The second scenario still considers one single attachment with the plate being excited at the same point, but in this case a flexible link in a form of an elastic spring is considered to be the connection between the plate and beam. The same three values for beam to plate bending wavenumber ratios were analysed and three different values for the spring stiffness were considered. The results for the point mobility of the system are shown in Figure 2.10. In (a), the beam to plate bending wavenumber ratio was kept constant, whilst in (b), the spring stiffness was kept constant. These results were calculated on the host structure, namely, the plate.

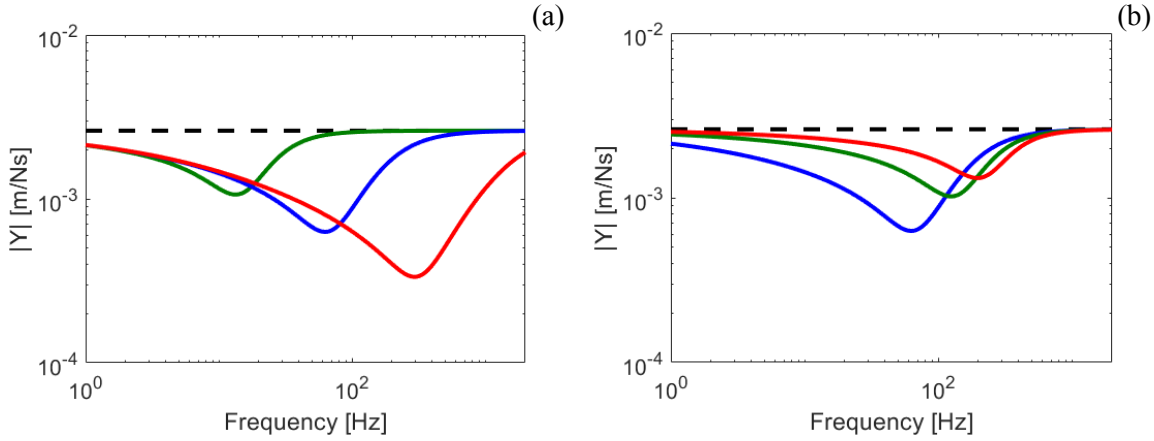

Figure 2.10 – Point mobility. Infinite beam attached to an infinite plate through one single elastic spring.

In (a), — $\frac{k_b}{kp} = 0.35$ and spring stiffness of 40 kN/m, — $\frac{k_b}{kp} = 0.35$ and spring stiffness of 400 kN/m and — $\frac{k_b}{kp} = 0.35$ and spring stiffness of 4000 kN/m. In (b), — $\frac{k_b}{kp} = 0.35$ and spring stiffness of 400 kN/m, — $\frac{k_b}{kp} = 1.00$ and spring stiffness of 400 kN/m and — $\frac{k_b}{kp} = 2.00$ and spring stiffness of 400 kN/m. — — is the plate mobility in both cases. The excitation is applied on the plate.

When an elastic spring is introduced for the connection, the coupled system has a dip in the coupled mobility response and it is governed by the mobility of the actual connection and the host structure at higher frequencies. The stiffer the link, the higher is the frequency of the minimum in the coupled mobility. The dip occurs when the absolute value of the mobility of the beam and plate in parallel matches the absolute value of the mobility of the elastic spring and plate in parallel.

The results for the input mobility of the beam are shown in Figure 2.11. Depending on the system properties, there is a frequency where the systems uncouple, and the response tends to the response of the host structure. In Figure 2.11, it is possible to see the drop of the mobility at the beam in the coupled system in the presence of an elastic spring compared to the mobility of the beam alone. This means that the motion of the beam decreases above this uncoupling frequency. This drop occurs after the uncoupling of the system, at around 70 Hz, for this particular case.

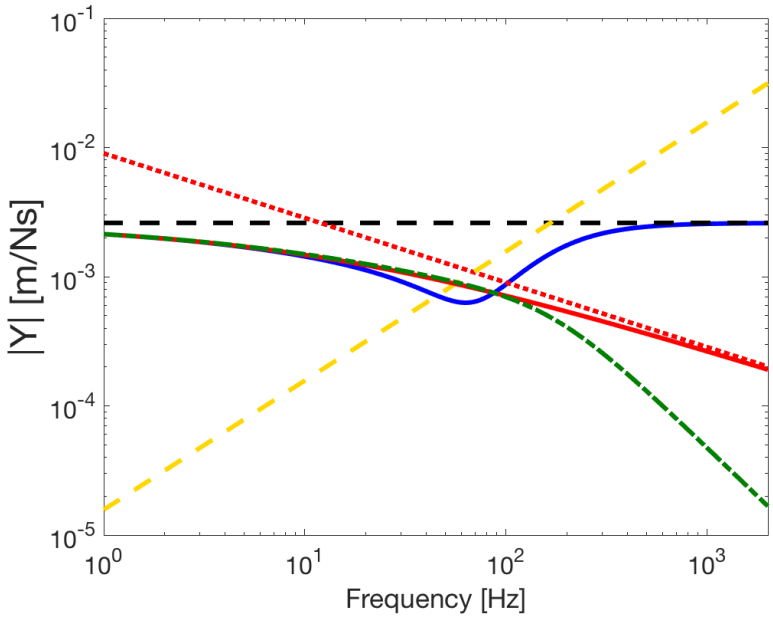

Figure 2.11 – Point mobilities. Uncoupling of the beam from the plate in the presence of an elastic spring. Excitation on the plate.

— is the response of the plate with $\frac{k_b}{kp} = 0.35$ and spring stiffness of 400 kN/m, — · — · is the response of the beam with $\frac{k_b}{kp} = 0.35$ and spring stiffness of 400 kN/m, — is $\frac{k_b}{kp} = 0.35$ and using a rigid link. — — is the plate mobility, ····· is the mobility of the beam and — — is the spring mobility.

Similarly to the case of the rigid link, a comparison between the equivalent system with lumped parameters, $Y = \left[\left(Y_K + Y^{c_{eq}^b} + Y^{m_{eq}^b}\right)^{-1} + Y^{c_{eq}^p}{}^{-1}\right]^{-1} = \left[\left(\frac{i\omega}{\kappa}\frac{1}{c_{eq}^b} + \frac{1}{i\omega m_{eq}^b}\right)^{-1} + \frac{1}{c_{eq}^p}{}^{-1}\right]^{-1}$, and the actual expressions for the mobilities are shown in Figure 2.12. Again, the response using the two modelling techniques agree.

It is possible to find some asymptotic behaviours for the different regions in the frequency spectrum, which are shown in Figure 2.13. Firstly, at lower frequencies, the response of the coupled system is given by the combination of the beam and plate alone. Then, there is a minimum of the response when the mobility of the combined plate and spring matches the mobility of the combined plate and beam and the system uncouples. At higher frequencies, the displacement of the attachment beam vanishes, i.e., its mobility drops, and the coupled system responds as the combination of the spring and host structure acting in parallel.

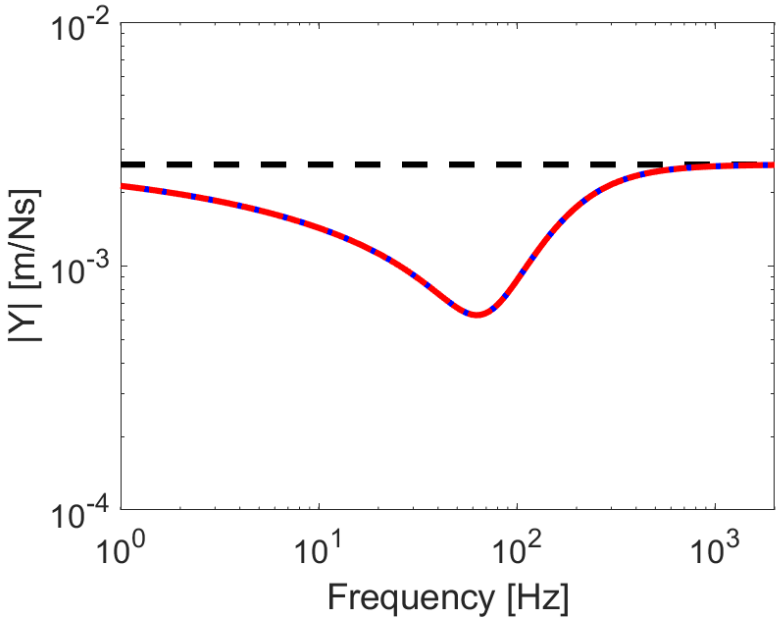

Figure 2.12 – Point mobility with elastic spring. Comparison between lumped parameter system and modelling.

— is the coupled system $\frac{k_b}{kp} = 0.35$, — · — · is the equivalent lumped parameter system and — — is the mobility of the plate. The spring stiffness is 400 kN/m. Excitation on the plate.

This equivalent lumped parameters systems are proposed in order to estimate the frequency at which the systems uncouple.

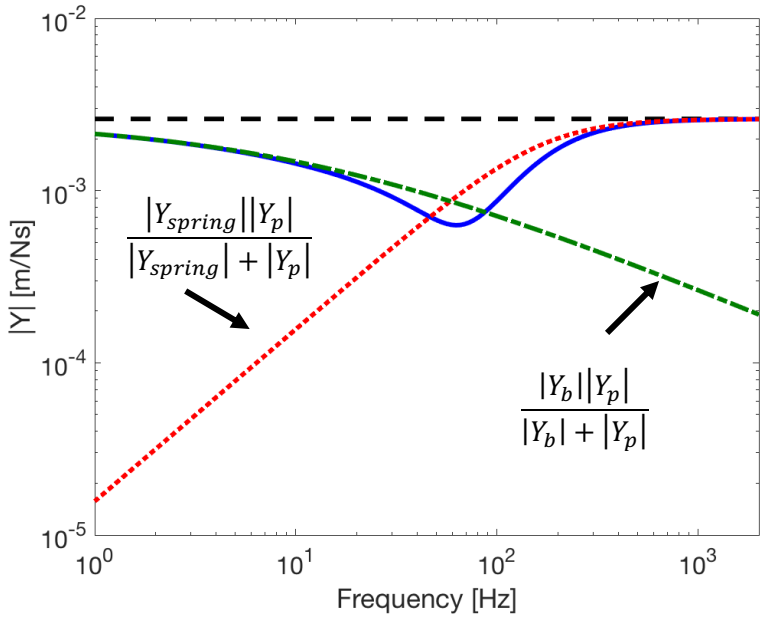

Figure 2.13 – Regions of behaviour for the coupled system with one spring attachment for the coupling

— is the coupled system $\frac{k_b}{kp} = 0.35$, — · — · is the combination of the mobilities of the spring and plate in parallel, ····· is the combination of the mobilities of the beam and plate in parallel whereas — — is the mobility of the plate. The spring stiffness is 400 kN/m. Excitation on the plate.

Above the uncoupling frequency, for the excitation applied to the plate then the displacement of the beam drops and the response of the coupled system is dominated by the spring and host structure. In contrast, below this frequency, the response of the system is dominated by the combination of the mobilities of the beam and the plate acting in parallel.

One way of estimating the frequency where the minimum of the response of the coupled system occurs is to analyse frequency by frequency when the mobilities of the two different subsystems are equal:

$$\frac{\left|Y_{spring}\right|\left|Y_p\right|}{\left|Y_{spring}\right|+\left|Y_p\right|}=\frac{|Y_b||Y_p|}{|Y_b|+\left|Y_p\right|} \tag{2.106}$$

where $\left|Y_{spring}\right|=\omega/\kappa$, which can be rewritten after some algebraic manipulation as:

$$\omega=\kappa|Y_b| \tag{2.107}$$

Therefore, if both the stiffness of the connection spring and the mobility of the attached one-dimensional waveguide are known, the frequency of the minimum can be estimated by finding the frequency ω which satisfies Equation (2.107). In the case presented in Figure 2.13, that would lead to a value of 69 Hz, whilst the actual minimum occurs at around 63 Hz.

The derivation of an expression for the uncoupling frequency using the lumped parameters properties is not easier than doing the actual numerical calculations using the mobility approach. This minimum point marks the uncoupling of the system.

2.6 Numerical results and discussion for infinite beams connected to homogeneous plates through multiple points

In this section, the results are shown through an extended simulation for a finite number of rigid links evenly spaced, then through elastic springs. After this analysis, the random spacing between the connection points is introduced. The random spacing is sampled from a uniform probability density function around the nominal value of the spacing. In all cases, the external harmonic force was applied on the plate at one of the attachment points. When multiple connections were considered, the load was applied to the central attachment. Once again, the results were obtained with codes written in Matlab.

2.6.1 *Results for multiple rigid links between a beam and a plate*

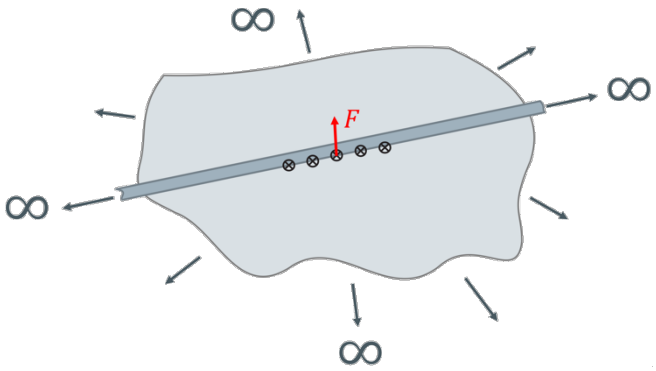

Figure 2.14 – Diagram for multiple connection points.

In this case, 5 connection points were considered. The external force is applied at the central connection point throughout this chapter.

Another point of interest to analyse is what is the effect of having a different number of attachments, but keeping the other properties, i.e. spacing and beam to plate bending wavenumber ratios constant. The results are shown in Figure 2.15, $\frac{k_b}{kp} = 0.35$, and in Figure 2.16, $\frac{k_b}{kp} = 2.00$. In both cases, the spacing is 0.1875 m and the different number of attachments are 3, 5, 7, 9, 11, 13. Since they are rigid links, the effect of the elastic springs at higher frequencies is lost and the coupled

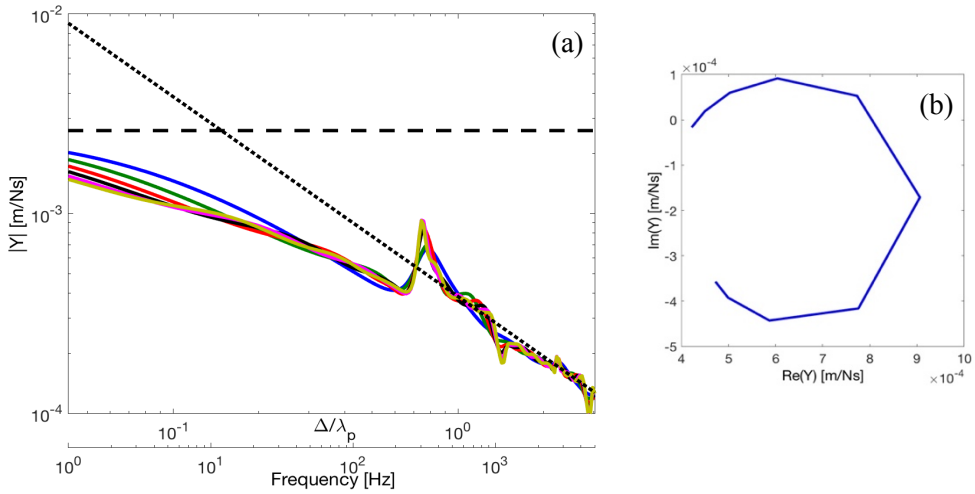

structure tend to the behaviour of the attached beam. When multiples attachments are considered, it is convenient to plot the results versus the dimensionless parameter Δ/λ, spacing Δ between the connections over bending wavelength λ. In this chapter the plate's wavelength was chosen as reference, as the plate properties are kept constant.

Figure 2.15 – The effects of having multiple rigid link attachments and an Argand plot of the coupled mobility.

$\frac{k_b}{kp} = 0.35$ and $\Delta = 0.1875$ m. In (a), the magnitude of the input mobility: — 3, — 5, — 7 — 9, — 11 and — 13 attachments. ····· is the mobility of the attached beam and — — is the mobility of the host plate. In (b), the peak around 300 Hz ($\Delta/\lambda \approx 0.8$) is plotted as the imaginary versus the real part of the coupled system input mobility.

The presence of multiple attachments allows for the presence of standing-wave-like behaviour between them, effectively creating local modes. Figure 2.15(b) shows the complex response of one of the systems plotted as the imaginary part versus real part, and a circular shape is found, which is a characteristic of a modal Nyquist response plot [**71**], confirming the modal behaviour of the coupled structure. The same happens to the peaks presented in Figure 2.16.

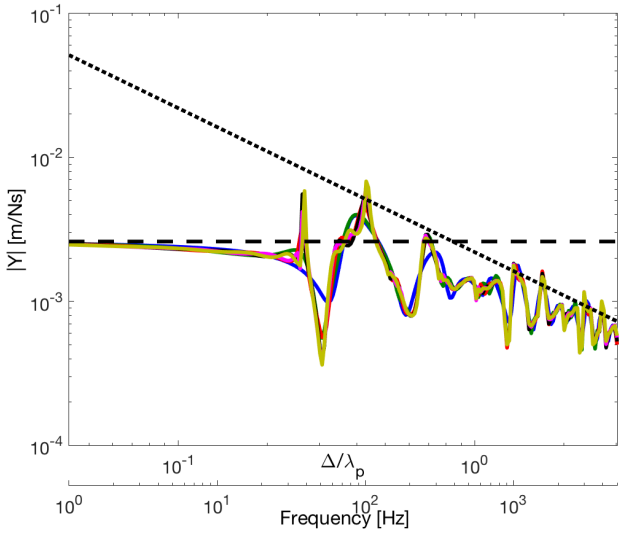

Figure 2.16 – The effect of having multiple rigid link attachments points.

Magnitude of the input mobility: — 3, — 5, — 7, — 9, — 11 and — 13 attachments. $\frac{k_b}{kp} = 2.00$ and $\Delta = 0.1875$ m. ····· is the mobility of the attached beam and — — is the mobility of the host plate.

Figure 2.17 shows the effect of the same number of attachment points, 5, but with a different regular spacing between them for each case, from 0.05 m to 1.175 m. It is possible to see that are peaks occurring in the same regions, around the same values of Δ/λ, which indicate they are the same kind of wave behaviour.

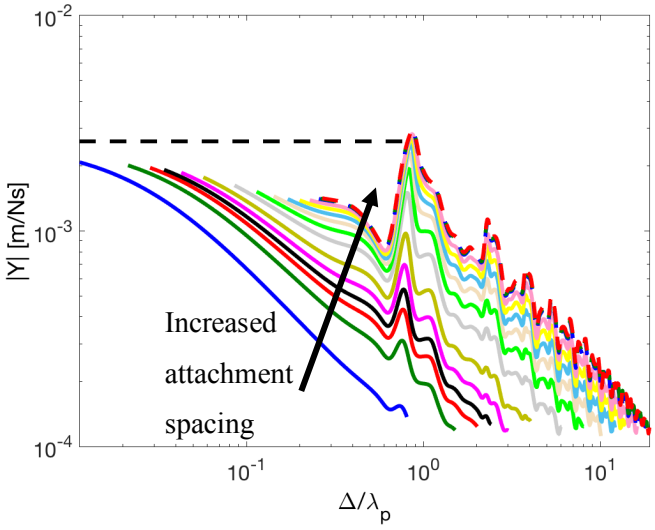

Figure 2.17 – The effect of having different attachment spacing Δ.

$\Delta = 0.5, 0.09375, 0.125, 0.15, 0.1875, 0.25, 0.375, 0.5, 0.625, 0.75, 0.875, 1.0, 1.125, 1.15, 1.175$ [m]. $\frac{k_b}{kp} = 0.35$ and — — is the input mobility of plate.

Figure 2.18(a) shows a contour plot of the real part of the velocity of the coupled system when the spacing is 0.1875 m, $\frac{k_b}{kp} = 0.35$ and $\Delta/\lambda \approx 0.8$, around the first peak. Even when the connection points are randomly spaced, Figure 2.18(b), the structure responds in a similar manner.

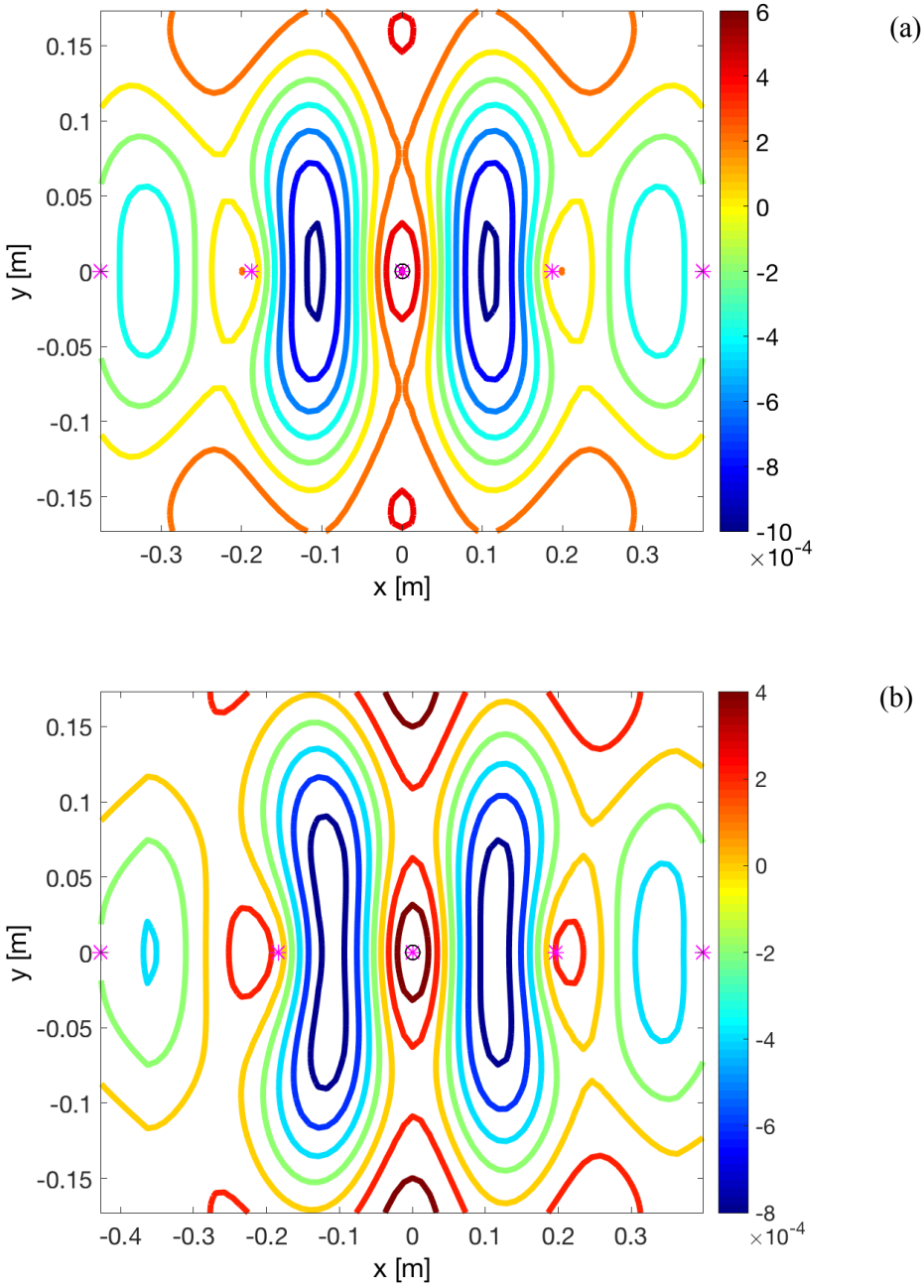

Figure 2.18 – Real part of the velocity of the coupled system.

The attachments are marked with $*$ and $\frac{k_b}{kp} = 0.35$. In (a), 5 evenly spaced attachments $\Delta = 0.1875$ m. In (b), 5 randomly spaced attachments. Load applied at the central attachment on the plate and $\Delta/\lambda_p \approx 0.8$ (or approximately 300 Hz).

Figure 2.19 shows the real part of the velocity of the connected plate and beam in cross-section cut out of the attachment region, $y = 0$ for the same peak at $\Delta/\lambda \approx 0.8$ and $\frac{k_b}{kp} = 0.35$. Figure 2.20 shows similar data, a contour plot of the real part of the velocity of the coupled system and real part

of the velocity of the connected beam and plate on a transverse cut of the connecting section, but now the beam to plate bending wavenumber ratio is 2.00. The dimensionless frequencies are; $\Delta/\lambda \approx 0.25$, $\Delta/\lambda \approx 0.40$, $\Delta/\lambda \approx 0.70$ and $\Delta/\lambda \approx 0.80$ for the more flexible beam. The spacing is equal to 0.1875 m in all cases.

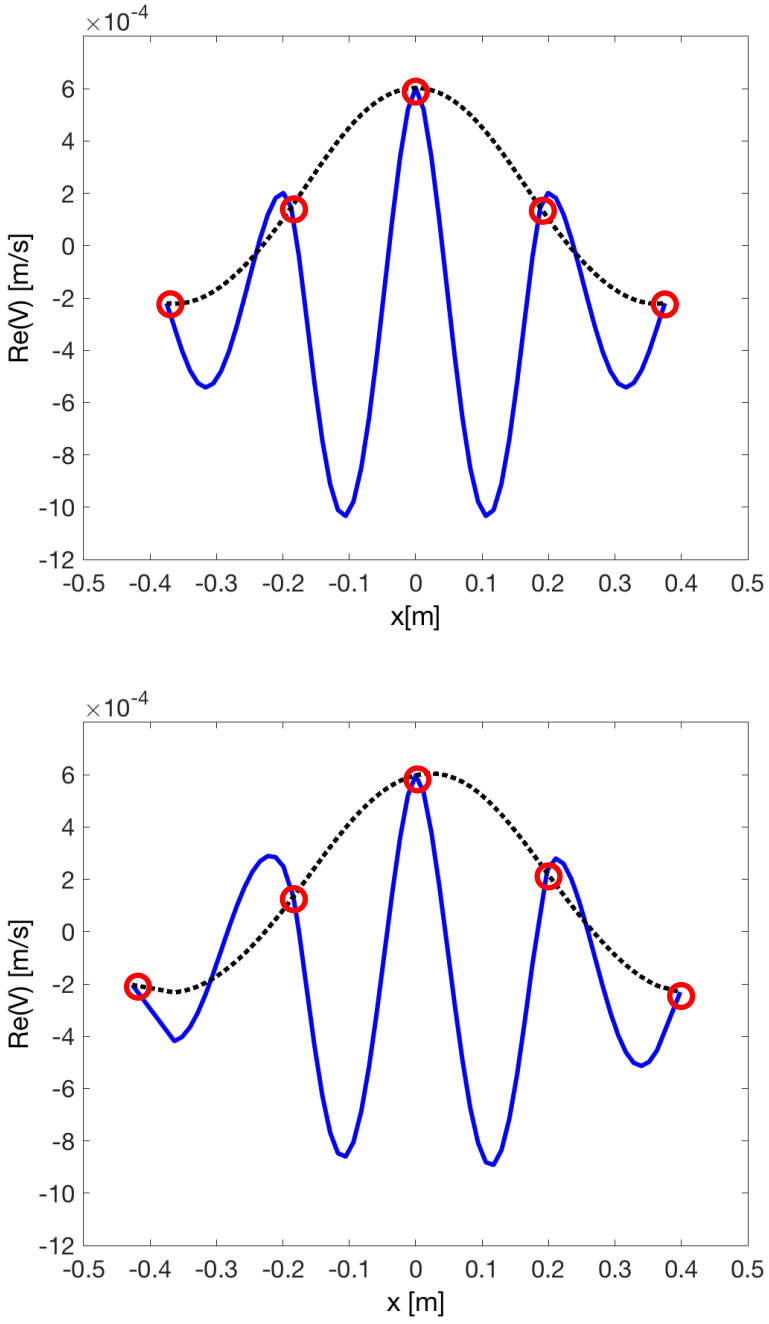

Figure 2.19 – Cross-section of the attachment region. Real part of the velocity.

— is the velocity of the plate and ····· is the velocity of the beam $\frac{k_b}{kp} = 0.35$. In (a), 5 evenly spaced attachments $\Delta = 0.1875$ m. In (b), 5 randomly spaced attachments. The connections points are marked by ○.

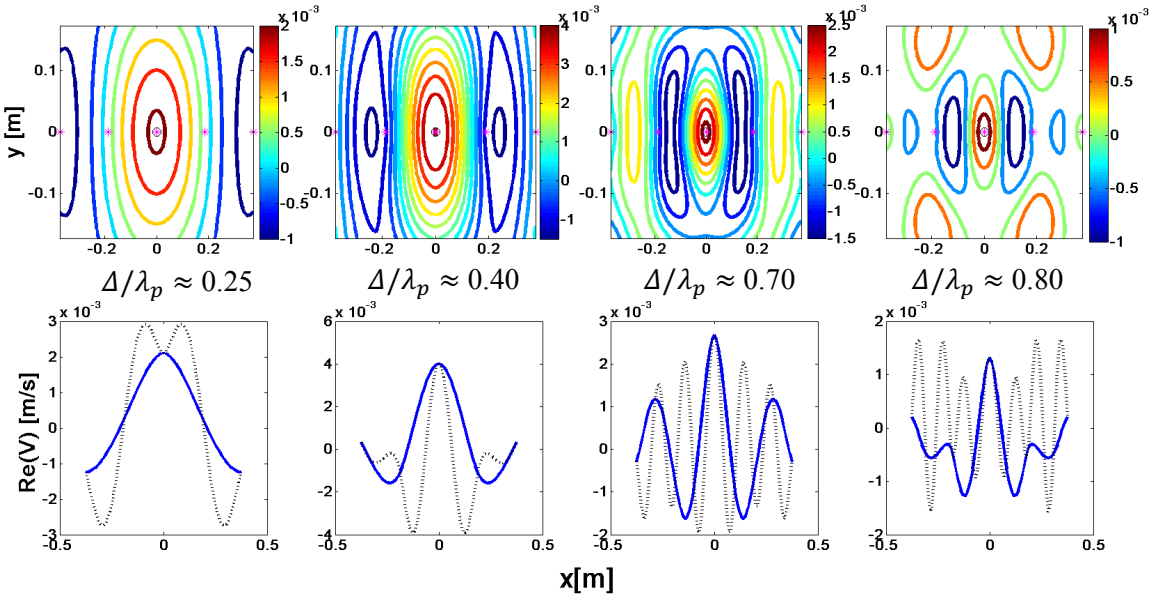

Figure 2.20 – The standing-wave-like behaviour of the coupled system at the frequency of the peaks in the coupled beam-plate mobility.

Contour plot of the real part of the velocity on top and real part of the velocity at the bottom. $\frac{k_b}{kp} = 2.00$ and ▬ is the velocity of the plate and ····· is the velocity of the beam. 5 evenly spaced attachments.

When multiple attachments points are considered, it is possible to note the presence of standing-wave-like behaviour for the coupled system. There are some amplifications of the response in a similar manner to a mode of a finite structure. It can be seen how the coupled mobility, when plotted as the imaginary part versus the real part, resembles a circle, which is the expected behaviour of the frequency response of a finite system mode [**71**]. The less stiff is the attached beam, more of the peaks in the mobility are present in the same frequency band. Moreover, they occur in the same Δ/λ_p frequency regions, indicating that they have similar shapes. The frequencies where these standing-waves occur are given by the spacing between the attachments and the beam to plate wavenumber ratio considered.

2.6.2 *Results for random properties – Uniform beam, elastic connections and five connection points*

Before advancing to the results in the presence of a beam with slowly varying properties, different parameters where allowed to vary around their nominal values, but still considering a uniform beam for the connected structures. In the following results, for each parameter, five hundred cases were calculated. The distributions from which the values were sampled are presented on a case by case basis. The beam is attached to the plate through 5 points with nominal spacing $\Delta = 375$ mm.

Firstly, the beam to plate bending wavenumber ratio was allowed to vary. The properties of the plate were kept constant, whilst the variation of the wavenumber ratio was translated into

variation of the beam's Young's modulus. The nominal values of $\frac{k_b}{kp} = 0.35$ and $\frac{k_b}{kp} = 2.00$ were considered and they varied accordingly to $\frac{k_b}{kp}_{random} = \frac{k_b}{kp}(1+\epsilon)$, where ϵ was sampled from a normal distribution, Figure 2.21(a), with mean equal to zero and standard deviation of 0.075; which, effectively, means that 95% of the samples are vary within $\pm$ 15% around the nominal value. The distribution for ϵ can be direct converted to a distribution for the beam to plate bending wavenumber ratio, Figure 2.21(b).

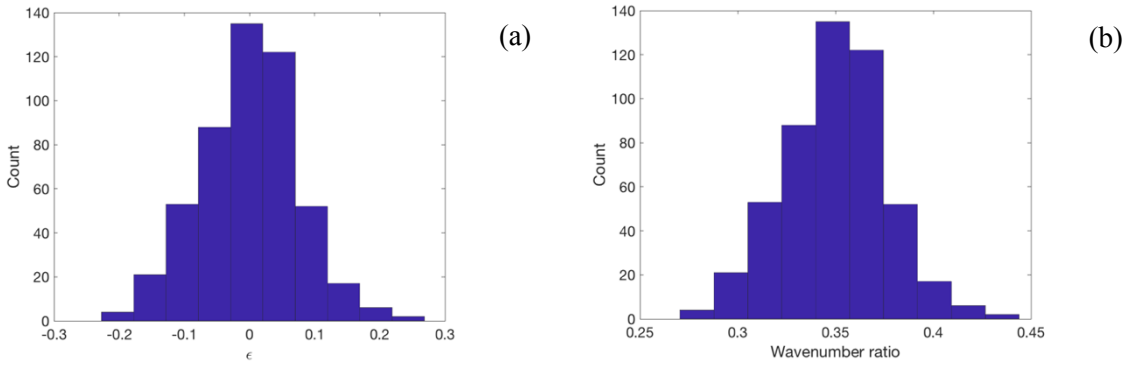

Figure 2.21 – Histograms for the uniform stiffer beam.
In (a), the histogram for ϵ. In (b), the histogram from the beam to plate bending wavenumber ratio.

From that, if all the other properties are kept constant, the different Young's modulus can be calculated by $E_{random} = \frac{1}{\frac{k_b}{kp}_{random}^4} \frac{\rho A}{I} \frac{B}{m}$, where ρ is the beam's density, A is the beam's cross-section area, I is the beam's second moment of area, B is the plate bending stiffness and m is the plate mass per unit area. This results in the following histogram for the Young's modulus, Figure 2.22, that will be used for the new uniform beam simulations.

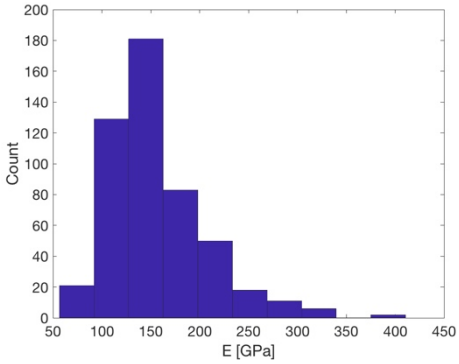

Figure 2.22 – Histogram for the uniform Young's modulus in the stiffer beam case.

The input mobilities considering these 500 different beams are shown in Figure 2.23 along with the nominal case, $\frac{k_b}{kp} = 0.35$ (Young's modulus of 146 GPa), the average of all cases, and the envelope showing the range within which 95% of the response lies. The colourmap given was normalised frequency-by-frequency in order to better show the distribution of the response. For each

frequency calculated, a kernel distribution was fitted and used to draw the colourmap. Darker colours in the colourmap represent a denser region of response, as in more different beams have the response in that region. An example of the histogram of the response and the fitted distribution is shown in Figure 2.24. The beam is connected to the plate through springs with a stiffness of 4000 kN/m.

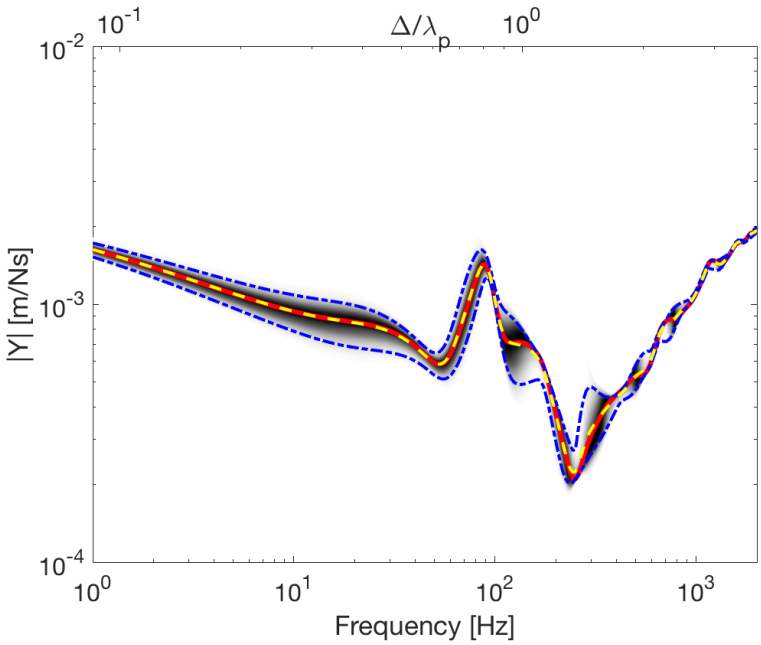

Figure 2.23 – Coupled beam-plate input mobility over a set of uniform beams. The stiffer beam case.

Nominal beam to plate bending wavenumber ratio $\frac{k_b}{kp} = 0.35$. Colourmap represents the density of the response, ▬ is the nominal case, ▬ ▬ is the mean of the different uniform beams and ▬ · ▬ is the envelope for where 95% of the response lies within. The random beam to plate bending wavenumber are in the format $\frac{k_b}{kp}(1+\epsilon)$, where ϵ was sampled from a normal distribution, with mean equal to zero and standard deviation of 0.075.

As expected, at lower frequencies, the spreading of the response around the nominal case is larger than at higher frequencies, when the systems uncouple, the response is then governed by the mobilities of the host structure and the elastic spring. The different beams also lead to some variation of the frequency where the local mode-like behaviour occurs, but they still appear in the same region of the spectrum, $\Delta/\lambda_p \approx 0.8$.

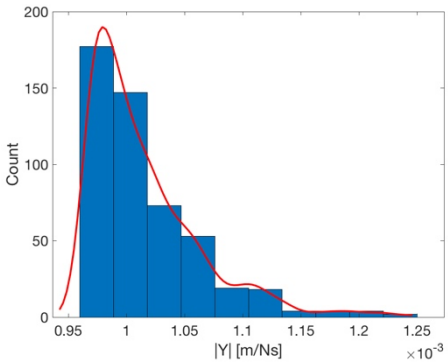

Figure 2.24 – Histogram of the response of the stiffer beams at 100 Hz and fitted distribution.

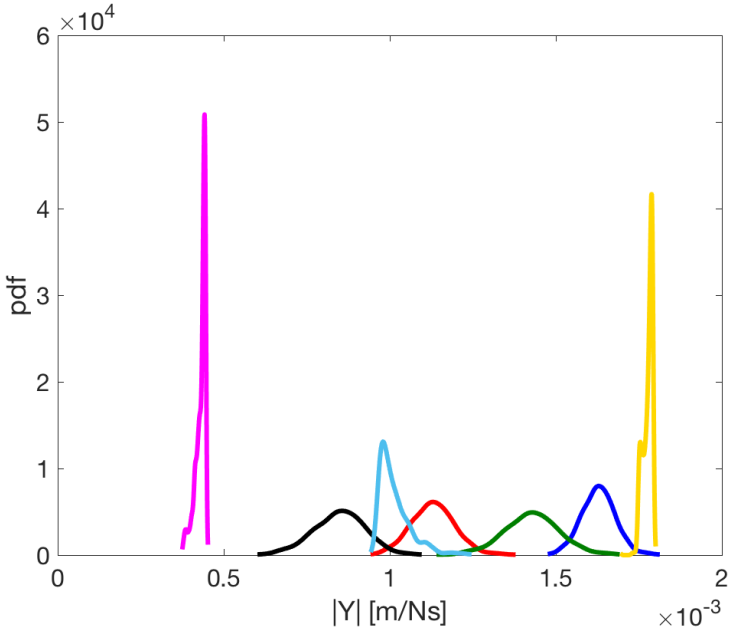

Figure 2.25 – Fitted probability density functions for the response of the coupled system at different frequencies when the stiffer beam is considered.

1 Hz, 4.5 Hz, 20 Hz, 89 Hz, 100 Hz (also shown in Figure 2.24), 397 Hz and 1770 Hz.

One can notice how the probability density functions of the response of the coupled system are narrower once the system is above the frequency at which the beam and the plate become uncoupled. Therefore, flexible connections can be used to reduce the uncertainties in the coupled structures due the variability in the attached beam. After this uncoupling the variability of the coupled system is only subject to the uncertainties in the host plate and the uncertainties in the stiffness of the connections.

This effect is also shown in Figure 2.26. Five hundred beams with uniform random Young's modulus were connected using a rigid link and then an elastic spring. In order to compare the results without the effect of the dip that changes the shape of the curves, the input mobility is plot in a dB scale referenced to each one of the nominal cases. It is clear how above the uncoupling frequency at

around 200 Hz, the spreading of the response of the system coupled through elastic springs is much smaller than that of the system coupled via rigid links.

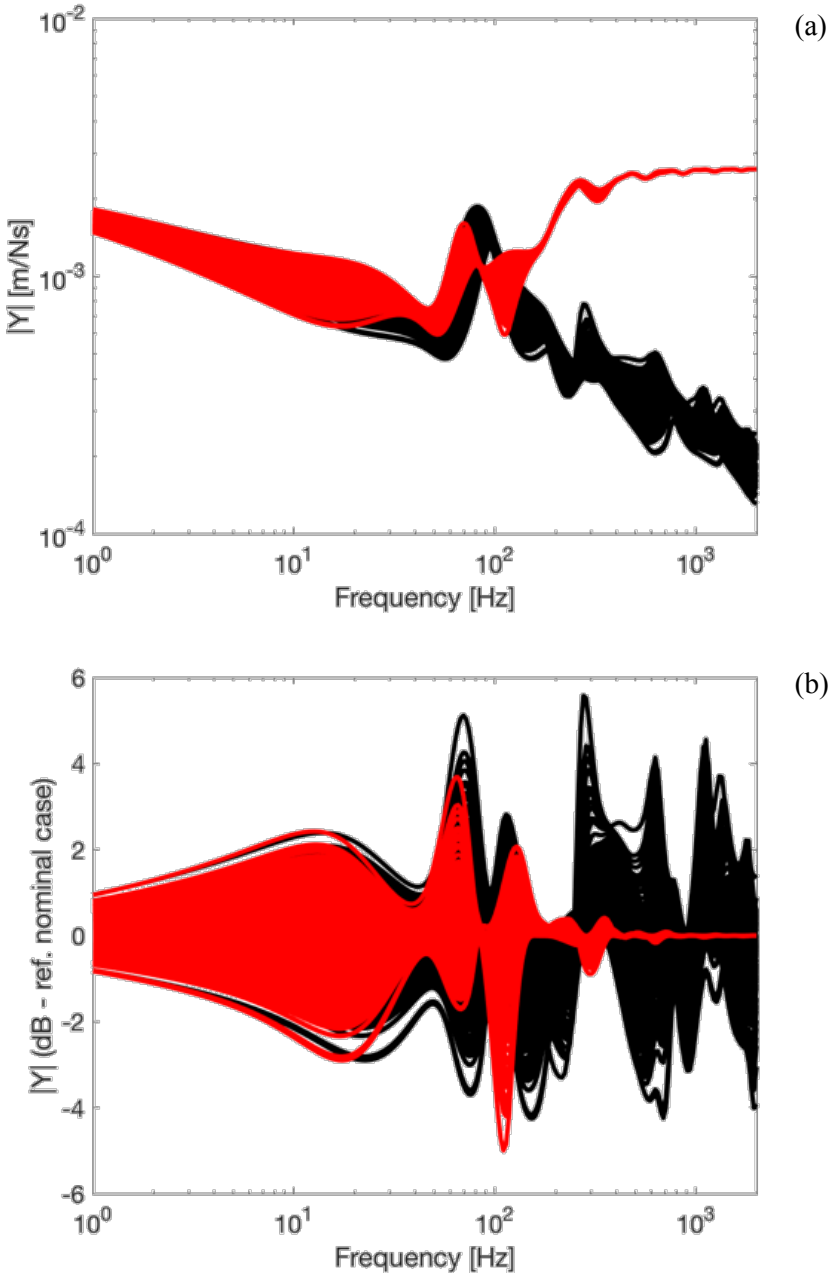

Figure 2.26 – Reduction in the uncertainties due the addition of flexible links.

Input mobility of 500 beams connected to a plate through 5 rigid links (—) and when flexible links are considered as the connections (—). In (a), the magnitude of the mobilities. In (b), the magnitude of the mobilities in a dB scale referenced to the appropriate nominal case (rigid links or spring connections). Nominal beam to plate bending wavenumber ratio $\frac{k_b}{kp} = 0.35$. Spring stiffness of 4000 kN/m. The random beam to plate bending wavenumber are in the format $\frac{k_b}{kp}(1+\epsilon)$, where ϵ was sampled from a normal distribution, with mean equal to zero and standard deviation of 0.075.

The same procedure and calculations were followed considering the more flexible beam, nominal beam to plate wavenumber ratio $\frac{k_b}{kp} = 2.00$ (Young's modulus of 0.137GPa), and the results are shown in Figure 2.27. The same distribution for ϵ was considered.

In this case, since the matching of the combination of the mobilities of the plate and beam in parallel and mobilities of the spring and plate in parallel happens at a higher frequency, a wider dispersion of the response around the nominal case is present over a broader frequency range. At lower frequencies, the parallel combination of plate and beam is dominated by the plate for this more flexible beam, so the response of the coupled system with random properties is similar to the response of the coupled system with nominal properties. However, one can still notice how the envelope of the response of the coupled systems gets narrower at the high frequency end of the frequency range analysed.

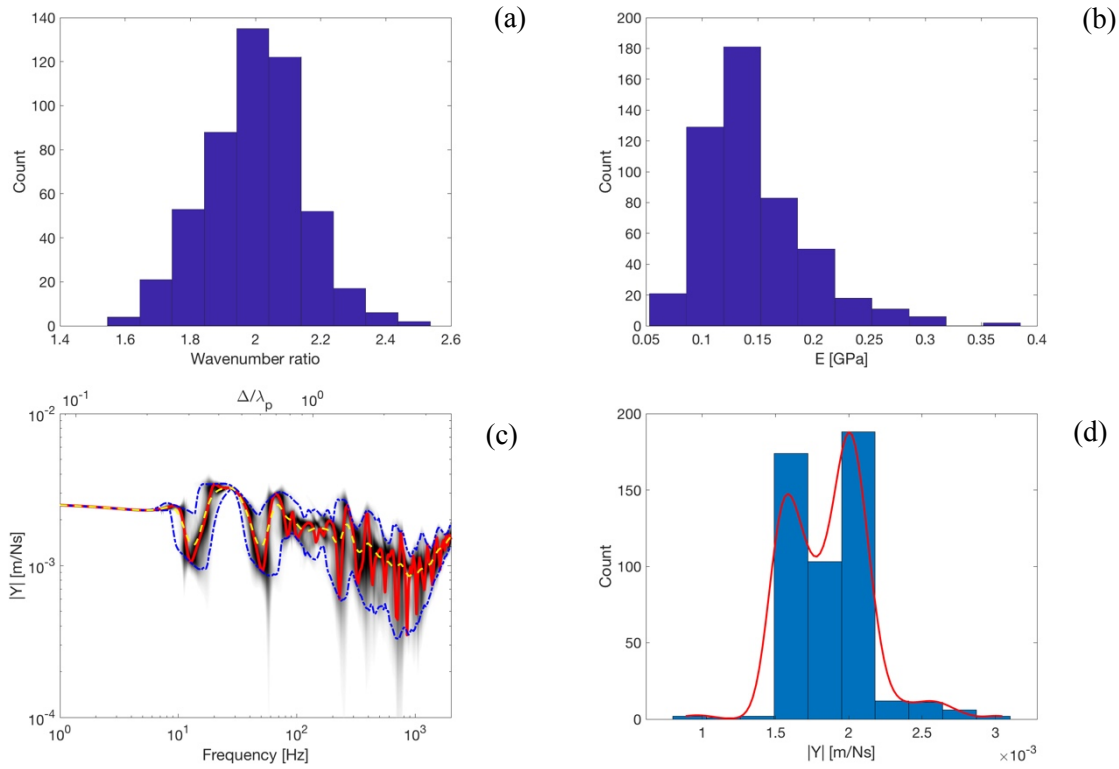

Figure 2.27 – Analysis of the coupled beam-plate system using the more flexible beam. 500 different random, but homogeneous beams.

In (a), the histogram of the beam to plate bending wavenumber ratio. The nominal case is $\frac{k_b}{kp} = 2.00$. In (b), the histogram of the modulus of elasticity using the sampled wavenumber ratios. In (c), colormap represents the density of the response, ▬ is the nominal case, ▬ ▬ is the mean of the different uniform beams and ▬ · ▬ is the envelope showing the range within which 95% of the response lies. In (d), histogram of the response of the 500 random uniform beams at 100 Hz.

The second parameter allowed to vary is the stiffness of the elastic springs, that act as the connection between the plate and the beam. Firstly, all of the five springs that link the structures vary by the same amount. Again, the stiffer and the more flexible beams were considered. The results are condensed in Figure 2.28. Secondly, each spring was allowed to vary independently of the others. The results of the input mobilities are virtually identical, since the response is governed by the local properties at the analysed point and in the two cases, the input distribution for the springs are the same. In both cases, the random spring stiffnesses are in the form $\kappa_{random} = \kappa(1 + \epsilon)$, with ϵ being sampled from a normal distribution, with mean equal to zero and standard deviation of 0.075.

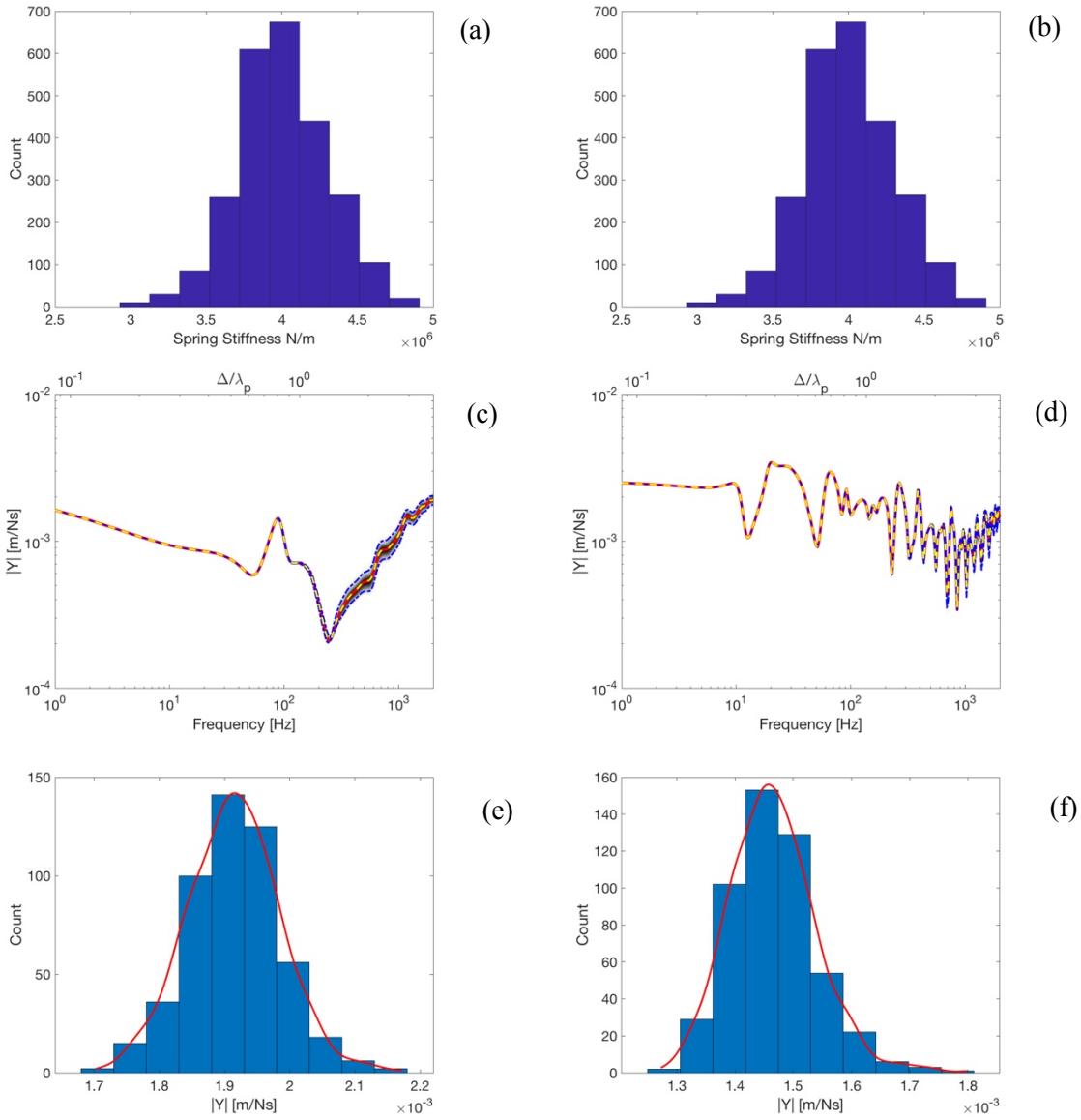

Figure 2.28 – Analysis the beam-plate coupled system through a different set of spring connections.

All the springs varied by the same amount in each individual case. Histograms of the springs stiffnesses $\frac{k_b}{kp}$ =0.35 in (a) and $\frac{k_b}{kp} = 2.00$ in (b). In (c), $\frac{k_b}{kp} = 0.35$, the histogram of the modulus of elasticity using the sampled wavenumber ratios. In (c), $\frac{k_b}{kp} = 0.35$, colormap represents the density of the response, — is the nominal case, — — is the mean of the different uniform beams and — · — is the envelope for where 95% of the response lies within. In (d), $\frac{k_b}{kp} = 2.00$, colormap represents the density of the response, — is the nominal case, — — is the mean of the different uniform beams and — · — is the envelope for where 95% of the response lies within. Histograms of the input mobility at 2000 Hz in (e), $\frac{k_b}{kp} = 0.35$, and in (f), $\frac{k_b}{kp} = 2.00$.

The effect of different spring stiffness only plays a role at higher frequencies, when the systems uncouple and where one can then see some spreading of the response around the nominal case.

The third and last parameter that was chosen to be varied in the presence of a uniform beam were the positions of the connection points, which translates into varying the spacing between the

attachment points. Once again, the parameter is defined in terms of varying around its nominal value in the form $x_{random} = x(1 + \epsilon)$, where ϵ was sampled from a uniform distribution between -0.15 and 0.15. Figure 2.29 shows the histograms of the $(1 + \epsilon)$ and of the spacing Δ.

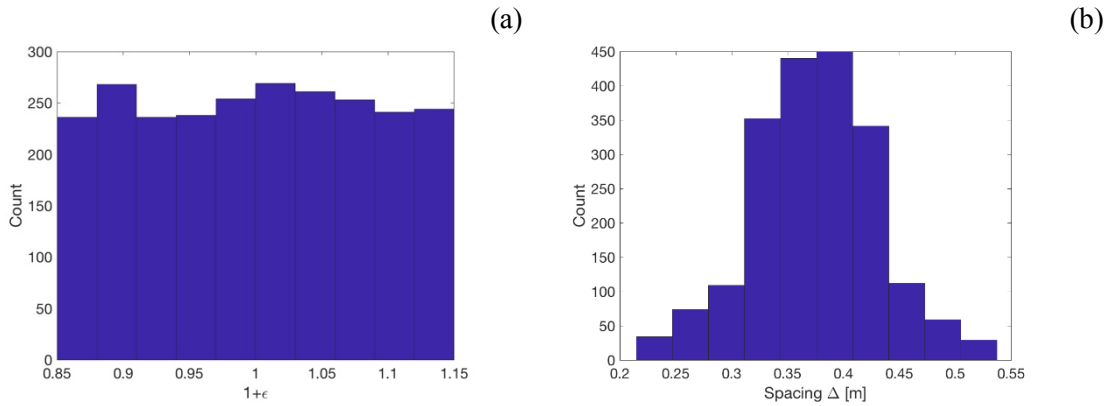

Figure 2.29 – Histograms of the random spacing.

In (a), the histogram of the $(1 + \epsilon)$ and in (b) the histogram of the spacing Δ resulting from the sampled ϵ.

The same two beam to plate bending wavenumber ratios were considered in this analysis and the input mobility of the connected system is presented in Figure 2.30 along with a typical histogram and fitted distribution of the response at a given frequency. The beam was attached to the plate using rigid links in these analyses and the random spacing affects the frequencies where the local mode-like behaviour happens, since they only occur because of finite connection points and the spacing between them.

In terms of random properties, the one that affects the coupled system the most is the case where randomly spaced connections are introduced. In this analysis, the nominal spacing $\Delta = 375$ mm and the distribution for the random spacing is a Normal distribution with mean 375 mm and standard deviation of 28 mm. Firstly, one can notice that even in the presence of that, the standing-wave-like behaviour persists. All of these standing waves are of the same kind as in the evenly spaced cases, they occur in the same attachment separation scale of the ratio Δ/λ_p. Since the more flexible beams allows for more of these localised modes to occur, they also lead to more spreading in the mobility amplitude around the nominal case when random spacing is considered. This is related to the fact that when a flexible beam is attached to the plate, the whole structure can accommodate more of these standing like waves and small variations of the frequencies at which these occur result. This then results in there is a greater discrepancy compared to the evenly spaced scenario.

2.6.3 *Beam with slowly varying Young's modulus attached to plate through five connection points*

This section focus on the numerical results involving the coupled system comprising an infinite beam with a strongly correlated random field for the Young's modulus attached to a homogeneous infinite

plate using the formulation developed in Sections 2.2, 2.3.1 and 2.4. The Young's modulus is assumed to be still varying slowly enough outside of the observed region so that there are no reflections due to this. The effect of different correlation lengths, spreading factors σ and nominal values for the beam's Young's modulus are presented. The convergence of the KL expansion is also presented. The properties for the four cases presented are summarised in Table 2.2. As in the previous section the beam is attached to the plate through 5 points with nominal spacing $\Delta = 375$ mm.

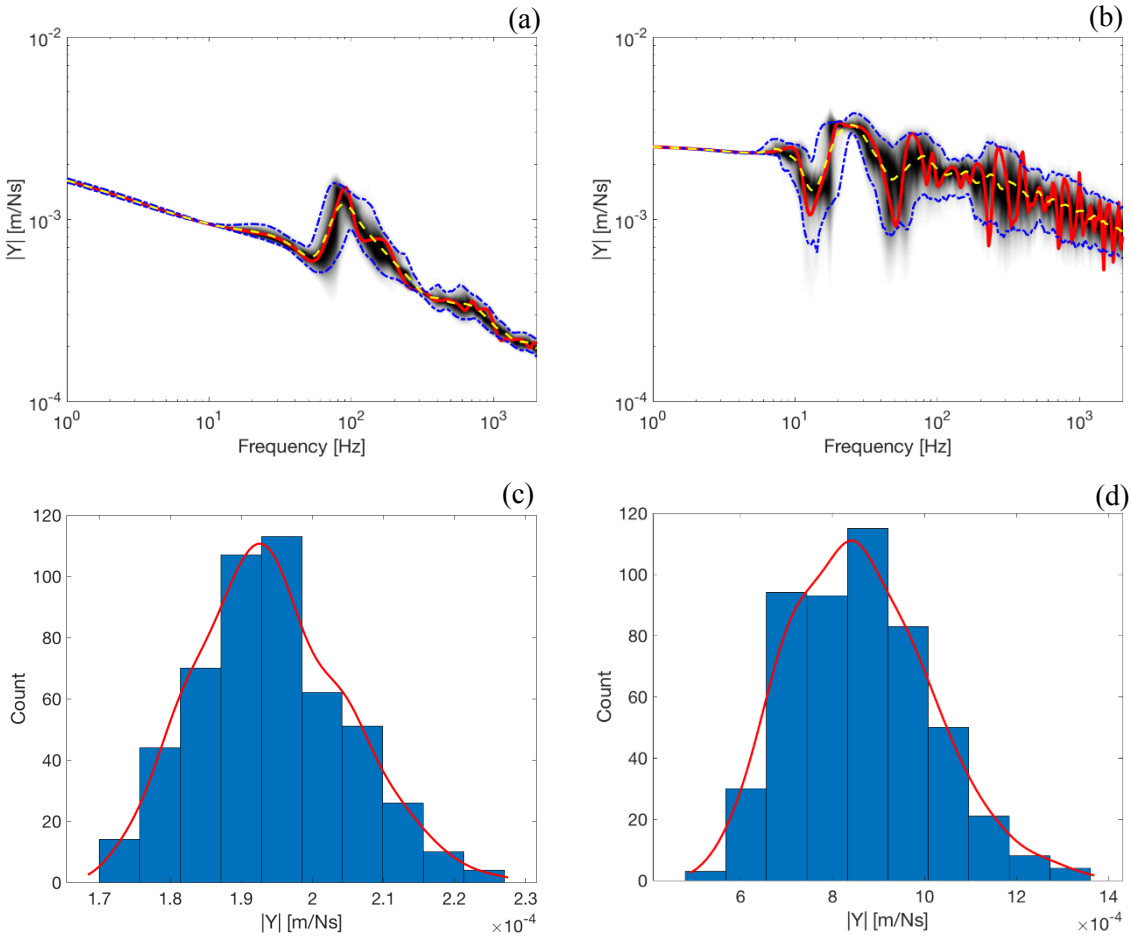

Figure 2.30 – Effects of random spacing on the coupled system. Input mobility.

Input mobilities in (a) $\frac{k_b}{kp} = 0.35$ and (b) $\frac{k_b}{kp} = 2.00$. In both cases, a colourmap represents the density of the response, ▬ is the nominal case, ▬ ▬ is the mean of the different uniform beams and ▬ · ▬ is the envelope for where 95% of the response lies within. The histogram of the response at 2000 Hz in (c) $\frac{k_b}{kp} = 0.35$ and (d) $\frac{k_b}{kp} = 2.00$.

Changes in the value of the Young's modulus result in different beam to plate wavenumber ratios, while a shorter correlation length means the random field varies more rapidly in the spatial sense and more terms in the truncated KL expansion are needed for convergence. The spreading factor σ is linked to how much around the nominal value the Young's modulus is allowed to vary. This dispersion is kept small in order to use the deductions from section 2.4. If larger values of σ are required, i.e., a larger yet still slowly variation of the field is present, numerical methods can be used to evaluate the integrals linked to the change in phase. One sample of the random field in the

observed region for each one of the cases and the convergence of the KL expansion is presented in Figure 2.31.

Table 2.2 – Properties for the slowly varying cases.

Property	Case 1	Case 2	Case 3	Case 4
Nominal Young's modulus of the beam, E_b	146 GPa	0.137 GPa	0.137 GPa	0.137 GPa
Correlation length, b_L	0.75 m	0.75 m	0.375 m	0.75 m
Number of modes KL expansion	16	16	16	16
Spreading factor, σ (see Eq. (2.95))	0.1	0.1	0.1	0.2

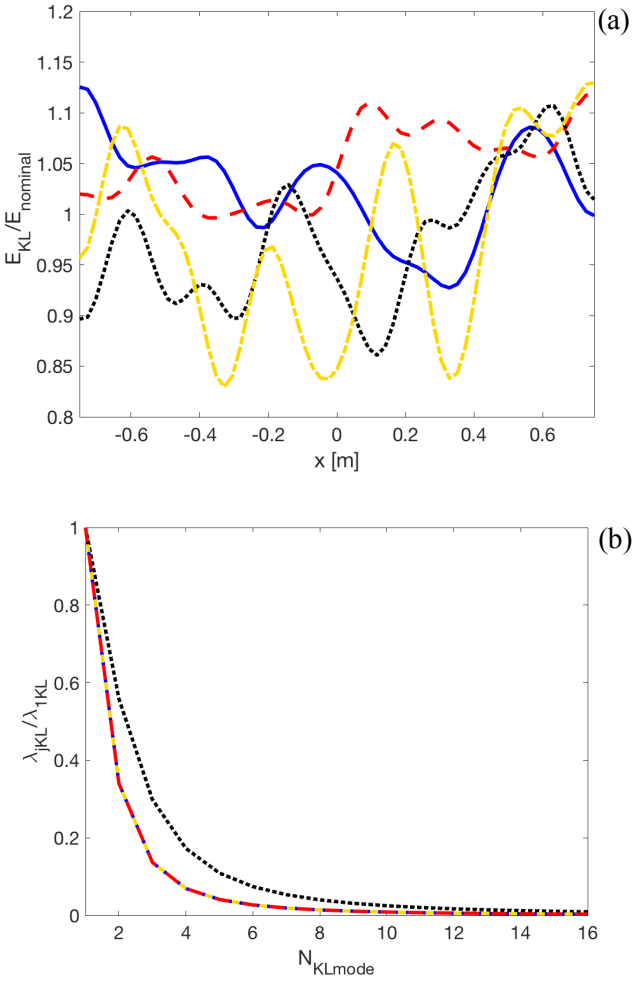

Figure 2.31 – Samples of the random field in the observed region and convergence of the KL expansion.

In (a), one sample of the beam's Young's modulus along its length for each case. In (b), the eigenvalue of each mode of the KL expansion normalised by the first eigenvalue. In both cases, ▬ case 1 ($E_b = 146$ GPa, $b_L = 0.75$ and $\sigma = 0.1$), ▬ ▬ case 2 ($E_b = 0.137$ GPa, $b_L = 0.75$ and $\sigma = 0.1$), ⋯ case 3 $E_b = 0.137$ GPa, $b_L = 0.375$ and $\sigma = 0.1$) and ▬ · ▬ case 4 ($E_b = 0.137$ GPa, $b_L = 0.75$ and $\sigma = 0.2$)

In Figure 2.31(b), one can see the effect of having a shorter correlation length has on the normalised eigenvalues and how more terms are necessary for the series convergence of them. However, in all cases, 16 terms were enough to adequately represent the KL expansion for the random field.

The input mobilities of the coupled systems for Cases 1-4 are shown in Figures 2.26-2.29, along with the distribution of the generated random fields for the beam Young's moduli and the input mobility of the infinite beam, plate and coupled system.

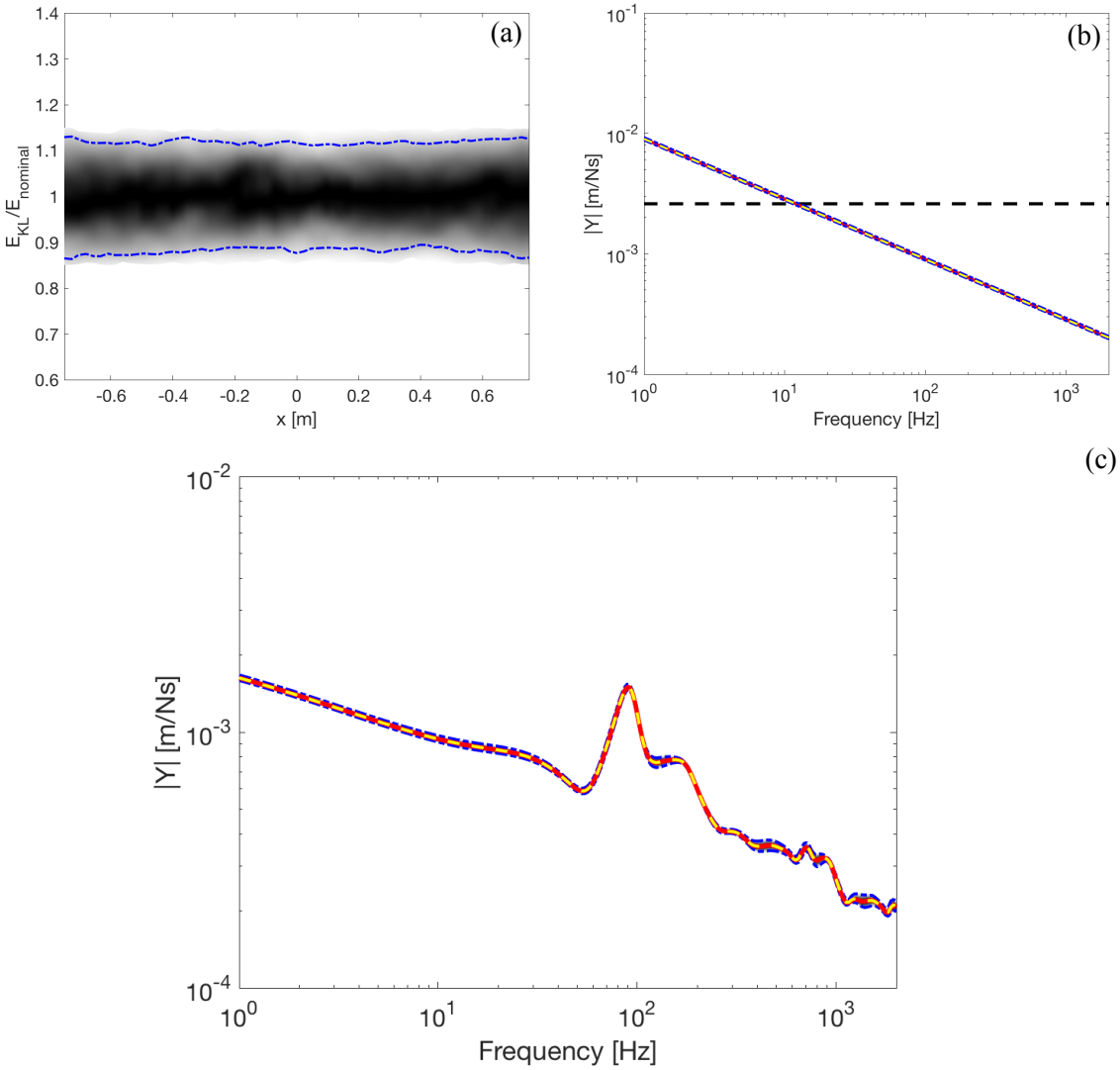

Figure 2.32 – Distribution of the Young's Modulus, input mobilities of the infinite beam and plate and input mobility of the coupled system: Case 1.

Case 1: nominal $\frac{k_b}{kp} = 0.35$, correlation length $b_L = 0.75$ m, $N_{KL} = 16$ and $\sigma = 0.1$. In (a), the colourmap is the normalised distribution of the Young's modulus along the beam's length and — · — limits the region where 95% of the samples are. In (b), the input mobilities of the separate systems; — — is the homogeneous plate, — is the beam with nominal properties, the colormap is the normalised distribution of the mobilities using the 500 slowly varying Young's moduli, — — is the mean of the responses and — · — limits the region where 95% of the response is. In (c), the input mobility of the coupled system; — is the connected system with nominal properties, the colormap is the normalised distribution of the mobilities using the 500 slowly varying Young's moduli, — — is the mean of the responses and — · — limits the region where 95% of the response is.

The spreading factor σ is kept small so the variation in the local properties are also small. The response of the infinite system is highly dominated by the local properties, so when the beams with slowly varying Young's modulus are introduced, the response of the coupled system do not change significantly.

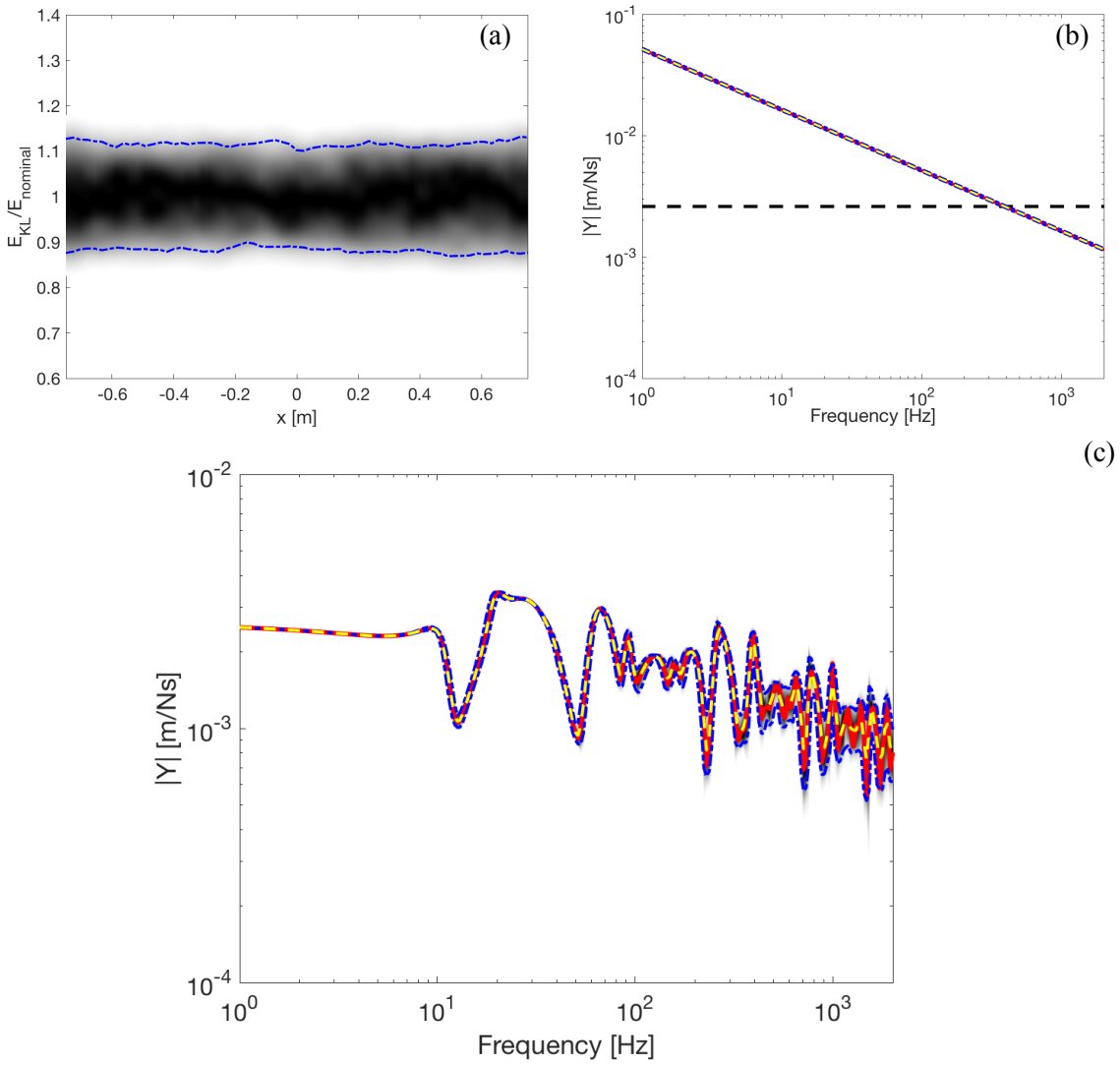

Figure 2.33 – Distribution of the Young's Modulus, input mobilities of the infinite beam and plate and input mobility of the coupled system: Case 2.

Case 2: nominal $\frac{k_b}{kp} = 2.00$, correlation length $b_L = 0.75$ m, $N_{KL} = 16$ and $\sigma = 0.1$. In (a), the colourmap is the normalised distribution of the Young's modulus along the beam's length and — · — limits the region where 95% of the samples are. In (b), the input mobilities of the separate systems; — — is the homogeneous plate, — is the beam with nominal properties, the colormap is the normalised distribution of the mobilities using the 500 slowly varying Young's moduli, — — is the mean of the responses and — · — limits the region where 95% of the response is. In (c), the input mobility of the coupled system; — is the connected system with nominal properties, the colormap is the normalised distribution of the mobilities using the 500 slowly varying Young's moduli, — — is the mean of the responses and — · — limits the region where 95% of the response is.

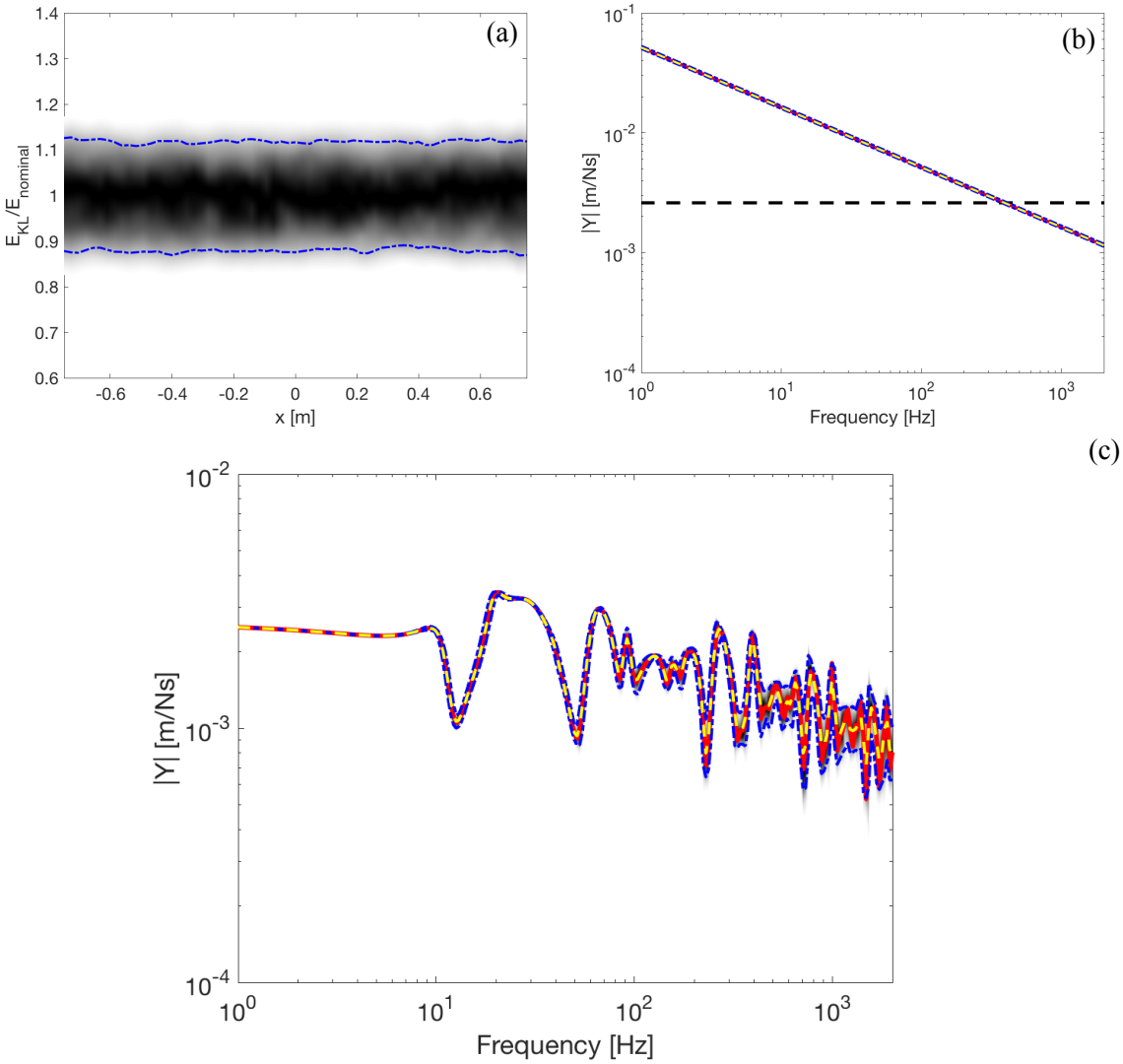

Figure 2.34 – Distribution of the Young's Modulus, input mobilities of the infinite beam and plate and input mobility of the coupled system: Case 3.

Case 3: nominal $\frac{k_b}{kp} = 2.00$, correlation length $b_L = 0.375$ m, $N_{KL} = 16$ and $\sigma = 0.1$. In (a), the colourmap is the normalised distribution of the Young's modulus along the beam's length and — · — limits the region where 95% of the samples are. In (b), the input mobilities of the separate systems; — — is the homogeneous plate, — is the beam with nominal properties, the colormap is the normalised distribution of the mobilities using the 500 slowly varying Young's moduli, — — is the mean of the responses and — · — limits the region where 95% of the response is. In (c), the input mobility of the coupled system; — is the connected system with nominal properties, the colormap is the normalised distribution of the mobilities using the 500 slowly varying Young's moduli, — — is the mean of the responses and — · — limits the region where 95% of the response is.

Once again, the response of the infinite system is highly dominated by the local properties, so the change in the correlation length does not significantly affect the response of the coupled system.

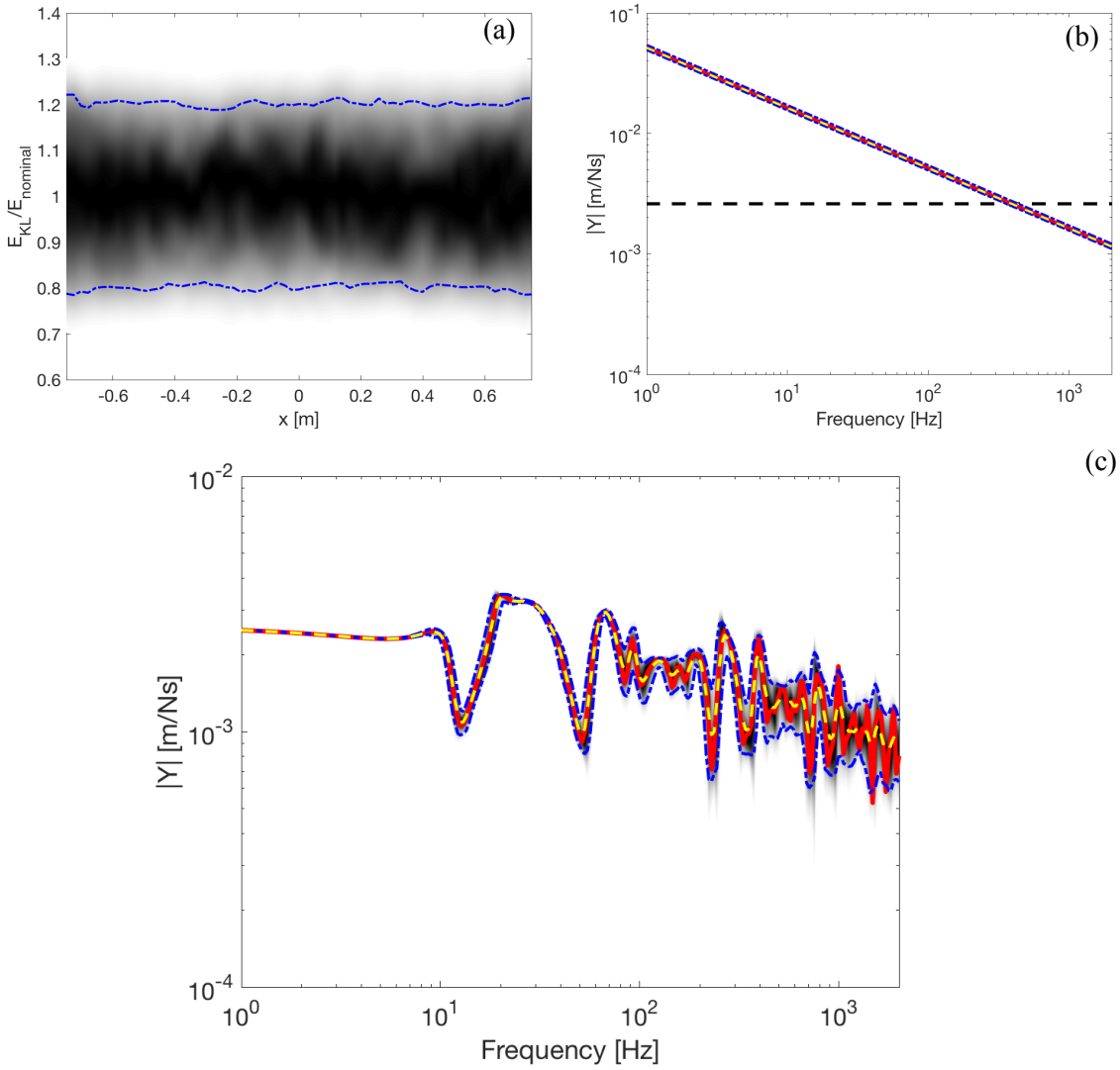

Figure 2.35 – Distribution of the Young's Modulus, input mobilities of the infinite beam and plate and input mobility of the coupled system: Case 4.

Case 4: nominal $\frac{k_b}{kp} = 2.00$, correlation length $b_L = 0.75$ m, $N_{KL} = 16$ and $\sigma = 0.2$. In (a), the colourmap is the normalised distribution of the Young's modulus along the beam's length and — · — limits the region where 95% of the samples are. In (b), the input mobilities of the separate systems; — — is the homogeneous plate, — is the beam with nominal properties, the colormap is the normalised distribution of the mobilities using the 500 slowly varying Young's moduli, — — is the mean of the responses and — · — limits the region where 95% of the response is. In (c), the input mobility of the coupled system; — is the connected system with nominal properties, the colormap is the normalised distribution of the mobilities using the 500 slowly varying Young's moduli, — — is the mean of the responses and — · — limits the region where 95% of the response is.

As expected, if the properties are allowed to vary by a larger amount, the envelope of the response of the coupled system gets wider between the upper and lower response bounds.

The convergence of the statistical properties of the response of the coupled system considering Case 4 are shown in Figure 2.36 and they are normalised by the quantities when the whole set of 500 samples are considered. Case 4 is the one that allows a larger spread around the nominal value,

therefore it is the worst-case scenario for convergence. It is possible to see how the unity plateau is frequency dependent.

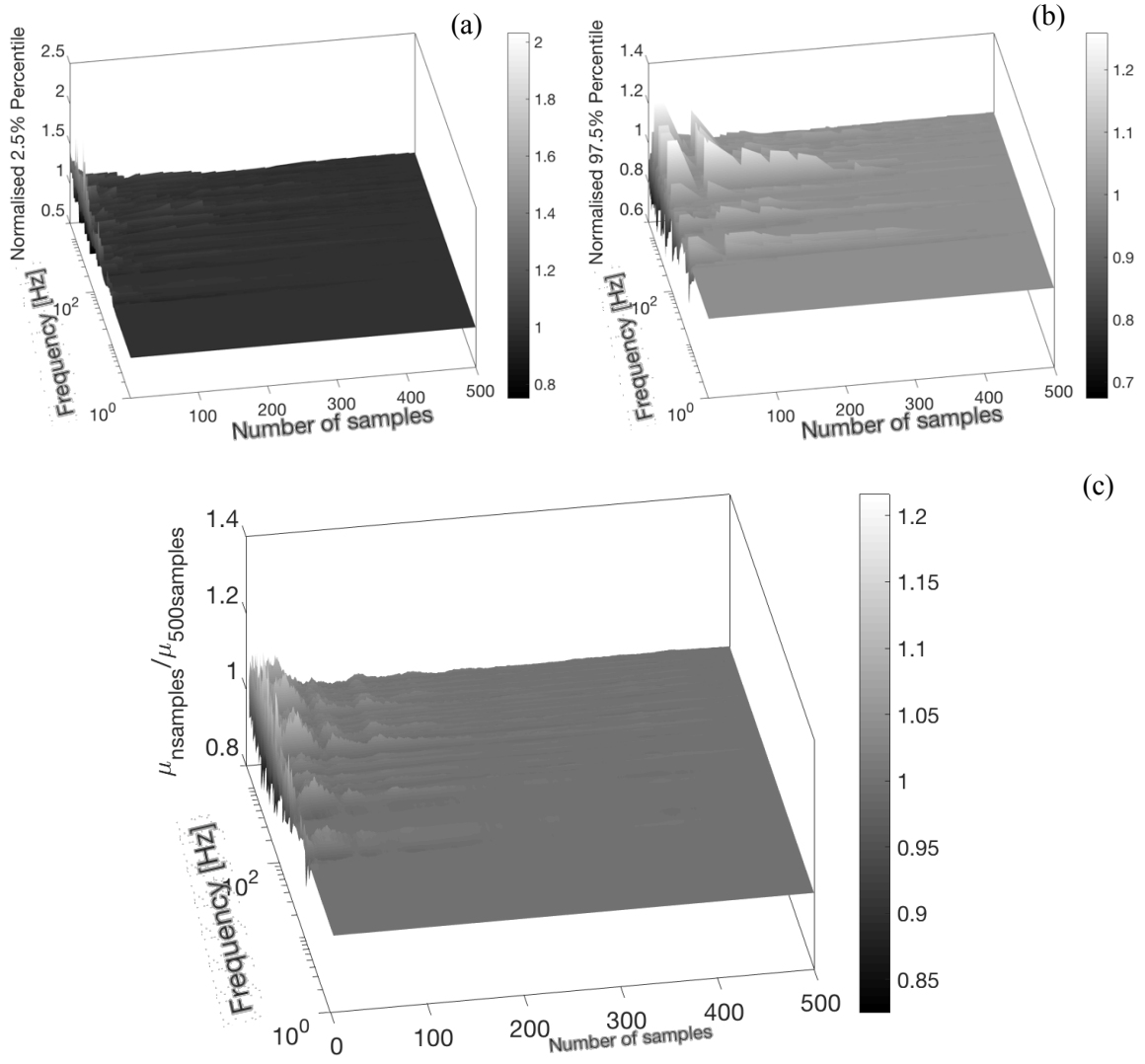

Figure 2.36 – Convergence of the statistical properties mean, 2.5% and 97.5% percentiles: Case 4.

In (a), the values for the 2.5% percentile considering a different number of samples used divided by the value for the 2.5% percentile using the 500 samples. In (b), the values for the 97.5% percentile considering a different number of samples used divided by the value for the 97.5% percentile using the 500 samples. In (c), the values of the mean considering a different number of samples normalised by the mean using the 500 samples.

The properties are shown normalised for a more convenient view. After 400 samples the fluctuations are negligible (normalised or not) and therefore using a sample size of 500 samples should be enough to infer the statistical properties of the response.

Another way of looking at the response of the coupled systems in the presence of slowly varying beams is to plot them on a dB scale referenced to the nominal case, so the effects of the slowly varying fields are more conveniently shown. These results are presented in Figure 2.37.

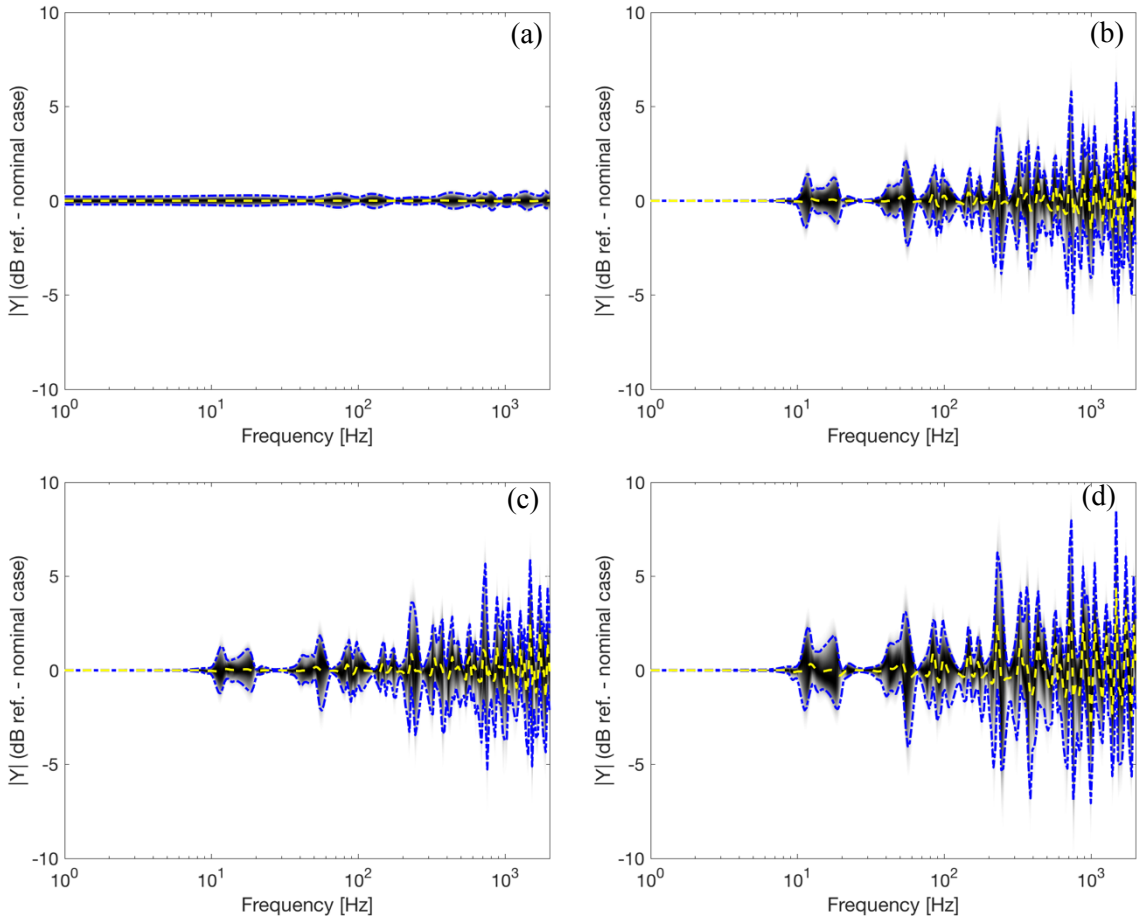

Figure 2.37 – Infinite system: All cases in a dB scale.

The response of the system in the presence of different slowly varying beam in a dB scale referenced to the system connected to the nominal beam. In (a), case 1; nominal $\frac{k_b}{kp} = 0.35$ (stiffer beam), correlation length $b_L = 0.75$ m, $N_{KL} = 16$ and $\sigma = 0.1$. In (b), case 2; nominal $\frac{k_b}{kp} = 2.00$ (flexible beam), correlation length $b_L = 0.75$ m, $N_{KL} = 16$ and $\sigma = 0.1$. In (c), case 3; nominal $\frac{k_b}{kp} = 2.00$, correlation length $b_L = 0.375$ m, $N_{KL} = 16$ and $\sigma = 0.1$. In (d), case 4; nominal $\frac{k_b}{kp} = 2.00$, correlation length $b_L = 0.75$ m, $N_{KL} = 16$ and $\sigma = 0.2$. In all cases, the colormap is the normalised distribution of the mobilities using the 500 slowly varying Young's moduli, — — is the mean of the responses and — · — limits the region where 95% of the response is.

The fluctuation in Figure 2.37 is caused by the shift in frequency of the peaks and valleys due to the changes in stiffness of the attached beams accordingly to the parameters of correlation length and spreading factor used to generate their random field. Once again, the effects are greater when more flexible beams are considered. On a dB scale referenced to the nominal case, the differences can be in the region of ±8 decibels. It is important to note that these changes come from slightly shifting the frequencies of the peaks and troughs in the response of the coupled system.

Finally, the last analysis conducted is related to the validity of the WKB approximation, described in Equation (2.48). Typical examples of Young's modulus generated by the KL expansion for cases 1-4 are used to compute the results and check how they compare to the unity, if they are indeed much smaller than 1 and, therefore, if the WKB approximation holds.

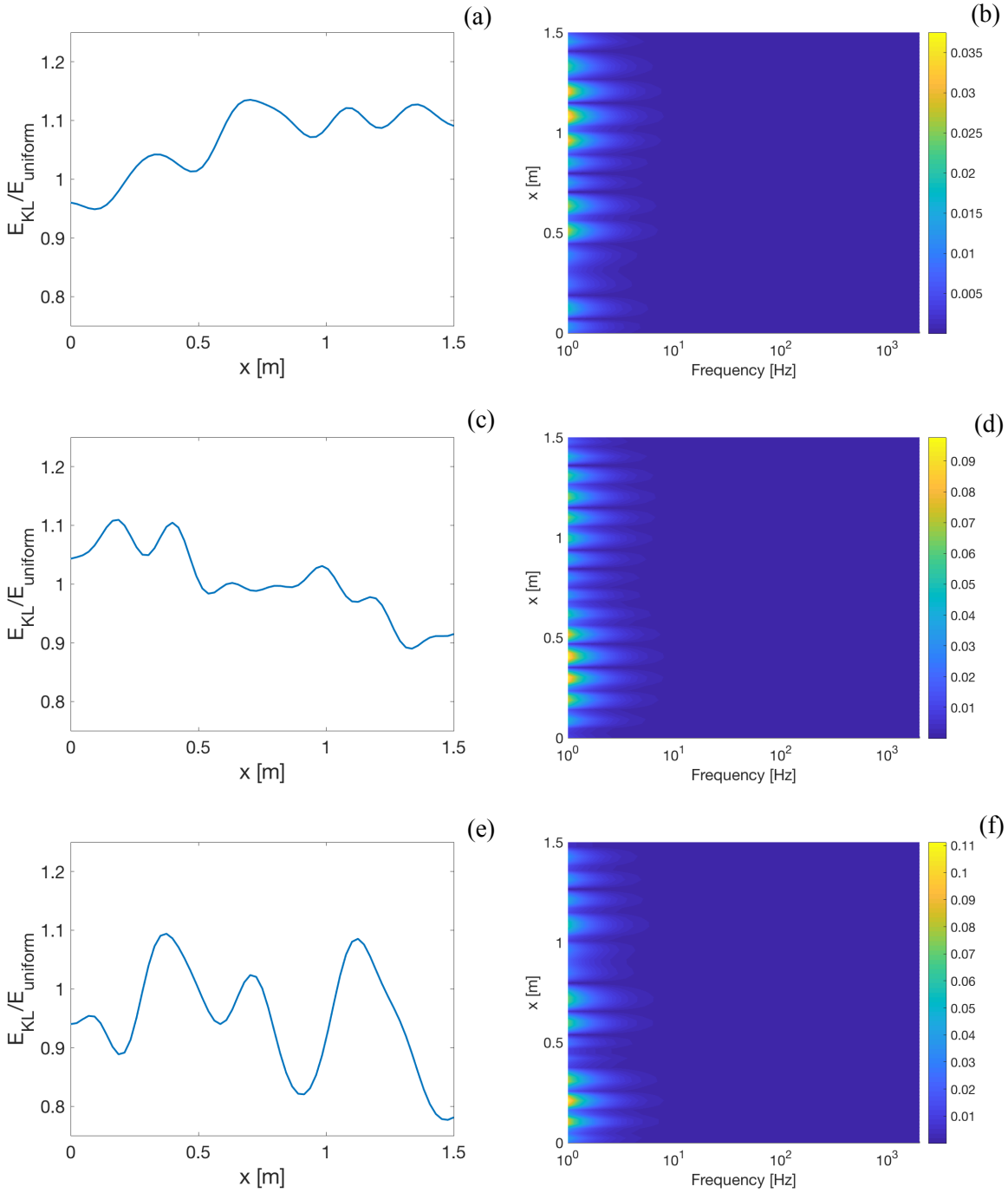

Figure 2.38 – Validity of the WKB approximation along the length of the beam and the frequency range.

In (a), a typical sample of the slowly varying random field for cases 1 ($E_b = 146$ GPa, $b_L = 0.75$ and $\sigma = 0.1$) and 2 ($E_b = 0.137$GPa, $b_L = 0.75$ and $\sigma = 0.1$). In (b), the colourmap shows the results when such typical sample is plugged into Equation (2.48). In (c) and (e), two typical samples for the slowly varying random Young's moduli in cases 3 ($E_b = 0.137$GPa, $b_L = 0.375$ and $\sigma = 0.1$) and 4 ($E_b = 0.137$GPa, $b_L = 0.75$ and $\sigma = 0.2$), respectively. Whilst (d) and (f) shown the validity of the WKB assumption for cases 3 and 4, respectively.

The higher values occur at low frequencies (around 1 Hz), but do not exceed 0.11. For most of the frequency spectrum, they are much smaller than 1 and the WKB approximation is considered to be held and safe to be used. As expected, the higher the frequency, the better is the approximation.

In the cases studied in this chapter, the assumption for the WKB approximation holds over the whole frequency range.

2.7 Conclusions

In this chapter, a model comprising coupled infinite beams and plates was considered in order to get a first grasp of the dynamic behaviour of connected structures. A mobility approach was used to model the point connections. Expressions for the point and transfer mobilities of both the infinite and homogeneous Euler-Bernoulli beams and classic thin plates are readily obtained in the literature.

To find the analytical solutions in the presence of slowly varying properties, the WKB approximation was used. Firstly, as an example and as an introductory case, the expressions for an infinite rod were derived. Subsequently, the expressions for the infinite beam were derived, which is the actual interest of this research. Here, the derivations for the beam were made considering a direct approach to calculate the flexural displacement, instead of the energetic approach found in the literature. The results are in full agreement. The main assumption of the WKB method is that the properties vary slowly enough and that there are no internal reflections of the waves. In order to achieve such a field, it is recommended to use the KL expansion. Expressions were derived and given considering that only the Young's modulus of the beam and rod were varying, but the method can be extended to other properties or even multiple properties. For convenience, a first order approximation of the integral related to the random field was made.

Once the point and transfer mobilities are known, it is possible to use them in a straightforward manner, using a matrix formulation, to model connected structures coupled through a finite number of point connections. However, the matrices involved in the process can become very large, as they are proportional to the square of the number of points of interest. The models developed have only considered translational displacement, but the analysis could be extended to incorporate rotational coupling as well. The offset of the neutral axis of the beam and plate were also neglected. The latter would then result in the potential coupling of in and out of plane displacement.

Using the proposed modelling techniques, the content of the chapter follows to show some numerical results considering different scenarios covering different beam to plate bending wavenumber ratios, the number of attachment points, spacing between the connection points, rigid or flexible connections and random beam properties.

Even when infinite structures were considered, the presence of the connection points produces local modes between the connections, governed by the spacing between the connection points and the properties of the beam and host plate. It is also important to note that the uncertainty in the positioning (or spacing) of these connection points can be as relevant and important as uncertainties in the mechanical properties of the structures.

Assuming that the excitation is applied to the plate, one possible way of reducing the uncertainty of the response of the coupled system due to uncertainties in the attached beam is using flexible links. This will result in the uncoupling of the two structures above a given frequency and the response of the system will be only governed by the host plate structure and the mobility of the links itself.

The next chapter deals with finite structures and, therefore, the coupled systems have natural frequencies and modes that can be affected by the slowly varying random fields. It will cover variation in both the beam and plate subsystems and try to generalise the behaviour and results.

Chapter 3 The coupling of finite structures using mobilities

This chapter addresses the modelling of finite beams and plates. The main difference from finite structures to the infinite structures considered in Chapter 2 is that the presence of boundaries i.e. the edges of the structures reflect the propagating waves, which leads to standing waves, or modes of the structures. The mobility approach shown in the previous chapter is used to couple beam and plate. For the point and transfer mobilities of the beam with slowly varying properties, an analytical solution is derived using again the WKB approximation. Variability in the plate is introduced by perturbing the matrices obtained using Finite Element Analysis. The strongly correlated random fields are described via the Karhunen–Loève expansion in both cases.

Results for three scenarios are presented comprising beams with slowly varying properties attached to a homogeneous plate, homogeneous beams attached to slowly varying plates and slowly varying beams attached to slowly varying plates. Similar to the previous chapter, when considering flexible links, they are modelled as elastic springs. The results only consider a slowly varying Young's modulus field, but this approach could be used to the other properties as well. The effects of random spacing are also analysed.

3.1 Mobilities of beams and plates

This section gives a brief overview of the mobilities of homogeneous plates and beams, which can be found in the literature. The Wentzel–Kramers–Brillouin approximation is used to find the waves in the slowly varying beam and that allows to find the input and transfer mobilities.

A modal approach is used to find the mobility of a finite Euler-Bernoulli beam. It can be written in terms of natural frequencies, modal shapes and summation of modal response [**53**] as:

$$Y(\alpha,\beta) = i\omega \sum_{n=1}^{\infty} \frac{\psi_n(\alpha)\psi_n(\beta)}{\rho A l[\omega_n^2(1+i\eta)-\omega^2]} \tag{3.1}$$

where $Y(\alpha,\beta)$ is the mobility for a force excitation at α and transverse velocity response at β, i is the imaginary unit, ω is the circular frequency, ψ_n is the modal shape, ρ is the density of the beam, A is the cross-section area of the beam and l is the length of the beam, whilst η is the loss factor and ω_n is the natural frequency given by $\omega_n = \sqrt{\frac{EI}{\rho A}} k_{nb}$. The modal shapes and natural wavenumbers depend on the boundary conditions.

Analogous to the modelling of a beam, modal summation can also be used to write the mobilities of finite plates [**72**]. Considering a rectangular plate of dimensions l_x and l_y, coordinate

system origin located at a corner of the plate, force excitation at point α and transverse velocity response at point β, the mobility can be written as [**72**] [**53**]:

$$Y(\alpha,\beta) = i\omega \sum_{m=1}^{\infty}\sum_{n=1}^{\infty} \frac{\psi_{mn}(\beta)\psi_{mn}(\alpha)}{\rho h l_x l_y[\omega_{mn}^2(1+i\eta)-\omega^2]} \tag{3.2}$$

where h is the thickness of the plate, ψ_{mn} is the $(m,n)^{th}$ bending natural mode and ω_{mn} is $(m,n)^{th}$ natural frequency.

Once again, the modal shapes and natural frequencies are dependent of the boundaries conditions. The natural frequencies for a rectangular plate can be generalised as [**73**] [**53**]:

$$\omega_{mn} = \sqrt{\frac{Eh^2}{12\rho(1-\nu^2)}}\left(\frac{\pi}{l_x}\right)^2 q_{mn} \tag{3.3}$$

where ν is the Poisson's ratio and $q_{mn} = \sqrt{G_x^4(m) + G_y^4(n)\left(\frac{l_x}{l_y}\right)^4 + 2\left(\frac{l_x}{l_y}\right)^2\left[\nu H_x(m)H_y(n) + (1-\nu)J_x(m)J_y(n)\right]}$. The constants G_j, H_j and J_j are defined accordingly to the boundary conditions.

This chapter considers that the boundary conditions of the beam are free-free, whilst the plate is pinned-pinned. The necessary natural wavenumbers, modal shapes, G_j, H_j and J_j are summarised in Table 3.1.

3.1.1 *Beam with slowly varying properties*

This chapter also assumes that there are no internal reflections of the waves due to the changes of the properties in the slowly varying field, which allows the use of the WKB approximation once again to find the solutions for the change in phase and in amplitude of the waves in finite beam. As in Section 2.2, the change in phase is given by the integral of the wavenumber, $\theta(x) = \int\left[\frac{\rho A(x)}{EI(x)}\right]^{\frac{1}{4}}\sqrt{\omega}dx$ and the change in amplitude is given by $\gamma = \ln\frac{\widetilde{W}(x_2)}{\widetilde{W}(x_1)}$, where $\widetilde{W}(x) = (\rho A)^{-\frac{3}{8}}(EI)^{-\frac{1}{8}}$ [**2**] [**40**].

A similar wave approach is used to find the input and transfer mobilities, but this time, taking into account the fact that the waves are reflected by the ends of the beam. The ongoing and reflected waves to one side of the beam are shown in Figure 3.1.

The KL expansion approach to describe a random field in Chapter 2 is also valid in this case of finite beams.

Table 3.1 – Boundary conditions and constants for the homogeneous beam and plate.

(Adapted from: [**53**])

Beam: Free-free $W''(0) = 0$ $W''(l) = 0$ $W'''(0) = 0$ $W'''(l) = 0$	n	$k_{nb}l$	$\psi_n(x)$
	Even rigid body mode		l
	Rocking rigid body mode		$\sqrt{3}(l - 2x/l)$
	1	4.73004	$\cosh k_{nb}x + \cos k_{nb}x - \sigma_n(\sinh k_{nb}x + \sin k_{nb}x)$ $\sigma_n = \dfrac{\cosh k_{nb}l - \cos k_{nb}l}{\sinh k_{nb}l - \sin k_{nb}l}$
	2	7.85320	
	3	10.9956	
	4	14.1372	
	5	17.2788	
	6, 7, …	$(2n + l)\,\pi/2$	

Plate: Pinned-pinned $W(0) = 0$ $W(l) = 0$ $W''(0) = 0$ $W''(l) = 0$	j	G_j	H_j	J_j	$\psi_{mn}(x, y)$
	1, 2, 3, …	j	j^2	j^2	$\sqrt{2}\sin\left(\dfrac{m\pi x}{l_x}\right)\sqrt{2}\sin\left(\dfrac{n\pi y}{l_y}\right)$

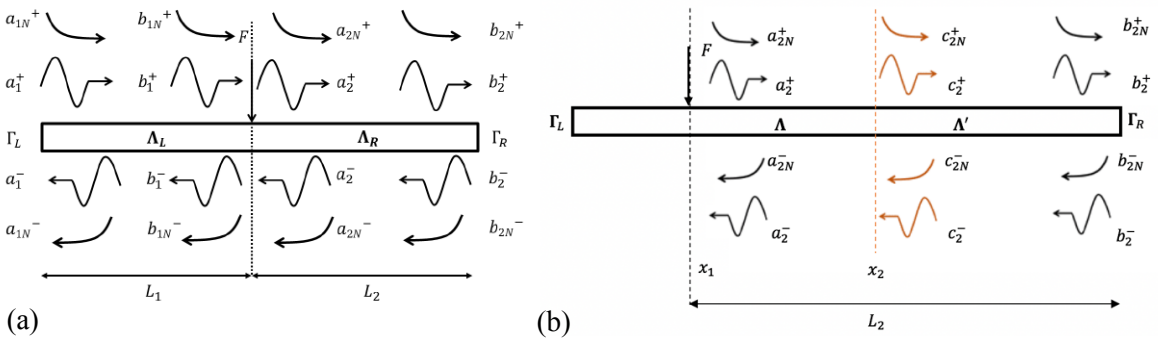

Figure 3.1 – Propagating waves and waves reflected by the boundaries on a finite beam.

In (a), the propagating waves from the excitation point and reflected waves by the boundaries, whilst (b) also includes the propagating waves at an arbitrary position x_2.
(Adapted from [**2**])

The point harmonic excitation force F creates the positive and negative going waves $\boldsymbol{q}^{\pm} = [q^{\pm}\ q_N^{\pm}]^T$ and the expression for the input mobility [**2**], can be generalised to find the amplitude of the waves $\boldsymbol{c}_2^{\pm} = [c_2^{\pm}\ c_{2N}^{\pm}]^T$ at an arbitrary position from $\boldsymbol{a}_2^{\pm} = [a_2^{\pm}\ a_{2N}^{\pm}]^T$ and $\boldsymbol{b}_2^{\pm} = [b_2^{\pm}\ b_{2N}^{\pm}]^T$.

Firstly:

$$\boldsymbol{b_1^+ = \Lambda_{L_{11}} a_1^+} \tag{3.4}$$

$$\boldsymbol{b_2^+ = \Lambda_{R_{11}} a_2^+} \tag{3.5}$$

$$\boldsymbol{b_1^- = \Lambda_{L_{22}} a_1^-} \tag{3.6}$$

$$\boldsymbol{b_2^- = \Lambda_{R_{22}} a_2^-} \tag{3.7}$$

$$\boldsymbol{a_2^+ = b_1^+ + q^+ = \Lambda_{L_{11}} a_1^+ + q^+} \tag{3.8}$$

$$\boldsymbol{b_1^- = a_2^- + q^- \Leftrightarrow \Lambda_{L_{22}} a_1^- = a_2^- + q^-} \tag{3.9}$$

$$\boldsymbol{a_1^+ = \Gamma_L a_1^-} \tag{3.10}$$

$$\boldsymbol{b_2^- = \Gamma_R b_2^+ = \Gamma_R \Lambda_{R_{11}} a_2^+} \tag{3.11}$$

where $\boldsymbol{\Lambda_J} = \begin{bmatrix} \boldsymbol{\Lambda_{J_{11}}} & \boldsymbol{0} \\ \boldsymbol{0} & \boldsymbol{\Lambda_{J_{22}}} \end{bmatrix}$, $\boldsymbol{\Lambda_{J_{11}}} = \begin{bmatrix} e^{-i\theta_J+\gamma_J} & 0 \\ 0 & e^{-\theta_J+\gamma_J} \end{bmatrix}$ and $\boldsymbol{\Lambda_{J_{22}}} = \begin{bmatrix} e^{i\theta_J+\gamma_J} & 0 \\ 0 & e^{\theta_J+\gamma_J} \end{bmatrix}$.

$$\boldsymbol{c_2^+ = \Lambda a_2^+} \tag{3.12}$$

$$\boldsymbol{b_2^- = \Lambda' c_2^- \ \Leftrightarrow c_2^- = \Lambda'^{-1} \Gamma_R \Lambda_{R_{11}} a_2^+} \tag{3.13}$$

where $\boldsymbol{\Lambda}$, $\boldsymbol{\Lambda'}$ and $\boldsymbol{\Lambda_{R_{11}}}$ are propagating matrices and $\boldsymbol{\Gamma_R}$ is the reflection matrix at the right end of the beam.

$$\boldsymbol{\Lambda} = \begin{bmatrix} e^{-i\int_{x_1}^{x_2} k(x)dx+\gamma_1} & 0 \\ 0 & e^{-\int_{x_1}^{x_2} k(x)dx+\gamma_1} \end{bmatrix} \tag{3.14}$$

$$\boldsymbol{\Lambda'} = \begin{bmatrix} e^{i\int_{x_2}^{L_2} k(x)dx+\gamma_2} & 0 \\ 0 & e^{\int_{x_2}^{L_2} k(x)dx+\gamma_2} \end{bmatrix} \tag{3.15}$$

$$\boldsymbol{\Lambda_{R_{11}}} = \begin{bmatrix} e^{-i\int_{x_1}^{L_2} k(x)dx+\gamma_{R_{11}}} & 0 \\ 0 & e^{-\int_{x_1}^{L_2} k(x)dx+\gamma_{R_{11}}} \end{bmatrix} \tag{3.16}$$

Thus:

$$\boldsymbol{c_2^+ + c_2^- = \Lambda a_2^+ + \Lambda' \Gamma_R \Lambda_{R_{11}} a_2^+ = (\Lambda + \Lambda' \Gamma_R \Lambda_{R_{11}}) a_2^+} \tag{3.17}$$

Combining Equations (3.8) and (3.10):

$$\boldsymbol{a_2^+ = \Lambda_{L_{11}} \Gamma_L a_1^- + q^+} \tag{3.18}$$

where $\boldsymbol{\Gamma_L}$ is the reflection matrix at the left end of the beam.

Which can be rewritten as:

$$\boldsymbol{a_2^+ = \Lambda_{L_{11}} \Gamma_L \Lambda_{L_{22}}^{-1} b_1^- + q^+ = \Lambda_{L_{11}} \Gamma_L \Lambda_{L_{22}}^{-1} (a_2^- + q^-) + q^+} \tag{3.19}$$

$$\boldsymbol{a_2^+ = \Lambda_{L_{11}} \Gamma_L \Lambda_{L_{22}}^{-1} (\Lambda_{R_{22}}^{-1} b_2^- + q^-) + q^+} \tag{3.20}$$

$$\boldsymbol{a_2^+ = \Lambda_{L_{11}} \Gamma_L \Lambda_{L_{22}}^{-1} b_1^- + q^+} \tag{3.21}$$

$$\boldsymbol{a_2^+ = \Lambda_{L_{11}} \Gamma_L \Lambda_{L_{22}}^{-1} (a_2^- + q^-) + q^+} \tag{3.22}$$

$$\boldsymbol{a_2^+ = \Lambda_{L_{11}} \Gamma_L \Lambda_{L_{22}}^{-1} (\Lambda_{R_{22}}^{-1} \Gamma_R \Lambda_{R_{11}} a_2^+ + q^-) + q^+} \tag{3.23}$$

From equilibrium of forces and continuity of displacement the infinite beam wave amplitudes are:

$$\boldsymbol{q^+ = q^- = q} = \frac{-1}{4EI(x_1)k_B^3(x_1)} \begin{bmatrix} i \\ 1 \end{bmatrix} F \tag{3.24}$$

Thus:

$$\boldsymbol{a_2^+ = \left(I - \Lambda_{L_{11}} \Gamma_L \Lambda_{L_{22}}^{-1} \Lambda_{R_{22}}^{-1} \Gamma_R \Lambda_{R_{11}}\right)^{-1} \left(I + \Lambda_{L_{11}} \Gamma_L \Lambda_{L_{22}}^{-1}\right) q} \tag{3.25}$$

Where $\boldsymbol{I}$ is the identity matrix.

Finally:

$$\boldsymbol{c_2^+ + c_2^-} = \left(\boldsymbol{\Lambda + \Lambda'^{-1}\Gamma_R\Lambda_{R_{11}}}\right)\left(\boldsymbol{I - \Lambda_{L_{11}}\Gamma_L\Lambda_{L_{22}}^{-1}\Lambda_{R_{22}}^{-1}\Gamma_R\Lambda_{R_{11}}}\right)^{-1}\left(\boldsymbol{I + \Lambda_{L_{11}}\Gamma_L\Lambda_{L_{22}}^{-1}}\right)\boldsymbol{q} \tag{3.26}$$

Once, the wave amplitudes $\boldsymbol{c_2^+ + c_2^-}$ at an arbitrary position are known, the generalised mobility at any point is given by:

$$Y(\omega) = \frac{i\omega(\boldsymbol{c_2^+ + c_2^-})}{F} \tag{3.27}$$

In the particular case of a free end, the reflection matrices $\boldsymbol{\Gamma_L}$ and $\boldsymbol{\Gamma_R}$ are given by [**74**]:

$$\boldsymbol{\Gamma_L} = \boldsymbol{\Gamma_R} = \begin{bmatrix} -i & 1+i \\ 1-i & i \end{bmatrix} \tag{3.28}$$

3.2 FEA model of a thin plate in flexure

Firstly, in order to introduce variability into the host structure, a plate is analysed using a finite element model comprising plate bending elements. The element chosen for the analysis is a thin rectangular and non-conforming element, also known as the ACM element [**13**]. This element, Figure 3.2, was firstly presented by Adini [**75**] and then, from another expansion, by Melosh [**76**]. It has 12 degrees-of-freedom and the displacement function has a polynomial form in ξ and η with twelve terms. To ensure that the element is geometrically invariant, meaning that the displacement pattern is independent of the direction of the coordinate axes, a complete cubic with two quartic terms are added from the Pascal's triangle, [**13**]:

$$w = \alpha_1 + \alpha_2\xi + \alpha_3\eta + \alpha_4\xi^2 + \alpha_5\xi\eta + \alpha_6\eta^2 + \alpha_7\xi^3 + \alpha_8\xi^2\eta + \alpha_9\xi\eta^2 + \alpha_{10}\eta^3 + \alpha_{11}\xi^3\eta + \alpha_{12}\xi\eta^3 \tag{3.29}$$

where $\xi = \frac{x}{a}$ and $\eta = \frac{y}{b}$.

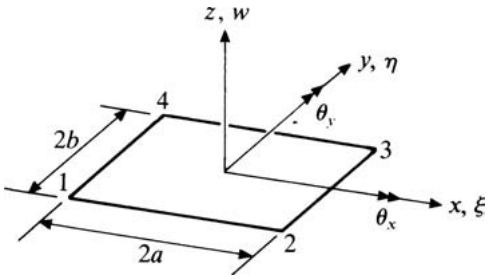

Figure 3.2 – Rectangular finite element for a plate.

(From: [**13**])

The ACM elements satisfy completeness and transverse deflection continuity, but they fail at normal slope continuity, it is only achieved at the four corner points [**77**]. Despite this fact, they are still used [**13**] and show good convergence when used for rectangular plates [**77**], the case of this analysis.

The element inertia and element stiffness matrices are given by Petyt [**13**], but it is worth noting the error pointed by Fabro (private conversation in January 8th, 2018) in the element stiffness matrix.

The element inertia matrix [**13**]:

$$[\boldsymbol{m}]_e = \frac{\rho hab}{6300}\begin{bmatrix} \boldsymbol{m}_{11} & \boldsymbol{m}_{21}^T \\ \boldsymbol{m}_{21} & \boldsymbol{m}_{22} \end{bmatrix} \tag{3.30}$$

where $[\boldsymbol{m}]_e$ is the element inertia matrix, ρ is the density, h is the plate's thickness and $2a$ and $2b$ are the size of the element's edges.

$$\boldsymbol{m}_{11} = \begin{bmatrix} 3454 & & & & & \\ 922b & 320b^2 & & & Sym & \\ -922a & -252ab & 320a^2 & & & \\ 1226 & 398b & -548a & 3454 & & \\ 398b & 160b^2 & -168ab & 922b & 320b^2 & \\ 548a & 168ab & 240a^2 & 922a & 252ab & 320a^2 \end{bmatrix} \tag{3.31}$$

$$\boldsymbol{m}_{22} = \begin{bmatrix} 3454 & & & & & \\ -922b & 320b^2 & & & Sym & \\ 922\text{a} & -252ab & 320a^2 & & & \\ 1226 & -398b & 548a & 3454 & & \\ -398b & 160b^2 & -168ab & -922b & 320b^2 & \\ -548a & 168ab & -240a^2 & -922a & 252ab & 320a^2 \end{bmatrix} \tag{3.32}$$

$$\boldsymbol{m}_{21} = \begin{bmatrix} 394 & 232b & -232a & 1226 & 548b & 398a \\ -232b & -120b^2 & 112ab & -548b & -240b^2 & -168ab \\ 232a & 112ab & -12a^2 & 398a & 168ab & 160a^2 \\ 1226 & 548b & -398a & 394 & 232b & 232a \\ -548b & -240b^2 & 168ab & -232b & -120b^2 & -112ab \\ -398a & -168ab & 160a^2 & -232a & -112ab & -120a^2 \end{bmatrix} \tag{3.33}$$

The element stiffness matrix [**13**]:

$$[\boldsymbol{k}]_e = \frac{Eh}{48(1-\nu^2)ab}\begin{bmatrix} \boldsymbol{k}_{11} & & Sym & \\ \boldsymbol{k}_{21} & \boldsymbol{k}_{22} & & \\ \boldsymbol{k}_{31} & \boldsymbol{k}_{32} & \boldsymbol{k}_{33} & \\ \boldsymbol{k}_{41} & \boldsymbol{k}_{42} & \boldsymbol{k}_{43} & \boldsymbol{k}_{44} \end{bmatrix} \tag{3.34}$$

where $[\boldsymbol{k}]_e$ is the element stiffness matrix, E is plate's Young's Modulus, h is the thickness of the plate, ν is the Poisson's ratio and $2a$ and $2b$ are the size of the element's edges.

$$\boldsymbol{k}_{11} = \begin{bmatrix} 4(\beta^2+\alpha^2)+\frac{2}{5}(7-2\nu) & & Sym \\ 2\left[2\alpha^2+\frac{1}{5}(1+4\nu)\right]b & 4\left[\frac{4}{3}\alpha^2+\frac{4}{15}(1-\nu)\right]b^2 & \\ 2\left[-2\beta^2-\frac{1}{5}(1+4\nu)\right]a & -4\nu ab & 4\left[\frac{4}{3}\beta^2+\frac{4}{15}(1-\nu)\right]a^2 \end{bmatrix} \quad (3.35)^{\dagger}$$

$$\boldsymbol{k}_{21} = \begin{bmatrix} -\left[2(2\beta^2-\alpha^2)+\frac{2}{5}(7-2\nu)\right] & 2\left[\alpha^2-\frac{1}{5}(1+4\nu)\right]b & 2\left[2\beta^2+\frac{1}{5}(1-\nu)\right]a \\ 2\left[\alpha^2-\frac{1}{5}(1+4\nu)\right]b & 4\left[\frac{2}{3}\alpha^2-\frac{4}{15}(1-\nu)\right]b^2 & 0 \\ -2\left[2\beta^2+\frac{1}{5}(1-\nu)\right]a & 0 & 4\left[\frac{2}{3}\beta^2-\frac{1}{15}(1-\nu)\right]a^2 \end{bmatrix} \quad (3.36)$$

$$\boldsymbol{k}_{31} = \begin{bmatrix} -\left[2(2\beta^2+\alpha^2)-\frac{2}{5}(7-2\nu)\right] & 2\left[-\alpha^2+\frac{1}{5}(1-\nu)\right]b & 2\left[\beta^2-\frac{1}{5}(1-\nu)\right]a \\ 2\left[\alpha^2-\frac{1}{5}(1-\nu)\right]b & 4\left[\frac{1}{3}\alpha^2+\frac{1}{15}(1-\nu)\right]b^2 & 0 \\ 2\left[-\beta^2+\frac{1}{5}(1-\nu)\right]a & 0 & 4\left[\frac{1}{3}\beta^2+\frac{1}{15}(1-\nu)\right]a^2 \end{bmatrix} \quad (3.37)$$

$$\boldsymbol{k}_{41} = \begin{bmatrix} 2(\beta^2-2\alpha^2)-\frac{2}{5}(7-2\nu) & 2\left[-2\alpha^2-\frac{1}{5}(1-\nu)\right]b & 2\left[-\beta^2+\frac{1}{5}(1+4\nu)\right]a \\ 2\left[2\alpha^2+\frac{1}{5}(1-\nu)\right]b & 4\left[\frac{2}{3}\alpha^2-\frac{1}{15}(1-\nu)\right]b^2 & 0 \\ 2\left[-\beta^2+\frac{1}{5}(1+4\nu)\right]a & 0 & 4\left[\frac{2}{3}\beta^2-\frac{4}{15}(1-\nu)\right]a^2 \end{bmatrix} \quad (3.38)$$

where $\alpha = a/b$ and $\beta = b/a$.

And [**13**] [**78**]:

$$\begin{aligned} &\boldsymbol{k}_{22} = \boldsymbol{I}_3^T \boldsymbol{k}_{11} \boldsymbol{I}_3; \\ &\boldsymbol{k}_{32} = \boldsymbol{I}_3^T \boldsymbol{k}_{41} \boldsymbol{I}_3; \quad \boldsymbol{k}_{33} = \boldsymbol{I}_1^T \boldsymbol{k}_{11} \boldsymbol{I}_1; \\ &\boldsymbol{k}_{42} = \boldsymbol{I}_3^T \boldsymbol{k}_{31} \boldsymbol{I}_3; \quad \boldsymbol{k}_{43} = \boldsymbol{I}_1^T \boldsymbol{k}_{21} \boldsymbol{I}_1; \quad \boldsymbol{k}_{44} = \boldsymbol{I}_2^T \boldsymbol{k}_{11} \boldsymbol{I}_2; \end{aligned} \quad (3.39)$$

where $\boldsymbol{I}_1 = \begin{bmatrix} -1 & 0 & 0 \\ 0 & 1 & 0 \\ 0 & 0 & 1 \end{bmatrix}$, $\boldsymbol{I}_2 = \begin{bmatrix} 1 & 0 & 0 \\ 0 & -1 & 0 \\ 0 & 0 & 1 \end{bmatrix}$ and $\boldsymbol{I}_3 = \begin{bmatrix} 1 & 0 & 0 \\ 0 & 1 & 0 \\ 0 & 0 & -1 \end{bmatrix}$.

Once the element inertia $[\boldsymbol{m}]_e$ and stiffness $[\boldsymbol{k}]_e$ matrices are built, the assembly process to move from local nodes to global nodes and build the global inertia $[\boldsymbol{M}]$ and stiffness $[\boldsymbol{K}]$ matrices is made by pre-multiplying them by a local-to-global nodes matrix that consists of zeros and ones. Natural frequencies and mode shapes can then be found solving the $[\boldsymbol{K}]\boldsymbol{w} = \omega^2[\boldsymbol{M}]\boldsymbol{w}$ eigenproblem

---

† In M. Petyt's book [**13**], two elements in this matrix are wrongly given as $\boldsymbol{k}_{11}(3,1) = 2\left[-2\beta^2 - \frac{1}{5}(1-4\nu)\right]a$ and $\boldsymbol{k}_{11}(3,3) = 4\left[\frac{4}{3}\beta^2 + \frac{1}{15}(1-\nu)\right]a^2$.

[**79**] [**80**]. The mobilities are then found by substituting the natural frequencies and mode shapes into Equation (3.2).

3.3 Perturbation method for a plate with slowly varying properties

Re-analysis methods are used to minimise computational costs, as they avoid solving the eigenvalue/vector problem in modal analysis by computing the fully dynamic response for one (or a few) cases and performing approximations [**1**] in the form of a perturbation method [**81**] or an interpolation method [**82**].

These methods can approximate the variation of the dynamic response in the presence of varying model parameters. The response of the new system can be updated from the previously computed response or the system modal parameters can be updated from previously computed modal parameters, which then allows one to compute the new response [**1**].

The simplest approximation that can be used to minimise computational costs is a linear approximation. In order to keep accuracy when using linear approximations, one has to ensure that the rate of change of the variable being approximated is also close to following a linear behaviour. This fact limits the linear approximation to the modal parameters, since the rate of change of the frequency response is very non-linear, especially around resonances [**1**].

The perturbation method was first introduced by Liu et al. [**81**] to analyse systems subject to uncertainties. If the response of the system for a given set of parameters is known, the method states that the variation in the response due to uncertain parameters can be calculated through first order approximations, assuming that the variations are small. Also, modal shapes are only significantly affected by large changes in the geometry of a system. Uncertainties in the mass or stiffness of the system will only change the frequencies where the mode resonates [**1**]. Since this work deals with slowly varying random properties with small dispersion, the perturbation method is considered to be adequate.

Assuming mass-normalised eigenvectors, the perturbation functions for undamped modes are given by [**1**] [**83**]:

$$\widetilde{\Delta}\lambda_m = \boldsymbol{\phi}_m^T\left[\Delta[\boldsymbol{K}] - \lambda_m\Delta[\boldsymbol{M}]\right]\boldsymbol{\phi}_m \tag{3.40}$$

where $\widetilde{\Delta}\lambda_m$ is the change in the m^{th} eigenvalue, $\boldsymbol{\phi}_m$ is the unperturbed m^{th} eigenvector, λ_m is the unperturbed m^{th} eigenvalue and $\Delta[\boldsymbol{K}]$ and $\Delta[\boldsymbol{M}]$ are the respective differences in the global stiffness and inertia matrices.

$$\widetilde{\omega}_m = \sqrt{\lambda_m + \widetilde{\Delta}\lambda_m} \tag{3.41}$$

where $\widetilde{\omega}_m$ is the perturbed natural frequency.

$$\widetilde{\Delta}\boldsymbol{\phi}_m = \frac{1}{2}(\boldsymbol{\phi}_m^T \Delta[\boldsymbol{M}]\boldsymbol{\phi}_m) - \sum_{i \neq m} \frac{\boldsymbol{\phi}_i^T [\Delta[\boldsymbol{K}] - \lambda_m \Delta[\boldsymbol{M}]]\boldsymbol{\phi}_m}{\lambda_i - \lambda_m} \boldsymbol{\phi}_i \tag{3.42}$$

where $\widetilde{\Delta}\boldsymbol{\phi}_m$ is the change in the m^{th} eigenvector.

As in the case of the one-dimensional waveguide, this chapter considers that only the Young's modulus of the plate is varying and, therefore, only the stiffness matrix changes. The midpoint method was first introduced by Der Kiureghian and Ke [**84**] and it uses a single random variable defined as the value of the field at the centroid of each element to approximate the random field in each element [**63**]. In this case, the sampled value for the Young's modulus from the random field for each one of the elements is then used in Equation (3.34) to find the element stiffness matrix and, once all the element stiffness matrices are defined, the new global stiffness matrix can be assembled. From that, it is possible to calculate the differences in the global stiffness matrix as:

$$\Delta[\boldsymbol{K}] = [\widetilde{\boldsymbol{K}}] - [\boldsymbol{K}] \tag{3.43}$$

where $[\widetilde{\boldsymbol{K}}]$ is the new global stiffness matrix from the sampled random field.

The global mass matrix $[\boldsymbol{M}]$ was not perturbed and the perturbed modal shapes $\Delta\boldsymbol{\phi}_m = \boldsymbol{\phi}_m + \widetilde{\Delta}\boldsymbol{\phi}_m$ are not mass normalised. They can be mass normalised to ensure that $\Delta\boldsymbol{\Phi}_m^T[\boldsymbol{M}]\Delta\boldsymbol{\Phi}_m = 1$ [**85**] and the mass normalised perturbed modal shape $\Delta\boldsymbol{\Phi}_m$ is given by:

$$\Delta\boldsymbol{\Phi}_m = \Delta\boldsymbol{\phi}_m / \Delta\boldsymbol{\phi}_m^T[\boldsymbol{M}]\Delta\boldsymbol{\phi}_m \tag{3.44}$$

Once again, the slowly varying random field is described by the Karhunen-Loève expansion and using separable autocorrelation functions, which allows the random field to be characterized by a multiplication of the expansion in the x direction and the expansion in the y direction [**61**].

In this work, the whole plate has variabilities associated with its Young's modulus, so all of the degrees-of-freedom are perturbed. The computational cost of the perturbation method in this case scales as $2(n_{modes} + 1)\mathcal{O}(N_{dof})$ operations while the eigenproblem scales with $\mathcal{O}(N_{dof}^2)$, where n_{modes} is the number of modes to be calculated and it always much smaller than the number of degrees-of-freedom N_{dof} of the system. Therefore, finding the perturbed modes and natural frequencies is requires only a small fraction of the computational power necessary to solve the eigenproblem [**1**].

3.4 Numerical results for a homogeneous plate and uncertain beam

This section presents the numerical analysis carried out to investigate the effects of coupling a finite beam with a strongly correlated random field for the Young's modulus to a homogeneous plate. This analysis is analogous to the previous chapter, but in this chapter, since the waves are reflected at the boundaries, it is possible to notice how the slowly varying random field affects the natural frequencies and modes. Once again, effects of different spreading factors and nominal values of the Young's modulus of the beam are presented. The absolute value of the correlation lengths analysed are different from those used in Chapter 2, but when b_L is normalised by the observed length (i.e., the distance between the first and the last points analysed in the case of the infinite structures) of the beam they are the same in both chapters. The nominal properties for beam and plate are given in Table 3.2, whilst the properties for the slowly varying beam are summarised in Table 3.3. The geometry of the system analysed is shown in Figure 3.3. For evaluation of the required mobilities, the uncertain beam is treated using the WKB approximation. For the plate, a perturbation method is used for the natural frequencies and modes, which are then used in Equation (3.2).

Table 3.2 – Nominal properties of the finite beams and plates.

Properties	Value
Density (kg/m^3)	7850
Plate thickness (m)	0.002
Length y – plate (m)	0.69
Length x – plate (m)	1.5
Plate Young's modulus (GPa)	200
Beam cross-sectional side (m)	0.02
Length beam (m)	1.0
Spacing between connections	0.21875
Poisson's ratio	0.30
Loss factor	0.001

Table 3.3 – Properties for the slowly varying beam.

Property	Case 1	Case 2	Case 3	Case 4
Nominal Young's modulus of the beam, E_b	146 GPa	0.137 GPa	0.137 GPa	0.137 GPa
Correlation length, b_L	0.5 m	0.5 m	0.25 m	0.5 m
Number of modes KL expansion	16	16	16	16
Spreading factor, σ	0.1	0.1	0.1	0.2

In all cases considered in this section, a point force was applied at the central attachment on the plate. Modes up to 4000 Hz for the plate were considered, therefore, the analysis of coupled

structures will be limited from 1 Hz to 2000 Hz. Figure 3.4 shows the input mobilities of the nominal cases for the individual beam, plate and also the coupled system.

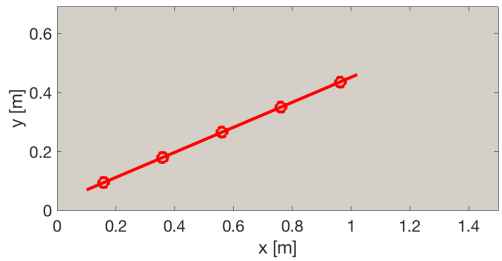

Figure 3.3 – Geometry of the coupled system.

One metre long beam (in red) attached to a rectangular homogeneous plate (in gray) through 5 point connections (O).

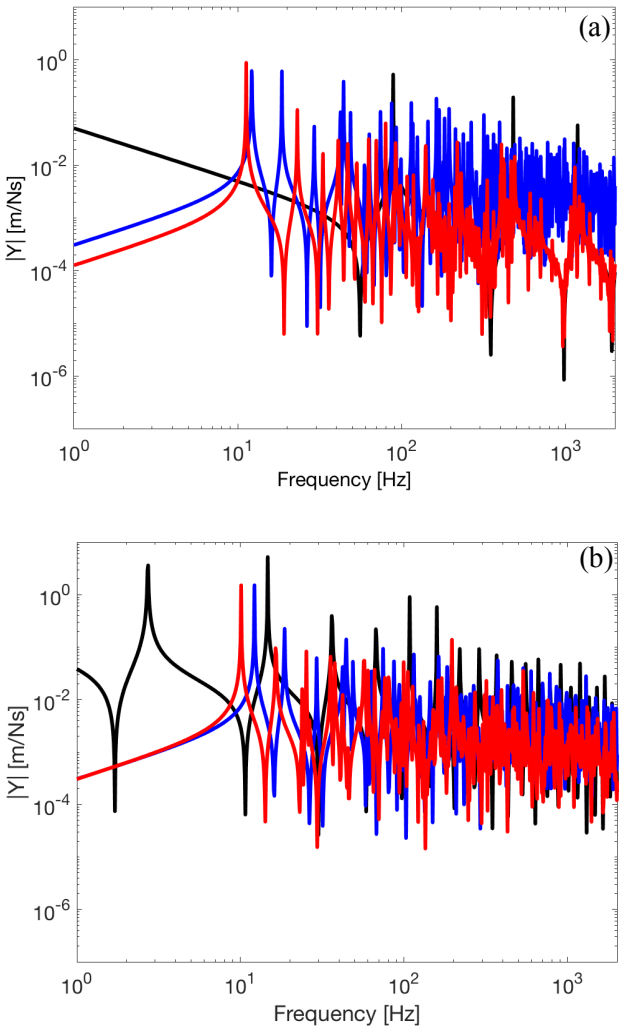

Figure 3.4 – Input mobilities of the nominal cases.

In (a), considering the beam with nominal Young's modulus of 146 GPa (case 1), while in (b), the beam with nominal Young's modulus of 0.137 GPa (cases 2, 3 and 4). In both cases, ▬ is the input mobility of the attached beam, ▬ is the input mobility of the host plate and ▬ is the input mobility of the coupled system.

It is possible to see how at lower frequencies the connected beam acts as an added mass, shifting down the natural frequencies of the coupled system when compared to the response of the

plate alone. At higher frequencies, the connection of the beam reduces the amplitude levels of the response of the coupled system. The coupled beam-plate system now possesses a higher modal density than the original plate. The observed effect is that the original plate resonant response is now shared into more modal response, with an apparent reduction in the peak resonance amplitudes. Some observers have considered this to be analogous to having additional damping.

The results for case 1, nominal $E_b = 146$ GPa, correlation length $b_L = 0.5$ m, $N_{KL} = 16$ and $\sigma = 0.1$, is given in Figure 3.5. Figure 3.6 summarises the results of the analysis of case 2, nominal $E_b = 0.137$ GPa, correlation length $b_L = 0.5$ m, $N_{KL} = 16$ and $\sigma = 0.1$, whilst the results of case 3, the same as case 2, but $b_L = 0.25$ m, can be seen in Figure 3.7 and finally, Figure 3.8 shows the result for case 4, nominal $E_b = 0.137$ GPa, correlation length $b_L = 0.5$ m, $N_{KL} = 16$ and $\sigma = 0.2$.

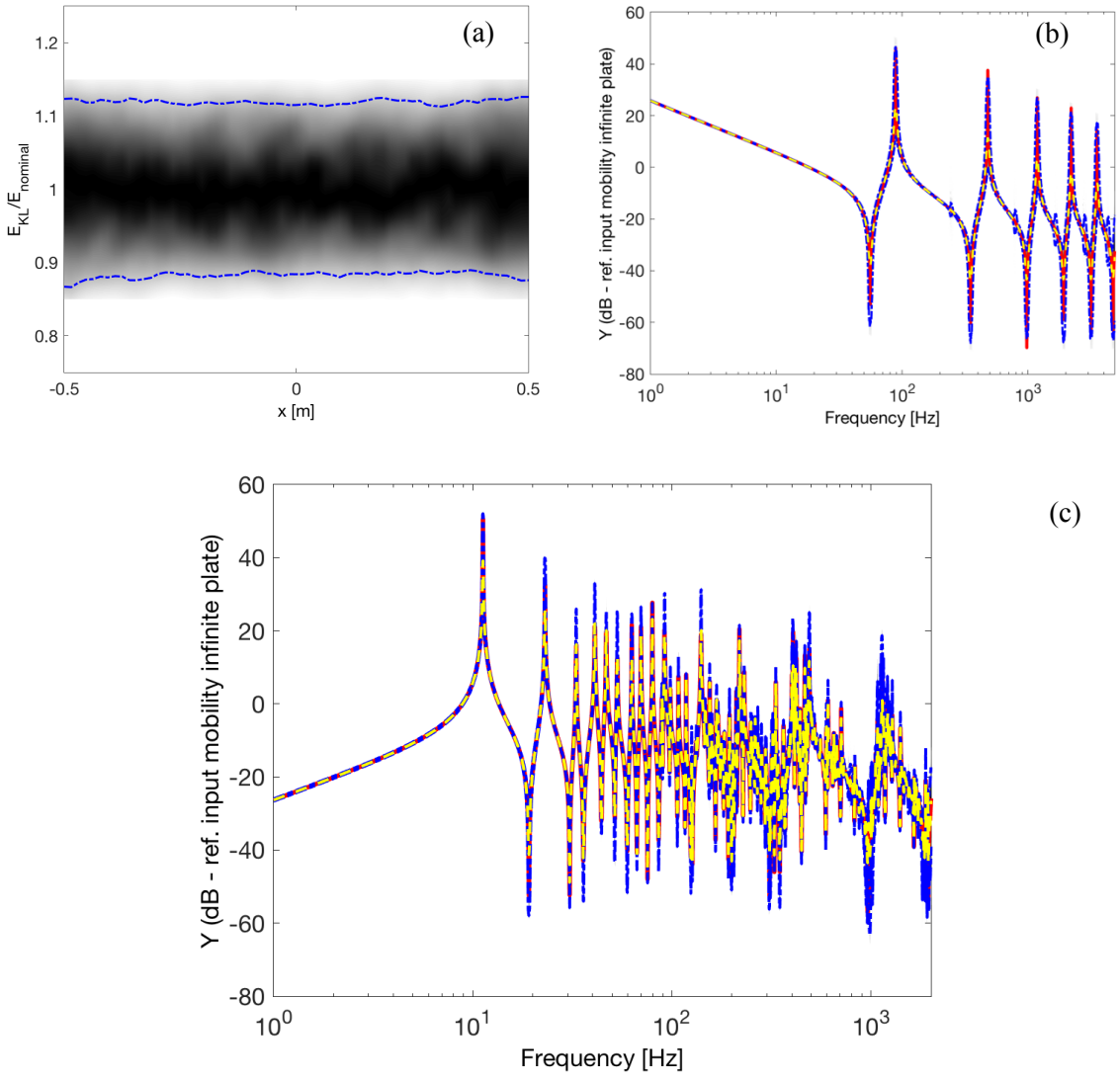

Figure 3.5 – Slowly varying beam and homogeneous plate: Case 1.

Case 1: nominal $E_b = 146$ GPa, correlation length $b_L = 0.5$ m, $N_{KL} = 16$ and $\sigma = 0.1$. In (a), the colormap is the normalised distribution of the Young's modulus along the length of the beam and — · — limits the region where 95% of the samples are contained within. In (b), the input mobility of the connected beam — is the beam with nominal properties, the colormap is the normalised distribution of the mobilities using the 1000 slowly varying Young's moduli, — — is the mean of the responses and — · — limits the region where 95% of the response is. In (c), the input mobility

of the coupled system; ▬ is the connected system with nominal properties, the colormap is the normalised distribution of the mobilities using the 1000 slowly varying Young's moduli, ▬ ▬ is the mean of the responses and ▬ · ▬ limits the region where 95% of the response is.

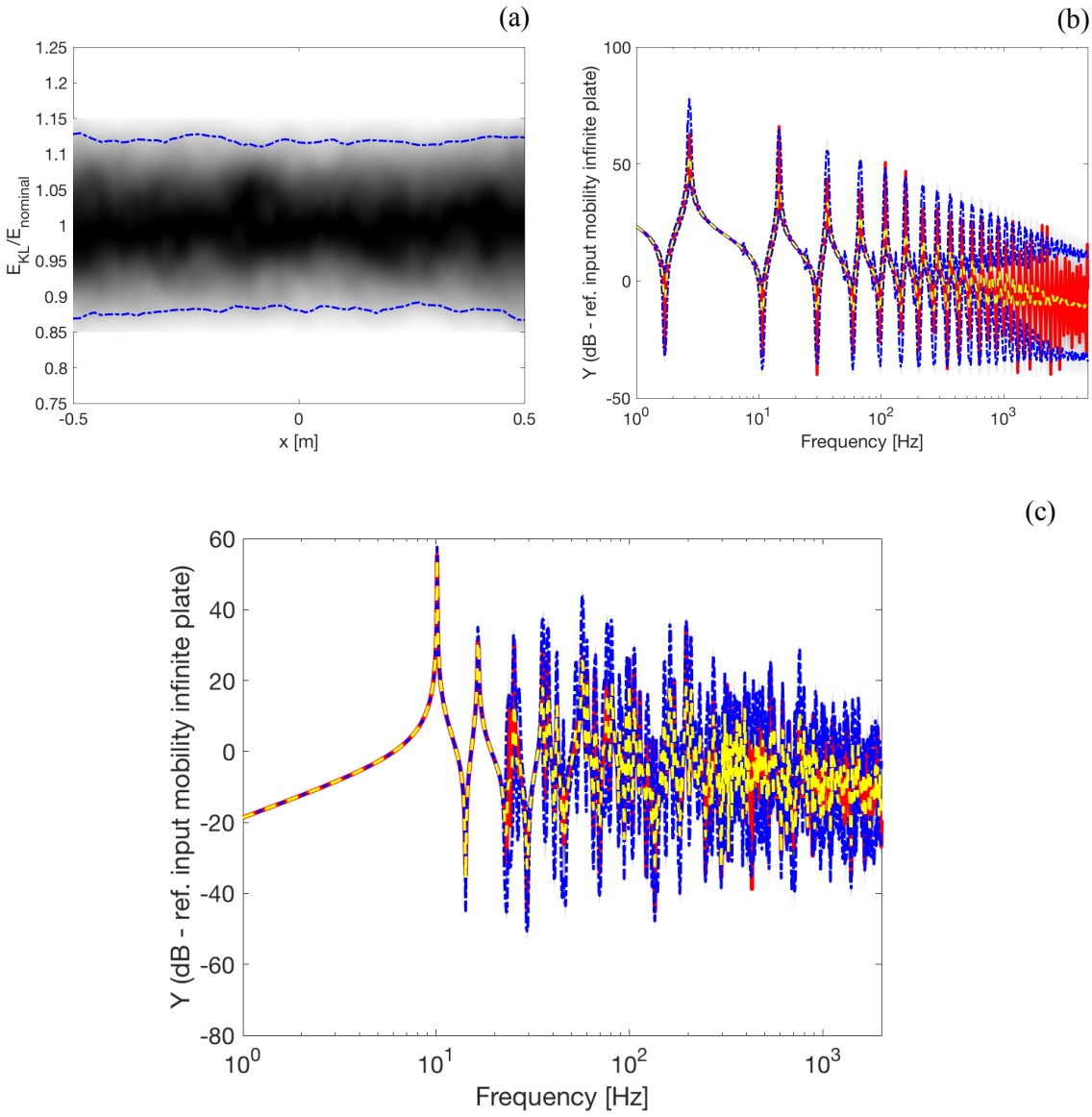

Figure 3.6 – Slowly varying beam and homogeneous plate: Case 2.

Case 2: nominal $E_b = 0.137$ GPa, correlation length $b_L = 0.5$ m, $N_{KL} = 16$ and $\sigma = 0.1$. In (a), the colormap is the normalised distribution of the Young's modulus along the length of the beam and ▬ · ▬ limits the region where 95% of the samples are contained within. In (b), the input mobility of the connected beam ▬ is the beam with nominal properties, the colormap is the normalised distribution of the mobilities using the 1000 slowly varying Young's moduli, ▬ ▬ is the mean of the responses and ▬ · ▬ limits the region where 95% of the response is. In (c), the input mobility of the coupled system; ▬ is the connected system with nominal properties, the colormap is the normalised distribution of the mobilities using the 1000 slowly varying Young's moduli, ▬ ▬ is the mean of the responses and ▬ · ▬ limits the region where 95% of the response is.

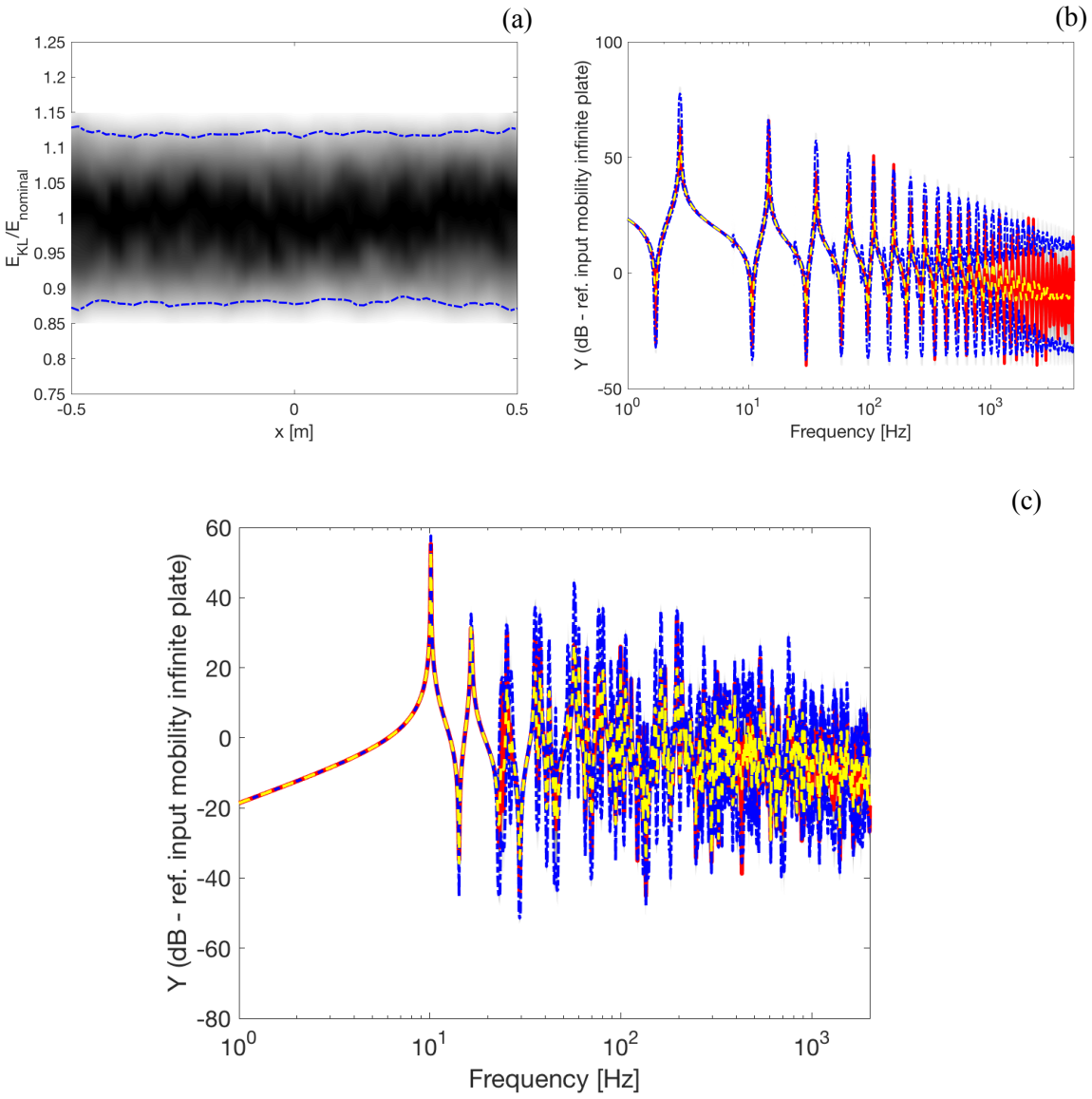

Figure 3.7 – Slowly varying beam and homogeneous plate: Case 3.

Case 3: nominal $E_b = 0.137$ GPa, correlation length $b_L = 0.25$ m, $N_{KL} = 16$ and $\sigma = 0.1$. In (a), the colormap is the normalised distribution of the Young's modulus along the length of the beam and — · — limits the region where 95% of the samples are contained within. In (b), the input mobility of the connected beam — is the beam with nominal properties, the colormap is the normalised distribution of the mobilities using the 1000 slowly varying Young's moduli, — — is the mean of the responses and — · — limits the region where 95% of the response is. In (c), the input mobility of the coupled system; — is the connected system with nominal properties, the colormap is the normalised distribution of the mobilities using the 1000 slowly varying Young's moduli, — — is the mean of the responses and — · — limits the region where 95% of the response is.

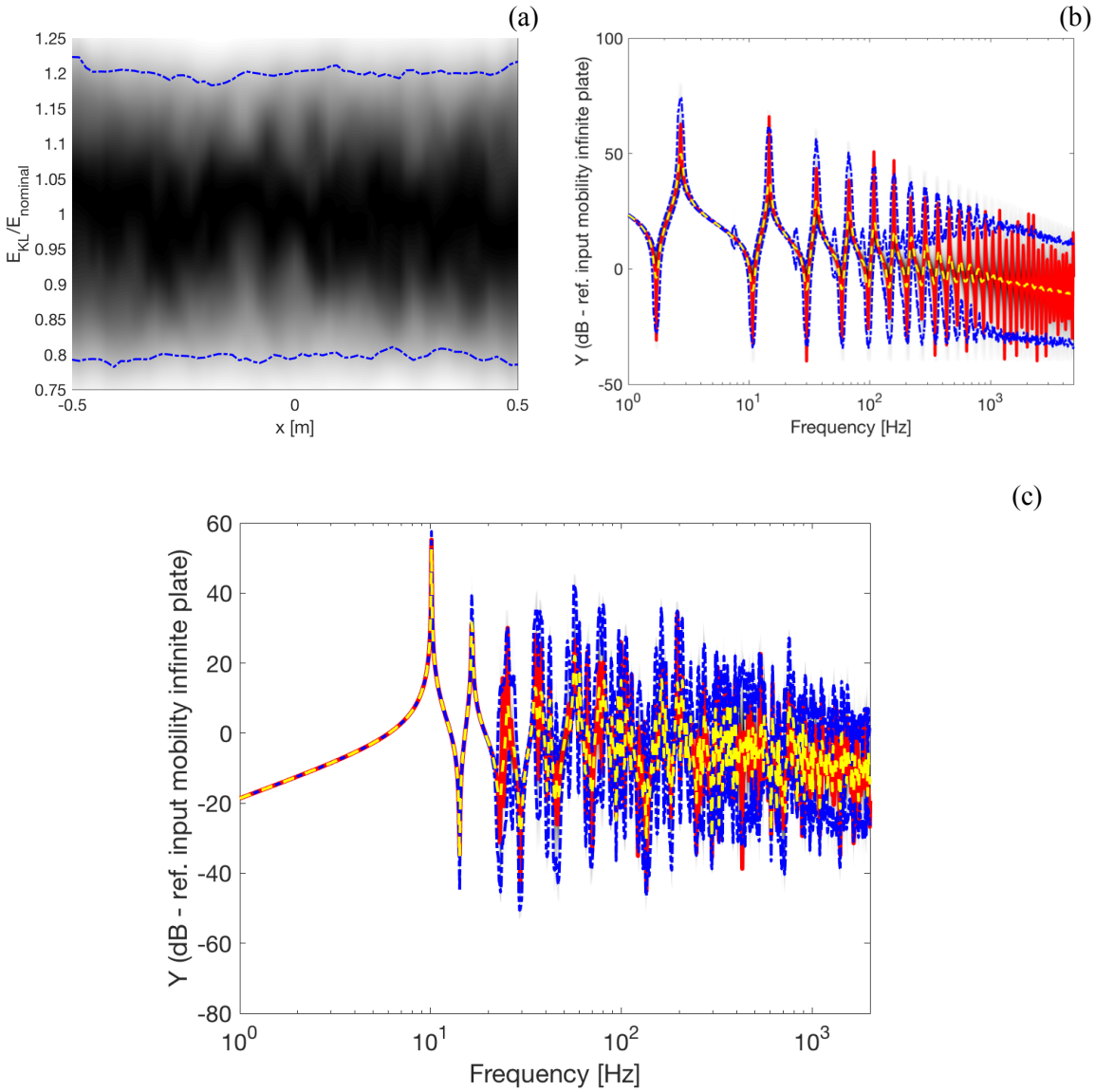

Figure 3.8 – Slowly varying beam and homogeneous plate: Case 4.

Case 4: nominal $E_b = 0.137$ GPa, correlation length $b_L = 0.5$ m, $N_{KL} = 16$ and $\sigma = 0.2$. In (a), the colormap is the normalised distribution of the Young's modulus along the length of the beam and — · — limits the region where 95% of the samples are contained within. In (b), the input mobility of the connected beam — is the beam with nominal properties, the colormap is the normalised distribution of the mobilities using the 1000 slowly varying Young's moduli, — — is the mean of the responses and — · — limits the region where 95% of the response is. In (c), the input mobility of the coupled system; — is the connected system with nominal properties, the colormap is the normalised distribution of the mobilities using the 1000 slowly varying Young's moduli, — — is the mean of the responses and — · — limits the region where 95% of the response is.

In order to more easily see the effects of the slowly varying properties, the responses of the coupled system are once again given in a dB scale referenced to the nominal case.

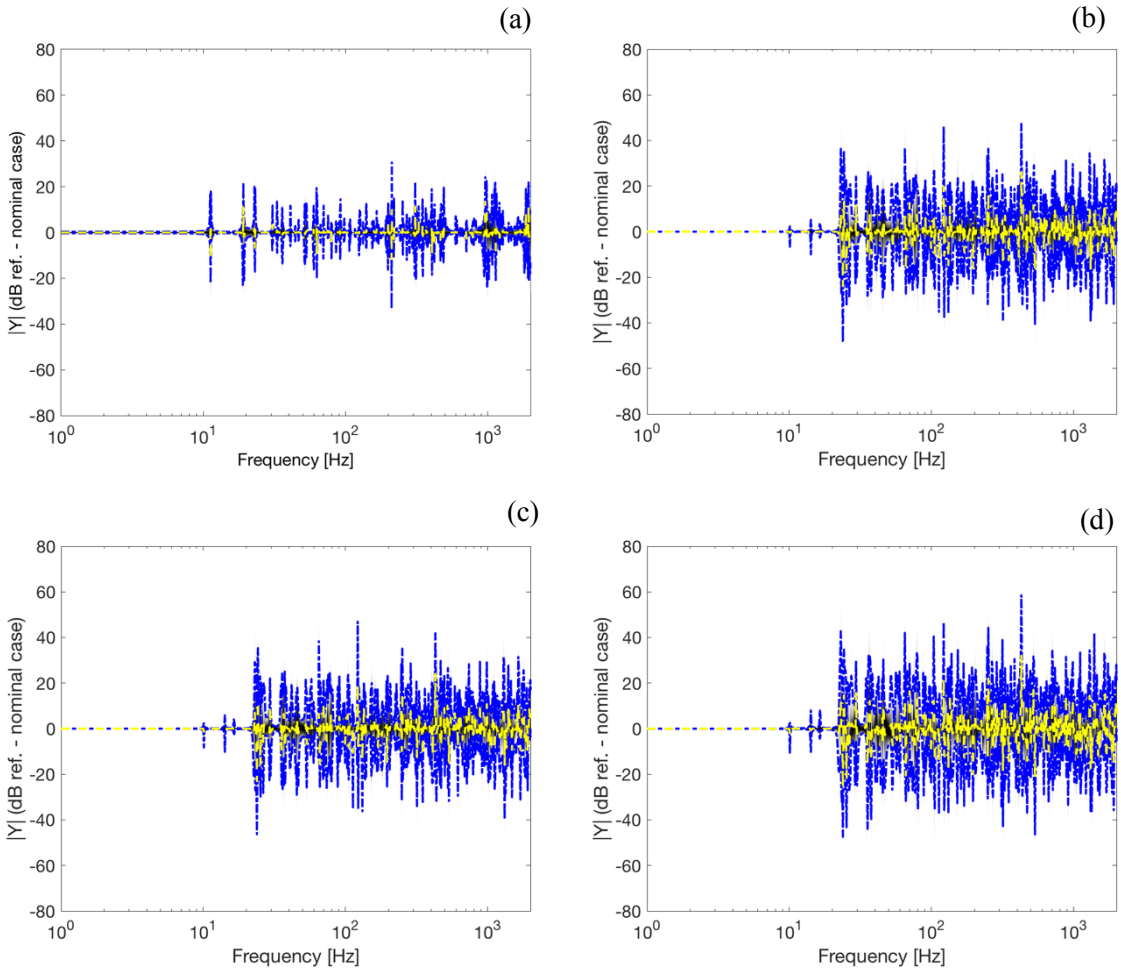

Figure 3.9 – Effects of the slowly varying Young's moduli of the attached beams.

The response of the system in the presence of different slowly varying beam in a dB scale referenced to the system connected to the nominal beam. In (a), case 1; nominal $E_b = 146$ GPa (stiffer beam), correlation length $b_L = 0.5$ m, $N_{KL} = 16$ and $\sigma = 0.1$. In (b), case 2; nominal nominal $E_b = 0.137$ GPa (flexible beam), correlation length $b_L = 0.5$ m, $N_{KL} = 16$ and $\sigma = 0.1$. In (c), case 3; nominal $E_b = 0.137$ GPa, correlation length $b_L = 0.25$ m, $N_{KL} = 16$ and $\sigma = 0.1$. In (d), case 4; nominal $E_b = 0.137$ GPa, correlation length $b_L = 0.5$ m, $N_{KL} = 16$ and greater spreading $\sigma = 0.2$. In all cases, the colormap is the normalised distribution of the mobilities using the 1000 slowly varying Young's moduli, — — is the mean of the responses and — · — limits the region where 95% of the response is.

The mass of the added beam is the same in all cases. At lower frequencies, the effect of the added mass is more dominant in the case of the more flexible beams, as it can be seen by the smaller 95% envelopes in the dB scale referenced to the nominal case. The stiffer beam has the effect of added mass along with adding stiffness to the coupled system, and therefore, the first natural frequencies of the coupled system are more sensitive to the different slowly random fields for the Young's modulus, e.g. Case 1 versus case 2 for instance at around 10 Hz. As in the case of infinite structures, the system with a more flexible attachment is more susceptible to variability in the presence of an uncertain stiffness of the beam. Comparing cases 2 and 4, as the level of dispersion from the nominal case increases, the differences in the response of the coupled system also increases. The correlation length might affect individual samples, but once numerous cases are analysed the statistical properties of the coupled system are the same, i.e. case 2 versus case 3.

The convergence of the statistical properties of the response of the coupled system are analysed for the case where most uncertainty is present, case 4. In this chapter, the analysis is made by comparing how the value of the mean changes when a different number of samples are considered, ranging from only 3 samples to the full set of 1000 samples. For a more convenient view, the convergence is considered to be given by $\mu_{MC} = 20\log\left(\frac{|\mu_{nsamples}(Y_{coupled})|}{|\mu_{1000samples}(Y_{coupled})|}\right)$, so a value of 0 is desired. The result of the convergence is shown in Figure 3.10.

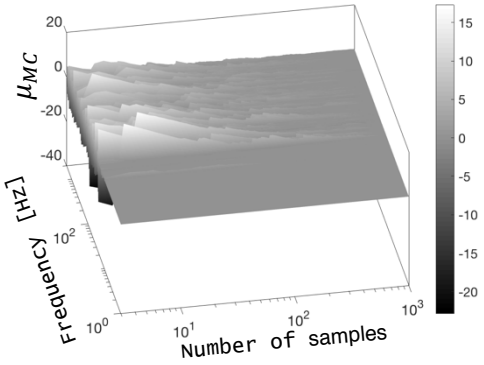

Figure 3.10 – Convergence of the mean: Case 4.

3.5 Numerical results for an uncertain plate

This section presents the results when variability is introduced into the plate. The solutions are calculated perturbing the eigenvalues and eigenvectors found using a modal analysis through a model generated using Finite Element analysis. Firstly, results of a perturbed two degrees-of-freedom are shown in order to give a grasp of how the method works. Secondly, a comparison of the same uncertain plate solved using via solving the eigenproblem associate with the FEA versus the solution found perturbing the homogeneous plate. Lastly, the solutions of the perturbed plate are used to calculate the mobility matrix for the plate and couple it to a beam. To summarise, the uncertain plate is considered to have a random Young's modulus field described by the KL expansion, which leads to small variations in the stiffness matrices and the perturbation method is used to find the new mode shapes.

3.5.1 *Introductory results for Perturbation Method*

Aiming to understand how the perturbation method works, a simple example comprising a 2-DOF system, Figure 3.11, is tested. This example is an adaption of the damped system in Mochales [**1**].

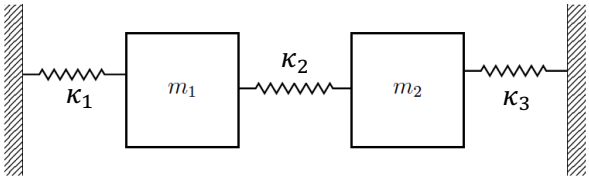

Figure 3.11 – System with two degrees-of-freedom.

Adapted from [**1**] and m_1 = 0.12 kg, m_1 = 0.1 kg, κ_1 = 1.5 kN/m, κ_2 = 1.0 kN/m and κ_3 = 2.0 kN/m.

The stiffness of the spring κ_3 is allowed to vary ±50% around its nominal value in 10% steps. For each one of the cases, the eigenvalues and eigenvectors associate with the free-vibration equations $\begin{bmatrix} m_1 & 0 \\ 0 & m_2 \end{bmatrix} \ddot{\boldsymbol{x}} + \begin{bmatrix} \kappa_1 + \kappa_2 & -\kappa_2 \\ -\kappa_2 & \kappa_2 + \kappa_3 \end{bmatrix} \boldsymbol{x} = \boldsymbol{0}$ are solved and then compared to the values found perturbing the nominal case. The results for the natural frequencies are shown in Figure 3.12, whilst the modal shapes are given in Figure 3.13.

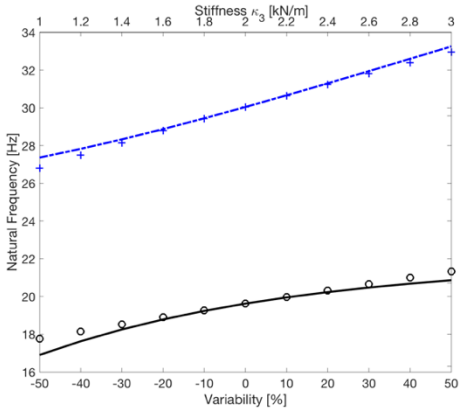

Figure 3.12 – Perturbation method: Variation in the natural frequencies.

In ▬ the first natural frequency from solving the eigen problem and in ▬ · ▬ the second natural frequency; + is the first natural frequency from the perturbation method and O is the second natural frequency from the perturbation method.

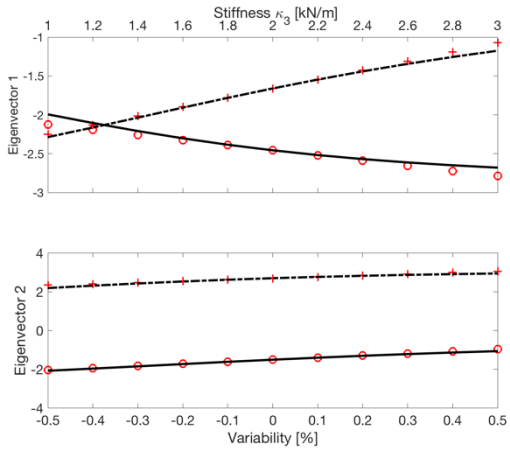

Figure 3.13 – Perturbation method: Variation in the modal shapes.
Modal displacement of the first mass from the eigenproblem ▬ and the second mass ▬ · ▬; modal displacements of the first mass from the perturbation method + and of the second mass O.

The perturbation method shows good agreement with the actual solutions of the eigenproblem, especially in the region of small dispersion, the region where this work is focused; ±20% around its nominal value.

3.5.2 *Comparison Eigenproblem versus Perturbation Method*

Although the results from the previous section show that the perturbation method is capable of accurately representing the natural frequencies and mode shapes in the presence of small dispersion around the nominal values of a property, a comparison applied to a plate with a slowly varying random Young's modulus was also carried out. A comparison was made between a modal analysis using FEA and the perturbation method.

The mesh used in the FEA model is shown in Figure 3.14 and it has 70 elements along the x direction and 32 in the y direction. The elements used were described in the section 3.2. The nominal properties of the plate are given in Table 3.4.

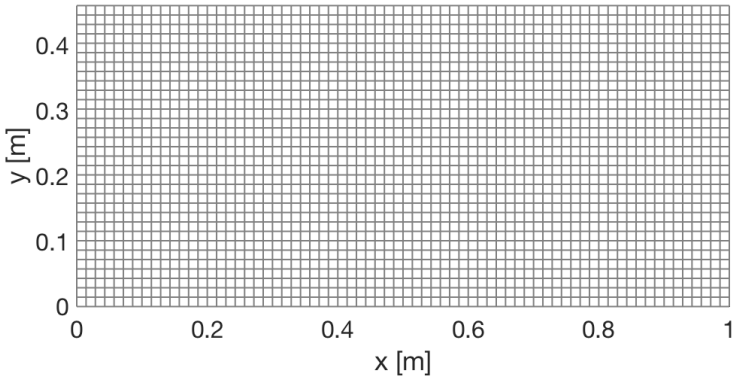

Figure 3.14 – Mesh used in the finite element analysis.

Table 3.4 – Nominal properties of the plate.

Properties	Value
Density (kg/m^3)	7850
Plate thickness (m)	0.002
Length y (m)	0.460
Length x (m)	1.0
Plate Young's modulus (GPa)	200
Poisson's ratio	0.30
Loss factor	0.001

Firstly, to validate the model, a brief comparison is shown between the results using the FE model and the analytical solutions. A modal analysis was performed to check the natural frequencies and modal shapes. The results are seen in Figure 3.15. Also, modes of the plate were considered up to around 4000 Hz, with a total of 290 modes. The analysis is then limited to the range of 1 Hz to 2000 Hz. In terms of the size of the elements, they were calculated considering that the plate's bending wavenumber is given by $k_B^p = \sqrt[4]{\frac{m}{B}}\sqrt{\omega} = \sqrt[4]{\frac{12\rho(1-\nu^2)}{Eh^2}}\sqrt{\omega}$, and that the wavelength is given

by $\lambda_B^p = \frac{2\pi}{k_B^p}$, which results to around 5 elements per wavelength at the highest frequency. Figure 3.16 shows the number of wavelength λ per elements in the x and y directions.

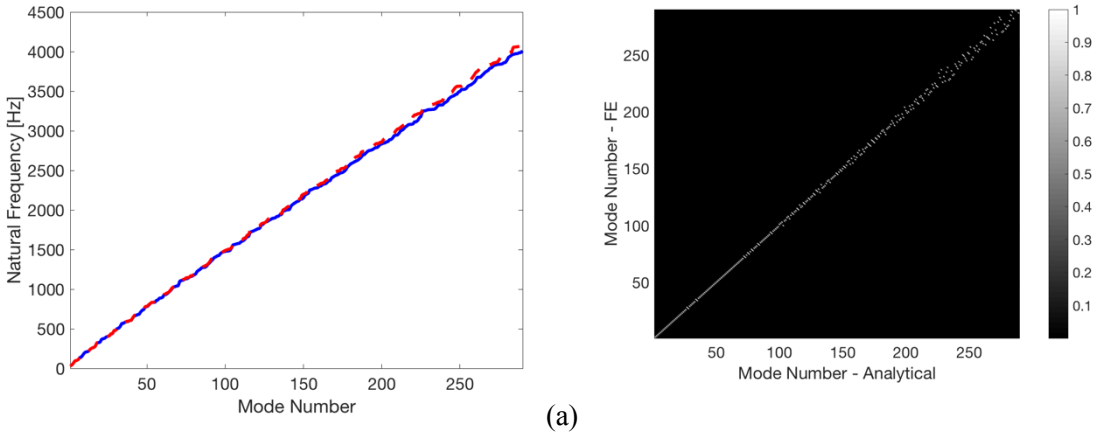

Figure 3.15 – Modal analysis of a plate: Analytical versus FEM

Simply supported plate. In (a), the first 290 natural frequencies of a plate; ▬ are the natural frequencies from the FE model and ▬ ▬ are the natural frequencies from analytical expressions. In (b), the Modal Assurance criterion (MAC) [**86**] between the modes extracted from the FEM and the analytical modal shapes.

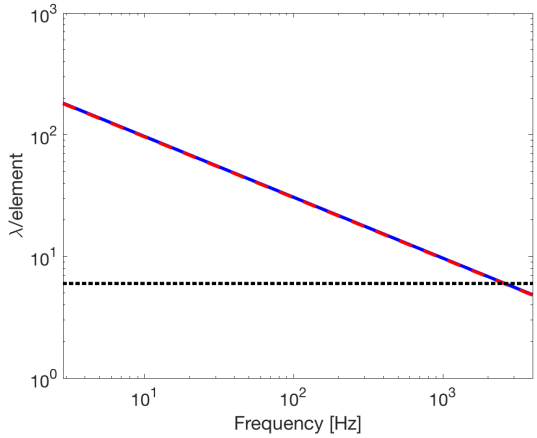

Figure 3.16 – Wavelength ratios per element length for the frequency range of analysis.

In ▬ relative to the x direction; in ▬ ▬ relative to the y direction and · · · is the line of 6 elements per wavelength.

Once the results are considerate satisfactory, it was possible to move onto the comparison of the solutions from the perturbation method versus the solutions from solving the eigenproblem for a plate with a slowly varying Young's modulus field. The KL expansion is used to describe a strongly correlated random field for the Young's modulus. The exponentially decaying autocorrelation function is used again to allow the use of analytical solutions and to describe the field as the multiplication of two one-dimensional expansions. The parameters used in the expansion are correlation length in the x direction $b_{Lx} = 0.5l_x$, correlation length in the y direction $b_{Ly} = 0.5l_y$, dispersion parameter $\sigma = 0.1$, total number of modes of the expansion in the x direction $N_{KLx} = 8$, total number of modes of the expansion in the y direction $N_{KLy} = 8$. The first 12 eigenfunctions of

the KL expansion are shown in Figure 3.17 and the normalised eigenvalues are shown in Figure 3.18. Finally, the random Young's modulus of the uncertain plate is shown in Figure 3.19.

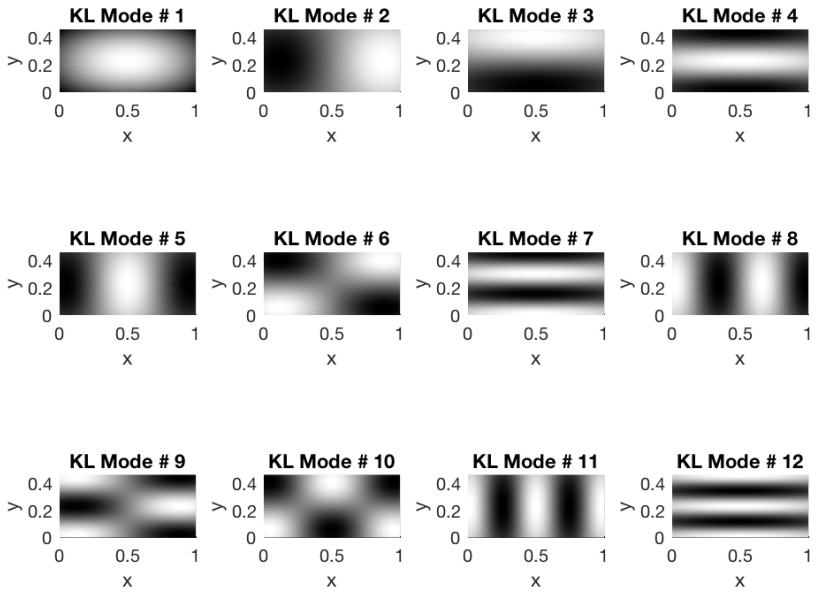

Figure 3.17 – First 12 eigenvectors (modes) of the KL expansion.

Parameters of the expansion: $b_{Lx} = 0.5l_x$, $b_{Ly} = 0.5l_y$, $\sigma = 0.1$, $N_{KLx} = 8$, $N_{KLy} = 8$.

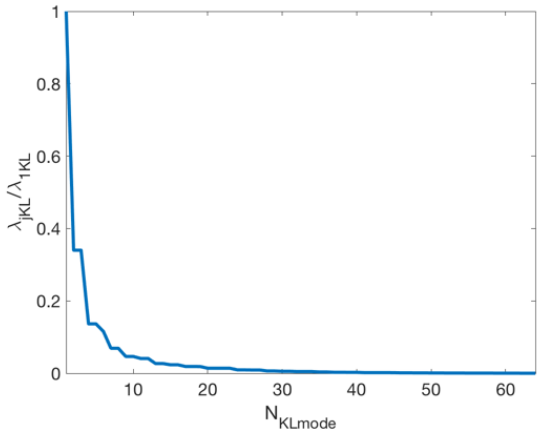

Figure 3.18 – Normalised eigenvectors of the KL expansion. Convergence of the expansion.

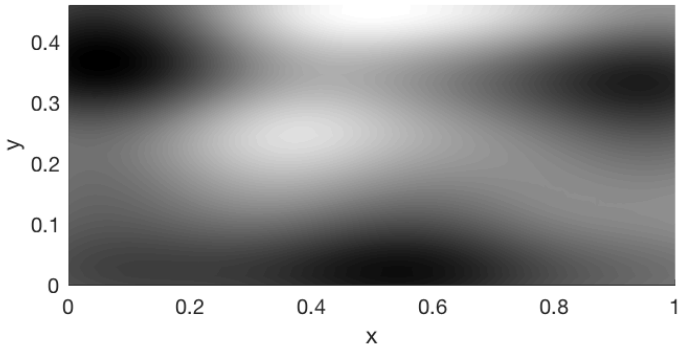

Figure 3.19 – Random field simulation for the Young's modulus of the plate.

Parameters of the expansion: $b_{Lx} = 0.5l_x$, $b_{Ly} = 0.5l_y$, $\sigma = 0.1$, $N_{KLx} = 8$, $N_{KLy} = 8$.

The random field is described at the nodes of the elements, the four corners of each element. The midpoint method is then used to interpolate the random field and find a single value for the random field at the centroid of each element. This value is then used to calculate the individual element stiffness matrix followed by the assembly of the global stiffness matrix. The interpolated random field along with the FEA mesh is shown in Figure 3.20.

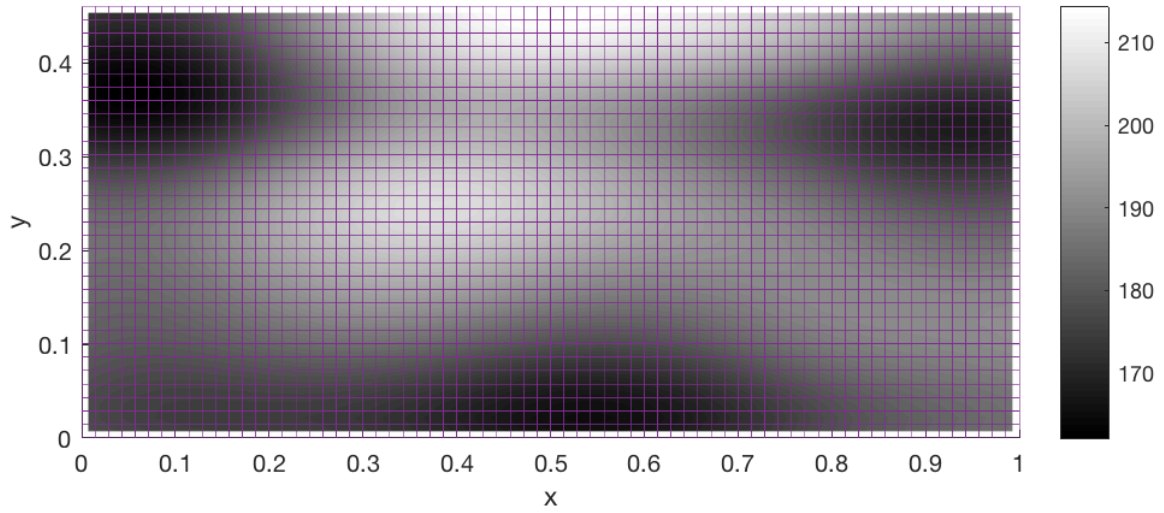

Figure 3.20 – Slowly varying Young's modulus via the midpoint interpolation method.
Nominal $E_p = 200$ GPa; Maximum $E_p = 214.14$ GPa and minimum $E_p = 162.17$ GPa.

A modal analysis solving the eigenproblem involving the mass matrix and stiffness matrix from the random field was performed to establish the base line of comparison. Subsequently, a modal analysis of the nominal case was perturbed in order to find the natural frequencies and modal shapes through the perturbation method. The results of the comparison are shown in Figure 3.21 in terms of natural frequencies and modal assurance criterion. Good agreement is observed.

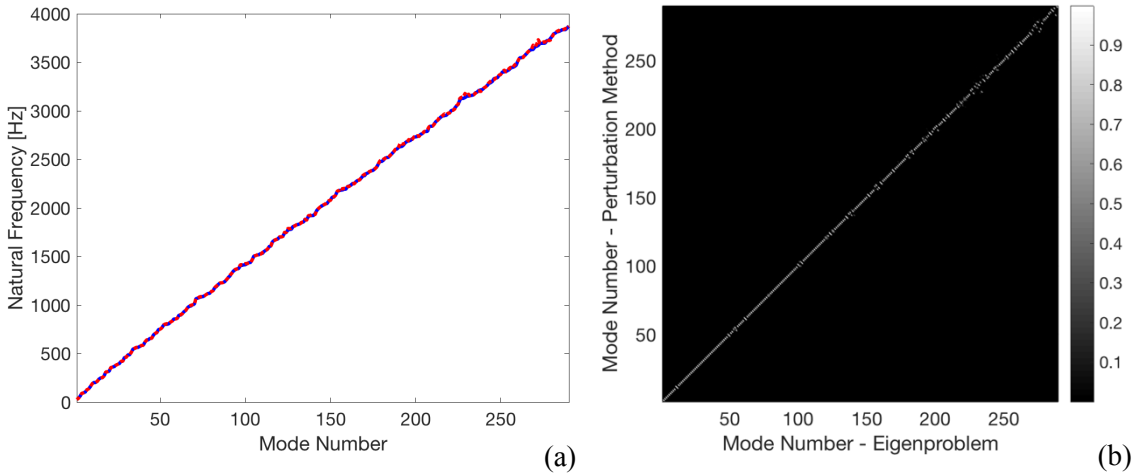

Figure 3.21 – Comparison between eigenproblem and perturbation method for a plate.
Simply supported plate. In (a), the first 290 natural frequencies of a plate; ▬ are the natural frequencies from the eigen problem and ▬ ▬ are the natural frequencies from the perturbation method. In (b), the MAC between the modes from the eigenproblem and the perturbation method.

3.5.3 *Coupled structures – finite beam attached to finite plate*

The last set of results of this chapter comprise the analysis of the plate with variability attached to a beam through a set of point connections. As in the previous sections, 5 connections were considered; a harmonic force is applied at the plate at the central attachment. The coupled system is shown in Figure 3.22.

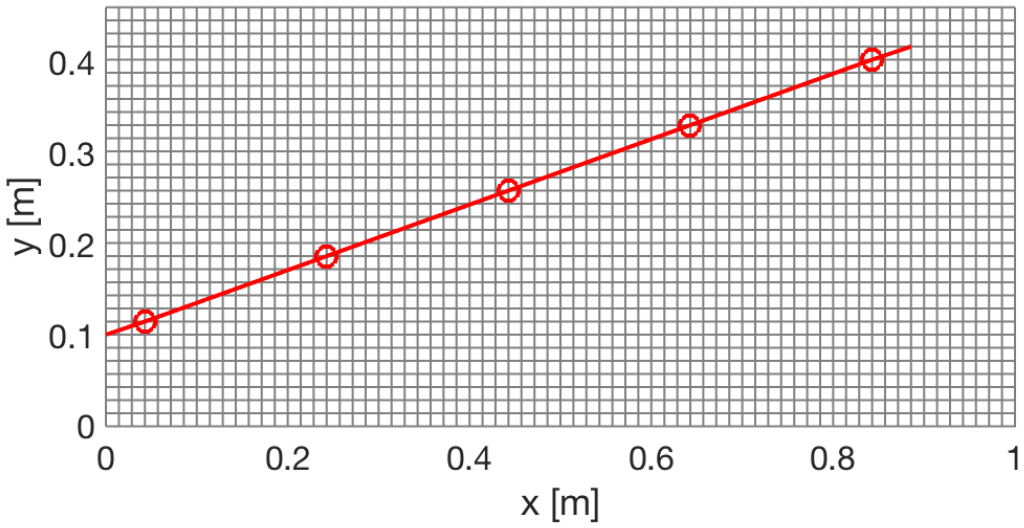

Figure 3.22 – Representation of the coupled system.

Mesh used in the FEA for the plate and the attached beam in —. The connection points are marked as O.

To perform a Monte Carlo analysis of the coupled system, a thousand plates and a thousand beams were considered. The nominal properties of the structures and the parameters for the KL expansions are given in Table 3.5. The input mobilities of the coupled system with nominal properties are shown in Figure 3.23.

Table 3.5 – Nominal properties of the coupled system and KL parameters.

Properties	Value
Density - plate (kg/m^3)	7850
Plate thickness (m)	0.002
Length y – plate (m)	0.460
Length x – plate (m)	1.0
Plate Young's modulus (GPa)	200
EI – beam (Nm^2)	1.0062
Length beam (m)	0.940
ρA – beam (kg/m)	0.1689
Spacing between connections	0.2125
Poisson's ratio	0.30
Loss factor	0.001
b_{Lx} – plate (m)	0.5
b_{Ly} – plate (m)	0.230
b_L – beam (m)	0.47
$N_{KLx} = N_{KLy}$ – plate	8
N_{KL} – beam	16
σ	0.1

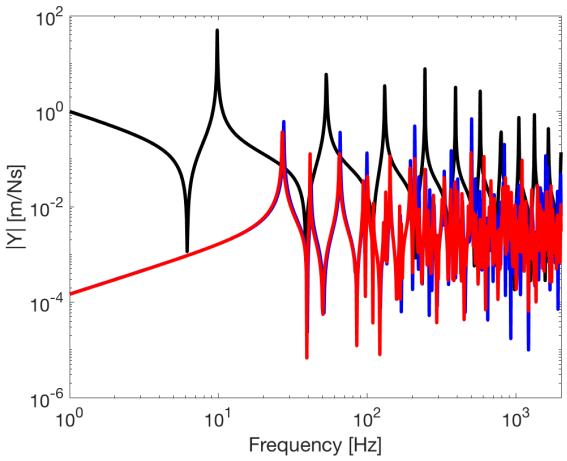

Figure 3.23 – Input mobilities of the coupled system with nominal properties.

— is the input mobility of the attached beam, — is the input mobility of the host plate and — is the input mobility of the coupled system.

As expected, at lower frequencies, the beam affects the coupled system mainly as an additional mass, whilst acting as a damper at higher frequencies. The response of the plate was calculated by a modal summation of the modes determined via solving the eigenproblem and the response of the beam was calculated analytically. The coupling of the system is made with the assistance of the mobility matrices.

The input mobility of the plates with varying Young's modulus is shown in Figure 3.24 and a distribution of the natural frequencies of the perturbed plates normalised by the natural frequency of the nominal plate is given in Figure 3.25.

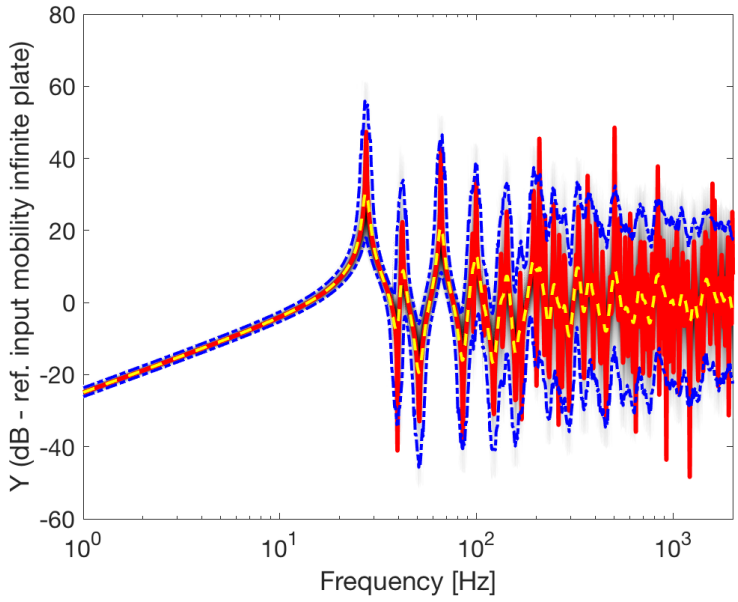

Figure 3.24 – Input mobility of the uncoupled uncertain plates.

Nominal $E_p = 200$ GPa, $b_{Lx} = 0.5$ m, $b_{Ly} = 0.230$ m, $N_{KLx} = N_{KLy} = 8$ and $\sigma = 0.1$. The colormap is the normalised distribution of the mobilities using the 1000 slowly varying Young's moduli fields — · — limits the region where 95% of the samples are contained within, — is the plate with nominal properties and — — is the average of all the cases

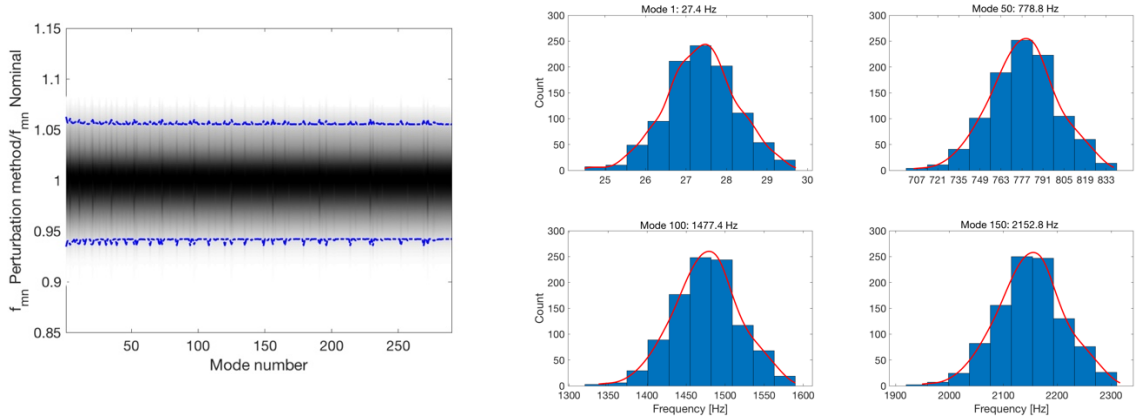

(a) (b)

Figure 3.25 –Distribution of the natural frequencies of the uncertain plates.

Nominal $E_p = 200$ GPa, $b_{Lx} = 0.5$ m, $b_{Ly} = 0.230$ m, $N_{KLx} = N_{KLy} = 8$ and $\sigma = 0.1$. In (a), the colormap is the normalised distribution of the first 290 natural frequencies of the plate using the 1000 slowly varying Young's moduli fields — · — limits the region where 95% of the samples are. In (b), the histogram and fitted distribution (—) of selected modes (1st, 50th, 100th and 150th). The natural frequencies of the nominal plate for these modes are 27.4 Hz, 778.8 Hz, 1477.4 Hz and 2152.8 Hz, respectively.

These 1000 different plates are then connected to the nominal beam and the results are shown in Figure 3.26.

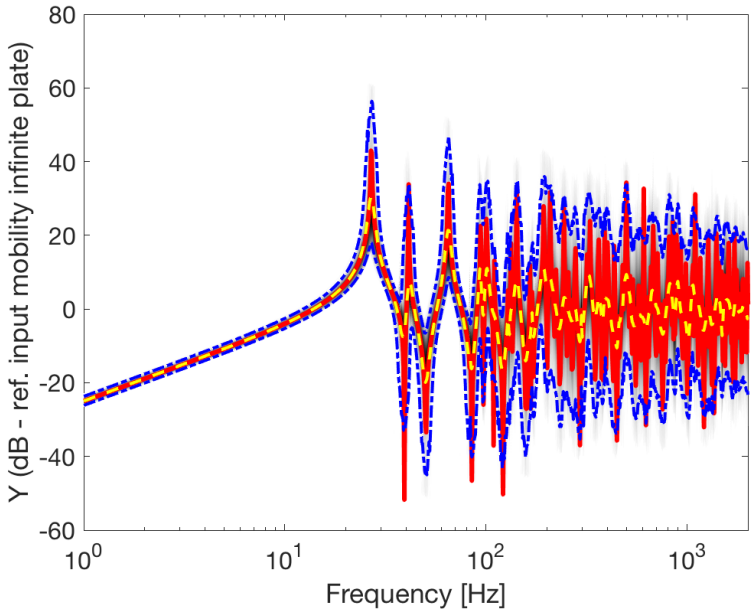

Figure 3.26 – Coupled system: Uncertain plates connected to a uniform nominal beam.

Nominal $E_p = 200$ GPa, $b_{Lx} = 0.5$ m, $b_{Ly} = 0.230$ m, $N_{KLx} = N_{KLy} = 8$ and $\sigma = 0.1$. The colormap is the normalised distribution of the mobilities using the 1000 slowly varying Young's moduli fields — · — limits the region where 95% of the samples are, — is the plate with nominal properties and — — is the average of all the cases

As the beam acts as a damper at higher frequencies, the envelope of containing 95% of the response levels are found to be slightly tighter. At lower frequencies, the uncertainty of the response of the coupled system is governed by the uncertainties in the plate.

In order to more easily visualise the effects of the uncertainties, once again the response of the coupled system is plotted on a dB scale referenced to the nominal uniform properties coupled system, Figure 3.27.

As done in previous sections, the convergence of the MC analysis was carried out. The analysis is made by comparing how the value of the mean changes when a different number of samples are considered, ranging from only 3 samples to the full set of 1000 samples. For a more convenient view, the convergence is considered to be given by $\mu_{MC} = 20\log\left(\frac{|\mu_{nsamples}(Y_{coupled})|}{|\mu_{1000samples}(Y_{coupled})|}\right)$, so a value of 0 is desired. The result of the convergence is shown in Figure 3.28.

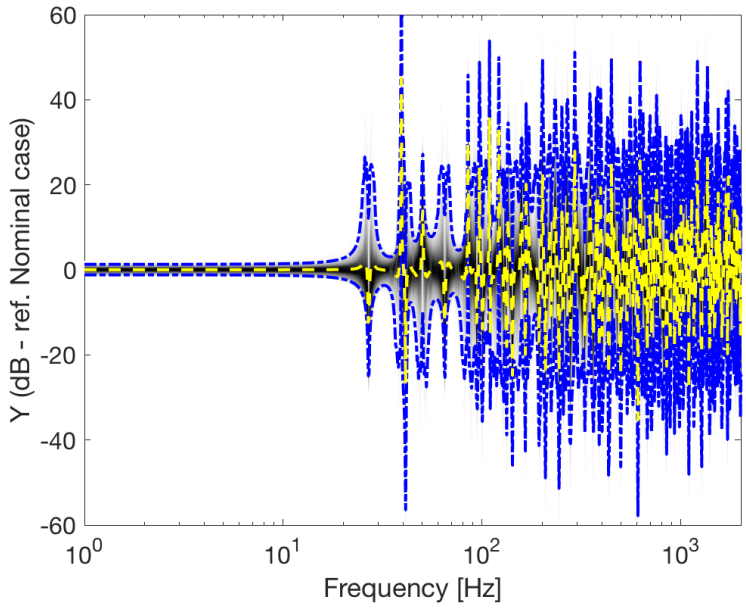

Figure 3.27 – Uncertain plates and nominal beam compared to the nominal case.

Nominal $E_p = 200$ GPa, $b_{Lx} = 0.5$ m, $b_{Ly} = 0.230$ m, $N_{KLx} = N_{KLy} = 8$ and $\sigma = 0.1$. The colormap is the normalised distribution of the mobilities using the 1000 slowly varying Young's moduli, — — is the mean of the responses and — · — limits the region where 95% of the response is.

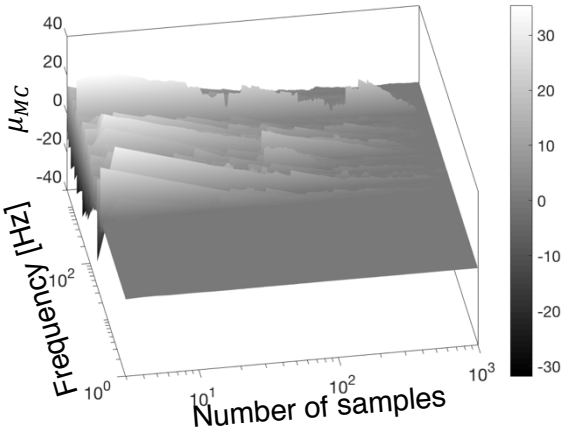

Figure 3.28 – Convergence of the mean of MC analysis of the coupled system.

A comparison between the following coupled systems was carried out; a nominal uniform plate and a beam with slowly varying Young's modulus, a plate with slowly varying Young's Modulus and a nominal uniform beam and, finally, both plate and beam with slowly varying Young's moduli. The results for the point mobilities are summarised in Figure 3.29.

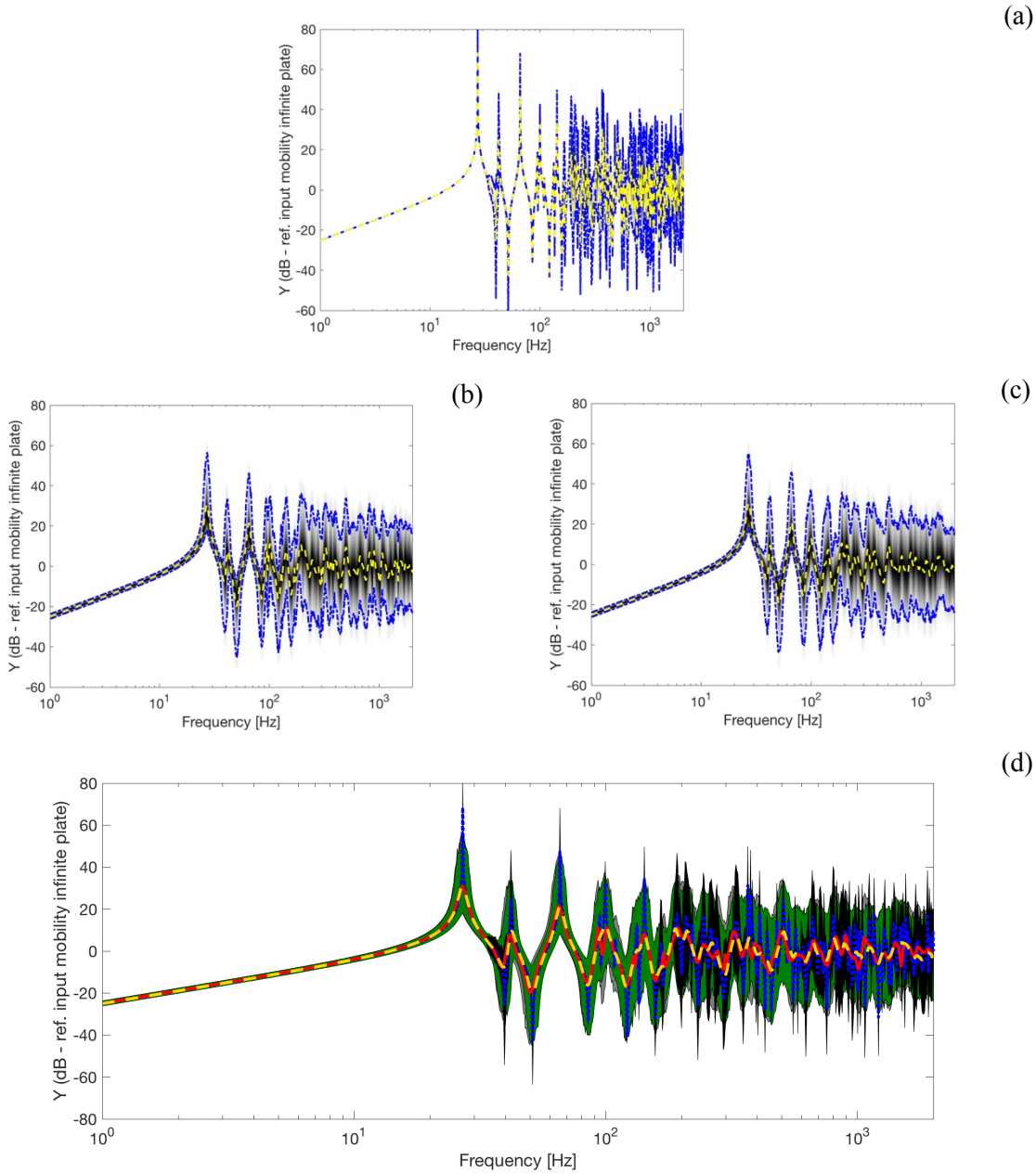

Figure 3.29 – Comparison of the different coupled systems.

Nominal $E_p = 200$ GPa and $EI_b = 1.0062$ Nm^2, $b_L = 0.470$ m, $b_{Lx} = 0.5$ m, $b_{Ly} = 0.230$ m, $N_{KL} = 16$, $N_{KLx} = N_{KLy} = 8$ and $\sigma = 0.1$. In (a), beam with slowly varying Young's modulus attached to a nominal uniform plate. In (b), a nominal uniform beam attached to plate with slowly varying Young's modulus. In (c), both beam and plate have slowly varying Young's moduli. In all three cases, the colormap is the normalised distribution of the mobilities using the 1000 slowly varying Young's moduli, — — is the mean of the responses and — · — limits the region where 95% of the response is. In (d), comparison of the 95% envelopes and averages. · · · is the average of the system with only uncertain beam and its 95% envelope ■, — is the average of the system with only uncertain plate and its 95% envelope ■, whilst — — is the average of the system with both uncertain plate and beam and its 95% envelope ■.

The last analysis consists of the study of the effects of having a flexible attachment connecting the beam to the plate. As in Chapter 2, these flexible links are considered to be elastic springs. In the automotive industry, the clips that hold in place cable bundles are made out of plastic and similar to the ones that Abolfathi et al. [**87**] measured. Modelling the mount system as a SDOF, the estimated stiffness has an average value of 1250 kN/m and a normalised standard deviation of 7% [**87**]. These values are used as a basis to construct a Gamma distribution, from which the stiffness of the elastic springs will be sampled and used in the calculations of the coupled system. The Gamma distribution therefore has a shape parameter $a_\Gamma = 204.0816$ and a scale parameter $b_\Gamma = 6125$. Five thousand values were sampled from the constructed Gamma distribution and the histogram of them along with the actual distribution are shown in Figure 3.30.

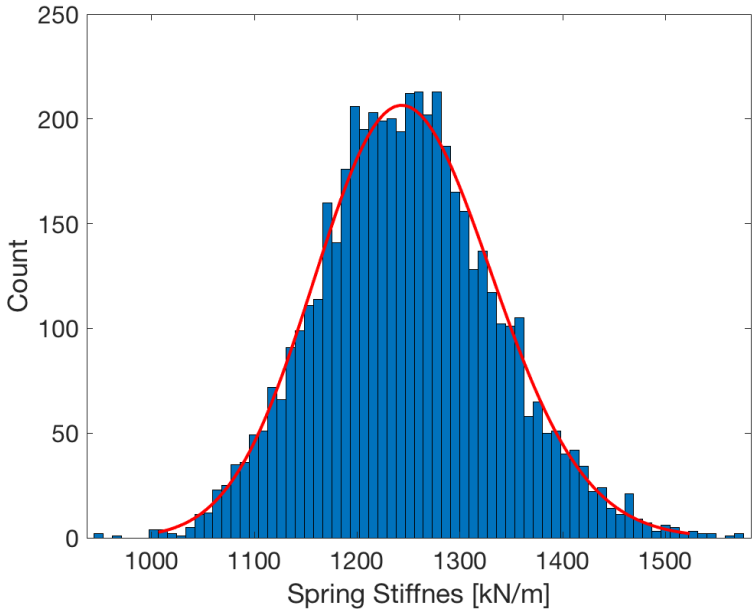

Figure 3.30 – Distribution of the stiffness of the clips.

The bars are the histogram of the values sampled from the Gamma distribution, in —.

For each one of the simulations, 5 values for the stiffness of the elastic springs are required. Firstly, the coupled system comprises both nominal plate and beam and the different sets of springs. In a second analysis, the coupled system comprises of the 1000 plates with slowly varying Young's modulus calculated before and the nominal plate. For each case, 1000 cases were calculated. In order to compare the effects, the 95% envelopes of the input mobility are shown in Figure 3.31.

As expected, from Chapter 2, the effects of varying the stiffness of the springs only show up at frequencies after the system uncouples, when the mobility of the combined plate and spring matches the mobility of the combined plate and beam. At lower frequencies, the uncertainty of the system is once again governed by the variability of the plate.

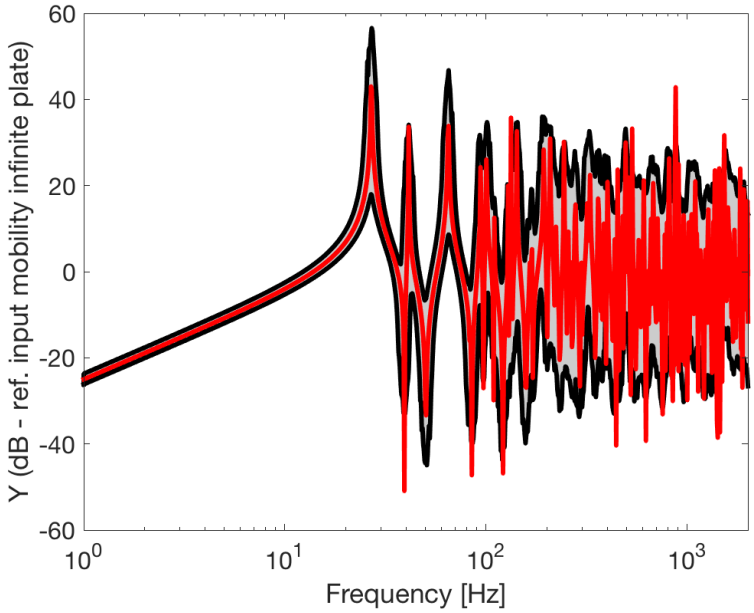

Figure 3.31 – 95% envelopes for the effects of variability of the stiffness of the connections.

In — the envelope for the nominal plate and beam and uncertain stiffness of the elastic springs; in — the envelope for the slowly varying plate and nominal beam, attached through uncertain connection points.

3.6 Discussion

In the case of applying a load at the central point of a beam, it can be noted that due to the fact that the random properties break the symmetry of the homogeneous beam, points that should be in a nodal response for even modes, can respond with those modes when the random properties are present. As shown in Figure 3.32. The nominal beam response is governed by the shape of the third mode, whilst the response of the beam with slowly varying Young's modulus is dominated by the shape of the second mode.

Also, when the beam is the only uncertain element in the structure, the response of the coupled system at lower frequencies is mostly dominated by the additional mass added, especially in the case of more flexible beams, as possibly cable bundles can be idealised. For stiffer beams, there is also a stiffness effect that can be relevant and more dependent on the random Young's modulus. Figure 3.33 shows the first two natural frequency of the coupled system normalised by the natural frequencies of the system with only masses at the connection points as function of different beam to plate bending wavenumber ratio.

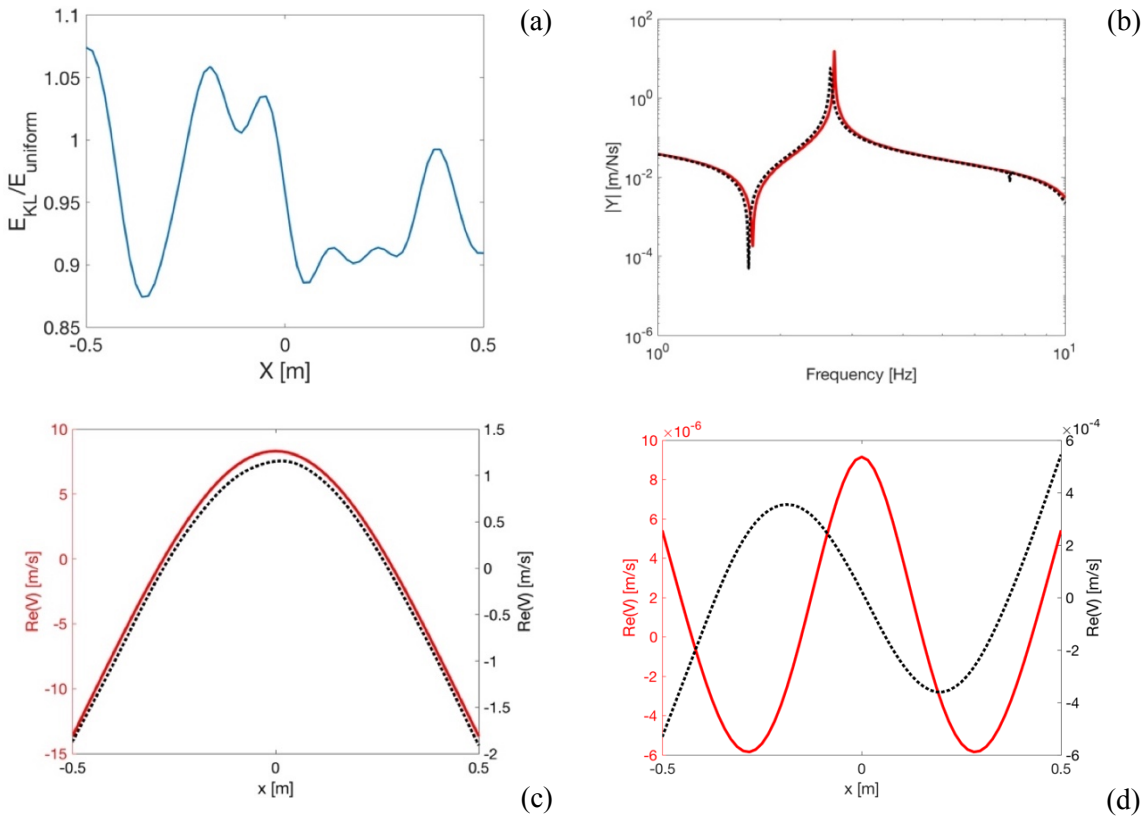

Figure 3.32 – Comparison of the velocity response of beams. Beam alone.

In (a) the normalised random Young's modulus of the beam with slowly varying properties. In (b), the point mobility of the central point of the beam. In (c), the real part of the velocity of the beam when excited with a unit point force at its central point at its first natural frequency, 2.71 Hz for the homogeneous one and 2.65 Hz for the slowly varying beam. In (d), the real part of the velocity of the beam when excited at its central point at the second natural frequency of the nominal beam, 7.48 Hz. In (b), (c) and (d), ▬ is the nominal beam and ⋯ is the beam with slowly varying Young's modulus.

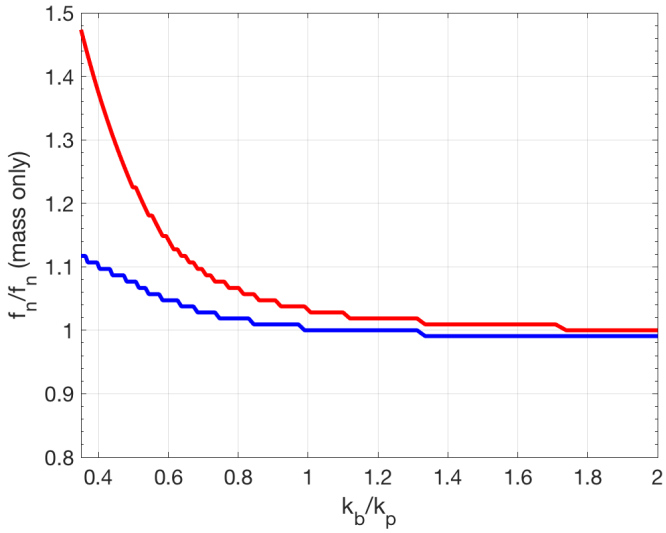

Figure 3.33 – Normalised first two natural frequencies of the coupled system.

The first natural frequency of the coupled system (beam attached to plate) normalised by the first natural frequency of the coupled system with only masses as attachments (▬) and the second one (▬). Larger beam to plate bending wavenumber ratio represent more flexible beams.

Figure 3.34 shows a comparison between coupling a beam to the plate versus coupling only masses at the connection points to the plate. The properties of the plate are given in Table 3.2 and the properties for the simulated cable are the ones identified in Chapter 5, which results in a beam to plate wavenumber ratio $\frac{k_b}{k_p} \approx 1.1$

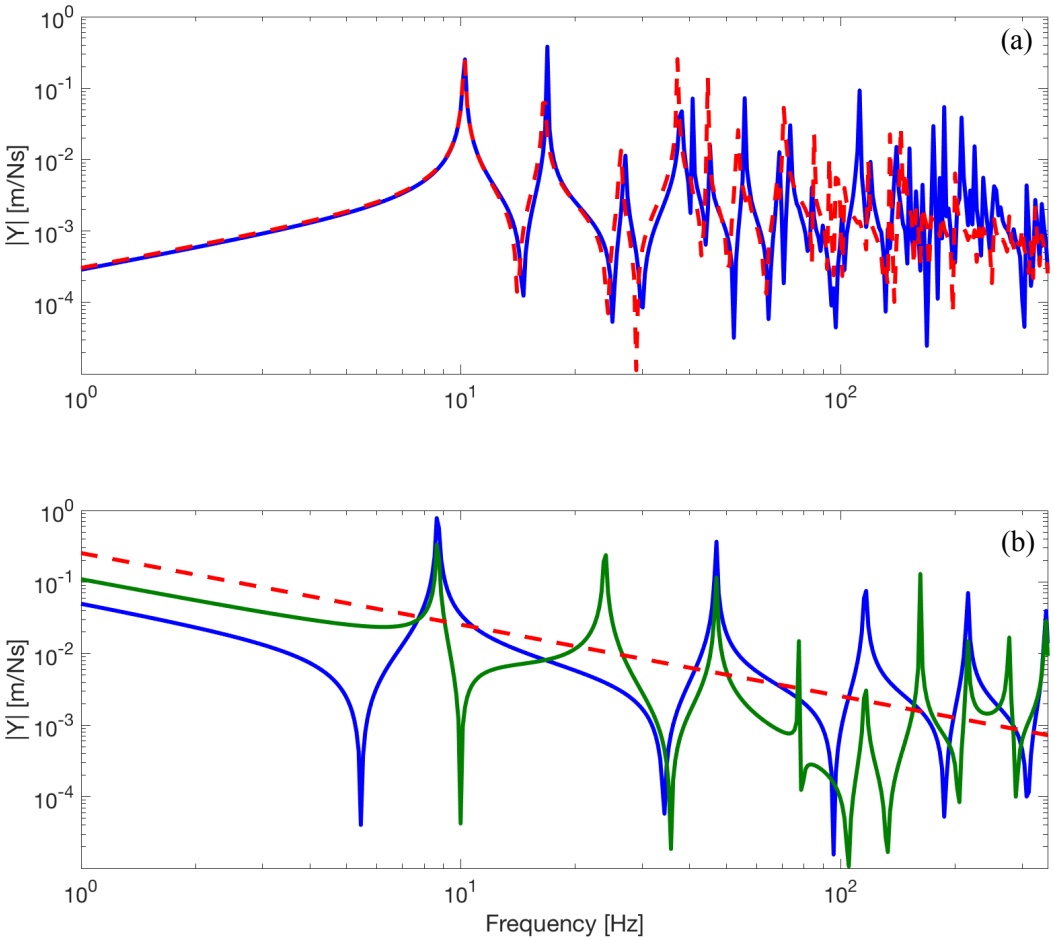

Figure 3.34 – Coupling a beam versus coupling masses to the plate.

Beam to plate bending wavenumber ratio $\frac{k_b}{k_p} = 1.1$. In (a), input mobility of the coupled system. Beam attached to plate through 5 point connections (—) or only using the divided mass of the beam equally among the 5 connections (— —). In (b), input (—) and one of transfer mobilities (—) of the attached beam versus the input mobility considering the attachment as only lumped masses (— —).

For the first few natural frequencies, the approximation of the cable bundle as only masses at the attachment points is accurate, the response of the coupled system is dominated by the stiffer element; the plate, in this case. But as the frequency increases and the mobilities of the attached beam and the host plate become comparable, the approximation of the cable bundle by masses only breaks. The mobility of the masses lacks the modal features that the attached beam adds to the system, which leads to a significant discrepancy between the two models. In this case, especially from 150 Hz onwards, lowering the predicted amplitudes of the response of the connected system.

For the cases of a coupled system comprising an uncertain plate, analyses comprising the attachment of homogeneous beam and also slowly varying beams were conducted. To obtain average values and the envelope that covers the response levels of 95% of the samples, a MC strategy was used with 1000 cases evaluated. The response of the system is mostly dominated by the uncertainty in the plate, for the beams mostly contribute as additional mass or damping. Aiming to proxy a cable bundle, the mechanical properties used for the beam in these simulations came from experimental identifications detailed in Chapter 5. The probability density functions for the natural frequencies of the uncertain plates, the responses of the plates and coupled systems were calculated by fitting a kernel distribution.

The analysis of the effects of the stiffness of the connectors was made by using properties found in the literature and generating values from a Gamma distribution that followed the average of the stiffness and standard deviation. Properties for a new clip were considered, as those of a worn clip would only change the frequency where effects of uncertain on the stiffness would appear. The actual level of variability between the new clip or worn out ones are similar, at around 7-8% for the normalised standard deviation [**87**].

The frequency-averaged behaviour of the coupled system can also be analysed and compared to the coupled system comprising infinite structures. This was done by a moving average. Three different window sizes were considered for the moving average; 35 Hz, 70 Hz and 140 Hz. The results are shown in Figure 3.35. The beam and plate properties are given in Table 3.2.

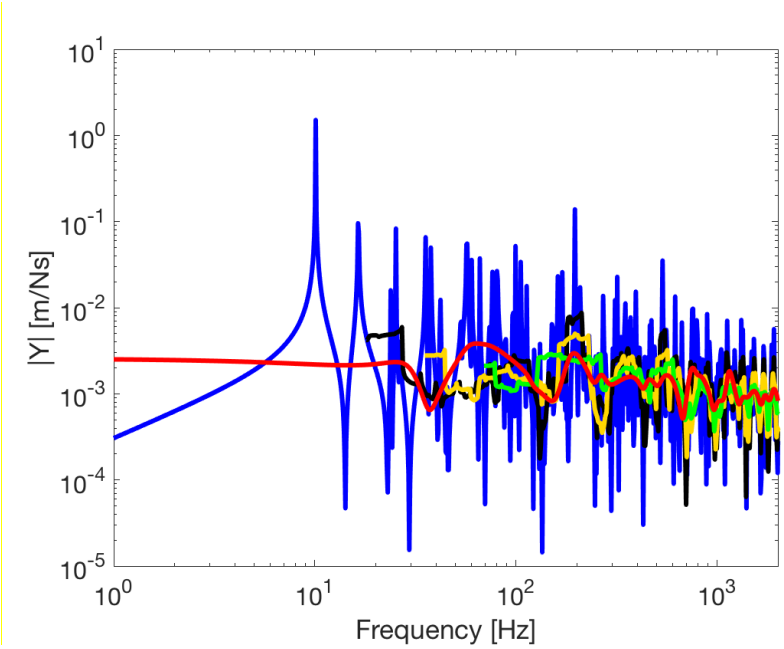

Figure 3.35 – Frequency-averaged finite system compared to infinite system.

Beam to plate bending wavenumber ratio $\frac{k_b}{k_p} = 0.35$. Coupled finite system (—), coupled infinite system (—), frequency-averaged finite system – 35 Hz window (—), frequency-averaged finite system – 70 Hz window (—) and frequency-averaged finite system – 140 Hz window (—).

As expected, it is possible to notice how the agreement between the frequency-averaged response and the infinite system increases at higher frequencies. The wider the averaging window, the better the agreement. However, even the narrower window captures the general features predicted by the infinite system, such as the increase in amplitude around the 200 Hz region of the spectrum.

3.7 Conclusions

This chapter extended the analysis shown in Chapter 2 to the case of finite structures comprising beams point attached to plates. The same mobility approach was used to connect the structures. The mobilities of the finite homogeneous Euler-Bernoulli beam and finite thin plate are also readily found in the literature. In all cases of the coupled systems, 5 point connections were considered and a harmonic point transverse force applied on the plate at the central attachment.

The work done here helps improving the standard modelling technique in the industry, which consists of considering only lumped masses at the attachment points. A computationally efficient method using analytical solutions allows one to include the modal features that an attached beam would add to the coupled system. These features are absent when only masses are considered as the attachments and lead to inaccurate results, especially at higher frequencies. The mobility of the coupled system is governed by the element with the lowest mobility. As the frequency increases, the mobility of the mass-only attachments becomes much smaller than that of the host structure and this fact along with the lack of modal features of the mass-only attachments, lead to unreasonable low values for the levels of the response coupled system.

In the case of the beam with slowly varying properties, the expressions for the changes in phase and amplitude of the waves found through the WKB approximation in the previous chapter are also valid in the case of the finite structure. One must only take into consideration the reflection due the presence of the boundaries of the beam when calculating the mobilities. A generalised expression to calculate point and transfer mobilities was derived in this chapter and is given in terms of the propagation and reflection matrices.

In order to introduce variability into the plate, a FE mode was constructed and the combined with the perturbation method. KL expansion was used once again to generate the slowly varying random field for the Young's modulus, which was sampled assuming that each element of the FE model has one particular value for the modulus of elasticity. A base line test was made solving the eigenproblem associate with the random plate and compared to the responses obtained through the perturbation method. Both the natural frequencies and mode shapes agreed in the comparison between solving the eigenproblem or perturbing the homogeneous case. Therefore, the perturbation method was used to solve a thousand random plates combining the KL expansion and mid-point sampling to the perturbation method. As stated by Mochales [**1**], even in the worst case where all degrees-of-freedom are perturbed, the perturbation method still has a lower computational cost than

solving the new eigenproblem. Since it allows one to find the perturbed modal shapes, the mobilities of the plate can be calculated via modal summation. Once the mobility matrix of the plate is obtained, the same approach as for the previous analyses was used to couple the beam and plate.

Chapter 4 Experimental investigation into the effect of random connection spacing on the vibration of coupled structures

This chapter presents the experimental validation to quantify the influence of the connection positions for attachments in specific coupled structural configurations. As only the spacing between the connections were measured, rather than the actual coordinates of the points relative to edges of the plates, the mobility measurements are compared to the previously developed analytical models in Chapter 2, which were for infinite structures. Previous experimental work [**88**] has measured the response of point-connected ribbed plates and compared the responses to results for infinite structures, but the effects of variability in the spacing of the discrete attachments or for differences in the bending wavenumber ratio for the connected structures components were not previously investigated. These parameters are taken into account in this study.

4.1 Experimental design

The experiment was designed to measure and quantify differences in the frequency response of a coupled system, comprising a finite beam attached to a finite plate. Variation in the spacing of the attachment points is considered in comparison to a uniform spacing arrangement. In order to obtain two different beam to plate bending wavenumber ratios, a more flexible beam and stiffer one; two different beams with different cross-sectional areas were used. The general properties of the plate and beams are given in Table 4.1. They were all made of mild steel.

Table 4.1 – General properties of the plate and beams.

Properties	Value
Density (kg/m^3)	7850
Young's modulus (GPa)	200
Plate dimensions (l x b, mm)	750 x 350
Plate thickness (mm)	0.9
Beam 1 height (mm)	3
Beam 1 width (mm)	6
Beam 2 height (mm)	10
Beam 2 width (mm)	10
Beams 1 and 2 length (mm)	750
Beam 1 to plate bending wavenumber ratio	0.56
Beam 2 to plate bending wavenumber ratio	0.31
Regular spacing Δ (mm)	150

The experiment consisted of attaching one of the beams to the plate at five points using Neodymium magnets. Each magnet has a diameter of 4 mm and a height of 3 mm. Grade N52 magnets were used. According to the manufacturer [**89**], each of the discs has a vertical pull of 9.3

N flush to a mild steel surface, which could have been verified using a standard pull test kit, but this was not part of the concerns of this research. Also, when comparisons with the numerical models were made, it was assumed that there is no incorporation of the magnets mass or rotational coupling between beam and plate. The numerical models assumed infinitely stiff attachments of negligible mass and size, i.e., rigid point connections.

The system was excited by a shaker through the plate at one of the attachment points and the input force was measured by an impedance head, Figure 4.1(a). It is possible to show theoretically that there is no difference in either exciting the beam or the plate when rigid attachments are considered. The response was measured on the opposite side of the coupled system, on the plate, with a laser vibrometer, Figure 4.1(b). The latter measures the out of plane bending velocity at a selected point. Figure 4.4(a) shows schematically the experiment.

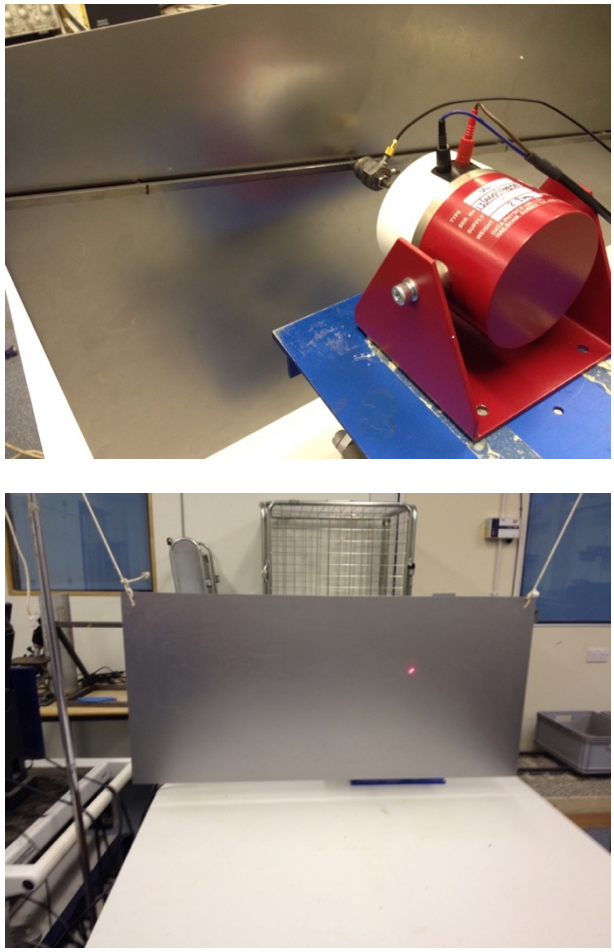

(a)

(b)

Figure 4.1 – Photos of the coupled system experiment.

The measurements were performed up to 6400 Hz, with a frequency resolution of 1 Hz and 20 averages, but due to drop in the excitation force and low coherence at higher frequencies, the analysis of the results is limited up to 2000 Hz. White noise was used for the excitation signal and Hanning windows were used on the signals. The sampling frequency used was 16.4 kHz. The shaker was attached to the beams using a stud glued to the beam, with a flexible stinger between the shaker and the stud, as shown in Figure 4.1(a). The vibrational response of the plate was measured using a

scanning laser. An example of the spectrum of the excitation load is shown in Figure 4.2 and a typical example of the measured coherence in Figure 4.3. In order to reliably obtain signals from the laser vibrometer, a reflective tape was used at the point of measurement.

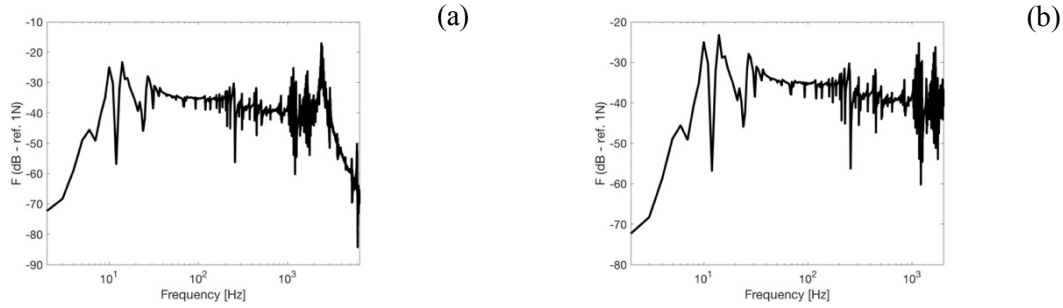

Figure 4.2 – Example of the spectrum of the force applied by the shaker.
In (a), over all of the frequency range. In (b), limited to 2000 Hz.

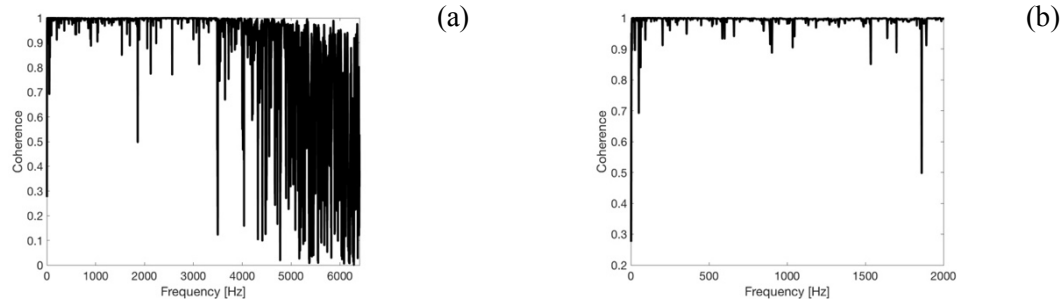

Figure 4.3 – Typical measured coherence.
In (a), over all of the frequency range. In (b), limited to 2000 Hz.

For each of the beams, 15 repeatability tests were conducted by performing a disassembly and reassembly of the coupled system. Sets of measurements were taken with a regular spacing Δ between the attachments. For the repeatability tests, the beams and magnets are at nominally the same locations on the plate in each case. Also, for each of the beams, 10 sets of random distributions of the spacing between the attachments were considered, with the distribution from which the spacing was sampled being a uniform distribution. The histogram of the sampled values for the spacing are shown in Figure 4.4(b). The spacing was allowed to vary up to 15% around its nominal equal spacing value of 150 mm. The attachment used as the excitation point was kept the same and the other points moved relative to this one. Considering as the origin of the coordinate system the end of the beam closest to the shaker, the coordinates where the magnets were placed to connect the structures are given in Table 4.2, along with the spacing for each case.

For beam 1, the beam to plate bending wavenumber ratio is 0.56 (i.e., the flexible beam), only one magnet was used at each attachment point, Figure 4.4(c). Whereas, in the case of beam 2, the beam to plate bending wavenumber ratio is 0.31 (i.e. a stiff beam). Due to its mass, for beam 2, two magnets, side-by-side, were required at each attachment point, as shown schematically by Figure 4.4(d).

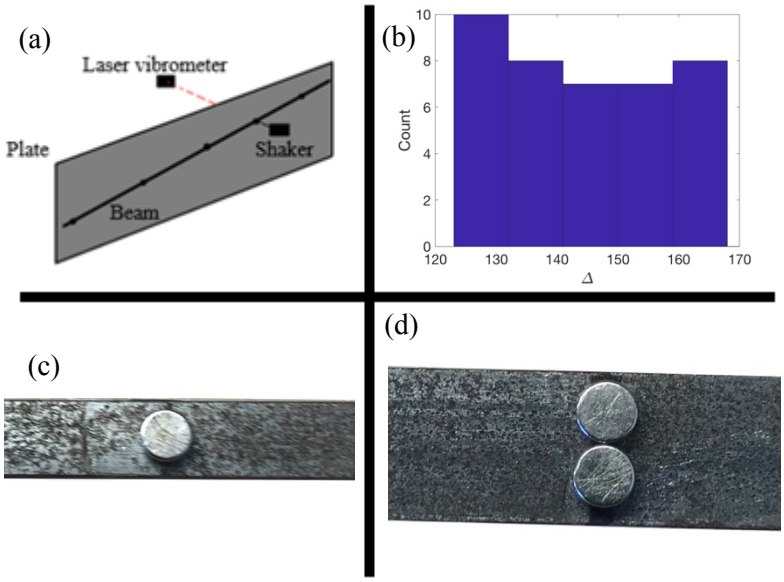

Figure 4.4 – Experimental design.

In (a), experimental schematics, histogram of the spacing (b), connection for beam 1 (c) and connection for beam 2 (d)

4.2 Results

The experimental data obtained is presented below. The results of point mobilities are compared to the infinite structures using the modelling described in Chapter 2. When mentioned, the equivalent infinite system is defined as having the same number of attachments and the same spacing of the measured system between said attachments. Differently from the previous chapters, the force here acts on the second attachment point and this change of the positioning of the point force is also considered in the modelling of the equivalent infinite system. Also, the infinite beams have the same cross-sectional area as the ones that were measured, whereas the infinite plate has the same thickness as the measured plate. The frequency range considered was from 10 Hz to 2 kHz, but the results are shown versus the dimensionless parameters Δ/λ_p and Δ/λ_b, where Δ is the regular spacing between the attachments, 150 mm, and λ_p and λ_b are the flexural wavelengths for the plate and beam, respectively. Figure 4.6 shows the difference that the random spacing produces on the measured point mobility. This is obtained by referencing the randomly spaced cases to the results for one of the evenly spaced case on a dB scale. Therefore, the reference level for 0 dB is the selected evenly spaced scenario. It also serves the purpose of showing the repeatability of the experiment and the inherent uncertainty in it.

In Figure 4.5 one can see that the variability in the response of the coupled system due to the randomly spaced connections starts to actually affect the coupled structural response in the frequency region corresponding to the attachment spacing to plate bending wavelength ratio $\Delta/\lambda_p \approx$ 0.4-0.6

onwards. This corresponds to a frequency where the wavelength on the plate is approximately equal to twice the spacing between the connections.

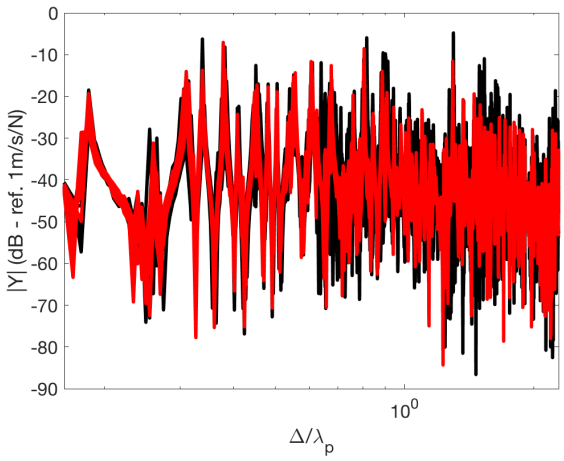

Figure 4.5 – Input mobility of the coupled system considering Beam 1.

The 10 randomly spaced cases in ▬ and the repeatability test of the regular spacing in ▬. The frequency range is 10 to 2000 Hz and the spacing Δ is the regular spacing 150 mm. Second attachment point as shown in Figure 4.4(a).

In both Figure 4.6(a) and (b), the black lines are the response of the 10 randomly spaced cases tested, the red line is the average of the 15 evenly spaced cases (when the system was disassembled and reassembled) and the yellow lines are the maxima and minima of these repeatability evenly spaced cases for each frequency. Figure 4.6(a) shows the results for beam 1, whereas Figure 4.6(b) shows the results for beam 2, the stiffest of the two beams.

Table 4.2 – Coordinates and spacing between the attachments.

Set	Coordinates (mm) **Spacing Δ (mm)**				
1	75	225	375	525	675
	150	**150**	**150**	**150**	
2	89	225	393	549	708
	136	**168**	**156**	**159**	
3	81	225	356	488	641
	144	**131**	**132**	**153**	
4	95	225	363	494	639
	130	**138**	**131**	**145**	
5	74	225	355	517	647
	151	**130**	**162**	**130**	
6	82	225	372	540	703
	143	**147**	**168**	**163**	
7	90	225	353	505	648
	135	**128**	**152**	**143**	
8	88	225	393	525	680
	137	**168**	**132**	**155**	
9	57	225	361	526	687
	168	**136**	**165**	**161**	
10	67	225	357	500	632
	158	**132**	**143**	**132**	
11	76	225	366	507	640
	149	**141**	**141**	**133**	

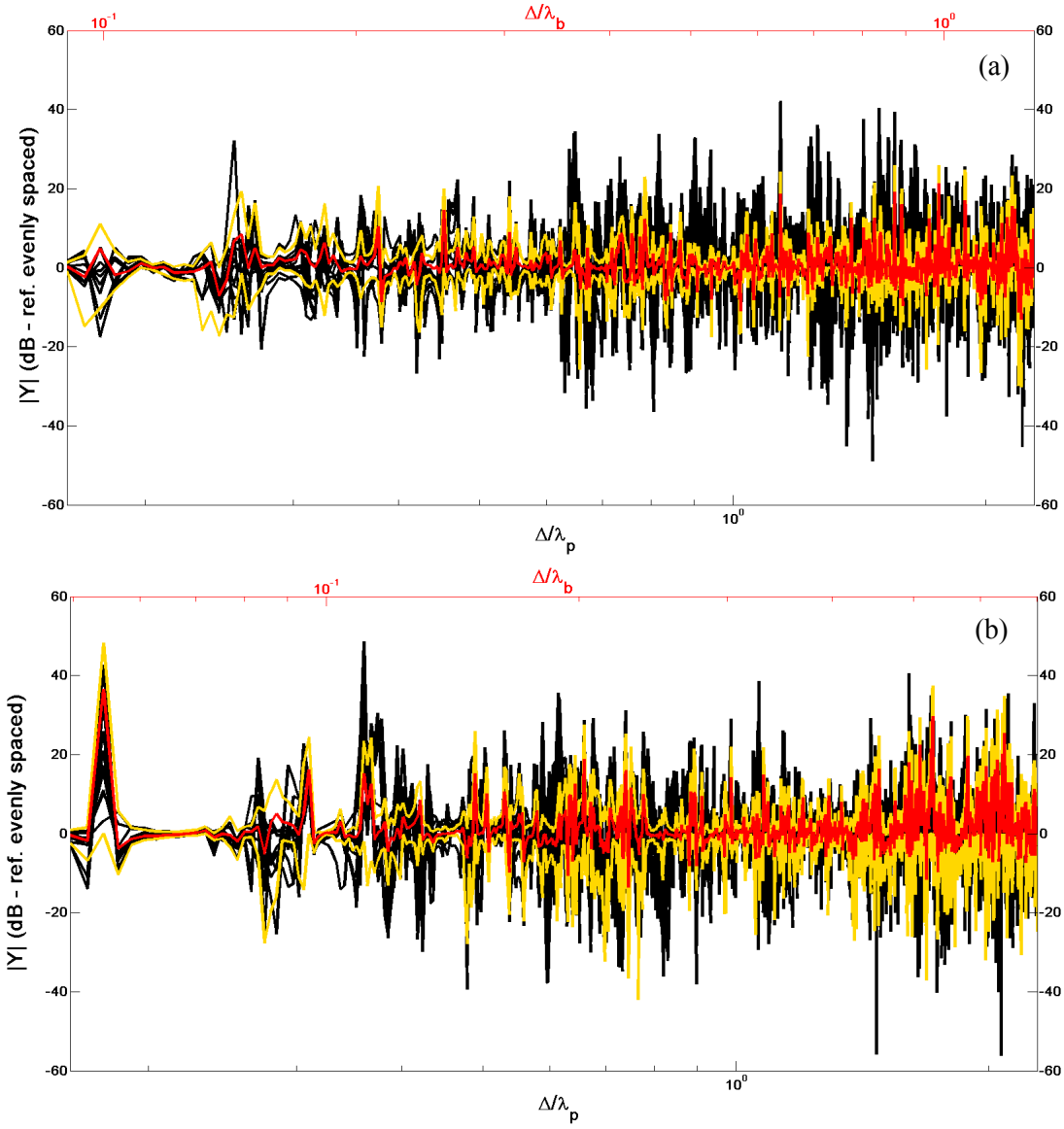

Figure 4.6 – Differences in the point mobility at an attachment point due to randomly spaced connection versus repeatability for equally spaced connections.

Beam 1 (less stiff beam) in (a) and beam 2 (stiffer beam) in (b). For both, ▬ are the randomly spaced cases, ▬ is the average of fifteen evenly spaced cases and the ▬ lines are the maxima and minima values for these evenly spaced cases at each frequency.

One can notice how at lower frequencies the random spacing does not have a significant effect on the coupled system, i.e., the levels of the response of the coupled system using 10 sets of random spacing is comparable to the levels of response of the repeatability test. However, for the case of the stiffer beam, which required 2 magnets per connection, the uncertainties of the positioning of these also increase the uncertainties in the repeatability test at higher frequencies.

In Figure 4.7, the mobility of one of the randomly spaced cases is compared to the equivalent infinite system. In both cases, Figures 4.7(a) and (b), the black lines are the measured mobility, the red lines are the infinite system and the yellow lines are the frequency averaged experimental data. A bandwidth of 35 Hz was used for the averaging.

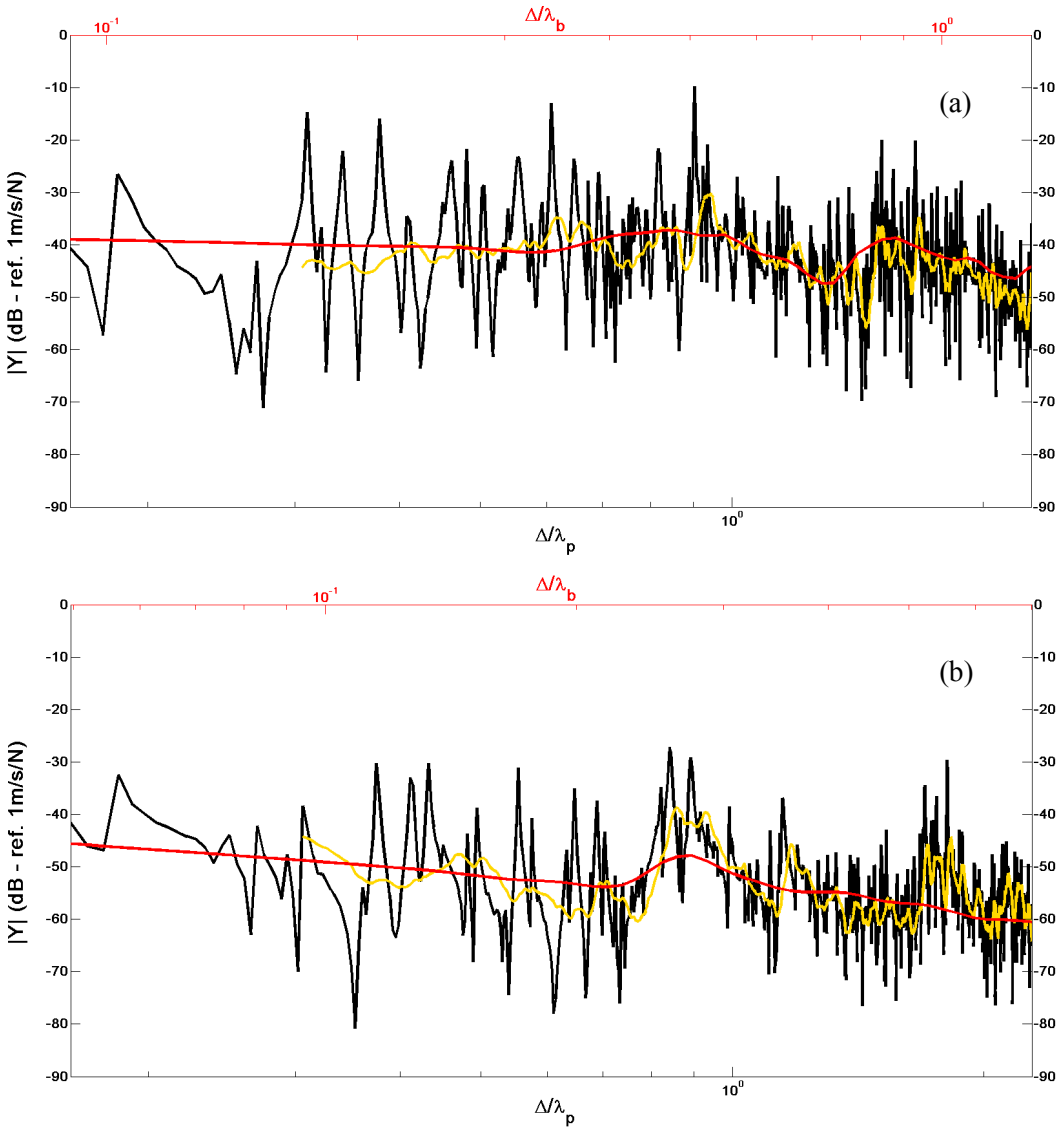

Figure 4.7 – The point mobility for randomly spaced connections, set number 3. Comparison with the infinite systems prediction model. Beam 1 in (a) and beam 2 in (b). For both, ▬ is the measured data, whereas ▬ is the equivalent modelled infinite system and ▬ is the frequency averaged experimental data.

These results serve to validate the connection model used in Chapter 2. Even the local modes between the connection points are captured when compared to the infinite equivalent system.

Figure 4.8 represents the same data as shown in Figure 4.7, but instead of referencing it to 1 m/s/N the evenly spaced case is used once again as 0 dB at each frequency line. For the experimental data, the reference is the data for the selected evenly spaced case. Whereas, for the infinite system the equivalent evenly spaced infinite system is the reference. As in Figure 4.7, for Figures 4.8(a) and (b), the black lines are the measured mobility, the red lines are the infinite system and the yellow lines are the frequency averaged experimental data.

Since all of the experimental data collected is referenced to the same value on a dB scale, 1 m/s/N, to change the reference for the evenly spaced case, one only needs to subtract the data from

the new reference value, namely the evenly spaced case. This is given by $\hat{Y}_{dB} = Y_{dB_r} - Y_{dB_e}$, where $\hat{Y}_{dB}$ is the experimental data now referenced to the evenly spaced case, Y_{dB_r} is the experimental data of the randomly spaced cases on a dB scale referenced to 1 m/s/N and Y_{dB_e} is the experimental data of the selected evenly spaced case, also on a dB scale referenced to 1 m/s/N.

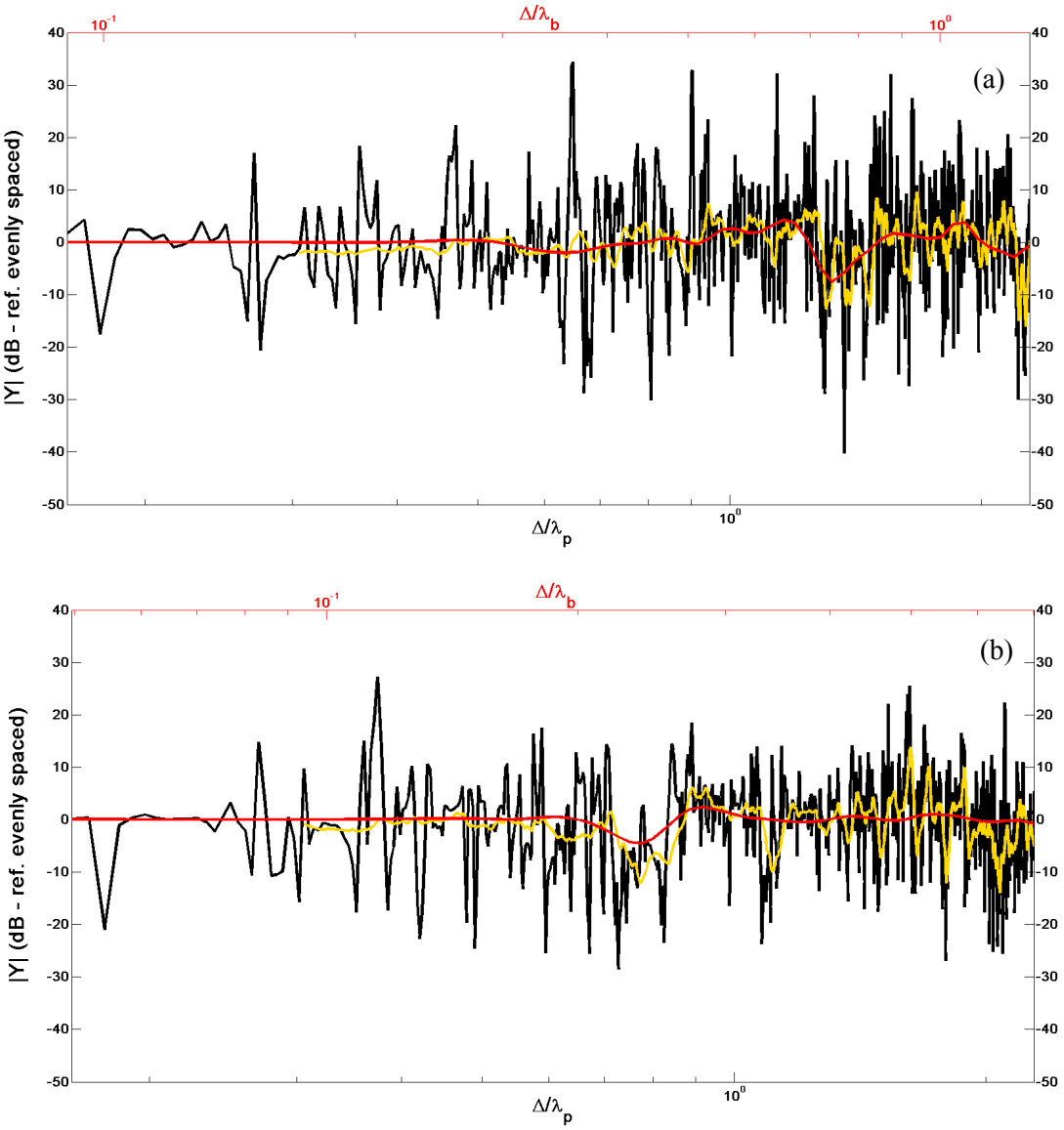

Figure 4.8 – The point mobility for randomly spaced connections, set number 3: dB scale. Finite system versus the equivalent infinite system, both referenced to the adequate evenly spaced case. Beam 1 (flexible) in (a) and beam 2 (stiffer) in (b). For both, ▬ is the measured data, whereas ▬ is the equivalent infinite system and ▬ is the frequency averaged experimental data.

In both cases, around 300 Hz, $\Delta/\lambda_p \approx 0.88$, there is an amplification of the mobility response of the equivalent infinite system. Figure 4.9 shows the spatial response given as contour levels for the experimental data and the equivalent infinite system at this frequency. In this case, a regular spacing of 150 mm between the attachments was considered. Although the contour level data is shown for the evenly spaced case, the randomly spaced cases also exhibit the same behaviour in this

region of the spectrum. The system was excited at the second connection point from right to left, as predicted in Chapter 2. The excitation was applied to the beam on the experiment and on the plate on the model. The results are shown for the combination of plate and beam 2, the stiff beam.

$\Delta/\lambda_p \approx 0.88$

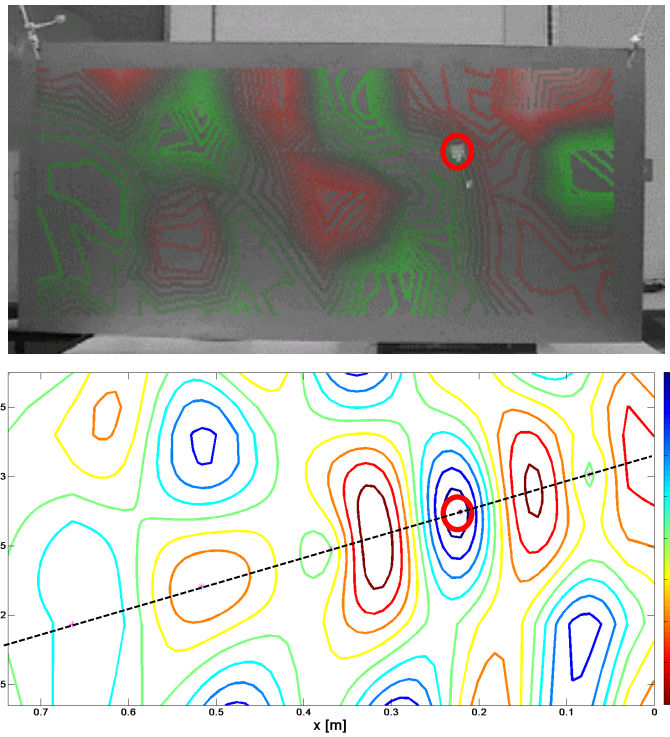

Figure 4.9 – Comparison of the spatial response of a plate with stiff beam attached at 300 Hz. Uniform spacing.

In (a), the experimental data versus equivalent infinite system, in (b). The beam is shown in shown in ▬▬, the attachments are represented by * and the point where the load was applied is marked as O.

4.3 Discussion

In Figure 4.6, one can notice that when compared to the evenly spaced scenario, the dynamic response for both beams with irregularly spaced connections produced variations that can be up to 40 dB, but most commonly reaching a difference up to 20 dB. Although, in Figure 4.6(b) it is also possible to see that the spread in the repeatability test is comparable to the variation for the random spacing response at several points, especially at higher frequencies. Another way to look at this would be to compare the standard deviation values divided by the mean values, σ/μ. This is also known as the coefficient of variation, for both the randomly spaced cases and the evenly spaced cases at each frequency, see Figure 4.10.

For beam 1, the coefficient of variation for frequency by frequency for the evenly spaced scenarios are oscillating around 0.25 at most frequencies (with a maximum of 1.8 around 1.5 kHz , $\Delta/\lambda_p = 1.97$), whereas the values for the randomly spaced cases are oscillating around 0.75. The coefficient of variation values, σ/μ, are also over 1.5 several times and could be up to 2.5, with a

maximum value being just greater than 2.5 at around 650 Hz , $\Delta/\lambda_p = 1.30$, for the randomly spaced cases.

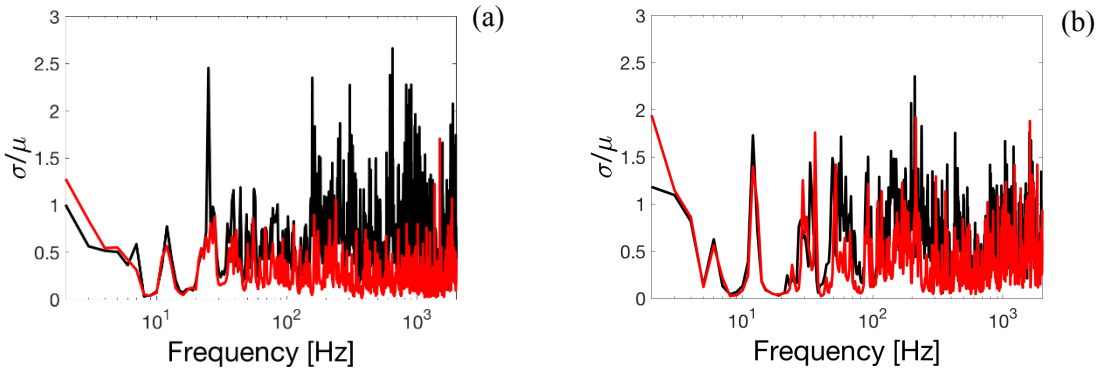

Figure 4.10 – Coefficient of variation comparing evenly spaced (repeatability test) connections versus randomly spaced connections.

— is from the randomly spaced cases, whereas — is from the repeatability test. In (a), the more flexible beam and in (b), the stiff beam is connected to the plate.

For the stiffer beam 2 with connections at evenly spaced points, the coefficient of variation also varies around 0.25 for most of the frequency range, but reaches up to 1.5 at several points, whereas the randomly spaced cases oscillate around 0.5, also reaching 1.5 multiple times with a maximum of 2.4 around 220 Hz, $\Delta/\lambda_p = 0.75$. Even though the values for σ/μ are larger when randomly spaced attachments are considered, there are frequencies when the magnitude of the response of the evenly spaced cases are comparable to the randomly spaced cases, especially at frequencies above 1 kHz ($\Delta/\lambda_p = 1.61$), where the data becomes less reliable with reduced coherence in the measured transfer function for the point mobility

The literature reports that the response of the finite system, when frequency-averaged, should tend to that of the equivalent infinite system [**55**]. Both Figures 4.7(a) and 4.7(b) are consistent with that observation and comment even for a coupled system (beam-plate). The frequency averaged experimental data was evaluated by a moving averaging with a window of a constant size of 35 Hz. Moreover, from the results in Chapter 2, it is reasonable to say that the magnets behave like rigid links for the frequency range considered. The presence of a flexible link would in this frequency range produces a dip in the frequency averaged results. In addition, the standing-wave-like response predicted to happen between the attachments of the infinite system seems to match the response of the finite system, as shown qualitatively in Figure 4.9.

In fact, even when the point mobilities were referenced on a dB scale to the evenly spaced case, Figures 4.8(a) and 4.8(b), the frequency-averaged response of the system oscillates around that predicted by the equivalent coupled infinite system with the same randomly spaced attachments. The

reference value for plotting the red line is the magnitude of the mobility of the evenly spaced infinite system.

4.4 Conclusions

This chapter proposed an experiment to investigate the effects of uncertainties in the positioning of the connection points and carried out a validation of the coupling method proposed in Chapter 2 via a mobility approach. In order to allow an easy repositioning of the connection points, ferromagnetic beams and plate were used and coupled together through Neodymium magnets. The spacing between the connection was sampled from a uniform distribution and allowed to vary ±15% around its nominal value. This value is not necessarily trying to simulate uncertainties in a manufacturing process, but just investigating what the effects of breaking the symmetry between connection points are.

Trying to analyse the attachment of beams with different stiffnesses, two beams with nominally identical mechanical properties but different cross-sectional areas were used. Unfortunately, the beam to plate bending wavenumber ratios, 0.561 (beam 1, more flexible) and 0.355 (beam 2, stiffer), were not sufficiently different to notice any significant difference in the response amplitude due to the small variation in the position of the attachment points introduced.

The need for two magnets per connection point for beam 2, the stiffer beam, could have added some extra uncertainties in the position of the connecting points and rotational inertia of the connections, therefore producing results that are more scattered in the repeatability test. For this case, it is possible to see the effects that varying the position of the attachments produce in the frequency range between 20 Hz and 500 Hz. Above the higher frequency, the inherent uncertainty of disassembling and reassembling the experiment gets comparable to the variation measured when random spacing was considered.

The repeatability test has less variability in the response of the coupled system when compared to the random spaced connections. However, there is a cut-on point where the random spacing starts to more significantly affect the coupled structures. Uncertainties in the positioning of the connections start to play a role from $\Delta/\lambda_p \approx$ 0.4-0.6 onwards. This corresponds to a frequency where the plate bending wavelength is approximately equal to twice the spacing between the connections. As the uncertainties in the spacing between the connection points slightly changes the natural frequencies of the coupled system, this results in a spread of the envelope of the response. Regions that would nominally be in a low level of vibration region can actually have higher levels of vibration due to the uncertain positioning of the attachments and the associated shift in the natural frequencies due to random spacing, requiring attention to check if the levels are acceptable. For instance, in Figure 4.5,

at around $\Delta/\lambda_p \approx 0.7$, the nominal response is in the region of -40 dB, but the randomly spaced connections can change this to be between -65 and -25 dB.

In terms of validation of the model, the frequency averaged responses of the measured coupled systems show good agreement with the predictions of the equivalent infinite system. A window of 35 Hz was used for the frequency averaging, but if more modes are included, i.e., increasing the frequency window, the better the agreement would be. However, because the end points were not included in the moving average, there is a trade-off; as the frequency window increases, the higher is the first frequency point for the frequency-averaged point. In other words, for a window of 35 Hz, the average is only calculated when there is a response for at least 17.5 Hz above and below this given point. The modal behaviour between the connection points was also captured by the equivalent infinite system, which also serves the purpose of validating the coupling model.

Chapter 5 The application of the Bayes inference for identification of bending stiffness of cable bundles

In this chapter, a combination of Bayesian inference and wavenumber estimation is proposed in order to identify the bending stiffness of cable bundles. Firstly, to familiarise the reader with Bayesian statistics, one classic example is given as an introduction. The chapter then follows to the particular case of bending stiffness identification. The combination of the two techniques allowed for the identification of global and local properties for the bending stiffness.

In order to understand the Bayesian approach to statistics, one must know that this approach assumes that since the value of a given parameter is uncertain, this parameter should be treated as a random variable. The Bayes theorem is then a tool to infer this parameter from a given set of data [**90**]. One classical example for starting to grasp the concept of a Bayesian approach is the following; consider a rare disease that affects 0.1% of population. A usual test to identify this disease will correctly identify 99% of people that have the disease, while testing positive for 1% of people that don't have the disease. After testing positive in one test, the actual chances of having the disease are lower than 99% and can be calculated via application of Bayes theorem. The theorem provides the probability that one hypothesis is true, given an event, as a function of the probability that the event is true, given the hypothesis, the probability of the event and the probability of the hypothesis as follows:

$$p(H|E) = \frac{p(E|H)p(H)}{p(E)} \tag{5.1}$$

where $p(H|E)$ is the probability of the hypothesis given the event, $p(E|H)$ is the probability of the event given the hypothesis, $p(H)$ is the probability of the hypothesis and $p(E)$ is the probability of the event.

In other words, $p(H|E)$, also known as the posterior distribution, is the probability of one having the disease, given that the result of the test was positive, while $p(E|H)$, or likelihood, is the probability of one testing positive, given one has the disease. The $p(H)$, the prior distribution, is the probability one having the disease before the test result. Finally, $p(E)$ is the probability of having the disease and testing positive, $p(H)\ p(E|H) = 0.001 \times 0.99$, plus the probability of not having the disease but being incorrectly identified positively, $p(-H)p(E|-H) = 0.999 \times 0.01$. This can be written as $p(E) = p(H)\ p(E|H) + p(-H)p(E|-H)$. Therefore, after one positive test for the disease, the actual probability of having it is 9.0%.

$$p(H|E) = \frac{p(E|H)p(H)}{p(E)} = \frac{0.99 \times 0.001}{0.001 \times 0.99 + 0.999 \times 0.01} = 9.0\%$$

The Bayesian approach can be used in an iterative way, updating the prior distribution with the now new knowledge, coming from the posterior just calculated, i.e., 9.0%. In this example, if a second independent test also resulted in a positive identification of the disease, the probability of having the disease after both tests came positive would increase to 90.7%.

Although in engineering the likelihood and prior are rarely known quantities, a Bayesian approach can still be used to identify parameters given that a set of data is available.

In this chapter, the bending wavenumber, k_B, is considered as an uncertain parameter through an uncertain bending stiffness, EI, and, therefore, treated as a random variable.

Firstly, before moving to the actual experiments and wavenumber estimations, a model to represent beams under axial load and have an initial knowledge of the behaviour of the flexural wavenumbers under said load is used.

5.1 Flexural beam waveguide under axial load

The experiment comprised a cable bundle typically found in the automotive industry. It was necessary that some tension was applied to the wiring in order to stretch it and keep it geometrically straight, which led to modelling of a beam in flexure consistent with that. The equation of motion of a uniform beam under a uniform static tension, Figure 5.1, is given by [**91**]:

$$\rho A \frac{\partial^2 w(x,t)}{\partial t^2} + EI \frac{\partial^4 w(x,t)}{\partial x^4} = T \frac{\partial^2 w(x,t)}{\partial x^2} \tag{5.2}$$

where ρ is the density of the beam, A is the cross-sectional area, $w(x,t)$ is the displacement, E is the Young's Modulus of elasticity, I is the second moment of area and T is the applied tension. The other properties namely ρ, A, E and I are all assumed to be constant.

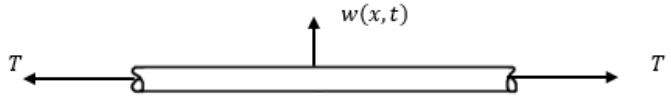

Figure 5.1 – Beam under axial load.

Assuming a flexural wave solution in the form $w(x,t) = Ce^{i(k_B x - \omega t)}$, it is possible to rewrite Equation (5.2):

$$-\omega^2 \rho A w(x,t) + EIk_B^4 w(x,t) = -Tk_B^2 w(x,t) \tag{5.3}$$

where ω is the circular frequency and k_B is the bending wavenumber.

The case when there is no flexural displacement is not of interest, so one can assume $w(x,t) \neq 0$. Hence the dispersion relationship and wavenumber can be derived for harmonic free wave propagation.

$$-\omega^2 \rho A + EIk_B^4 = -Tk_B^2 \Leftrightarrow EI = \frac{\omega^2 \rho A - Tk_B^2}{k_B^4} \tag{5.4}$$

Substituting $k_B^2 = K$:

$$EI\mathrm{K}^2 + T\mathrm{K} - \omega^2 \rho A = 0 \tag{5.5}$$

which is a quadratic equation and, therefore, with solutions given by $K = \frac{-T \pm \sqrt{T^2 + 4EI\rho A\omega^2}}{2EI}$.

Finally, one can then write the bending wavenumbers of a beam under axial load as:

$$k_B = \pm \left[\frac{-T \pm \sqrt{T^2 + 4EI\rho A\omega^2}}{2EI} \right]^{\frac{1}{2}} \tag{5.6}$$

where ρ is the density of the beam, A is the cross-sectional area, E is the Young's Modulus of elasticity, I is the second moment of area, T is the applied tension and ω is the circular frequency. Equation (5.6) reduces to the free bending wavenumber of a beam with no axial load applied if $T = 0$.

The theoretical model then produces the typical numerical results presented in Figure 5.2 for different values of the axial load applied. Two of these wavenumbers are purely real, which indicate propagating waves, and are given by $k_B = \pm \left[\frac{-T + \sqrt{T^2 + 4EI\rho A\omega^2}}{2EI} \right]^{\frac{1}{2}}$, while two of them are purely imaginary, given by $k_B = \pm \left[\frac{-T - \sqrt{T^2 + 4EI\rho A\omega^2}}{2EI} \right]^{\frac{1}{2}}$, and represent near-field or evanescent waves. The numerically simulated model comprised a rectangular beam with cross-sectional area of 6 mm by 3 mm (base x height) and standard stainless steel properties; Young's modulus of 200 GPa and density of 7850 kg/m^3. Therefore, the bending stiffness, given by the product of the Young's modulus and the second moment of area, is 2.70 Nm^2. The range of the masses applied to create the axial load was from 0 to 250 kilograms, which, assuming that the yield strength for the steel is 330 MPa, the stress ($m_{applied} * g/A$) would be in the range equivalent to 0% to 41.3% of the yield strength.

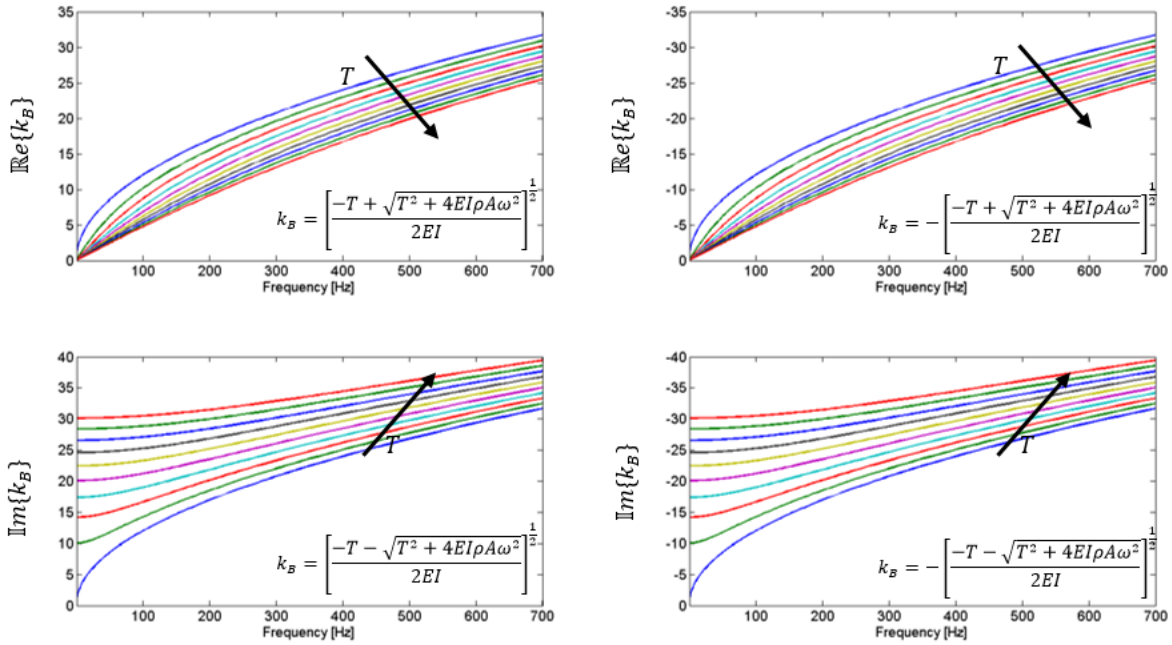

Figure 5.2 – Bending wavenumbers of a beam under axial load.

Real and Imaginary parts of the bending wavenumber of a beam under a constant axial load for different values of the applied tension ($EI = 2.7\ [Nm^2], \rho A = 0.1413\ [kg/m], m_{applied} = [0, 250][kg]$, which is equivalent to $T = [0, 2452.5][N]$)

5.2 Parameter identification strategy

The experimental data can be used within a Bayesian strategy in order to update the prior probability density function [**92**] of the bending wavenumber of a beam under axial load. Assuming that the only knowledge one has about the prior distribution is its lower and upper limits, a uniform distribution gives the maximal uncertainty for an uncertain variable, i.e., if there is no other strong grounds for assuming a different prior, a uniform distribution would be the best start [**93**]. That is a result of the Maximum Entropy Principle [**94**] [**95**] [**96**]. Any other information considered about the prior distribution would result in a non-uniform distribution and the random variable would have less entropy or, in another words, more information, which would put less weight in the role of the experimental data updating the prior distribution [**97**]. The measured data is usually assumed to be of an additive Gaussian noise in the form of $\boldsymbol{y}(\boldsymbol{\theta}) = \boldsymbol{q}(\boldsymbol{\theta}) + \boldsymbol{e}$, where $\boldsymbol{q}(\boldsymbol{\theta})$ is the system output of a model under the same excitation $\boldsymbol{\theta}$, $\boldsymbol{y}(\boldsymbol{\theta})$ is the measured data and $\boldsymbol{e}$ is the prediction error that accounts for the difference between $\boldsymbol{y}(\boldsymbol{\theta})$ and $\boldsymbol{q}(\boldsymbol{\theta})$ [**98**] [**99**].

Assuming the measured data $\boldsymbol{y} = [y_1, y_2, \dots, y_N]$, in a Bayesian context, the posterior distribution of the set of model parameters $\boldsymbol{\theta}$, given the data $\boldsymbol{y}$, is [**98**]:

$$p(\boldsymbol{\theta}|\boldsymbol{y}) = \frac{p(\boldsymbol{y}|\boldsymbol{\theta})p(\boldsymbol{\theta})}{p(\boldsymbol{y})} \tag{5.7}$$

where $p(\boldsymbol{y}|\boldsymbol{\theta})$ is the likelihood function, $p(\boldsymbol{\theta})$ is the prior distribution and $p(\boldsymbol{y})$ is a normalising constant.

In other words, at every frequency, $p(\boldsymbol{y}|\boldsymbol{\theta})$ is the probability of the observed data $k_{B_{observed}}$, or bending stiffness via Equation (5.6), given a wavenumber k_B from the prior distribution, which is assumed to be uniform. The prior, $p(\boldsymbol{\theta})$, is the distribution of the modelled wavenumber k_B. The probability density function $p(\boldsymbol{y})$ is the pdf of the observed data and can be treated as a simple normalising constant that does not affect the identification of the parameter of interest.

A first attempt at the Bayesian inference was made using numerical simulation as a proxy for experimental data. Eight dispersion curves were produced with the introduction of an additive noise in the form of $k_{B_{synth}} = k_B[1 + \epsilon(\omega)]$. In this pseudo-experiment, $k_{B_{synth}}$ represents $k_{B_{observed}}$. Figure 5.3 shows the synthetic dispersion curves and the nominal case. The distributions for $\epsilon(\omega)$ are show in Figure 5.4 and a value for it was sampled at each frequency for each one of the cases.

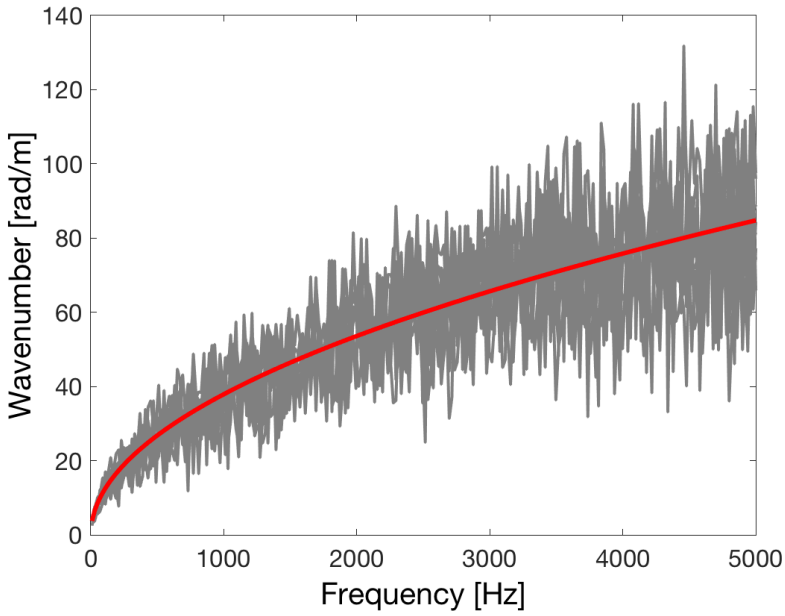

Figure 5.3 – Synthetic bending wavenumber data.

Nominal case in ▬ and, in ▬, the eight synthetic cases.

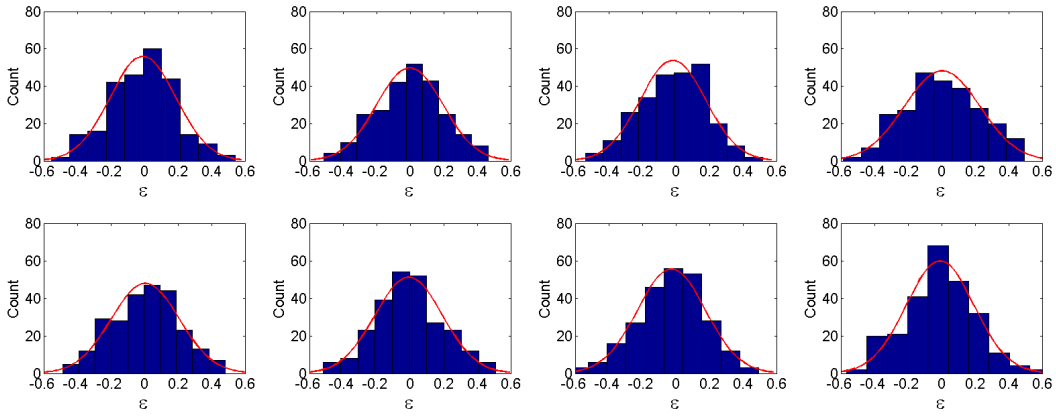

Figure 5.4 – Histogram of the added noise for each pseudo-experiment to build the synthetic data and fitted Gaussian distribution.

For convenience, the likelihood function is often formulated in terms of the negative log-likelihood function [**98**]:

$$L(\boldsymbol{\theta}) = -\ln p(\boldsymbol{y}|\boldsymbol{\theta}) \tag{5.8}$$

Hence, combining Equations (5.7) and (5.8):

$$p(\boldsymbol{\theta}|\boldsymbol{y}) \propto e^{-L(\boldsymbol{\theta})} \tag{5.9}$$

If $\boldsymbol{e}$ is assumed to be independent and identically Gaussian distributed with zero mean and standard deviation σ_S, one can write [**98**]:

$$p(\boldsymbol{y}|\boldsymbol{\theta}) = \prod_{i=1}^{N} \frac{1}{\sqrt{2\pi}\sigma_s} e^{\left\{\frac{-1}{2\sigma^2}[\boldsymbol{y}_i(\boldsymbol{\theta})-\boldsymbol{q}_i(\boldsymbol{\theta})]^2\right\}} \tag{5.10}$$

In this particular case, $\boldsymbol{y}_i(\boldsymbol{\theta})$ are the synthetic bending wavenumbers, $k_{B_{synth}}$, at a given frequency and $\boldsymbol{q_i}(\boldsymbol{\theta})$ is a bending wavenumber k_B sampled from the uniform prior distribution. The uniform prior distribution assumes that k_B is between 0 and 200 rad/m. The analysis is made every 1 Hz sampling a value of k from the prior and using it as $\boldsymbol{q}(\boldsymbol{\theta})$.

For instance, for a given index i, there is an associate value for k_B that comes from the assumed uniform prior distribution. Whilst $\boldsymbol{y}_i(\boldsymbol{\theta})$ comes from the synthetic data. Therefore, in this example, for every index i, $\boldsymbol{y}_i(\boldsymbol{\theta})$ is a vector with 8 values for the wavenumber from the pseudo or simulated experiment. The individual value $q_i(\boldsymbol{\theta}) = k_B(i)$ is repeated n times to match the size of the vector $\boldsymbol{y}_i(\boldsymbol{\theta})$ and then form the vector $\boldsymbol{q}_i(\boldsymbol{\theta})$. These values are the inputs for Eq. (5.10) and the calculations were performed using Matlab. Finally, it is possible then to find a likelihood $p(\boldsymbol{y}|\boldsymbol{\theta})$ associated with each index i. At every i, equivalent to a k_B value, the value of the prior distribution is multiplied by the value of the likelihood distribution, resulting in a value proportional to the posterior distribution. For purposes of parameter identification, it is only required to know which k_B (or index i) maximises the result of this multiplication.

Once the whole range of the prior was considered (varying the index i), the process is repeated for the next frequency. The results of the analysis of the synthetic data are shown in Figure 5.5. The parameter is identified as the value that maximises the posterior distribution. For each frequency, these values are shown in Figure 5.6.

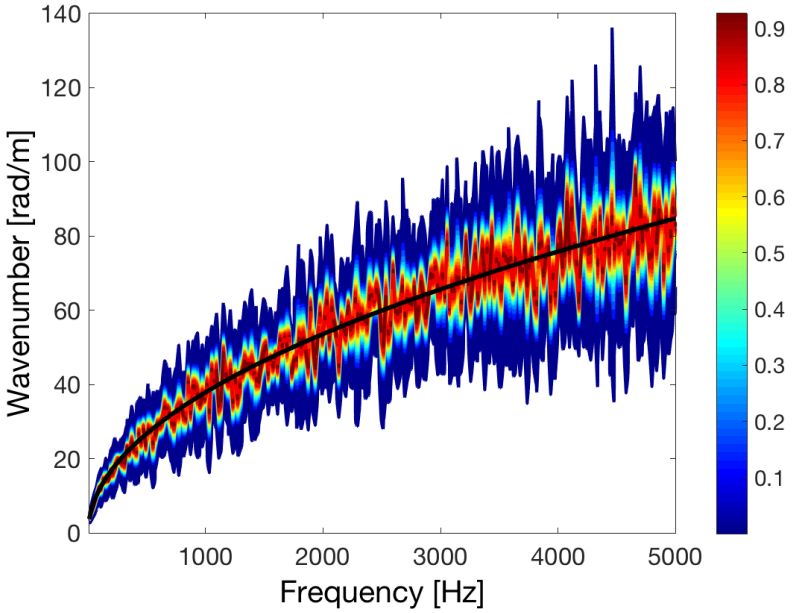

Figure 5.5 – Posterior distribution after the Bayesian inference has been applied.
Colormap is the estimated distribution and the actual value of k_B at each frequency (—).

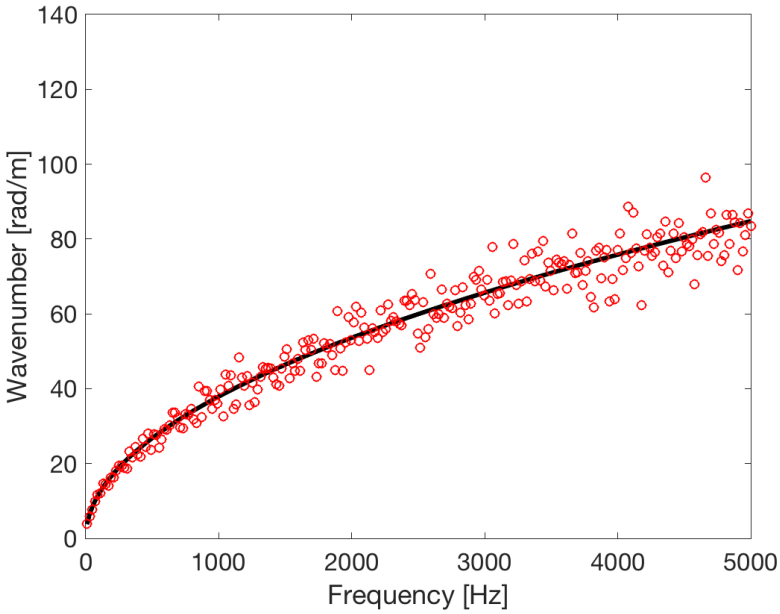

Figure 5.6 – Wavenumbers selected via Bayesian inference.
Values that maximise the posterior (○) and the actual value of k_B (—) at each frequency.

One can also look at the results frequency by frequency. Figure 5.7 shows the posterior and prior distributions along with the actual value of the bending wavenumber at 3000 Hz. It also shows the relative error from each of the dispersion curves and the wavenumber identified via the Bayesian framework, which is the value that maximises the posterior distribution. The wavenumbers from the synthetic data are also shown, and at this frequency some of them differ substantially from the actual wavenumber (theoretical and noiseless data). This is especially the case for samples 4 and 6. The value that maximises the posterior is taken as the identified wavenumber for each frequency.

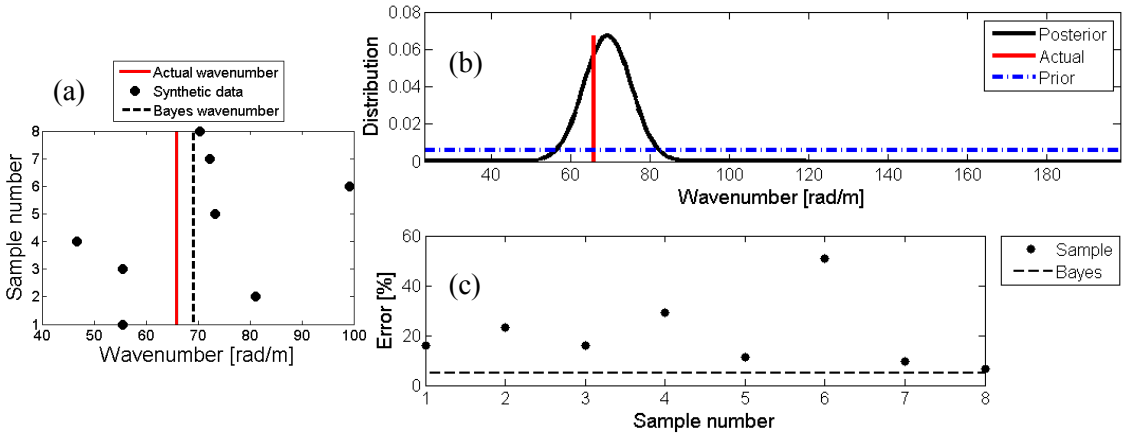

Figure 5.7 – Wavenumbers at 3000 Hz.

Wavenumbers from each one of the pseudo-experiments in (a), the posterior distribution at 3000 Hz in (b) and magnitude of the error associated in the wavenumber with the Bayes identification versus the different synthetic data (c).

The frequency-averaged errors (the average of the errors frequency-by-frequency) for each of the wavenumbers calculated using the synthetic data are around 15%, but can reach up to 18.16%, in the case of sample 4. After using the Bayesian inference, the frequency-averaged error reduces to 5.90%, even in the presence of strongly noisy data, as shown in Figure 5.7(c).

5.3 Experimental analysis of a cable bundle

A cable bundle was fixed at one end and attached to a rope that went through a pulley at the other end, supporting a mass of 16 kilograms. The applied load was chosen to ensure that the cable bundle is kept straight. A general schematic of the experiment is presented in Figure 5.8. Ten points equally spaced along the length of the wiring were measured. The velocity response covered a total measurement length of 315 mm. The flexural velocity at the points were measured with a scanning laser vibrometer and the cable was excited using an electromagnetic shaker. Measurements were taken up to 700 Hz with a frequency resolution of 1 Hz. A white noise signal was used for the shaker and the excitation signal to the shaker amplifier was used for the reference channel when evaluating the transfer functions. As in the previous chapter, reflective tape was necessary at the measurement points to assure the strength of the reflected laser signal. Given the random excitation signal, Hanning windows were used for both the signals and 15 averages were performed in the calculation of the FRFs. The shaker stood on a small fixed platform. In order to assume that only propagating bending waves were present, the response points were considered to be away from any boundaries, such as the fixed end and the pulley or the point of excitation. The cable bundle tested is a typical sample of a harness used in the automotive industry and it can be seen in Figure 5.9. Its properties are mass of 0.20 kilograms, length of 1.184 m and approximate diameter of 10.1 mm. Two examples of typical frequency response function and coherence measured are shown in Figure 5.10.

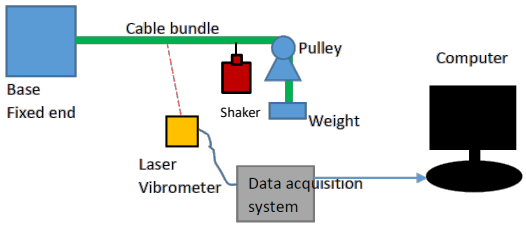

Figure 5.8 – Experimental setup.

Figure 5.9 – Measured cable bundle; typical wiring from the automotive industry.

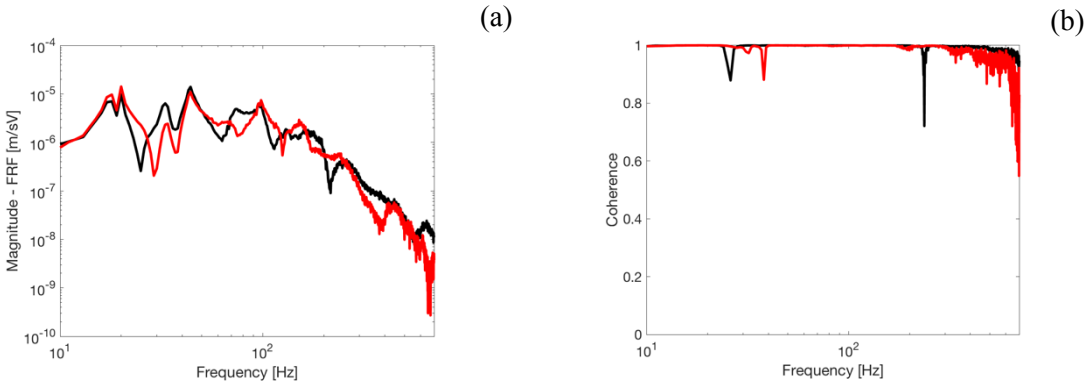

Figure 5.10 – Example of measured FRF data between the excitation signal to the shaker and the cable velocity.

In (a), the magnitude of two typical frequency response functions measured with the laser vibrometer. In (b), the measured coherence.

Once the complex frequency response functions were obtained, a correlation technique [**100**] [**101**] was used to identify the flexural wavenumbers present in the cable bundle vibrational response. Since only one cable sample was available, to introduce some variability, between each measurement, the system was dismantled and reassembled. Measurements were also made at

different times. One advantage of this wave identification approach is that the method does not require any prior knowledge of the structure such as boundary conditions, material properties or cross-sectional dimensions [**102**]. Adapting the two-dimensional wavenumber correlation case [**100**] [**101**], the wavenumbers are identified when the absolute value of the following correlation function reaches a maximum:

$$\hat{Y}(k_{tx},\omega) = \frac{l}{N_p}\sum_{j=1}^{N_p} Y(x_j,\omega)e^{-ik_{tx}x_j} \tag{5.11}$$

where l is the length of the cable measured, N_p is the number of points measured, $Y(x_j,\omega)$ is the complex transfer function measured at the point x_j at the frequency ω and k_{tx} is the trial wavenumber to be estimated. The trial wavenumbers are real numbers.

The data obtained for the wavenumber and hence dispersion curves via the correlation technique is shown in Figure 5.11:

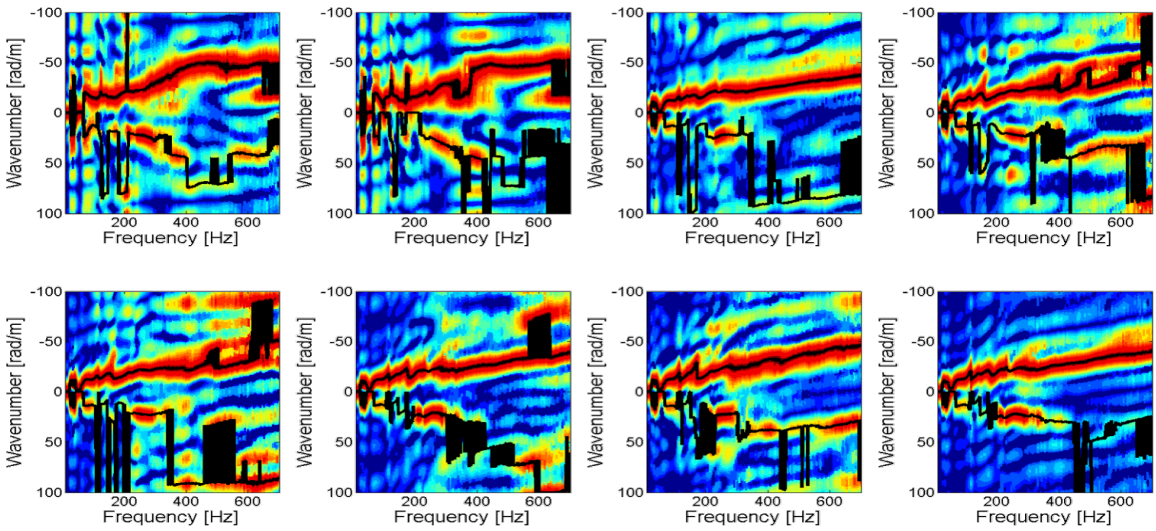

Figure 5.11 – Wavenumber identification via correlation technique.

Black lines represent the real value for the wavenumber that maximises the amplitude of the complex value of the correlation function. Each colourmap is a different individual measurement, i.e. a repetition of the FRF measurement on eight occasions.

The wavenumbers identified in Figure 5.11 (black solid lines) show the behaviour of the purely real wavenumbers predicted by the theory, which represents the propagating waves. This is especially the case for the negative wavenumber values, which, in this case, are the directly excited waves propagating from the exciting point, rather than the waves reflected by the boundary and then measured. For convenience, since the negative wavenumbers identified in the experiment show a stronger response and what seems to be only one single kind of wave, they were chosen as the input to the Bayesian framework. Once a set of wavenumbers are defined, the same procedure as used for the simulated synthetic data can be applied to the measured data and an updated posterior can be found.

The updated posterior after considering a uniform distribution as a prior for each frequency is shown in Figure 5.12(a). The wavenumber that produces the maximum value of the updated posterior distribution is then selected and can be used as an input in Equation (5.4) to calculate the value of the bending stiffness of the cable bundle, Figure 5.12(b).

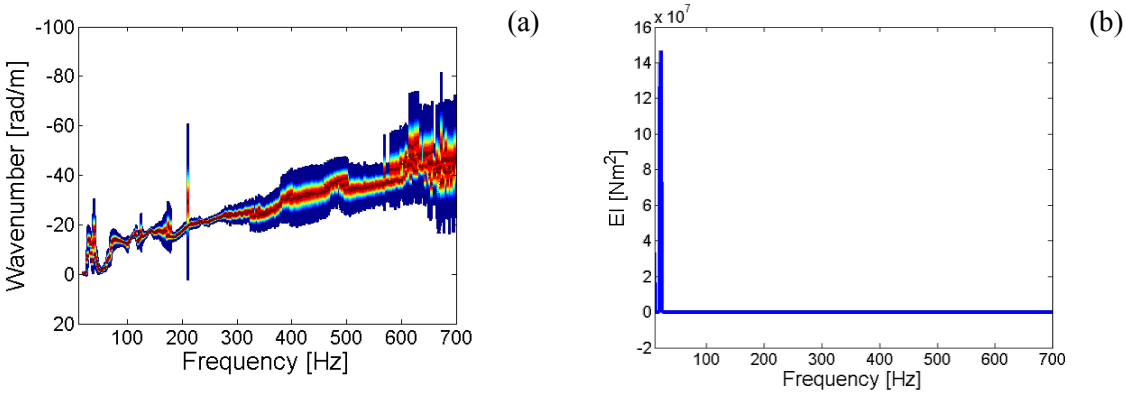

Figure 5.12 – Updated posterior and estimated bending stiffness of the cable bundle.

In (a), the updated posterior distribution after the Bayesian analysis of the 8 experimental data. In (b), the measurement data at low frequencies (<20 Hz) is unreliable, leading to gross error in the estimated bending stiffness.

Since the identification of the wavenumbers at lower frequencies is poor, producing results for the bending wavenumbers $k_B \approx 0$, the corresponding values for EI approach non-physical values, as shown in Figure 5.12(b). These values at lower frequencies are subsequently ignored and the data without these outliers is presented in Figure 5.13(a), while Figure 5.13(b) shows the histogram of these values. The histogram indicates a bending stiffness $EI \approx 1$ Nm^2, whilst the fitted Gamma distribution (shape parameter $a_\Gamma = 4.79$ and a scale parameter $b_\Gamma = 0.253$) has mean of 1.214 Nm^2 and standard variation of 0.554 Nm^2. The Gamma distribution is suited for modelling non-negative random variables [**103**] and its expected value is given by $\mathbb{E}[x] = a_\Gamma b_\Gamma$ and its variance is given by $\sigma^2 = a_\Gamma b_\Gamma^2$.

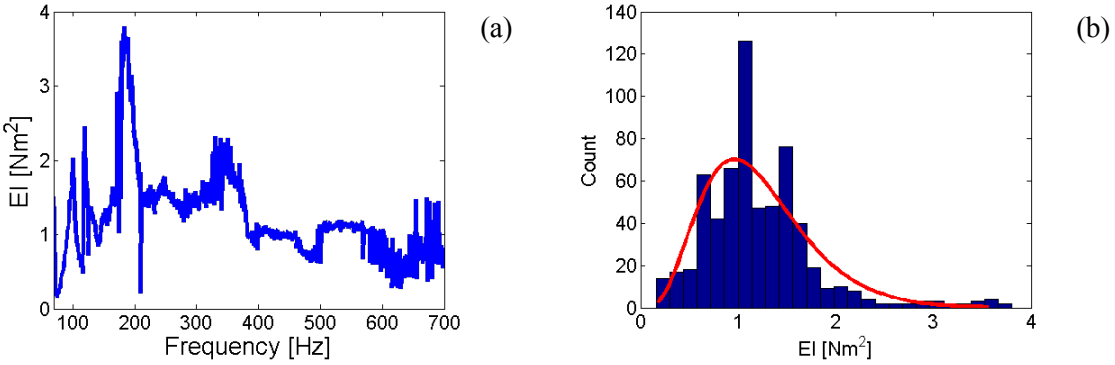

Figure 5.13 – Processed bending stiffness data from the identified dispersion curve.

In (a), the values for the bending stiffness when the outliers (non-physical values) are discarded and for results plotted over a reduced frequency range. In (b), the histogram of the values for estimated the bending stiffness and (—) the fitted Gamma distribution (shape parameter $a_\Gamma = 4.79$ and a scale parameter $b_\Gamma = 0.253$).

Assuming that the bending stiffness is frequent independent, it is possible, using the minimum and maximum values for the bending stiffness in Figure 5.13, to define a range of analysis and comparison with the bending wavenumber identified through the Bayesian inference. The bending stiffness is identified to be between 0.1574 Nm^2 and 3.806 Nm^2. This range is then sampled in equally divided intervals and the sampled bending stiffnesses are used in Equation (5.6) to calculate the bending wavenumbers. A convergence test was made changing the number of division from 10 to 2000. Figure 5.14(a) shows an example when said range is divided into 16 equally spaced values for the estimated bending stiffness and the corresponding theoretical bending wavenumbers. Figure 5.14(b) shows the maximum coefficient of determination R^2 found versus different numbers of divisions whilst Figure 5.14(c) shows the bending stiffness that maximises R^2 versus different numbers of divisions. The system converges to a maximum $R^2 = 0.8974$ and bending stiffness $EI = 1.0062$ Nm^2. The whole frequency range was considered in this test, in contrast to when the histogram was calculated when only frequencies higher than 100 Hz were used.

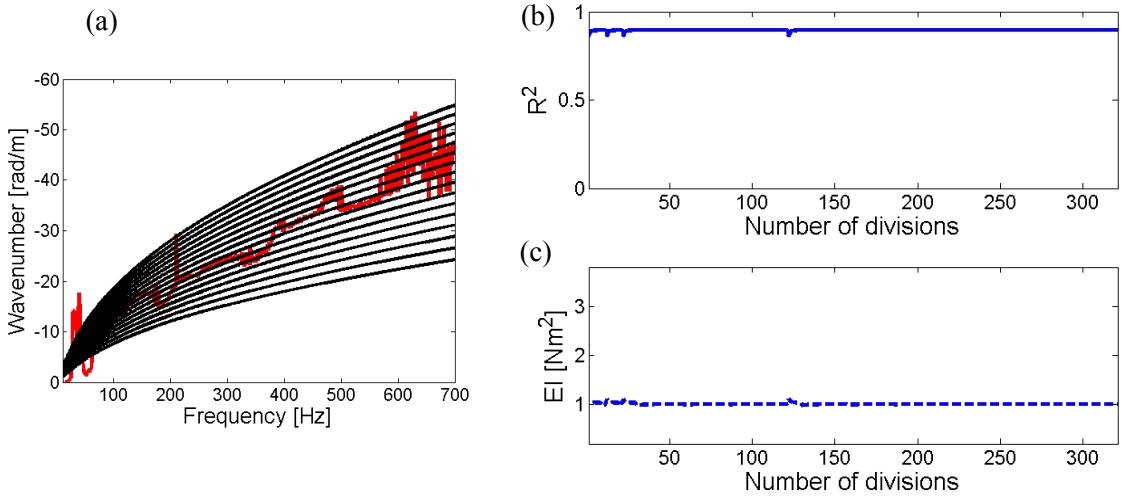

Figure 5.14 – Convergence test of the bending stiffness that maximises the coefficient of determination.

In (a), wavenumbers calculated using the different bending stiffness (—) compared to the Bayesian inferred wavenumber (—). In (b) the maximum value for the coefficient of determination R^2 and in (c) the corresponding value of the bending stiffness EI that produces such R^2.

Once the bending stiffness is chosen, it is possible to use it to compare the bending wavenumbers with the fitted EI to the values identified via the Bayes' approach and calculate the residual between them. The results for it are shown in Figure 5.15.

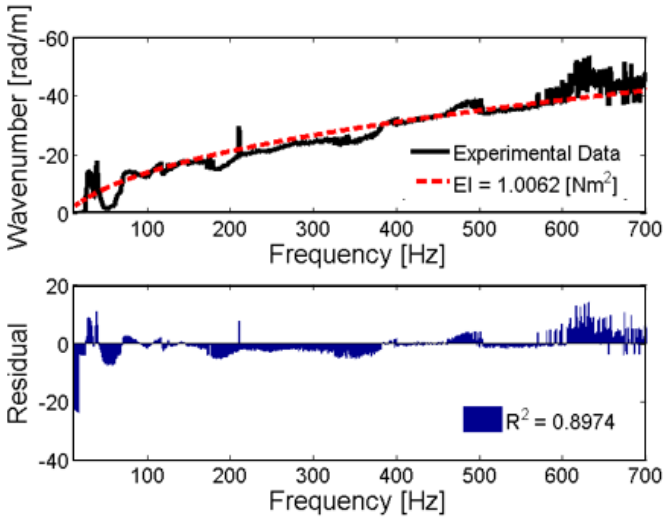

Figure 5.15 – Identified bending stiffness using Bayes inference and residual of the fit.

The dispersion curve identified via Bayesian inference from the 8 sets of experimental data (—) and the theoretical wavenumber using Eq. (5.6) which used the fitted bending stiffness *EI* (— —).

Then using the parameters of the fitted Gamma distribution, it is possible to find the cumulative distribution function. The values that limit to 95% of the identified bending stiffness are, as shown in Figure 5.16. Once these values are known, one can compare the dispersion curves using different bending stiffnesses, such as the mean of the Gamma distribution, 1.214 Nm^2; the lower value of the 95% interval, 0.382 Nm^2; the upper value of the 95% interval, 2.518 Nm^2; the best fit, 1.0062 Nm^2; and the experimental data. The corresponding calculated wavenumbers are shown in Figure 5.17.

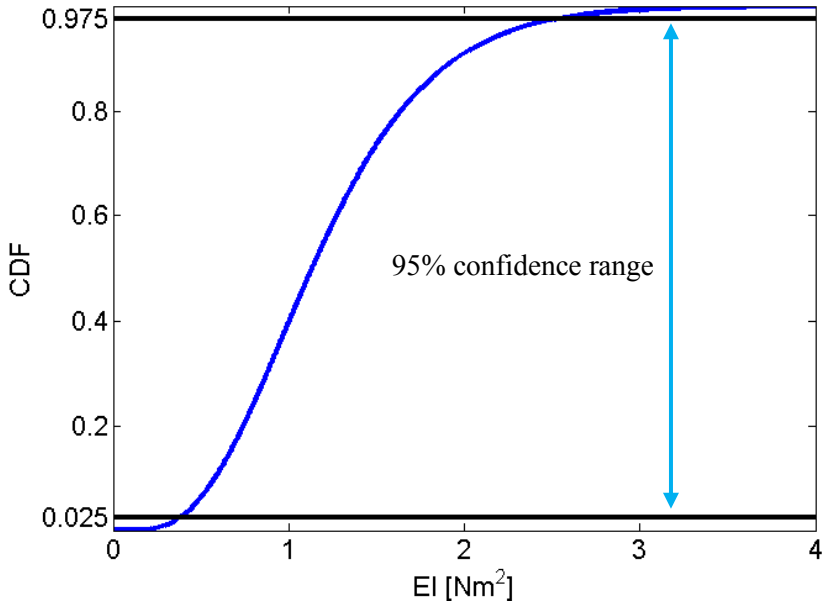

Figure 5.16 – Cumulative distribution function.

(—) Cumulative distribution function, (—) upper (2.518 Nm^2) and lower (0.382 Nm^2) values of the 95% interval.

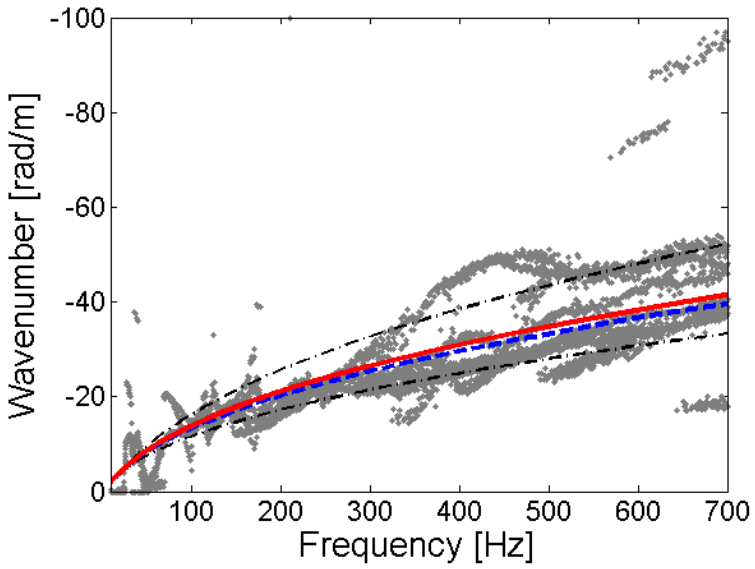

Figure 5.17 – Experimental data versus the dispersion curve calculated using the identified constant bending stiffness and its 95% interval.

— is the wavenumber using the identified bending stiffness of 1.0062 Nm^2, – – is the wavenumber using the mean of the fitted Gamma distribution (1.214 Nm^2), —•— is the limits of the 95% interval and • for the 8 sets of experimental data.

Using the identified bending stiffness $EI = 1.0062$ Nm^2 and the linear density of the cable $\rho A = 0.20/1.184$ kg/m, it is possible simulate how sensitive the wavenumber is to the value of the applied tension in the cable bundle, using Equation (5.6). As the tension increases and dominates the behaviour of the bending wavenumber, the closer to 0 is the real part of the wavenumber over all of the frequency range. The corresponding imaginary part tends to a constant given by $\sqrt{T/EI}$. Considering the applied mass of 16 kilograms, the tension is observed to not being high enough to dominate the value of the corresponding bending wavenumber, Figure 5.18.

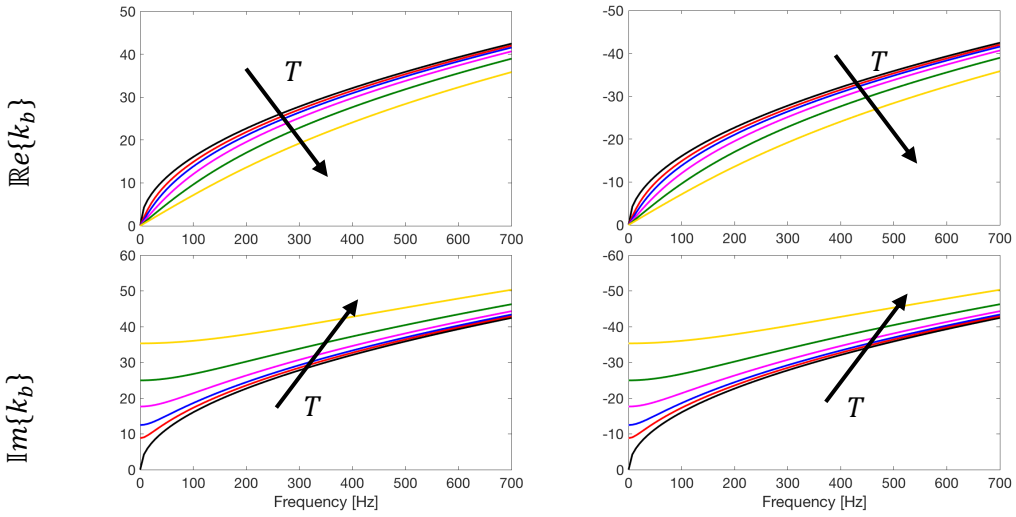

Figure 5.18 – Simulated cable: sensitivity to the applied mass and hence tension.

Real and Imaginary parts of the bending wavenumber of a simulated beam under a constant axial load for different values of the applied tension considering the properties of the measured cable bundle ($EI = 1.0062\ [Nm^2], \rho A = 0.20/1.184\ [kg/m]$, applied mass — 0, — 8, — 16, — 32, — 64, — 128 $[kg]$. T is given by the applied mass multiplied by $g = 9.81\ m/s^2$).

One can also use the identified bending stiffness to predict the behaviour of the system if the tension applied to the cable is changed. Figure 5.19 shows the result when a mass of 11 kilograms is used to tension the cable bundle. In the region between 100 Hz and 400 Hz, the results are mostly within the bounds, but at higher frequencies the agreement between experimental data and prediction deteriorates due partially because of the inherent varying properties of the cable bundle and also due to poor coherence at the higher end of the frequency range. Also, the correlation technique can erroneously estimate wavenumbers that are integer multiples of the actual wavenumber, which can be the case for some of the outliers in both Figures 5.18 and 5.19. This is due to the finite length of the measurements. The subsequent window effect on the calculated correlation function has not one single maximum but multiple smaller maxima at integer multiples of the actual wavenumber. The window creates "ripples" in the correlation function.

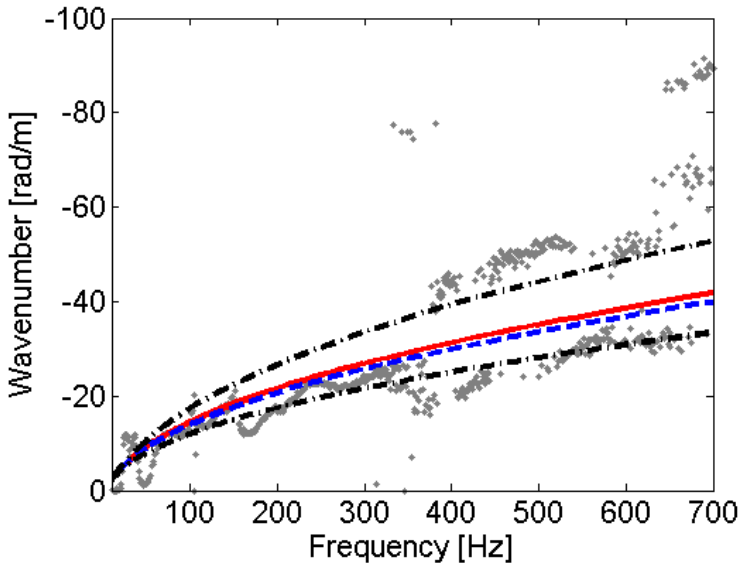

Figure 5.19 - Experimental data versus the dispersion curve calculated using the identified constant bending stiffness and its 95% range interval when 11 kg act on the cable bundle. — is the wavenumber using the identified bending stiffness of 1.0062 Nm^2, — — is the wavenumber using the mean of the fitted Gamma distribution (1.214 Nm^2), — • — is the limits of the 95% interval and • for 1 set of experimental data.

5.4 Bayesian identification of a random field of the Young's modulus of a cable bundle using synthetic data and wavenumber estimation

The correlation technique to find the bending wavenumbers can only find an average behaviour of the structure. Even though it managed to capture the general response of the cable bundle, a not insignificant part of the measured points fell outside the 95% confidence interval found. Also, it does not capture values for the local bending stiffness if these change in the structure. In order to achieve a better insight of the behaviour of the bending stiffness along the length of the cable bundle, a

different combination of the correlation technique and the Bayes inference is proposed. A simply supported beam model is simulated and used as a reference for this proposal.

The simulated beam has a slowly varying Young's modulus of elasticity along its length. This random field is described by the Karhunen-Loève expansion, while the response of the beam can be calculated using the Wentzel–Kramers–Brillouin approximation, as in section 3.1.1. The Young's modulus of elasticity for a typical example can be seen in Figure 5.20 and the uniform beam referenced has the standard properties of stainless steel. The second moment of area is considered to be constant, so the changes in the Young's modulus of elasticity translate directly into changes in the bending stiffness EI.

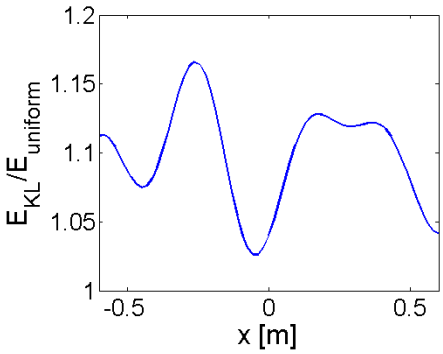

Figure 5.20 – Random field for the Young's modulus of elasticity.

Eighteen points along the beam were considered as locations of interest, i.e., points where the local wavenumbers will be calculated. For each of these locations, the response of 5 points to the right of them and 5 to the left of them were calculated in the form of the flexural velocity of the structure. It is not necessary that these points are equally spaced [**100**], so they were randomly sampled to be at distances d_1, d_2 , d_3, d_4 and d_5 to the right and to the left of the reference location. Symmetry is not necessary, but it is convenient. For each of the 18 locations of interest, 10 sets of measurements were simulated, with different sets of distances between the reference location and the additional measured points. The total length of the beam is 1.2 m and the 18 locations of interest are located in the span of 0.5624 m of the beam, which is to start and end at 0.3188 m from each end of the beam. These locations are equally spaced. Therefore, in this pseudo-experiment, the velocity at a total of 1980 points was calculated. The frequency range is 10 to 5000 Hz and the wavenumbers when each one of the reference locations were considered are shown in Figure 5.21.

It is possible then to use the 10 sets of wavenumber values found using the correlation technique for each reference point as an input to the Bayes inference discussed in Section 5.3 finding a most probable value for the wavenumber to each one of them frequency by frequency. In other words, the proceeding method discussed in Section 5.2 is repeated at each one of the 18 points of interest, which results in 18 dispersion curves inferred via a Bayesian approach that would fit the pseudo experimental data. In a similar manner to Section 5.3, the inferred wavenumbers can then be related

to a bending stiffness. Again, the outliers at lower frequencies are discarded and a distribution for the local bending stiffness is show in Figure 5.22.

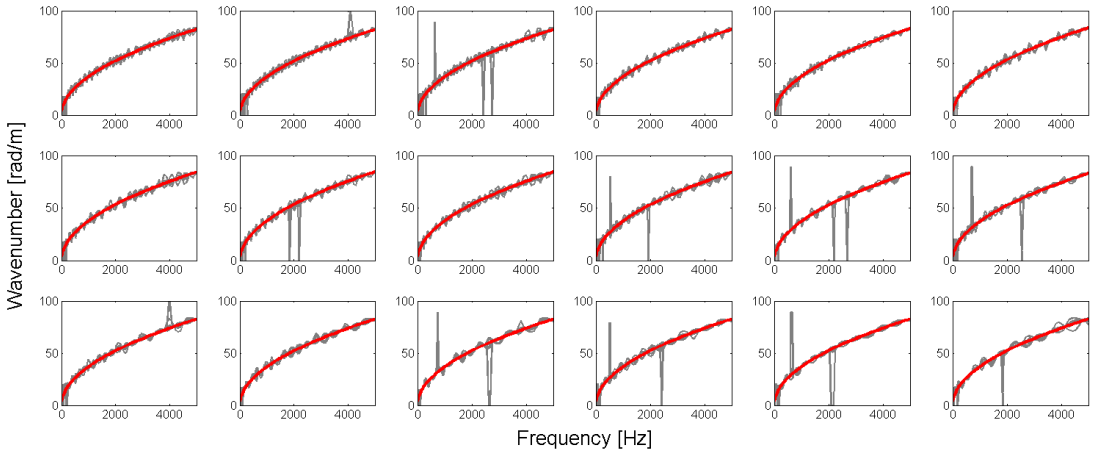

Figure 5.21 – Wavenumbers at the 18 reference locations.

The actual local wavenumber in ▬ and the 10 sets of calculated wavenumbers in ▬.

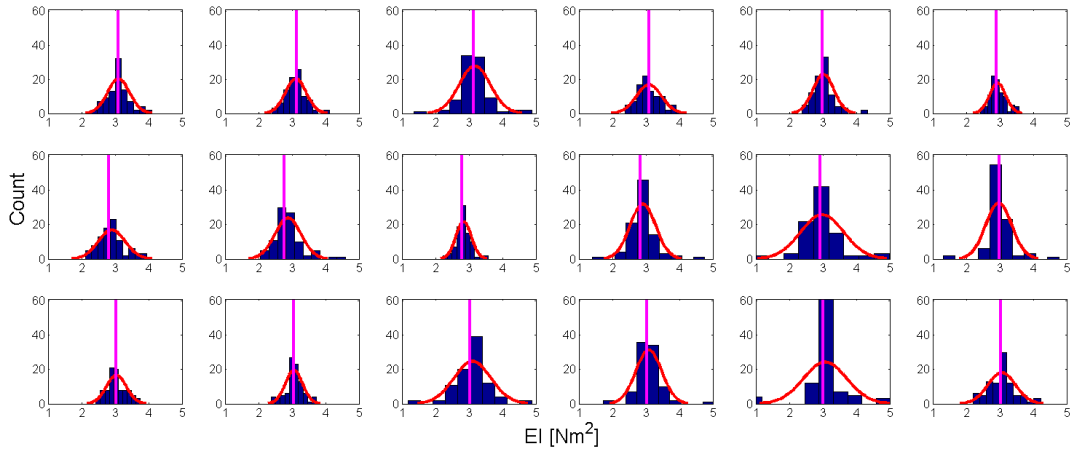

Figure 5.22 – Local bending stiffness.

Histogram from the synthetic data in blue, ▬ is the fitted distribution and ▬ is the actual local bending stiffness.

Gaussian distributions were used to fit the local bending stiffness. The fitted distributions were used as support for reconstruction of the random field and their mean were used as the identified value for the bending stiffness for that particular point. The results are shown in Figure 5.23(a). The scale of the colormap was normalised accordingly to each one of the fitted distributions in order to facilitate the visualisation of the results. Figure 5.23(b) shows the results when Gaussian noise was added to the simulated velocities, in a similar fashion of the noise added in Section 5.2.

In both cases, noiseless and polluted synthetic data, the technique is able to identify the random field. The measurement would require a considerable amount of points to be measured, but it could be made with the assistance of an automatic scanning laser vibrometer.

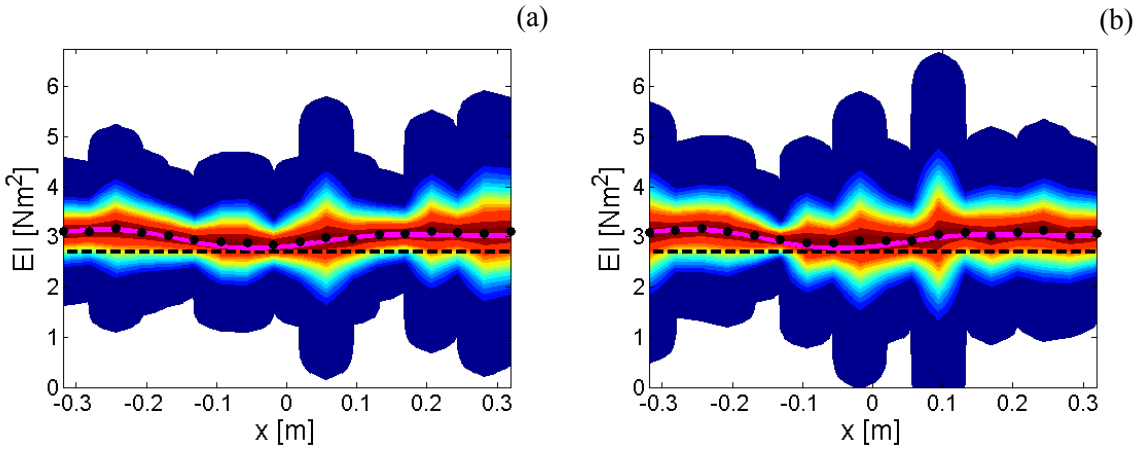

Figure 5.23 – Reconstructed random field for the bending stiffness.

The colormaps are the fitted distributions, ▬ is the actual random field, • is the identified value for the local bending stiffness and ▬ ▬ is the bending stiffness of a homogeneous beam with stainless steel properties.

5.5 Discussion

The experiment was conducted with the cables under an axial load and the results show the behaviour predicted by the theory. The correlation technique approach was chosen due to the fact that it is independent of the boundary conditions, as long as propagating bending waves are assumed, in other words, if the measurements are made far enough away from the boundaries and the source of excitation.

Firstly, as a proof of concept, a pseudo-experiment was conducted. A known wavenumber was polluted with additive Gaussian noise to generate synthetic data that was used to feed into the Bayesian framework. Even with high levels of noise added, up to +/- 60% around the nominal value, the Bayesian inference tool reduces the error when identifying the bending stiffness via the synthetic data. In this particular case, a reduction of the order of one-third compared to the individual pseudo-experiments was made. After the positive results of the pseudo-experiment, the same framework was applied to real experimental data.

Once the bending wavenumber was selected via the Bayesian approach, it was then possible to identify a distribution for the bending stiffness within the frequency range analysed. As there are no reasons for considering that the bending stiffness is frequency dependent in this range, 0 to 700 Hz, the bending stiffness was assumed to be constant. The distribution given by the wavenumber inference gave a range of values that served as a support to refine the value of the bending stiffness that would best fit the experimental data, maximising the coefficient of determination (R^2) value. This value is then used to find a confidence interval around it and compared again with the experimental data. This Bayesian model assumes a Gaussian error in the whole experimental setup, but if any other information is known it would be possible to change the formulation to match the

extra piece of information. One limitation of this approach is that the correlation technique can only find an averaged wave behaviour that would best fit the data measured. Even though this shed some light on the general response of the cable bundle, a significant part of the measured data is outside the bounds of the confidence interval calculated. This could be addressed if one finds values for the local bending stiffness for the structure of interest.

This was put to test with another pseudo-experiment. The velocity data used as input into the correlation technique came from a simulated simply supported beam model with slowly varying properties along the length of propagation of the bending waves. The set of measurements combined with the Bayesian framework was then able to reconstruct the random field. The latter describes the Young's modulus and, if the other properties are considered to be constant, the bending stiffness of a one-dimensional waveguide. The other mechanical properties, such as density, area and second moment of area, are trivial to measure and were only considered constant for convenience. When noise was added to the simulated velocity data, the proposed technique also managed to reconstruct the bending stiffness field. The distributions identified offer insight into the spatial spread of the random field and should give some guidance to the confidence of the results. This method required a considerable amount of measurement points, but this should not be a problem with the use of scanning laser vibrometers or other whole area optical measurements, such as Digital Image Correlation (DIC) or reflectometry.

5.6 Conclusions

This chapter addresses the issue of how to identify uncertain properties in cable bundles. It focused on the bending stiffness, but the same technique could be used for other properties. The estimated bending stiffness was used as an input parameter for some of the models in Chapter 3. Although the results here are estimated over a frequency range, it was assumed that the bending stiffness does not depend on the frequency. Therefore, the identified distribution for the bending stiffness was translated to a support for local, or spatial, dependent bending stiffness.

Moreover, this chapter successfully offers a novel way of combining an established correlation technique to find wavenumbers within a Bayesian framework to identify mechanical properties and estimate variability in the samples. The correlation technique is usually applied to identify global wave behaviours, but the work done here shows that if enough points are measured, even local properties can be estimated. This allows the estimation of properties described by random fields. The case studied focused on a typical cable bundle used in the automotive industry, but this same technique could be implemented in different scenarios, such as corroded pipes. For instance, one could identify regions where the pipes would be more susceptible to leakage due to reduction of the wall thickness.

Future work could be done to estimate the effective Young's modulus of the cable bundle, considering the geometry of the cross-sectional area of the bundle and individual diameters and properties of the wires, along with the distribution of copper in them. This requires assumptions on the properties and geometry. Also, the proposed technique could be tested further on other real experimental data. For particular applications in the automotive or aerospace industries, for instance, the identified cable properties could now be included within an FE beam model to represent them and replace the simplistic and more approximate point lumped mass attachment typically adopted. The automotive industry might be more interested in the distribution of the properties and envelopes for the responses due the large-scale production, whereas the aerospace industry could be interested in the actual properties of individual cables that will be used in their systems. The technique proposed here offers insight in both cases.

Chapter 6 Conclusions and further work

This study concerned the variability in the vibrational response due to uncertainties in coupled structures. A mobility approach was used to attach one-dimensional waveguides to thin plates. Mobilities were used because they have closed analytical solutions for the infinite system and finite beam. Depending on the boundary conditions, if necessary, the input and transfer mobilities for the finite plate can be calculated through the mode shapes found via FEM or analytically.

Firstly, infinite uniform beams and plates were considered for the coupled structures. These structures allow one to get a first grasp of the dynamic behaviour of the coupled systems, whilst maintaining analytical and concise expressions for the input and transfer mobilities. They can also be seen as an approximation to the frequency averaged response of finite structures. Finite structures were also subsequently considered in this study.

In the case of the one-dimensional waveguides, the WKB approximation was used to treat structures with spatial slowly varying properties. This approximation assumes that the properties vary slowly enough so that there are no reflected waves due to these small changes, or that they can be neglected. A wave propagation approach was used to derive expressions for the mobilities of the infinite beam and a generalised expression for the finite beam. Comparisons were made against existing results or numerical (FE) simulations.

For the uncertain plates, a combination of a FEA model along with the perturbation method was used to calculate the input and transfer mobilities. Aiming to keep the computational costs low, the perturbation method was chosen to avoid solving similar eigenproblems repeatedly.

In both cases, the KL expansion was used to describe the slowly varying random fields. This series expansion is recommended for strongly correlated random fields and it requires the minimum number of terms to adequately represent a random field with a truncated series. In principle, other random fields descriptions could be equally incorporated.

Experimental investigations regarding the effects of uncertain positioning of the attachment points and experiments to estimate the bending stiffness a typical cable bundle used in the automotive industry were also carried out. A Bayesian approach was used for the parameter estimations in the latter case.

6.1 Conclusions

This section summarises the main conclusions regarding the behaviour of the coupled structures, the effects of uncertainties and possible industrial implications.

6.1.1 *Basic features of the coupled system*

When rigid links are considered, the response of the coupled system is governed by the least mobile structure. At lower frequencies, this would generally be the host plate, whereas at higher frequencies, this would be attached beam. When a single elastic spring is used to simulate a flexible connection, there is a frequency at which the system uncouples. This frequency can be identified approximately from the mobilities of the beam, plate and elastic spring. In the case of the external load applied to the plate, this occurs when the magnitude of the point mobility of the beam and plate system acting in parallel matches the magnitude of the mobility of the spring and plate also acting in parallel. The stiffer the link, the higher is the frequency of the minimum in the mobility of the coupled system. Moreover, in this case, the motion in the attached beam decreases above the uncoupling frequency and the response of the coupled plate is only determined by the mobilities of the plate and spring. Below this frequency, both the response of the attached beam and the host plate are dominated by the combination of the beam and the plate mobilities acting in parallel. A lumped parameter equivalent system could be used to estimate this frequency, but the calculations for this are not particularly easy compared to the calculation of the actual coupled system response.

Even for the case comprising infinite structures, it is possible to note the occurrence of local modes in the section between the finite number of point connections. These localised modes are governed by the spacing between the connections and the stiffness of the individual structures. In the case of the infinite system, increasing the number of attachments, accentuates the appearance of the local modes between the connections. In the same frequency range, the system with a less stiff beam attachment allows more of these local modes to occur.

For the finite systems, the attached beam at different frequencies can act as an additional mass or additional mass and damping. More details are given in section 6.1.3. The frequency-averaged response of the coupled system comprising finite structures shows good agreement with the response of the infinite system. Especially at higher frequencies, when the modal density increases.

6.1.2 *The effects of uncertainties*

Regarding the effects of uncertainties in the spatial properties such as Young's modulus, a study showing how the WKB approximation holds for the case of flexural motion was shown. Also, the response from a combination of mid-point sampling and a perturbation method for the uncertain plate agrees well with the solution of the FE eigenproblem, but it significantly lowers the computational cost when multiple cases have to be studied in a Monte Carlo framework.

One can note how uncertainty in the positioning of the connections, or equivalent to the spacing, can be observed to be as important as uncertainties in the varying mechanical properties of the structures. In chapter 4, good agreement was observed between the experimental data and the

numerical models when random spacing between the attachments were considered. Uncertainties in the spacing start to play a role from frequencies above a spacing to plate bending wavelength ratio of $\frac{\Delta}{\lambda_p} \approx 0.5$. Unfortunately, the two beams used in the experiment were not sufficiently different in terms of bending stiffness to notice any additional features when compared to more flexible or stiffer beams as had been simulated.

In the case of slowly varying properties for the infinite system, they do not result in a large variability in the response of the coupled system. The response is highly governed by local properties and since only small dispersion was considered there is no significant difference. For the case of finite systems, the slowly varying properties change the natural frequencies of the system. At lower frequencies, the uncertainties in the response of the coupled system are dominated by the uncertainties in the host plate structure, whereas at higher frequencies, there is also a contribution from the uncertainties in the attached beam. One can also note that the slowly varying properties break the symmetry present in the attached beam. In the case of applying a load at the central point of a beam, points that should be a nodal response for even modes can respond in these modified modes when the random properties are present.

Uncertainties in the stiffness of the links that couple the structures together only played a role above the uncoupling frequency of the system. Below that frequency, the behaviour tends to that of a system comprising rigid links between the beam and plate. Another effect of the flexible links is that since the system uncouples above a given frequency, the flexible links can be used to reduce the uncertainties in the response of the combined system due to one of the elements. In the case presented here with the external load acting on the plate, the flexible links reduce the response variability due the attached beam.

6.1.3 *Industrial implications*

This thesis proposed an alternative approach to the standard technique used in the industry of considering the cable bundles attached to structures as simply lumped masses located at the connection points.

The use of mobilities to couple the structures also allows one to capture behaviour that would not be present when only masses are considered, such as the stiffness and modal features of the attached beam. At lower frequencies, the attached beams could be seen as an additional mass, shifting down the natural frequencies of the coupled system. However, this approximation breaks down at higher frequencies, where the attached beam contributes to some additional stiffness and it also reduces the amplitude levels of the response of the coupled system. This arises due to the fact that the coupled system has a higher modal density and the response of the coupled system is shared into more modes, which lead to an apparent reduction in the amplitude of the resonances. This is similar to apparently having additional damping in the system.

Also, the use of mobilities matrices for the description of the dynamics of the attached beams could be combined and implemented along with standard commercial available FE software. It would require obtaining the mobility matrix for the host structure at the connection points from the FE models.

The novel approach combining wavenumber estimation and Bayesian inference was able to identify local wavenumbers and, therefore, local bending stiffnesses when a random field was considered to describe the Young's modulus of a slowly varying beam. This could be used, for example, to estimate properties of critical cable bundles in structures such as satellites, which are not under a large volume production regime. It can also offer insight of the distribution of the properties that could be of interest for the case of the automotive industry, for instance. The example given was for the bending stiffness of cable bundle, but in principle it could be applied to other properties and even other structures, to identify the thickness of corroded pipes, for instance. The wavenumber correlation technique offers the advantage of being independent of the boundary conditions, which are typically unknown. It is also independent of the knowledge of the natural frequencies. This technique only requires the measurement of FRFs, it is not necessary to perform a modal analysis. However, the measurements need to be taken far away from boundary conditions and excitation points, to assume only propagating waves. For the correct identification of local properties, the measurement at large number of points might be required.

6.2 Future work

This study focused on the fundamental level research of variability in the response of connected structures with uncertain properties based on a mobility approach for structures in flexure. However, only the translational displacements were considered throughout this thesis. Therefore, the most obvious suggestions for future work would be to extend this analysis to include the rotations involved in the coupled structures and the offset of the links that couple the structures together. This might introduce significant modelling complexity. Moreover, different links can be considered, as only perfectly rigid links or translational elastic springs were used in this study. In both cases, they were massless.

Furthermore, in all cases, the beam is attached to the plate in a straight line, which is not necessarily the case in real applications. One could choose to investigate different configurations for the distribution of the attached beam, possibly trying to work on an optimization problem to achieve a given feature in the response of the coupled system, as the beam can act as an additional mass and damping and the spacing between the connections can create local modes. The analysis of different random spacing distributions could also be investigated, sampling the spacing from spatially correlated random fields.

Experimental work can be done using cable bundles and varying the positioning of the attachment points. Also, experimental work using the proposed technique to identify local properties should be carried out, as only synthetic data was used in this study. Work could also be done in terms of estimation of the random field when other geometrical measurable quantities such as thickness, width, bundle diameter are uncertain.

Other random field models using non-Gaussian distributions and different autocovariance functions could be investigated in the description of the spatially correlated random fields via the KL expansion.

In addition, one might also be interested in the sensitivity analysis of the coupled response to property variation and means to reduce the coupled system variability, also including an analysis of the importance of the $\frac{k_b}{k_p}$ ratio and taking into account cable to host structure mass ratio, as well.

Appendix A – Expressions for the mobilities of homogeneous beams and plates

For an infinite and uniform Euler-Bernoulli beam, the equation of motion for flexural vibration due to a transverse distributed force per unit length is given by [**53**] [**104**]:

$$EI\frac{\partial^4 w(x,t)}{\partial x^4} + \rho A\frac{\partial^2 w(x,t)}{\partial t^2} = f_z(x,t) \tag{A.1}$$

where E is the Young's modulus, I is the second moment of area about the neutral axis, ρ is the density, A is the cross-sectional area and $f_z(x,t)$ is transverse distributed force per unit length.

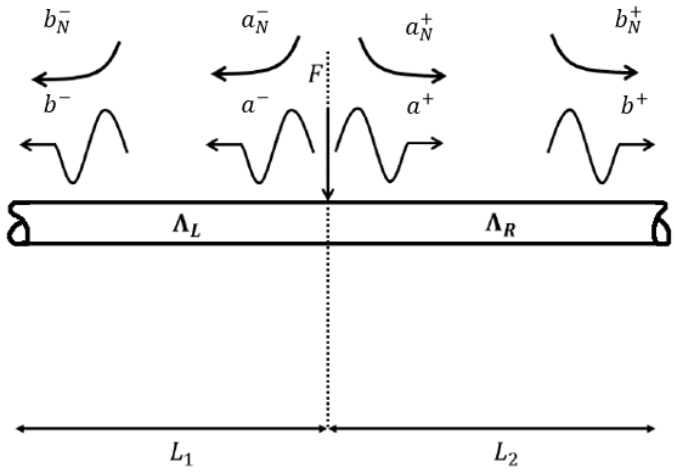

Figure A.1 – Infinite beam under a point harmonic excitation and the propagating waves and near-field waves.

(adapted from: [**2**])

For a harmonic response and free vibration, i.e. $f_z(x,t) = 0$, Equation (A.1) has a solution in the form:

$$W(x) = a^+e^{-ik_bx} + a_N^+e^{-k_bx} + a^-e^{ik_bx} + a_N^-e^{k_bx} \tag{A.2}$$

where a_N^+ and a_N^- are the amplitude of the transverse right and left near-field waves, respectively, and a^+ and a^- are the propagating right-going and left-going waves. k_b is the free wave bending wavenumber of the beam at the particular harmonic frequency.

The equilibrium and continuity boundary conditions for an infinite beam subjected to a point force at $x = 0$ are that the internal shear force equals the applied force:

$$F = 2EI\frac{\partial^3 W(0)}{\partial x^3} \tag{A.3}$$

Appendix A – Expressions for the mobilities of homogeneous beams and plates

The internal beam bending moment to the left of the applied force equals the beam bending moment to the right of the applied force:

$$EI\frac{\partial^2 W_L(0)}{\partial x^2} = EI\frac{\partial^2 W_R(0)}{\partial x^2} \tag{A.4}$$

The displacement to the left of the force equals to the displacement to the right of the applied force:

$$W_L(0) = W_R(0) \tag{A.5}$$

The rotation to the left of the force equals to the rotation to the right of the applied force:

$$\frac{\partial W_L(0)}{\partial x} = \frac{\partial W_R(0)}{\partial x} \tag{A.6}$$

These first two relationships, (A.3) and (A.4), together are known as the force equilibrium conditions and the second two, (A.5) and (A.6), as the continuity conditions.

As a result of applying the boundary conditions to the solution given by Equation (A.2), the wave amplitudes are $a_N^+ = a_N^- = \frac{-F}{4EIk_b{}^3}$ and $a^+ = a^- = \frac{-iF}{4EIk_b{}^3}$. Therefore, the mobility of the infinite Euler-Bernoulli beam for $x \geq 0$ can be determined substituing a^+ and a_N^+ into Equation (A.2) with $a_N^- = a^- = 0$ and differentiating it with respect to time. In other words, assuming point harmonic excitation, multiplying it by $i\omega$.

$$Y_b(\alpha,\beta) = \frac{\dot{W}_\beta(x)}{F_\alpha} = \frac{-\omega}{4EIk_b{}^3}\left(ie^{-k_b x} - e^{-ik_b x}\right) \tag{A.7}$$

where $\alpha = 0$ and $\beta = x$.

Rearranging for the distance between the points:

$$Y_b(\alpha,\beta) = \frac{-\omega}{4EIk_b{}^3}\left(ie^{-k_b r} - e^{-ik_b r}\right) \tag{A.8}$$

where $Y_b(\alpha,\beta)$ is the transfer mobility of an infinite beam between points α and β, ω is the angular frequency, E is the Young's modulus, I is the second moment of area about the neutral axis, k_b is the bending wavenumber of the beam and r is the distance between the points. To obtain the driving point mobility, one needs to set r to zero.

The bending wavenumber of a beam is given by:

$$k_b = \left[\frac{\rho A}{EI}\right]^{\frac{1}{4}}\sqrt{\omega} \tag{A.9}$$

The host structure is assumed to be an infinite and uniform homogeneous thin plate. From the classical plate theory for thin plates, the equation of motion for the transverse displacement subject to a distributed transverse force per unit area $p_z(x,y,t)$ is [**105**] [**43**] [**53**]:

$$B\left[\frac{\partial^4 w(x,y,t)}{\partial x^4}+\frac{2\partial^4 w(x,y,t)}{\partial x^2\partial y^2}+\frac{\partial^4 w(x,y,t)}{\partial y^4}\right]+m\frac{\partial^2 w(x,y,t)}{\partial t^2}=p_z(x,y,t) \qquad \text{(A.10)}$$

where $B=\frac{EI}{(1-\nu^2)}$ is the bending stiffness, E is the Young's modulus, ν is the Poisson's ratio, $I=\frac{h^3}{12}$ is the cross-sectional second moment of area per unit width, h is the thickness of the plate, $m=\rho h$ is the mass per unit area, ρ is the density of the plate material and $p_z(x,y,t)$ is the distributed transverse force per unit area.

It is possible to determine the characteristics of the wave motion in the plate in a similar way to the one used previously for the beam using a cylindrical coordinate description. After some algebraic manipulation, the mobility is given by [**53**]:

$$Y_p(\alpha,\beta)=\begin{cases}\dfrac{\omega}{8Bk_p^2}\left[H_0^{(2)}(k_p r)-\dfrac{2i}{\pi}K_0(k_p r)\right], & \alpha\neq\beta\\ \dfrac{1}{8\sqrt{Bm}}, & \alpha=\beta\end{cases} \qquad \text{(A.11)}$$

where $Y_p(\alpha,\beta)$ is the mobility for the infinite plate, $H_i^{(2)}$ is an ith order Hankel function of the second kind, K_i is an ith order modified Bessel function of the second kind, $k_p=\sqrt[4]{\frac{m}{B}}\sqrt{\omega}$ is the flexural wavenumber in the plate, ω is the circular frequency and r is the distance between points α and β in the plate.

Appendix A – Expressions for the mobilities of homogeneous beams and plates

Appendix B – A reciprocity check for a beam rigidly connected through a finite number of points to a plate

Reciprocity should still be valid in the case one is interested on the load being applied to the beam and it could be verified as it follows:

Assuming the response in both cases will be the same in the case of rigid links, the the velocity vectors at the point of connection will be equal, i.e.:

$$\dot{\boldsymbol{w}}^{p_1} = \dot{\boldsymbol{w}}^{p_2} \tag{B.1}$$

where $\dot{\boldsymbol{w}}^{p_1}$ is the response when the plate is excited, whereas $\dot{\boldsymbol{w}}^{p_2}$ is the response when the external force is applied to the beam. In both cases, the excitations are located at one of the rigid link locations.

Let $\boldsymbol{Y}^p$ and $\boldsymbol{Y}^b$ be the plate and beam mobilities, respectively. Then:

$$\dot{\boldsymbol{w}}^{p_1} = \boldsymbol{Y}^p(\boldsymbol{f} - \boldsymbol{f}') \text{ and } \dot{\boldsymbol{w}}^{p_2} = \boldsymbol{Y}^p\boldsymbol{f}_2' \tag{B.2}$$

where $\boldsymbol{f}'$ is the vector of transmitted internal forces from the plate to the beam when the external load $\boldsymbol{f}$ is applied to the plate, whilst $\boldsymbol{f}_2'$ is the vector of transmitted internal forces from the beam to the plate when the external load $\boldsymbol{f}$ is applied to the beam.

$$\boldsymbol{Y}^p(\boldsymbol{f} - \boldsymbol{f}') = \boldsymbol{Y}^p\boldsymbol{f}_2' \tag{B.3}$$

$$\boldsymbol{f}_2' = \left(\boldsymbol{Y}^p + \boldsymbol{Y}^b\right)^{-1}\boldsymbol{Y}^b\boldsymbol{f} \tag{B.4}$$

$$\boldsymbol{Y}^p\boldsymbol{f} - \boldsymbol{Y}^p\left(\boldsymbol{Y}^p + \boldsymbol{Y}^b\right)^{-1}\boldsymbol{Y}^p\boldsymbol{f} = \boldsymbol{Y}^p\left(\boldsymbol{Y}^p + \boldsymbol{Y}^b\right)^{-1}\boldsymbol{Y}^b\boldsymbol{f} \tag{B.5}$$

Multiplying all the terms by $\boldsymbol{Y}^{p\,-1}$ from the left side:

$$\boldsymbol{Y}^{p\,-1}\boldsymbol{Y}^p\boldsymbol{f} - \boldsymbol{Y}^{p\,-1}\boldsymbol{Y}^p\left(\boldsymbol{Y}^p + \boldsymbol{Y}^b\right)^{-1}\boldsymbol{Y}^p\boldsymbol{f} = \boldsymbol{Y}^{p\,-1}\boldsymbol{Y}^p\left(\boldsymbol{Y}^p + \boldsymbol{Y}^b\right)^{-1}\boldsymbol{Y}^b\boldsymbol{f} \tag{B.6}$$

$$\boldsymbol{I}\boldsymbol{f} - \boldsymbol{I}\left(\boldsymbol{Y}^p + \boldsymbol{Y}^b\right)^{-1}\boldsymbol{Y}^p\boldsymbol{f} = \boldsymbol{I}\left(\boldsymbol{Y}^p + \boldsymbol{Y}^b\right)^{-1}\boldsymbol{Y}^b\boldsymbol{f} \tag{B.7}$$

Now, multiplying all the terms by $(\boldsymbol{Y}^p + \boldsymbol{Y}^b)$ from the left side:

$$\left(\boldsymbol{Y}^p + \boldsymbol{Y}^b\right)\boldsymbol{f} - \boldsymbol{Y}^p\boldsymbol{f} = \boldsymbol{Y}^b\boldsymbol{f} \tag{B.8}$$

$$\boldsymbol{Y}^p\boldsymbol{f} + \boldsymbol{Y}^b\boldsymbol{f} - \boldsymbol{Y}^p\boldsymbol{f} = \boldsymbol{Y}^b\boldsymbol{f} \tag{B.9}$$

Appendix B – A reciprocity check for a beam rigidly connected through a finite number of points to a plate

$$\boldsymbol{Y}^{b}\boldsymbol{f} = \boldsymbol{Y}^{b}\boldsymbol{f} \tag{B.10}$$

Q.E.D

List of References

[1] L. C. Mochales, "Vibration analysis using approximate methods for heavily damped systems with variability," University of Southampton, Ph.D. Thesis 2016.

[2] A. T. Fabro, "Propagation In Waveguides With Slowly Changing Variability," University of Southampton, Ph.D. Thesis 2014.

[3] D. M. Coombs et al., "Dynamic Modeling and Experimental Validation of a Cable-Loaded Panel," *Journal of Spacecraft and Rockets*, vol. 48, no. 6, pp. 958-974, November-December 2011.

[4] Ji Woo Yoo, "Dynamic modelling of beam-plate systems in the mid-frequency region," Faculty of Engineering, Science and Mathematics, University of Southampton, United Kingdon, Ph.D. Thesis June 2005.

[5] M. S. Kompella and R. J. Bernhard, "Measurement of the statistical variation of structural acoustic characteristics of automotive vehicles," in *Proceedings of SAE noise and vibration Conference*, 1993.

[6] F. J. Fahy, "Statistical energy analysis: a critical overview," *Philosophical Transactions of the Royal Society of London*, vol. A346, pp. 431-447, 1994.

[7] S. H. Sung and D. J. Nefske, "Assessment of a vehicle concept finite-element model for predicting structural vibration," in *SAE Technical papers*, 2001.

[8] M. J. Moeller, R. S. Thomas, H. Maruvada, N. S. Chandra, and M. Zebrowski, "An assessment of a FEA NVH CAE body model for design capability," in *Proceedings of the 2001 Noise and Vibration Conference*, Traverse City, MI, USA, 2001.

[9] M. I. Friswell and J. E. Mottershead, *Finite Element Model Updating in Structural Dynamics*. Netherlands: Kluwer Academic Publishers, 1995.

[10] A. J. Jerry, "The Shannon sampling theorem - Various extensions and applications: A tutorial review," *Proceedings of IEEE*, vol. 65, pp. 1565-1596, 1977.

[11] S. Marburg, "Six boundary elements per wavelength: Is that enough?," *Journal of Computational and Acoustics*, vol. 10, pp. 25-51, 2002.

[12] P. Schmiechen, "Travelling wave speed coincidence," University of London, Ph.D. Thesis 1997.

[13] M. Petyt, *Introduction to finite element vibration analysis*. Cambridge, United Kingdom: Cambridge University Press, 1990.

[14] O. C. Zienkiewicz and R. L. Taylor, *The Finite Element Method: Basic Concepts and Linear Applications*, 3rd ed. London, United Kingdom: McGraw Hill, 1989.

[15] P. L. Riebero, "Hierarchical finite element analyses of geometrically non-linear vibration of beams and plane frames," *Journal of Sound and Vibration*, vol. 246, pp. 225-244, 2001.

[16] W. Han and M. Petyt, "Linear vibration analysis of laminated rectangular plates using the hierarchical finite element method," *Computers and Structures*, vol. 61, pp. 705-712, 1996.

[17] ESDU IHS, "An Introduction to Statistical Energy Analysis," 1999.

[18] B. R. Mace and J. Rosenberg, "Energy flow between two coupled plates: finite element and statistical energy analyses," in *Proceedings of Inter-Noise '95*, 1995, pp. 1271-1274.

[19] B. R. Mace, "Power flow between two continuous one-dimensional subsystems: a wave solution," *Journal of Sound and Vibration*, vol. 154, pp. 289-319, 1992.

[20] R. G. DeJong, "An approach to the Statistical Energy Analysis of strongly coupled systems," in *Proceedings of IUTAM symposium on Statistical Energy Analysis*, 1997, pp. 71-82.

[21] R. H. Lyon and R. G. DeJong, *Theory and Application of Statistical Energy Analysis*. Boston: Butterworth-Heinemann, 1995.

[22] R. M. Grice. and R. J. Pinnington, "A method for the vibration analysis of built-up structures, Part I: Introduction and analytical analysis of the plate-stiffened beam," *Journal of Sound and Vibration*, vol. 230, pp. 825-849, 2000.

[23] C. T. Hugin, "A Physical Description of the Response of Coupled Beams," *Journal of Sound and Vibration*, vol. 203, pp. 563-580, 1997.

[24] Alexis Castel, Rabah Hadjit, and Massimiliano Calloni, "A hybrid FE-SEA model reduction method to obtain detailed responses at chosen locations from a large launch vehicle model," in *7th European Conference for Aeronautics and Space Sciences*, Milan, Italy, 2017.

[25] R. S. Langley and P. Bremner, "A hybrid method for the vibration analysis of complex structural-acoustic systems," *Journal of the Acoustical Society of America*, vol. 105, pp. 1657-1671, 1999.

[26] N. Metropolis and S. Ulam, "The Monte Carlo Method," *Journal of the American Statistical Association*, vol. 44, pp. 335-341, 1949.

[27] F. Fontanela, "Análise robusta de modelos estruturais utilizando métodos probabilísticos," Engenharia Mecânica, UFSC, Florianópolis, MSc Dissertation (in Portuguese) 2015.

[28] Paul Gausserman, *Monte Carlo Methods in Financial Engineering*. New York: Springer, 2003.

[29] A. Cunha Jr, R. Nasser, R. Lopes, H. Sampaio, and K. Breitman, "Uncertainty quantification through the Monte Carlo method in a cloud computing setting," *Computer Physics Communications*, vol. 185, pp. 1355-1363, 2014.

[30] J. S. Liu, *Monte Carlo Strategies in Scientific Computing*. New York: Springer, 2001.

[31] R. W. Shonkwiller and F. Mendivil, *Explorations in the Monte Carlo Methods*. New York: Springer, 2009.

[32] C. P. Robert and G. Casella, *Monte Carlo Statistical Methods*. New York: Springer, 2010.

[33] Dongbin Xiu and G. E. Karniadakis, "The Wiener-Askey Polynomial Chaos for Stochastic Differential Equations," *Journal on Scientific Computing*, vol. 24, pp. 619-644, 2006.

[34] H. Benaroya and M. Rehak, "Finite Element Methods in Probabilistic Structural Analysis: A Selective Review," *Applied Mechanics Reviews*, vol. 41, pp. 201-213, 1988.

[35] E. Zio and N. Pedroni, "Possibilistic methods for uncertainty treatment applied to maintenance policy assessment.," Foundation for an Industrial Safety Culture, Toulouse, France, Industrial Safety Cahiers 2014.

[36] H. De Gersem, D. Moens, W. Desmet, and D. Vandepitte, "Dynamic interval analysis of FE models with uncertain substructures," in *PROCEEDINGS OF ISMA2006*, Heverlee, Belgium, 2006, pp. 4077-4090.

[37] L. Wasserman, *All of Statistics: A concise Course in Statistical Inference*.: Springer, 2004.

[38] A. Papoulis, *Probability, random variables, and stochastic processes*. New York: McGraw-Hill, 1991.

[39] A. Cunha Jr, "Lecture 2 - Elements of Statistical Inference," Florianópolis, Brazil, Notes of the Short course on UQ - Uncertainties 2018 2018.

[40] A. T. Fabro, N. S. Ferguson, T. Jain, R. Halkyard, and B. R. Mace, "Wave propagation in one-dimensional waveguides with slowly varying random spatially correlated variability," *Journal of Sound and Vibration*, vol. 343, pp. 20-48, 2015.

[41] A.D. Pierce, "Physical Interpretation of the WKB or Eikonal Approximation for Waves and Vibrations in Inhomogeneous Beams and Plates," *The Journal of the Acoustical Society of America*, vol. 48, pp. 275-284, 1970.

[42] A. T. Moorhouse and B. M. Gibbs, "Calculation of the Mean and Maximum Mobility for Concrete Floors," *Applied Acoustics*, vol. 45, pp. 227-245, 1995.

[43] L. Cremer, M. Heckl, and E. E. Ungar, *Structure-Borne Sound*, 2nd ed.: Springer, 1988.

[44] J. Renno and N. S. Ferguson, "Cable Bundles in Automotive Vehicles," University of Southampton, Visit Report 2014.

[45] J. C. Gooding, V. Babuška, D. T. Griffith, B. R. Ingram, and L. M. Robertson III, "Study of Free-Free Beam Structural Dynamics Perturbations due to Mounted Cable Harnesses," in *48th AIAA/ASME/ASCE/AHS/ASC Structure, Structural Dynamics, and Materials Conference*, Honolulu, Hawaii, 2007.

[46] V. Babuška et al., "Modeling and Experimental Validation of Space Structures with Wiring Harnesses," *Journal of Spacecraft and Rockets*, vol. 47, no. 6, November-December 2010.

[47] A. Lefebvre, "L'influence de câbles sur le mouvement d'une poutre," ENSTA ParisTech and University of Southampton, Internship Report (in French) 2010.

[48] M. Moshrefi-Torbati, C. Simonis de Cloke, and A. J. Keane, "Vibrational optimization of a mass-loaded stepped plate," *Journal of Sound and Vibration*, vol. 213, pp. 865-887, 1998.

[49] A. J. Keane, "Experiences with optimizers in structural design," in *Proceedings of the Conference on Adaptive Computing in Engineering Design and Control*, Plymouth, 1994.

[50] D. J. Mead, "Wave propagation and natural modes in periodic systems: I. Mono-coupled systems.," *Journal of Sound and Vibration*, vol. 40, pp. 1-18, 1975.

[51] D. J. Mead, "Wave propagation and natural modes in periodic systems: II. Multi-coupled systems, with and without damping.," *Journal of Sound and Vibration*, vol. 40, pp. 19-39, 1975.

[52] R.G. White, "Chapter 26 - Vibration control (II)," in *Noise and Vibration*, R.G. White and J.G. Walker, Eds.: Ellis Horwood Publishers, 1986.

[53] P. Gardonio and M.J. Brennan, "Chapter 9 - Mobility and impedance methods in structural dynamics," in *Advanced Applications in Acoustic, Noise and Vibration*, F. Fahy and J. Walker, Eds.: Spon Press, 2004.

[54] E. Skudrzyk, "Vibrations of systems with finite or infinite number of resonances," *Journal of the Acoustical Society of America* , vol. 30, pp. 1140-1152, 1958.

[55] E. Skudrzyk, *Simple and Complex Vibratory Systems*. London: The Pennsylvania State University Press, 1968.

[56] J.P. Arenas and M.J. Crocker, "A note on a WKB application to a duct of varying cross-section," *Applied Mathematics Letters*, vol. 14, pp. 667-671, 2001.

[57] F.B. Jensen, M.B. Porter W.A. Kuperman, and H. Schimidt, *Computational Ocean Acoustics*. New York: Springer, 2011.

[58] P. Filippi, D. Habault, J.P. Lefebvre, and A. Bergassoli, *Acoustics: Basic Physics, Theory and Methods*.: Academic Press, 1999.

[59] D. J. Thompson, "3. Waves in beams - forcing, reflection and transmission," University of Southampton, Lecture notes 2015.

[60] S.P. Huang, S.T. Quek, and K.K. Phoon, "Convergence study of the truncated Karhunen-Loeve expansion for simulation of stochastic processes," *International journal for numerical methods in engineering*, vol. 52, pp. 1029-1043, 2001.

[61] E. Vanmarcke, *Random Field: Analysis and Synthesis*, 2nd ed. Cambridge, MA, USA: Word Scientific, 2010.

[62] R. Ghanem and P. Spanos, *Stochastic Finite Elements: A Spectral Approach*.: Dover Publications, 1991.

[63] B. Sudret and A. Der Kiureghian, *Stochastic Finite Element Methods and Reliability: A State-of-Art Report*. Berkeley: University of California, 2000.

[64] G. Stefanou, "The stochastic finite element method: Past, present and future," *Computer Methods in Applied Mechanics and Engineering*, vol. 198, pp. 1031-1051, 2009.

[65] G.I. Schueller, "A state-of-art report on computational stochastic mechanics," *Probabilistic Engineering Mechanics*, vol. 12, pp. 197-321, 1997.

[66] K. Fukunaga and W.L.G. Koontz, "Application of the Karhunen-Loève expansion to feature selection and ordering," *IEEE Transactions on Computers*, vol. C-19, April 1970.

[67] S. Watanabe, "Karhunen-Loève expansion and factor analysis," *Trans. 4th Prague Conference on Information Theory*, 1965.

[68] S. Watanabe, "Evaluation and selection of variables in pattern recognition," in *Computer and Information Sciences Vol. 2.*: New York: Academic Press, 1967.

[69] T. M. Cover and J. A. Thomas, *Elements of Information Theory*, 2nd ed.: John Wiley & Sons, Inc., 1991.

[70] H.L. Van Trees, *Detection, Estimation and Modulation Theory, Part 1*. New York: Wiley, 1968.

[71] D. J. Mead, *Passive Vibration Control*. Chichester: Wiley, 1999.

[72] W. Soedel, *Vibrations of Shells and Plates*, 2nd ed. New York: Marcel Dekker Inc, 1993.

[73] G.B. Warburton, "The Vibration of rectangular plates," *Proceedings of the Institute of Mechanical Engineering*, vol. 168, pp. 371-384, 1951.

[74] B. R. Mace, "Wave reflection and transmission in beams," *Journal of Sound and Vibration*, vol. 97(2), pp. 237-246, 1984.

[75] A. Adini and R. W. Clough, "Analysis of Plate Bending by the Finite Element Method," Report submitted to the National Science Foundation, G7337 1961.

[76] R. J. Melosh, "Basis for derivation of matrices for the direct stiffness method," *AIAA J*, vol. 1, pp. 1631-7, 1963.

[77] University of Colorado at Boulder, *Advanced Finite Element Methods (ASEN 3637) - Chapter 22.*, 2017.

[78] C. V. Smith, "Finite Element Model, with Applications to Buildings and K-33 and K-31," Union Carbide Corporation Report Number CTC-29 1970.

[79] S. S. Rao, *Mechanical Vibrations*, 5th ed.: Pearson, 2010.

[80] M. Petyt and P. Gardonio, "Chapter 10 - Finite element techniques for structural vibration," in *Advanced Applications in Acoustic, Noise and Vibration*, F. Fahy and J. Walker, Eds.: Spon Press, 2004.

[81] W. K. Liu, T. Belytschko, and A. Mani, "Probabilistic finite elements for nonlinear structural dynamics," *Computer Methods in Applied Mechanics and Engineering*, vol. 56, pp. 61-81, 1986.

[82] A. Bhaskar, S. Sahu, and B. Nakra, "Approximations and reanalysis over a parameter interval for dynamic design," *Journal of Sound and Vibration*, vol. 248, pp. 178-186, 2001.

[83] R. L. Fox and M. P. Kapoor, "Rates of change of eigenvalues and eigenvectors," *AIAA Journal*, vol. 6, pp. 2426-2429, 1968.

[84] A. Der Kiureghian and J.-B. Ke, "The stochastic finite element method in structural reliability," *Prob. Eng. Mech.*, vol. 3, pp. 83-91.

[85] Anil K. Chopra, *Dynamics of structures: Theory and Applications to Earthquake Engineering*. New Jersey, USA: Prentice Hall, 1995.

[86] M. Pastor, M. Binda, and T. Harčarik, "Modal Assurance Criterion," *Procedia Engineering*, vol. 48, pp. 543-548, 2012.

[87] A. Abolfathi, D. J. O'Boy, S. J. Walsh, Amy M. Dowsett, and S. A. Fisher, "The uncertainty in stiffness and damping of an automotive vehicle's trim-structure mounts and its effect on the variability of the vibration transfer function," *Proceedings of the Institution of Mechanical Engineers, Part C: Journal of Mechanical Engineering Science*, vol. 232, pp. 2587-2598, 2017.

[88] A.R. Mayr and B.M. Gibbs, "Point and transfer mobility of point-connected ribbed plates," *Journal of Sound and Vibration*, vol. 330, pp. 4798-4812, 2011.

[89] Spider Magnetics Ltd, Barnsley, Manufacturer report 2015.

[90] W.M. Bolstad, *Introduction to Bayesian Statistics*, 2nd ed. New Jersey, USA: Wiley-Interscience, 2007.

[91] Francis S. Tse, Ivan E. Morse, and Rolland T. Hinkle, "Continous Systems," in *Mechanical Vibrations. Theory and applications*, Second ed. Boston, USA: Allyn and Bacon, 1979, ch. 7, pp. 268-269.

[92] T.G. Ritto, R. Sampaio, and R.R. Aguiar, "Uncertain boundary condition Bayesian identification from experimental data: A case study on a cantilever beam," *Mechanical Systems and Signal Processing*, vol. 68-69, pp. 176-188, 2016.

[93] J.L. Beck and L.S. Katafygiotis, "Updating models and their uncertainties I: Bayesian statistical framework," *Journal of Engineering Mechanics*, pp. 455-461, April 1998.

[94] E. Jaynes, "Information theory and statistical mechanics.," *Phys Rev*, vol. 106(4), pp. 1620-1630, 1957.

[95] E. Jaynes, "Information theory and statistical mechanics II," *Phys Rev*, vol. 108, pp. 171-190, 1957.

[96] J.N. Kapur, *Maximum entropy models in science and engineering*.: Wiley, 1990.

[97] T.G. Ritto and L.C.S. Nunes, "Bayesian model selection of hyperelastic models for simple and pure shear at large deformations," *Computers and Structures*, vol. 156, pp. 101-109, 2015.

[98] P. Liu and S-K. Au, "Bayesian parameter identification of hysteric behavior of composite walls," *Probabilistic Engineering Mechanics*, vol. 34, pp. 101-109, 2013.

[99] T.G. Ritto, "Bayesian approach to identify the bit-rock interactions parameters of a drill-string dynamical model," *Journal of the Brazilian Society of Mechanical Sciences and Engineering*, vol. 37, pp. 1173-1182, 2015.

[100] N. S. Ferguson, C. R. Halkyard, B. R. Mace, and K. H. Heron, "The estimation of wavenumbers in two-dimensional structures," in *ISMA2002: International Conference on Noise and Vibration Engineering*, Leuven, 2002.

[101] J. Berthaut, M. N. Ichchou, and L. Jezequel, "K-space identification of apparent structural behaviour," *Journal of Sound and Vibration*, vol. 280, pp. 1125-1131, 2005.

[102] J. G. McDaniel and W. S. Shepard Jr, "Estimation of structural wave numbers from spatially sparse response measurements.," *Journal of the Acoustical Society of America*, vol. 108, no. 4, pp. 1674-1682, 2000.

[103] Robert V. Hogg, Joseph W. McKean, and Allen T. Craig, "Some Special Distributions," in *Introduction to Mathematical Statistics*, 7th ed.: Pearson, 2012, ch. 3, pp. 156-168.

[104] R.E.D. Bishop and D.C. Johnson, *The Mechanics of Vibration*.: Cambridge University Press, 1960.

[105] J.N. Reddy, *Energy and Variational Methods in Applied Mechanics*. New York: John Wiley & Sons, 1984.